Fisheries New Zealand

Tini a Tangaroa

Cyclone impacts on fisheries

Daniel Leduc, Charine Collins, Mark Gall, Carolyn Lundquist, Helen Macdonald, Kevin Mackay, Joshu Mountjoy, Mark Morrison, Alan Orpin, Matt Pinkerton, Erica Spain, Finn Barry, Charlotte Bodie, Ethan Carson-Groom, Amelia Connell, Mark Fenwick, Grace Frontin-Rollet, Jane Halliday, Eva Leunissen, Brooke Madden, Gemma Mason, Alicia Maurice, April Nepia-Su'a, Greg Olsen, Rachael Peart, William Quinn, Rob Stewart, Niketi Toataua

March 2024

Te Kāwanatanga o Aotearoa
New Zealand Government

Please cite this report as:

Leduc, D.; Collins C.; Gall M.; Lundquist, C.; Macdonald, H.; Mackay, K.; Mountjoy J.; Morrison, M.; Orpin, A.; Pinkerton, M.; Spain, E.; Barry, F.; Bodie, C.; Carson-Groom, E.; Connell, A.; Fenwick, M.; Frontin-Rollet, G.; Halliday, J.; Leunissen, E.; Madden, B.; Mason, G.; Maurice, A.; Nepia-Su'a, A.; Olsen, G.; Peart, R.; Quinn, W.; Stewart, R.; Toataua, N. (2024). Cyclone impacts on fisheries. *New Zealand Aquatic Environment and Biodiversity Report No. 326.* 167 p.

TABLE OF CONTENTS

Plain language summary

Increasingly frequent and intense extreme weather events such as Cyclone Gabrielle are likely to impact seafloor marine ecosystems by accelerating soil erosion and sediment transport to the ocean by rivers.

The objective of this project was to understand sediment impacts from the February 2023 Cyclone Gabrielle event on marine environments of the Hawke's Bay and Gisborne regions to enable rapid fisheries management decisions.

We conducted two vessel surveys in June and October 2023 focusing on offshore seabed environments deeper than 15 metres. As part of these surveys we mapped selected areas of the seafloor, surveyed life on the seabed using a towed underwater camera, and obtained sediment core samples.

An ocean current and sediment transport model was designed and implemented to investigate the transport and deposition of sediments after Cyclone Gabrielle. Concentrations of suspended sediments and other parameters in the surface ocean along the east coast of the North Island were estimated from satellite images. This satellite information was used to inform the sediment transport model and to characterise the spatial extent and longevity of the offshore sediment plumes generated by Cyclone Gabrielle. A Seafloor model was used to explore impacts and recovery of seafloor ecosystems following the cyclone.

The analysis of satellite images suggest that the influence of Cyclone Gabrielle lasted approximately two to three months across the Hawke's Bay and Gisborne coastal marine areas, with surface ocean parameters largely returning to normal by May. The concentrations of suspended sediment at the ocean surface in February were significantly elevated, but they did not exceed values typical of winter months. Seabed mapping revealed areas of significant sediment erosion, and deposition up to about one metre in thickness, at Pania Reef, Tangoio Reef and Clive outfall area in Hawke Bay. Elsewhere, sediment core observations suggested the presence of fresh muddy deposits of up to about 15 centimetres. Swell waves were resuspending muddy sediments at shallow locations for several months after the cyclone, as was evident by the low underwater visibility during camera deployments.

The abundance and diversity of the sediment fauna sampled in Hawke's Bay and Gisborne before (2010) and after Cyclone Gabrielle (June and October 2023) tended to increase away from the shore and into deeper waters. Sediment fauna were less abundant in June 2023 when compared with 2010, but appeared to be recovering by October 2023.

Seafloor animal and plant communities are highly likely to have been impacted by sediments at 11 of the 36 locations we surveyed using the towed underwater camera, as assessed by observations including (1) fresh mud layer on the seafloor, (2) animal/plant life in poor condition, and/or (3) absence of seaweed at shallow depths. However, for most of these locations a direct link to Cyclone Gabrielle cannot be demonstrated because no information on the distribution of seafloor organisms is available from before the cyclone. The likely exception is Wairoa Hard in Hawke Bay, where available information shows that kelp and sponges were present before the cyclone but were almost completely or completely absent after the cyclone. Whether this loss of habitat has led to reductions in associated fish populations is unclear.

Although limited by the availability of data, the ocean current and sediment transport model produced realistic predictions of suspended sediment concentrations and deposition at the seafloor. In the days following the cyclone, sedimentation in Hawke Bay was predicted to occur mainly close to shore in the western and central parts of the bay. In the Gisborne region, there was deposition of up to about 10 centimetres of sediments offshore of Poverty Bay and along a narrow band of the coast to the north near Tokomaru and Tolaga bays. These model predictions are broadly consistent with observations from the sediment core samples.

The Seafloor model showed small declines in structure-forming organisms such as sponges for Hawke's Bay following Cyclone Gabrielle. These declines were not substantial, most likely because the region is already impacted by decades of fishing and increased sedimentation. The Seafloor model predicted weaker cyclone impacts for Gisborne than Hawke's Bay and indicated that continued trawling may slow down recovery of seafloor communities following extreme weather events.

The lack of pre-cyclone information was a major obstacle in assessing the potential impacts of the cyclone on seabed ecosystems. Information collected as part of this project now form a valuable baseline that will inform future impact assessments in the region. Another limitation is the inability to use towed cameras to survey inshore habitats for extended periods because of poor underwater visibility. A precautionary approach could be warranted in the period following an extreme weather event until key habitats and ecosystems can be surveyed, and fish stocks and catch levels should be carefully monitored in the years following the event.

Sediment transport modelling is a promising tool for rapidly identifying areas most at risk from sedimentation following extreme weather events. However targeted sampling of sediment and water parameters under normal and flood conditions would help improve the accuracy and reliability of model predictions. The Seafloor model could be used to explore how spatial changes in fishing effort could enhance recovery following extreme weather events and could be improved through better information on the distribution of seafloor sediment and reefs and their associated animal and plant communities, particularly in the Gisborne region.

The impact of extreme weather events is made worse by decades of increased sedimentation in New Zealand's marine environments. Addressing the long-term issue of sedimentation in marine ecosystems and the impacts of extreme weather events will require addressing the factors that have made New Zealand's catchments more prone to erosion.

EXECUTIVE SUMMARY

Leduc, D.[1]; Collins C.; Gall M.; Lundquist, C.; Macdonald, H.; MacKay, K.; Mountjoy J.; Morrison, M.; Orpin, A.; Pinkerton, M.; Spain, E.; Barry, F.; Bodie, C.; Carson-Groom, E.; Connell, A.; Fenwick, M.; Frontin-Rollet, G.; Halliday, J.; Leunissen, E.; Madden, B.; Mason, G.; Maurice, A.; Nepia-Su'a, A.; Olsen, G.; Peart, R.; Quinn, W.; Stewart, R.; Toataua, N. (2024). Cyclone impacts on fisheries.

Increased sedimentation from rivers is considered the most important land-based stressor on New Zealand coastal fisheries. Sedimentation rates on the New Zealand coast have increased by about one order of magnitude since human colonisation due to deforestation and land-use changes. Increasingly frequent and intense extreme weather events such as cyclones will, in addition to having devastating impacts on affected communities, likely put further stress on seafloor marine ecosystems by accelerating soil erosion and sediment yield to the ocean via rivers. The objective of this project was to understand sediment impacts from the Cyclone Gabrielle event in February 2023 on marine environments of the Hawke's Bay and Gisborne regions to enable rapid fisheries management decisions.

We designed and conducted two RV *Kaharoa* surveys in June and October 2023 focusing on offshore seabed environments (> 15 m depth). We used a multibeam echosounder to quantify changes in seafloor topography, conducted seabed camera transects to investigate potential impacts on seafloor communities, and obtained sediment core samples to describe potential cyclone-related changes in sediment characteristics and sediment fauna. A coupled hydrodynamic and sediment transport model was designed and implemented to investigate the transport and deposition of sediments after Cyclone Gabrielle. Satellite imagery data were used to parameterise this model and to characterise the spatial extent and longevity of the Cyclone Gabrielle event by assessing concentrations of surface suspended sediments and other parameters on the east coast of the North Island. Finally, a model of seafloor ecosystem dynamics (Seafloor model) was parameterised based on these sediment transport outputs to explore impacts and recovery of seafloor ecosystems following Cyclone Gabrielle.

Analyses of satellite data products showed more pronounced short-term impacts in Hawke's Bay relative to Gisborne in terms of total suspended solids, horizontal visibility, and light intensity in the days and weeks following the cyclone. This difference likely reflects the relatively shallow seabed and sheltered aspect of Hawke Bay, which will favour the retention of fine sediments for longer than in the Gisborne region, even though rivers in the Gisborne region typically transport far greater amounts of sediments to the coast. Mean monthly total suspended sediment concentrations in February were significantly elevated, but they did not exceed values typical of winter months. The influence of Cyclone Gabrielle on surface ocean parameters lasted approximately 2–3 months across the Hawke's Bay and Gisborne coastal marine areas, with surface ocean parameters largely returning to normal by May.

Comparison of multibeam data obtained pre- and post-cyclone revealed areas of significant sediment deposition up to ~1.0 m thick and erosion at Pania Reef, Tangoio Reef, and Clive outfall area in Hawke Bay. Minor patterns of deposition were noted at the Wairoa Hard and no notable areas of erosion or deposition were observed at Clive Hard (both in Hawke Bay). Sediment samples taken from areas of sediment deposition at Pania Reef and Tangoio Reef were sand. Elsewhere, sediment core observations during the June RV *Kaharoa* survey suggested the presence of variable fine sediment deposits of up to ~15 cm. Most of these deposits were still present when a subset of the coring sites were revisited in October; however, it is not clear whether these deposits were directly the result of Cyclone Gabrielle or

---

[1] All authors: National Institute of Water and Atmospheric Research (NIWA), New Zealand.

subsequent reworking. Swell waves and oscillatory near-bed water motions were resuspending fine-grained substrates at inner shelf sites and winnowing the seabed, as was evident by the high near-bed turbidity seen on camera deployments. Some shallow sites off Ngaruroro, Wairoa, and Waiapu rivers and off Tokomaru Bay consisted of variably stratified muds, which suggests retention of fine sediments at these locations.

Infaunal abundance, taxon richness, and community structure were generally positively correlated with mud content and water depth in both pre-cyclone (2010) and post-cyclone (2023) datasets, which could reflect the negative impact of wave-induced physical disturbance and/or river sediment discharges on macrofauna communities at the shallow sites nearest to river mouths. No relationship was seen with sediment organic matter content (a proxy of food availability) or woody debris content of the sediment. Macrofauna abundance was significantly lower, and the community structure significantly different, in the June 2023 samples relative to the 2010 samples. A significant increase in abundance (back to 2010 values) and shift in macrofauna community structure was then seen four months later in October 2023. This pattern could reflect an impact on macrofauna communities from the deposition of river-borne sediments during and immediately after the cyclone, followed by recovery later in the year, or may reflect natural seasonal and interannual variability. If macrofauna communities were indeed impacted by the cyclone, the data gathered in October indicate that recovery is likely to be occurring some eight months later, and that the infaunal communities in the Hawke's Bay and Gisborne region are adapted to disturbed conditions and can recover following extreme weather events.

Over 70 towed camera transects were conducted at 36 sites along the Hawke's Bay and Gisborne regions to assess the likelihood of sediment impacts to benthic ecosystems. Key observational evidence includes: (1) fresh muddy deposits and sediment smothering of benthos; (2) organisms in poor condition; (3) absence of macroalgae at shallow depths. Using these qualitative measures sediment impacts are highly likely to have occurred at 11 locations. However, for most of these locations, demonstrating a direct link to Cyclone Gabrielle and drawing quantitative conclusions remains problematic without survey data prior to the event. The likely exception is Wairoa Hard, where comparison of pre- and post-cyclone data from imagery shows that while kelp, other macroalgae, and sponges were present before the cyclone they were almost completely or completely absent after the cyclone. Whether this loss of biogenic habitat has led to reductions in associated fish populations is unclear; however, turbidity levels in the wake of the cyclone are likely to have been sufficiently elevated to cause direct deleterious impacts on fish in the area. Sediment impacts may also have occurred at Cape Kidnappers; but at that location kelp was absent in both pre- and post-cyclone imagery, indicating that chronic sediment impacts may pre-date Cyclone Gabrielle. In Gisborne, several inshore reefs off Poverty Bay, Anaura Bay, Waipiro Bay, Whakariki Point, and Waikori Bluff were assessed as having a high likelihood of sediment impacts. However, another inshore reef located just north of Poverty Bay showed no indication of being strongly impacted by sediment. Collectively, these observations suggest a range of benthic disturbance from river plumes that affect parts of the Gisborne coastline differently. Offshore reefs near the edge of the continental shelf off Poverty Bay and at Table Cape also showed signs of sediment impacts despite being located further seaward of riverine sources. It is likely that most, if not all, of the locations impacted by sediments are naturally exposed to high turbidity conditions near-bed, and periods of deposition. However, the scale of Cyclone Gabrielle will likely have exacerbated suspended sediment loads in the region through an abundance of sediment supply.

Although limited by the lack of data to describe riverine sediment inputs associated with the cyclone, the coupled hydrodynamic and sediment transport model produced realistic prediction of suspended sediment concentrations and deposition at the seafloor. In both regions, the spatial footprint was broader and concentration of near-bed suspended sediment greater than suspended sediment concentrations at the surface, most likely because of sediment resuspension occurring along the coast and inner shelf. In the days following the cyclone, sedimentation in Hawke Bay was predicted to occur mainly close to shore in the western and central parts of Hawke Bay, which is consistent with observations of distinct, stratified mud layers at the top of cores recovered from the region. Sediment deposition in the vicinity of Ngaruroro River mouth persisted in the model when riverine sediment inputs were removed. This indicates that sedimentation was at least partly due to deposition of material resuspended by waves and

currents from areas of erosion elsewhere in the region. There was also significant deposition of up to ~0.5 m of sediment off the Mohaka River mouth. There was net erosion on the Gisborne continental shelf which likely represents resuspension from waves and currents. In the days following Cyclone Gabrielle, there was deposition of up to about 10 cm of sediments offshore of Poverty Bay, which is broadly consistent with the observed soft mud layer at the top of cores obtained in the region, and along a narrow band along the coast to the north near Tokomaru and Tolaga bays. The model performed less well near East Cape and the Waiapu River, where sediment deposition was likely underestimated due to dampening of riverine inputs and boundary condition effects.

The Seafloor model showed small declines in most functional groups (e.g., epifaunal biogenic structure-forming invertebrates) for the Hawke Bay following Cyclone Gabrielle. These declines were not substantial, most likely because the pre-cyclone model state suggests the region is already impacted by decades of fishing and sediment stressors. Some functional groups showed limited impact or rapid recovery following the cyclone, i.e., opportunistic groups, predators/scavengers, and deep-burrowing invertebrates, which were parameterised as having a strong tolerance of high mud content. In contrast, the Seafloor model showed a shrinking in the distribution older age classes of epifaunal biogenic structure-forming invertebrates in Hawke Bay during the Cyclone Gabrielle sedimentation event due to increased mortality at offshore locations. The expected sediment inputs and seafloor deposition from the hydrodynamic and sediment transport model was predicted to be lower in Gisborne than in Hawke's Bay, resulting in a more muted impact of the cyclone on seafloor communities. This difference in impact between the regions is also likely to be partly due to an underestimation of the extent of hard substrates (and their associated communities) in the Gisborne region due to fewer data being available. The Seafloor model suggests that continued trawling may slow down recovery of seafloor communities following events such as Cyclone Gabrielle.

A major impediment in assessing the potential impacts of the cyclone on seabed ecosystems was the paucity of baseline information. Data collected and described in this project now form a valuable baseline dataset that will inform future impact assessments in the region. Another limitation is the inability to use towed cameras to survey inshore habitats and organisms most likely to be impacted by sedimentation for extended periods (8 months in the case of Cyclone Gabrielle), because of the high levels of turbidity and poor underwater visibility. Although biogenic reef habitats may persist after a cyclone event, high levels of near-bed suspended sediments may reduce the extent to which these ecosystems are used by commercially and recreationally harvested species, with potential flow-on impacts on fish stock levels that will not be observable for up to several years. Therefore, a precautionary approach could be warranted in the period following an extreme weather event until key habitats and ecosystems can be surveyed, and fish stocks and catch levels should be carefully monitored in the years following the event.

Sediment transport modelling is a promising tool for rapidly identifying areas most at risk from sedimentation following extreme weather events. The model developed for the east coast of the North Island provided a realistic picture of sediment transport in the region, albeit that further calibration is required with targeted sampling of sediment and water parameters under normal and extreme conditions. The Seafloor model could be used to explore how spatial changes in fishing effort could enhance recovery following extreme weather events and could be improved through better information on the spatial distribution of seafloor substrates and communities, particularly in the Gisborne region.

The impact of extreme weather events is exacerbated by decades of increased sedimentation in New Zealand's marine environments. Addressing the long-term issue of sedimentation in marine ecosystems and the impacts of extreme weather events will require addressing the factors that have made New Zealand's catchments more prone to erosion.

1. INTRODUCTION

Increased sedimentation from rivers is considered to be one of the main threats to marine ecosystems in New Zealand (MacDiarmid et al. 2012) and the most important land-based stressor on New Zealand coastal fisheries (Morrison et al. 2009). Increased sediment input to the ocean can impact fisheries productivity through direct effects including clogging of filter-feeders, reduction in larval/juvenile settlement success and survival, sublethal effects on adults (e.g., respiratory efficiency), and reduced foraging efficiency of visual predators such as fish, and indirect effects including loss of nursery habitats and reduction in the abundance of invertebrate prey species (Morrison et al. 2009). Sedimentation rates in New Zealand estuaries, harbours, and inlets have increased by about one order of magnitude since human colonisation due to deforestation and land-use changes (e.g., Swales et al. 2002, 2005). Extreme weather events (such as Cyclone Bola in March 1988 and Cyclone Gabrielle in February 2023) are expected to become more intense as a result of climate change (Harrington et al. 2023) and may put further stress on seafloor marine ecosystems already under pressure.

Cyclone Gabrielle caused devastating and widespread damage to infrastructure in catchments and the coastal zone of the Te Matau-a-Māui/Hawke's Bay and Tairāwhiti/Gisborne regions, with severe impacts on dwellings, businesses, and crops. Over 300 000 landslides occurred along the east coast of the North Island in the wake of the cyclone, leading to the erosion of an estimated 300 million tonnes (M/t) of soil across the region (MacMillan et al. 2023), a substantial proportion of which was transported to the coast by rivers. The presence of extensive and pervasive coastal plumes of turbid floodwater in the days and weeks following the cyclone, the frequent sighting of woody debris, and difficulties to some fisheries operations caused by accumulation of sediment and logs on the seafloor show the initial impacts of the cyclone on fisheries. Given the magnitude of the Cyclone Gabrielle weather event, longer term impacts to marine benthic ecosystems and fisheries habitats may be significant and widespread.

The continental shelf adjacent to the Hawke's Bay, Gisborne, and East Cape coastline receives large quantities of riverine sediment and suspended material, delivered to the coastal environment by New Zealand's muddiest rivers (Hicks et al. 2011). These East Coast rivers drain steep, deforested catchments in the Raukumara and coastal ranges, composed of strongly jointed, friable, and clay-rich lithologies, resulting in highly unstable landforms (e.g., Berryman et al. 2000, Fuller & Marden 2010). Sediment yields in these upper catchments are among the highest recorded on Earth (Walling & Webb 1996). The East Coast (East Cape to Hawke's Bay) receives an estimated 80 Mt/yr of sediment, around 38% of the national sediment delivery of 209 Mt/yr to the ocean. The bedload component (sands and gravels) of East Coast rivers is typically very low; for example, the Waipaoa River is <1% of the suspended load (Gomez et al. 2009).

The Waiapu River is New Zealand largest single contributor of suspended sediment to the ocean at 35 Mt/yr, the Waipaoa River is second at 15 Mt/yr, and the Uawa-Hikuwai River contributes 5 Mt/yr (Hicks et al. 2011). The Wairoa and Mohaka rivers in Hawke's Bay have suspended sediment yields of 1.1 and 1.4 Mt/yr, respectively (Hicks et al. 2011). Up to four decades of river gauge records before 2001 show flood discharges for East Coast rivers might approach or exceed the critical suspended sediment concentration to generate dense, bottom-hugging, mud plumes at river mouths (Hicks et al. 2004). Anecdotal evidence from cyclone Bola suggested a fluid mud layer, ~2 m thick, formed on the Poverty Bay continental shelf (Foster & Carter 1997), following flood discharge of ~36 Mt of suspended sediment from the Waipaoa River, more than twice its mean annual yield. Such events may occur at the Waipaoa River mouth every ~40 years, but at the Waiapu and Uawa-Hikuwai rivers they may occur annually (Hicks et al. 2004, Ma et al. 2008).

Modern material discharged from East Coast rivers is accumulating in shelf, outer shelf, and slope depocentres (e.g., Kniskern et al. 2010) and centennial sediment accumulation rates vary spatially (Kniskern et al. 2010, Miller & Kuehl 2010). Accumulation rates on the shallow shelf (20–50 m depth) are lower because vigorous reworking of the seabed by waves and currents, transporting resuspended sediment along the shelf and seaward. Riverine material is distributed across the shelf and even the

upper slope, over days to months after a flood, suggesting that material is readily resuspended, reworked, and transported (e.g., Walsh et al. 2014), dispersing sediments across and possibly along the shelf margin throughout the year (Alexander et al. 2010, Kniskern et al. 2010, Moriarty et al. 2015). More sediment is trapped on the inner shelf in Poverty Bay than elsewhere (Kuehl et al. 2016), partly due to protection afforded by the deep shape of the embayment.

NIWA has conducted a variety of research projects on the ecology of seafloor ecosystems in the Hawke's Bay and Gisborne Coastal Marine Areas (CMAs) (Figure 1), and further offshore to the edge of the continental shelf, which are of relevance in assessing the impacts of Cyclone Gabrielle on fisheries habitats and benthic ecosystems. In Hawke's Bay, this includes recent work on key ecological areas of the Hawke's Bay CMA (Lundquist et al. 2020), modelling of seafloor impacts on benthic structure (Lundquist et al. 2022a), and a report on 2020 baseline of existing scientific information on the Maungaharuru-Tangitū Hapū Application Area in Hawke's Bay (Pinkerton et al. 2020). In Gisborne, biogenic habitats work was undertaken on the distribution of continental shelf biogenic habitats (Jones et al. 2018). In addition, hydrodynamic and sediment transport models have been developed for the Waiapoa shelf (Moriarty et al. 2014) and hydrodynamic modelling work has been conducted for Hawke's Bay Regional Council (HBRC) (Collins & Plew 2020).

The objective of this project was to understand sediment impacts in affected marine environments of Hawke's Bay and Gisborne to enable rapid fisheries management decisions. We designed and conducted two RV *Kaharoa* surveys in June and October 2023 focusing on seabed environments at water depths of ~15–100 m. During these surveys, we used a multibeam echosounder to map seafloor topography, conducted seabed camera transects to investigate potential impacts of sedimentation on seafloor communities, and obtained sediment core samples to describe potential cyclone-related changes in sediment characteristics and sediment fauna. Alongside this fieldwork a coupled hydrodynamic and sediment transport model was designed and implemented to investigate the transport and deposition of sediments in Hawke's Bay, Gisborne, and the adjacent continental shelf during and after Cyclone Gabrielle. Satellite imagery data were used to parameterise this model and to characterise the spatial extent and longevity of the Cyclone Gabrielle event by assessing concentrations of surface suspended sediments and other parameters on the east coast of the North Island. The effects of sediment stressors on habitat-structure forming epifaunal invertebrates (animals that live at and above the surface of the seafloor such as those that form sponge gardens, and bryozoan reefs) were investigated using a modified and expanded version of a previously developed seafloor model of disturbance impacts on benthic structure in Hawke Bay.
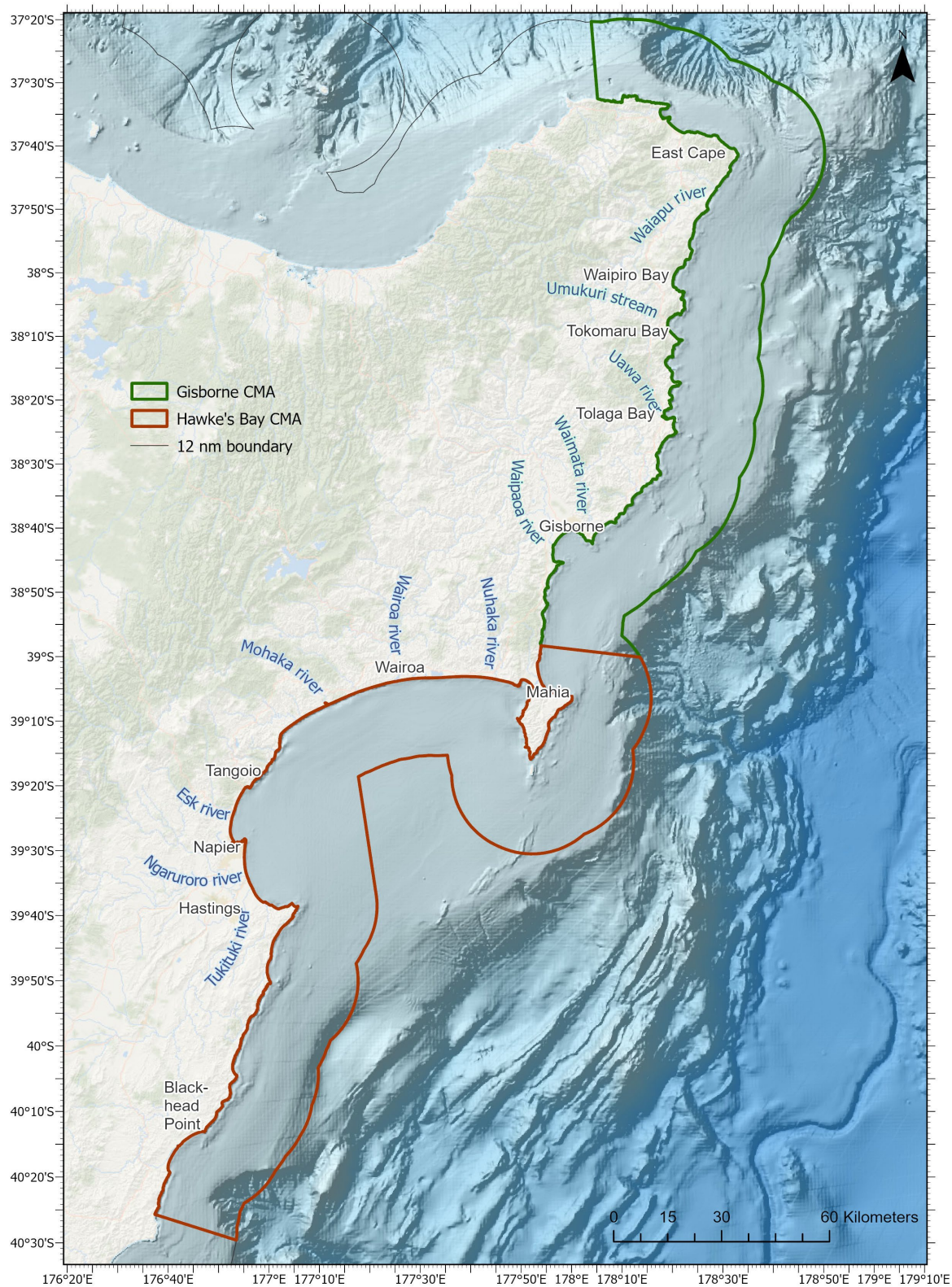
Figure 1: **Map of study region showing the Hawke's Bay and Gisborne CMAs.**

2. METHODS

2.1 General approach and report structure

Prior to this project, multibeam mapping was conducted by NIWA at selected locations in Hawke Bay to evaluate cyclone-related changes in seabed topography (18–29 April 2023; RV *Ikatere* voyage IKA2303). Details of the methods and results from this survey are included in Sections 2.3.2 and 3.2.1 of this report.

The first priority for this project, which began in late May 2023, was to obtain samples and data from the field as quickly possible in order to capture as much information as possible on potential impacts from the Cyclone Gabrielle event (that took place on the night of 13/14 February) on seafloor ecosystems of Hawke's Bay and Gisborne. The first RV *Kaharoa* voyage KAH2303 began on 2 June, over 3 months after the cyclone event, followed by another RV *Kaharoa* voyage KAH2306 in early October, almost eight months after the event. Analyses of remote sensing data and the development of the coupled hydrodynamic and sediment transport model took place alongside this field work. Data from the field surveys, remote sensing, and sediment transport modelling fed into the model of seafloor disturbance impacts. In this report, research components are presented in the following order:

1. Remote sensing
2. Research vessel surveys
3. Hydrodynamic and sediment transport modelling
4. Model of seafloor disturbance impacts.

Remote sensing data are presented first to provide a broader context around the Cyclone Gabrielle event both temporally (from daily to weekly, seasonal, and interannual variability) and spatially (e.g., individual CMAs) for surface ocean parameters such as suspended sediments. This is followed by data from the June and October 2023 field surveys, including seafloor bathymetry, sediments, and seafloor fauna, which are used to assess potential impacts on seafloor ecosystems in targeted areas. The coupled hydrodynamic and sediment transport model provides spatial footprints of near-bed suspended sediment and sedimentation across the Hawke's Bay and Gisborne regions and, together with the remote sensing and field survey data, feeds into the model of seafloor disturbance impacts. The latter model enables the estimation of likely seafloor impacts across the entire region, highlighting the main areas of concern which may negatively impact fisheries.

Note that detailed sediment analysis from the samples collected in this project will be presented in an upcoming New Zealand Aquatic Environment and Biodiversity Report from the associated project SEA2022-13: Cyclone Gabrielle sediment analyses (Swales et al. in prep).

2.2 Remote sensing

To interpret spatial and temporal patterns in satellite coastal ocean observations it is useful to consider the timing of river stormflow during the Cyclone Gabrielle event, and the general seasonal patterns of river stormflow inputs into coastal regions. We used flow data from Wairoa River, the largest river in Hawke's Bay, obtained from the HBRC website (https://www.hbrc.govt.nz/environment/river-levels/). Similar patterns in the timing of peak flows were observed for other major rivers in Hawke's Bay and Gisborne (https://www.gdc.govt.nz/environment/maps-and-data/river-flows). Wairoa River flow data were plotted to identify the timing and duration of the acute phase of Cyclone Gabrielle, and flow data from 2009 to 2023 were plotted to visualise long-term seasonal trends.

Satellite data from NASA's Moderate Resolution Imaging Spectrometer on the Aqua satellite (MODIS-Aqua) provide a long-term (from mid-2002) foundation for observation of surface waters and capturing ever changing physical processes (e.g., Dickey et al. 2006, Gall et al. 2022). MODIS Aqua Level-2 (L2) datasets overlapping the New Zealand region were sourced via direct download (several daily overpass netcdf format files) from NASA's Ocean Biology Distributed Active Archive Center (OB.DAAC). Data

were processed from raw L1A sensor data to atmospherically corrected geophysical parameters (L2) on a 1000 m pixel scale, by National Aeronautics and Space Administration's (NASA) Ocean Biology Processing Group (OBPG), using processing version R2022.0 (SeaDAS l2gen software). L2 files were further processed to L3 spatially (500 × 500 m) and temporally aggregated (week, month, seasonal, and year) following the NIWA-SCENZ (Seas, Coasts, and Estuaries New Zealand) workflow (Gall et al. 2022). NIWA-SCENZ data version 5.0 differs from version 3.0 (Gall et al. 2022) in the source of L2 data, improvements in blending across clear open-ocean products and coastal turbid water products, and monthly interpolation and extrapolation of all products into coastlines (version 4.0, Pinkerton et al. 2023).

Satellite water observations at times are blocked by cloud cover, which impacts observational adequacy or representativeness in capturing natural variability and extremes during episodic and transient events. Nonetheless, signatures of events often remain in subsequent daily observations under cloud free conditions. We produced gap-free daily maps from a simple linear time interpolation method using the approximate function in the R *terra* package (Hijmans et al. 2022).

For this report, we have focused our analyses on the Hawke's Bay and Gisborne CMAs. The Hawke's Bay CMA covers 7246 km^2, equating to about 28 985 500 × 500 m pixels. The Gisborne CMA is comparatively smaller (5598 km^2 or 22 393 pixels). The Hawke's Bay CMA is shallower (mean water depth ~40 m) than the Gisborne CMA (mean water depth ~60 m) and has over twice as many shallow pixels at 10–30 m water depth than the Gisborne CMA (Figure 2). The Hawke's Bay CMA is also more sheltered due to the shape of its coastline, which together with a relatively shallow topography, is likely to result in the retention of fine suspended sediment.
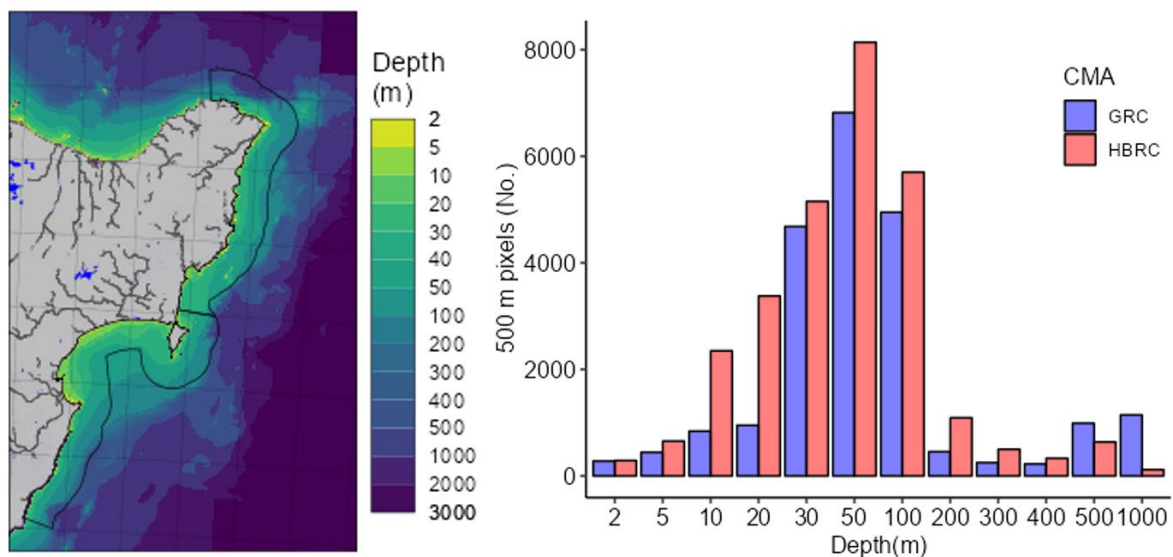
Figure 2: **Comparison of bathymetry in the HBRC and Gisborne District Council (GDC) CMAs. Depth bands are approximate and used to provide context to compare the number of satellite remote sensing pixels (500 × 500 m) at each depth band.**

Analyses of trends at the scale of CMAs provides an overview of trends at a relatively large scale but masks potentially different patterns that may occur at smaller scales, such as individual reefs or river mouths. While it is not possible to include analyses of remote sensing data across all areas of interest in this report, patterns can be visualised across a range of spatial and temporal scales by accessing the Cyclone Gabrielle Daily-SCENZ website via the NIWA-SCENZ portal, where daily observed and gap-free products from MODIS and OLCI sensors for the month of February 2023 are provided as web accessible layers for user interaction using the "project" tab (https://data-niwa.opendata.arcgis.com/documents/7454241f76b74f8891e3c55b8a78045c). Users can navigate and zoom in to regions of interest and overlay and compare products. Remote sensing products in localised

areas or regions of interest can be downloaded for more in-depth analyses in either Shiny-SCENZ or alternative software. Instructions on how to visualise data are included on the webpage.

The context of Cyclone Gabrielle over longer time scales can be explored and analysed on the Cyclone Gabrielle Trendy-SCENZ via the NIWA-SCENZ portal. An updated MODIS-Aqua data version 5.0 is provided in a reanalysis from mid-2002 to August 2023 and includes national scale water quality maps in time-step medians (week, month, season, and year) for analysing time series, climatologies (means), and anomalies (time series-climatologies). As with Daily-SCENZ, products in localised areas or regions of interest can be explored and data downloaded for more in-depth analyses at smaller spatial scales. In this report, we focus on monthly averages, which adequately describe seasonal patterns, interannual variability, and long-term trends against which the impact of the Cyclone Gabrielle event can be assessed.

Long-term trends from January 2002 to August 2023 were investigated to provide seasonal and interannual context for the Cyclone Gabrielle event. Satellite data were de-seasonalised using monthly anomalies to eliminate the influence of seasonal cycles on long-term change estimates. An alternative spline smooth method yielded nearly identical results (data not shown). Temporal trends for each pixel were determined using the Sen slope method (Sen 1968) applied to monthly anomalies. Statistical significance was evaluated using the Mann-Kendall Z statistic and p-values (Mann 1945, Kendall 1948). Correction for autocorrelation was made using the method of Yue & Wang (2004) to reduce the effective degrees of freedom, minimising type 1 errors while potentially increasing type 2 errors. The non-parametric Sen slope and Mann-Kendall test were chosen over linear regression for their distribution-free nature and independence from the assumption of normal data distribution. The insensitivity of the Sen slope to outliers makes it the preferred non-parametric method for estimating linear trends (Hipel & McLeod 1994). Trends are presented using percentage change per decade, aligning with the standardisation approach suggested by Larned et al. (2016).

We used the trend direction assessment procedures and guidelines of McBride et al. (2014) and McBride (2019) to categorise interannual trends into likelihood categories, indicating confidence in the correct direction (positive or negative) rather than merely distinguishing from zero (i.e., absence of trend; Table 1). Given the relatively short duration of satellite observations (typically around 40 years or less) and the high variability in natural systems, this approach offers a more meaningful way to assess trend significance than relying solely on Mann-Kendall p-values. For simplicity, the "Unlikely" category is used for all categories with p-values above 0.33 and probabilities less than 0.835.

Table 1: Comparison between trend likelihood categories determined from posterior probability distributions of slope direction (McBride et al. 2014, McBride 2019) with Mann-Kendal p-values and probability of non-zero slope.

Mann-Kendal p-value	Probability of non-zero slope	Trend likelihood
0 – 0.01	0.995 – 1	Virtually certain
0.01 – 0.05	0.975 – 0.995	Very likely
0.05 – 0.10	0.950 – 0.975	Likely
0.1 – 0.33	0.835 – 0.950	Possible
>0.33	<0.835	Unlikely

For the impact of Cyclone Gabrielle, our analyses included estimates of Total Suspended Solid concentration (TSS, g m^{-3}), Chlorophyll a concentration (CHL; mg m^{-3}), visual clarity (Horizontal VISibility distance of a black disk; HVIS, m), and the vertical visibility distance of a SECchi disk (SEC, m), diffuse light attenuation (K) of Photosynthetically Active Radiation (400–700 nm) with depth (KPAR, m^{-1}), and the intensity of light Energy reaching the seaBED (EBED, M m^{-2} d^{-1}) (see Appendix 1 for details of methods used to derive these metrics). In this report, we present data on the spatial and temporal extent of river plumes using TSS. We also show the extent of potential plume effects on visual predators (e.g., fish) using HVIS and on macroalgal primary producers (e.g., kelp) using EBED. Chlorophyll data are also shown as a proxy of surface primary productivity.

2.3   Research vessel surveys

2.3.1   *Study area and survey design*

The present study focused on offshore seabed ecosystems of the Hawke's Bay and Gisborne regions, from water depths of about 15 m (the shallowest depth that can be safely sampled using RV *Kaharoa*) and extending to the edge of the continental shelf. Two field surveys were conducted using RV *Kaharoa*. The first voyage was conducted on 2–20 June 2023 (KAH2303; referred to as 'June survey' hereafter) and the second voyage was conducted on 12–23 October 2023 (KAH2306; 'October survey').

The two RV *Kaharoa* surveys consisted of the following main components:

1. **Multibeam sonar mapping.** Several areas were mapped to fill gaps in the coverage of the RV *Ikatere* survey in April 2023 (see Section 2.3.2) to assess potential changes in seafloor topography following the cyclone. Several reefs were also mapped for the first time, and single pass multibeam transects were conducted to ensure safe and effective multicorer and towed camera deployments.

2. **Towed camera transects.** A towed camera system was deployed to obtain images and video of the seabed and assess potential impacts on the fauna and flora. Areas of rocky reefs and soft substrate were targeted across the two regions.

3. **Sediment coring.** Sediment core samples were obtained for analyses of sediment parameters and infauna.

A small beam trawl was also deployed during the June RV *Kaharoa* survey to obtain physical samples of seabed organisms; however, no sample was kept.

Target sites for the first RV *Kaharoa* survey in June were selected based on the following criteria:

1. Focus on areas of interest to Māori, stakeholders (e.g., councils), and/or commercial fisheries. We engaged with iwi, HBRC, Gisborne Regional Council (GDC), Ministry for Primary Industries (MPI)/Fisheries New Zealand, Department of Conservation (DOC), and local fishers.

2. Areas with pre-cyclone information (e.g., seabed topography, camera transects, sediment data). Conducting pre- and post-cyclone comparisons is more likely to yield meaningful insights into whether an ecosystem has been impacted by Cyclone Gabrielle than inferring impacts based on areas not sampled before the cyclone.

3. Areas in proximity to river mouths likely to have been impacted. We used existing information from earlier sediment dispersal studies offshore of the Waipaoa and Waiapu rivers and river sediment loads (Hicks & Shankar 2003) to identify which locations are most likely to have been influenced by sedimentation. Although the majority of the most impacted areas will be inshore, in some cases impacts may extend to the edge of the shelf due to the magnitude of expected riverine sediment inputs, coastal currents, and exposure to wave-resuspension events.

Significant Conservation Areas (SCAs) identified by HBRC (e.g., Lundquist et al. 2020) were targeted by the RV *Kaharoa* surveys. The surveys focused on the following SCAs extending beyond the shallow subtidal (from south to north): Aramoana-Blackhead Beach (SCA3), Clive Hard (SCA9), Pania Reef (SCA13), Wairoa Hard (SCA14), Portland Island (SCA17), and Long Point (SCA16) (Figure 3). These SCAs were surveyed using towed camera transects and multibeam mapping and sampled by coring. Areas previously sampled by camera tows/drops by DOC, HBRC, or NIWA were also identified as target sites for the RV *Kaharoa* surveys (i.e., Blackhead Point, Paoanui Point, Motuokura Reef, Wairoa Hard, Cape Kidnappers, Ariel Bank, and Table Cape; Funnell et al. 2005, Jones et al. 2018). Tangoio Reef and Lachlan Ridge in Hawke Bay were also identified as areas of interest, as they provide examples of shallow and deep reefs, respectively, which could potentially differ in their exposure to

cyclone-related sediment plumes. Tairāwhiti iwi and hapū indicated a number of inshore sites to target within their rohe, including reef features and areas where commercial fishing had ceased since Cyclone Gabrielle.

Coring was conducted along six inshore-offshore transects (T1–T6) that traverse depth and presumed sedimentation gradients across the shelf, along with a few additional targeted sites (Figure 3 and Figure 4). Three transects in Hawke Bay (T1–T3) capture variable benthic habitats, including sandy and muddy substrates of the broad continental shelf away from major rivers (i.e., Ngaruroro, Wairoa, and Nuhaka rivers). Locations span the zone of terrestrial and oceanic influence (Kuehl et al. 2016), straddling the "normal" sand-mud transition of wave-grading (Dunbar & Barrett 2005). In addition, locations adjacent to large riverine inputs and in depocentres (areas of maximum sediment deposition) traverse through the zone of stratified deposits, proposed from sediment studies in Poverty Bay and East Cape (T4 and T6; e.g., Kniskern et al. 2010, Rose & Kuehl 2010, Walsh et al. 2014). Placement of coring sites along Transect 4 off Poverty Bay was aligned with the location of coring sites sampled in 2010 during RV *Kaharoa* voyages KAH1006 and KAH1010 (Kniskern et al. 2014, Walsh et al. 2014). Sediment accumulations of more than one metre in thickness identified from bathymetric difference analyses around Pania Reef and Tangoio Reef were also targeted using the multicorer (see Section 2.3.3).

Sites sampled during the June RV *Kaharoa* survey (KAH2303) are listed in Appendix 2 and shown on Figure 3 and Figure 4. The weather was adverse throughout the majority of the survey period, with significant swell and high winds. Very poor inshore water visibility was experienced, particularly at inshore locations, reducing the number of CoastCam deployments that could be conducted. Some of the coring transects could not be completed due to the unfavourable conditions. Nevertheless, a total of 41 CoastCam deployments and 23 corer deployments were conducted across the Hawke's Bay and Gisborne regions. Some multibeam mapping was conducted in Hawke Bay during the first half of the voyage; however, a malfunction during the survey prevented mapping operations in the Gisborne region.

The second RV *Kaharoa* survey in October (KAH2306) followed a similar sampling approach as for the June survey. It provided the opportunity to re-visit sites from the first voyage that were not surveyed or sampled adequately due to adverse weather and water visibility conditions, re-visit sites sampled during the first voyage to monitor potential temporal changes, and sample additional sites (Appendix 2 and Figure 5 and Figure 6). Generally good weather conditions and improved underwater visibility enabled 43 CoastCam deployments and 11 corer deployments across the Hawke's Bay and Gisborne regions. Multibeam mapping mainly concentrated on a number of reef features in the Gisborne region.
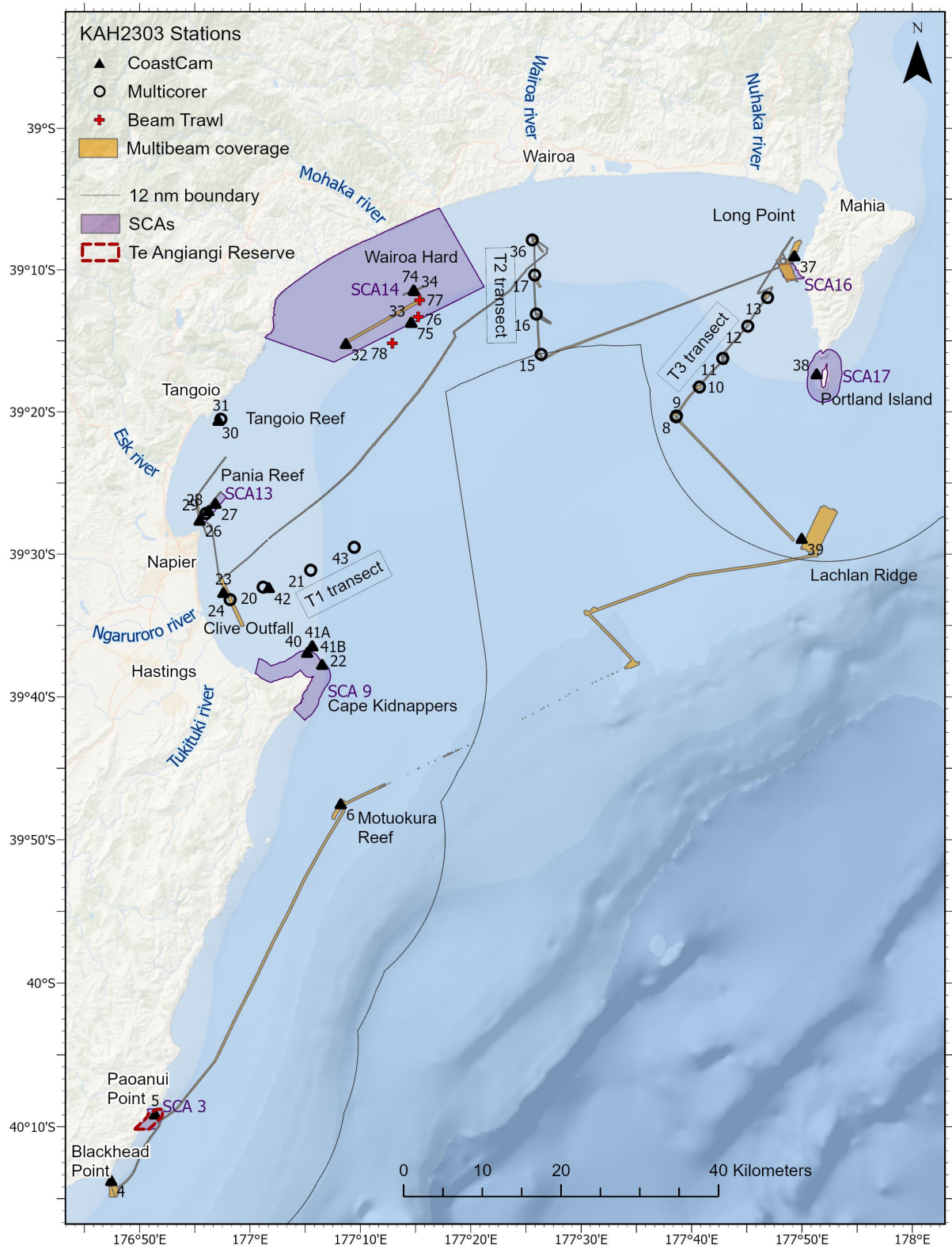
Figure 3: Location of Hawke's Bay sampling sites and multibeam coverage during June 2023 RV *Kaharoa* survey KAH2303. Numbers indicate station numbers (see Appendix 2). SCA, Significant Conservation Area; nm, nautical mile.

Figure 4: Location of Gisborne sampling sites during June 2023 RV *Kaharoa* survey KAH2303. Numbers indicate station numbers (see Appendix 2). Multibeam and camera transects surveyed in 2011 (RV *Tangaroa* voyage TAN1108; Jones et al. 2018) are shown. nm, nautical mile.
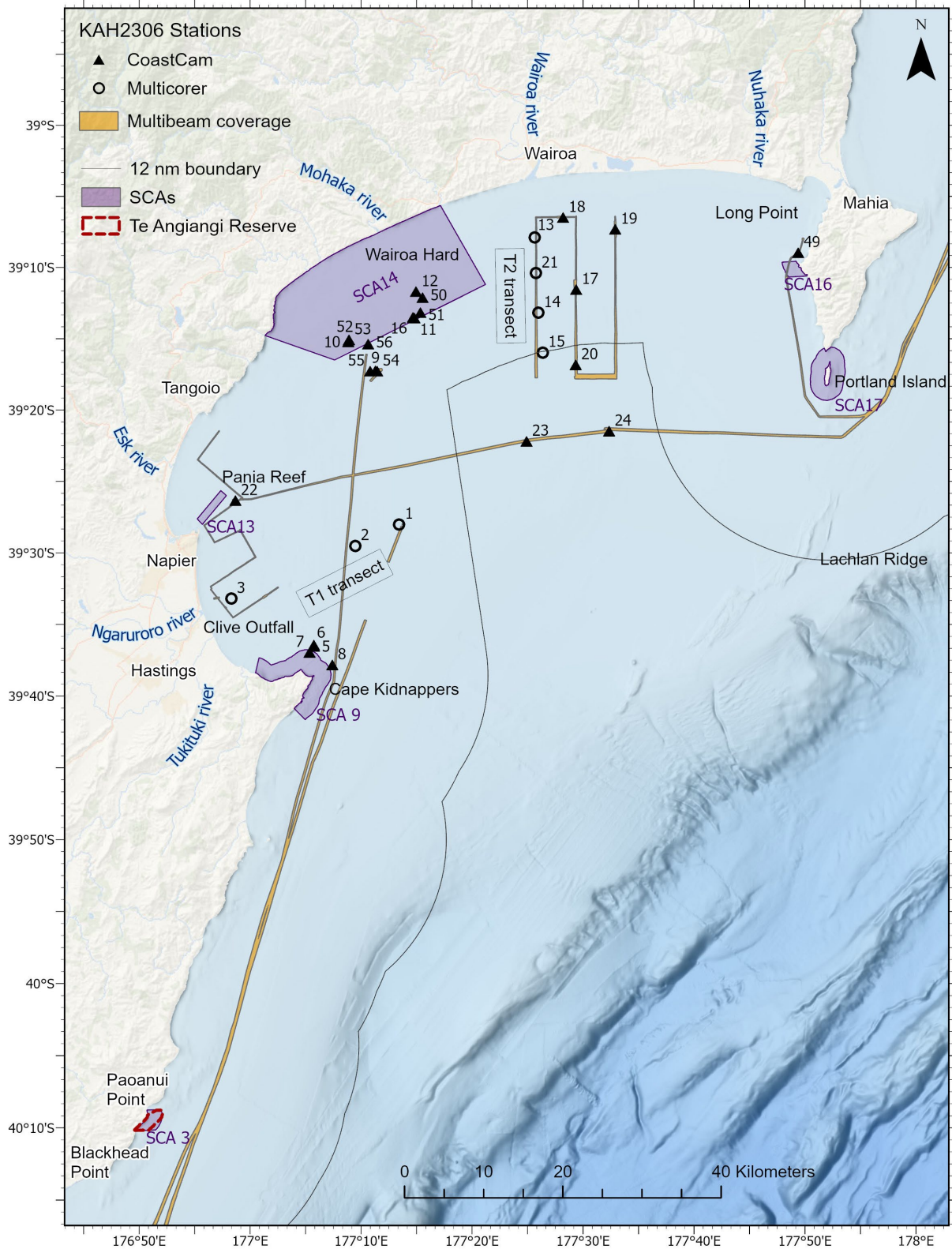
Figure 5: Location of Hawke's Bay sampling sites and multibeam coverage during October 2023 RV *Kaharoa* survey KAH2306. Numbers indicate station numbers (see Appendix 2). SCA, Significant Conservation Area; nm, nautical mile.

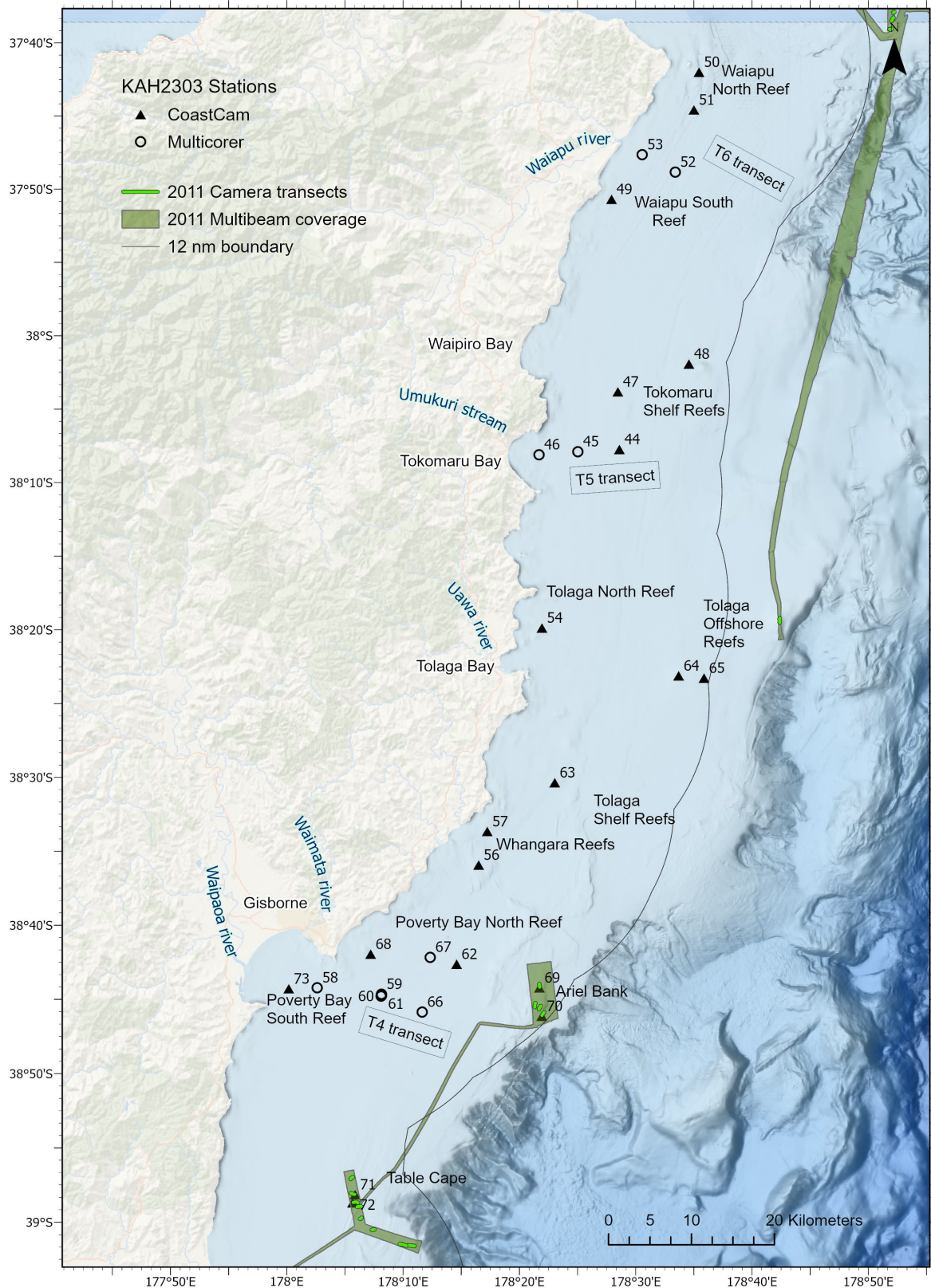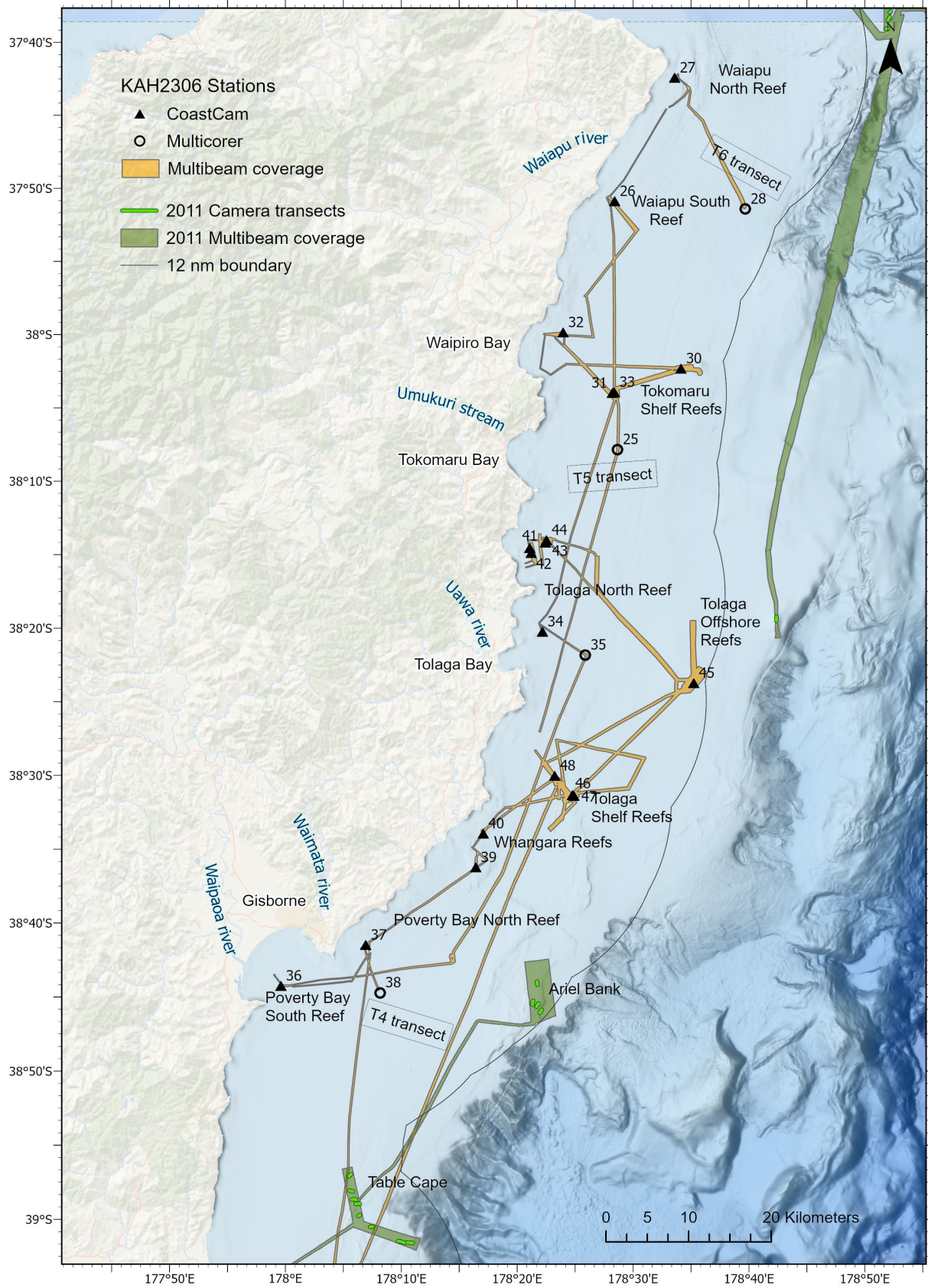**Figure 6:** Location of Gisborne sampling sites during October 2023 RV *Kaharoa* survey KAH2306. Numbers indicate station numbers (see Appendix 2). Multibeam and camera transects surveyed in 2011 (RV *Tangaroa* voyage TAN1108; Jones et al. 2018) are shown. nm, nautical mile.

2.3.2   Seafloor mapping

Initial survey data (IKA2303) were acquired between 18th April and 29th April 2023, encompassing Wairoa Hard, Clive Hard, Clive outfall, Pania Reef, and Tangoio Reef (Figure 7). These areas were the focus due to the presence of legacy multibeam data (from NIWA and LINZ surveys) with which to undertake change detection analysis (Table 2).
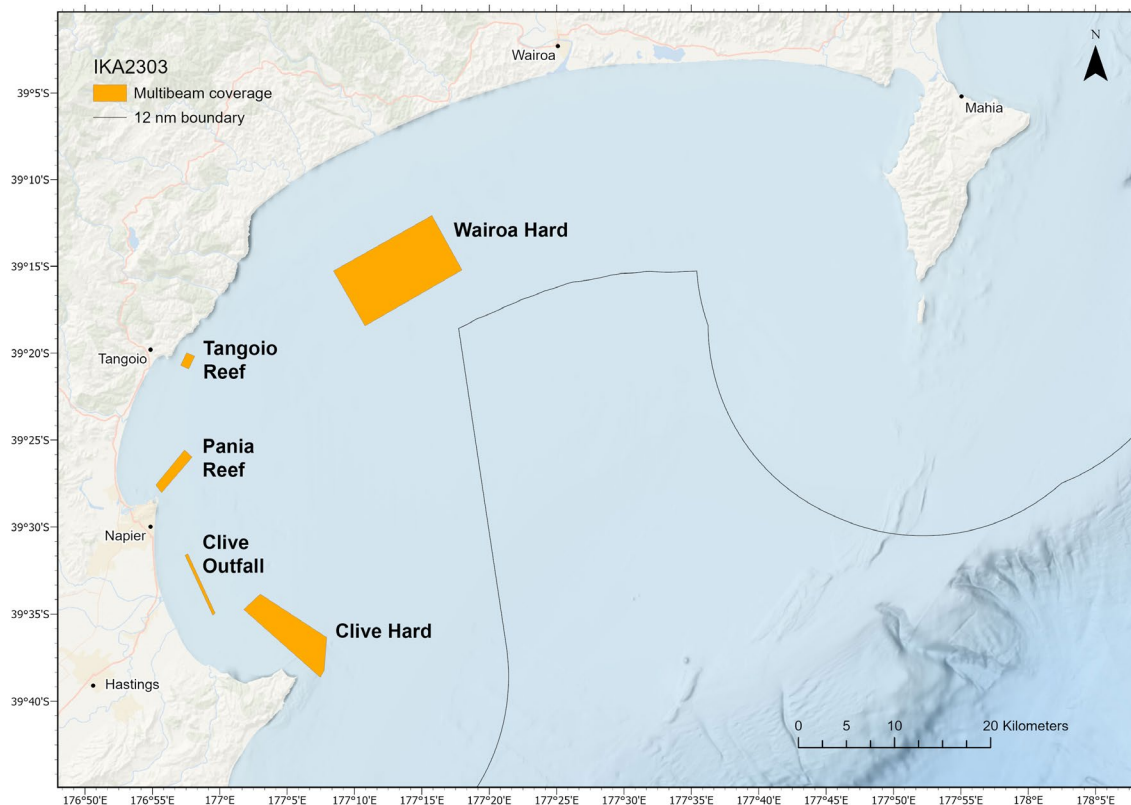
Figure 7:   **Map showing five areas of Hawke Bay covered during a multibeam mapping voyage using RV *Ikatere* in April 2023 prior to the beginning of this project. These five areas were targeted post-cyclone due to the existence of pre-cyclone multibeam data.**

Table 2:   **Legacy multibeam data in Hawke Bay.**

Area	Survey	Surveyor	Dates
Wairoa Hard	IKA18_Wairoa Hard	NIWA	13/04/2018–25/04/2018
Clive Hard	IKA19_Clive Hard	NIWA	11/06/2019–16/06/2019
Clive outfall	IKA2203_Hawkes Bay	NIWA	24/02/2022–27/02/2022
Pania Reef	HS68 Approaches to Napier	LINZ	21/05/2019–19/06/2019
Tangoio Reef	IKA2101_Hawkes Bay	NIWA	31/01/2021–04/02/2021

Additional multibeam data were obtained during the June and October 2023 RV *Kaharoa* surveys (KAH2303 and KAH2306, respectively). In the June survey, further mapping of Wairoa Hard and Clive Hard (Figure 3) was conducted to complement data obtained in April on IKA2303. Mapping was also conducted off Blackhead Point in the southern Hawke's Bay region, at Motuokura Reef, Lachlan Ridge (south of Mahia Peninsula), on the western coast of Mahia Peninsula in and around the Long Point Significant Conservation Area, and along the T2 and T3 coring transects. During the October survey, multibeam data were acquired at Poverty Bay, Whangara Reefs, Tolaga Shelf Reefs, Tolaga Offshore Reefs, Tolaga North Reef, Tokomaru Shelf Reefs, Waipiro Bay, Waiapu South Reef, and Waiapu North Reef (Figure 6).

The IKA2303 survey used a Kongsberg dual-head EM2040D 0.7° × 0.7° multibeam echosounder (MBES) operating at 200 and 300 kHz (depth dependent) with maximum beam angles of 75°/75°. The KAH2303 and KAH2306 surveys used a Kongsberg single-head EM2040 0.7° × 0.7° multibeam echosounder (MBES) operating 300 kHz with maximum beam angles of 75°/75°. Navigation was derived using Applanix Pos/MV GPS antennae, differentially corrected by a Fugro MarineStar XP Wide Area Differential GPS (WADGPS), with sub-metre accuracy. Sound velocity profiles (SVPs) were taken at the start of each survey block and periodically during each survey day.

Multibeam data obtained at Wairoa Hard, Clive Hard, Clive Outfall, Pania Reef, and Tangoio Reef were analysed and compared with pre-cyclone multibeam data to identify areas of sediment deposition and erosion. Data were processed using QPS Qimera v2.5.4 for bathymetry and QPS GeoCoder Toolbox (FMGT) v7.10.3 for seafloor backscatter. Data were corrected for tidal changes using NIWA's tidal model. Data were projected to NZTM projection and loaded into ArcGIS Pro for analysis.

2.3.3 Sediments

Sediment sampling was conducted using an Ocean Instruments MC-800A multicorer, a well-established system for reliably recovering intact sediment core samples (9.5 cm in diameter) that penetrate up to 70 cm depth into the seafloor and preserve the sediment-water interface (Figure 8). The corer comprised a hydraulically damped head-weight and core-tube carrier, with a triggered tube closure mechanism, with the tube top seal creating a vacuum-tight seal. The typical lack of sediment disturbance and deformation from the damped freefall makes the multicorer ideal for recovering benthic samples. The multicorer allows for the synchronous extraction of up to eight core tubes, allowing for some processing contingency and the choice of the best sample recoveries when operating in challenging conditions, e.g., rough sea states. The MC-800A multicorer is optimised for soft, muddy substrates rather than compact sand.

Core samples were collected for analyses of infauna (Section 2.3.4), sediment granulometry (particle size), organic matter content, isotopic analyses (bulk and compound-specific), and intact subcores for fine-scale sedimentary features (X-ray CT) (Table 3). Detailed methods used for the analyses of sediment parameters will be included as part of Swales et al. (in prep.).

Sediment samples were analysed for particle size using a Beckman Coulter LS 13 320 dual-wavelength laser particle sizer, which spans a size range 0.4–2000 μm, displayed as volume percent across 92 discrete size classes. For sandy or muddy samples, this method offers several advantages over traditional sieve stacks, including much improved efficiency, accuracy, resolution, and repeatability. Operational protocols followed well established laboratory procedures for heterogeneous marine sediments, with the exception of dispersal considerations. To achieve appropriate obscuration (a function of turbidity), approximately 0.5–1 cm^3 of sediment was initially dispersed in a 50 mL container with weak washing solution, sonicated in a bath for approximately 10 seconds, and then flushed through a 1.6 mm sieve into the laser sizer's sample bath containing approximately 1 L of 1 μm filtered tap water. Pre-sieving is required because any gravel-sized particles can block and damage the laser sizer plumbing and optical cell. Any visual estimates of the quantity and nature of the gravel components left on the sieve are recorded and a decision is made whether to also sieve the sample to measure the coarse fraction.

Raw results from the laser sizer were checked after each analysis to ensure correct instrument operation and exported into Excel for data manipulation and presentation. Any gravel fraction was added and normalised into the percentage size-class data. Granulometric analyses were achieved in Excel using GRADISTAT version 9.1 (Blott 2020 – after Blott & Pye 2001), which calculates the standard granulometric statistics, textural descriptions, and size fraction percentages. Size statistics are outputted using both arithmetic and graphic methods. Sediment textural descriptions follow the well-established guidelines of Udden (1914) and Wentworth (1922). To align with hydrographic definitions, "gravel" refers to all material >2 mm. As a nomenclature rule, size-class components need to be >5% by volume to be included as a textural modifier if appropriate, e.g., slightly sandy shelly mud. The clay fraction in

GRADISTAT is output as <2 µm and very fine silt is the 2–4 µm fraction. In more general applications the clay fraction is stated as <4 µm (Udden-Wentworth scale), and to that end dataset herein lists the clay fraction as <4 µm.

Total organic matter (TOM) for the less than 2 mm fraction of each sample was derived using a standard Loss on Ignition method (weight loss following combustion at 400 °C for 6 hours), and stable isotope analyses were conducted at NIWA's Sediment Laboratory, and Environmental and Ecological Stable Isotope Analytical Facility in Wellington.

Figure 8: **Multicorer deployed from RV *Kaharoa* to recover sediment cores during the post-Cyclone Gabrielle June survey (left). It can collect up to eight 70 cm long cores simultaneously (right top). Shuttles capturing the core samples are placed in racks for further processing (right bottom).**

Table 3: **Allocation of cores from a typical multicorer deployment and their treatment.**

Core Number	Sample type	Sediment core processing and subsampling protocols
1	Macrofauna	0–5, 5–10, 10–15 cm
2	Meiofauna and sediment archive	0–5 cm (subcore for meiofauna)
3	Sediment properties (particle size, total organic matter)	0–10 cm at 1 cm intervals; 10 cm to base at 2 cm intervals
4	Sediment samples for bulk and compound specific stable isotopes analyses	0–10 cm at 1 cm intervals; 10 cm to base at 2 cm intervals
5	Push-core of 6.7 cm diameter polypropylene for X-ray computed tomography (CT) scans	Entire core length
6–8	Spare	

2.3.4 Infauna

Samples for analyses of sediment fauna were obtained using the multicorer (Ocean Instruments MC-800A) during the June and October surveys. Macrofauna and meiofauna samples were collected from a total of 23 and 22 sites, respectively, during the June survey at 15–76 m water depth, mainly along the six coring transects and also at Pania Reef and Tangoio Reef in Hawke Bay (see Figure 3 and Figure 4). In the October survey, macrofauna and meiofauna samples were collected from 10 sites along the

coring transects, including sites sampled during the June survey and sites not previously sampled (15–146 m water depth) (Figure 5 and Figure 6). Macrofauna and meiofauna samples were also collected at a site offshore of Tolaga Bay. At each site (except Tangoio Reef sampled in June 2023 where no meiofauna sample was collected), one core was processed for macrofauna analysis and one core was processed for meiofauna analysis. Due to time constraints, meiofauna samples collected during the October survey were not processed.

Analyses focused on the top 5 cm of sediments because this is typically where the majority of infaunal organisms are found (Giere 2009). Meiofauna subcores were obtained using a cut-off syringe (29 mm internal diameter). The top 5 cm of sediment was preserved in 5% buffered formalin upon collection. In the laboratory, samples were sieved on a 63 μm mesh to retain meiofauna, which were then extracted from the sediments using the ludox flotation technique (Somerfield & Warwick 1996). Meiofauna were counted and identified to broad taxa (e.g., nematodes, copepods, kinorhynchs) using a dissecting microscope. The top 5 cm of each macrofauna core was sliced upon recovery and sieved using a 300 μm mesh at sea to retain the macrofauna. The macrofauna samples were immediately preserved in 5% buffered formalin. In the laboratory, samples were stained using Rose Bengal and fauna were counted and identified to broad taxa (e.g., polychaetes, amphipods, bivalves) under a dissecting microscope. Some crustacean (amphipods, cumaceans, and isopods) and mollusc taxa (gastropods and bivalves) from both June and October surveys were identified to the lowest taxonomic level possible (generally species or morphospecies) by taxonomists. Polychaetes sampled in the June Survey were also identified to the lowest taxonomic level possible. Time constraints prevented the identification of polychaetes to species/morphospecies from the October survey samples.

Pre-cyclone information on macrofauna communities was obtained by processing samples collected in May and September 2010 from the Poverty Bay area during RV *Kaharoa* surveys KAH1006 and KAH1010, respectively, conducted as part of the MARGINS Source-to-Sink project (9 sites from each survey; Table 4, Figure 9). The macrofauna cores were collected and processed using the same methods as the cores obtained in the June and October 2023 surveys (Walsh et al. 2014). These samples had been partially processed prior to this project; however, no counts or identification data have yet been obtained. As for the 2023 samples, fauna were counted and identified to broad taxa under a dissecting microscope and gastropod and bivalve molluscs were identified to the lowest taxonomic level possible by taxonomists. Time constraints prevented the more detailed identification of crustaceans and polychaetes from the 2010 samples.

Table 4: **Details of macrofauna core samples obtained in May (KAH1006) and September 2010 (KAH1010) from the Poverty Bay region which were used to provide pre-cyclone information.**

Survey	Station	Latitude °S	Longitude °E	Water depth (m)
KAH1006	203	38.7017	178.2069	50
	204	38.7322	178.1847	47
	206	38.7228	177.9842	18
	208	38.7717	178.0612	30
	209	38.786	178.0784	35
	210	38.7447	178.1344	35
	217	38.8084	178.0777	40
	232	38.7355	178.0416	25
	237	38.7491	178.0608	27
KAH1010	317	38.7345	178.0431	24
	318	38.7876	178.0839	35
	323	38.8237	178.1840	58
	329	38.746	178.1320	37
	332	38.7025	178.2066	50
	333	38.7318	178.1829	46
	334	38.8303	178.0699	42
	339	38.7185	177.9779	18
	352	38.7702	178.1172	36
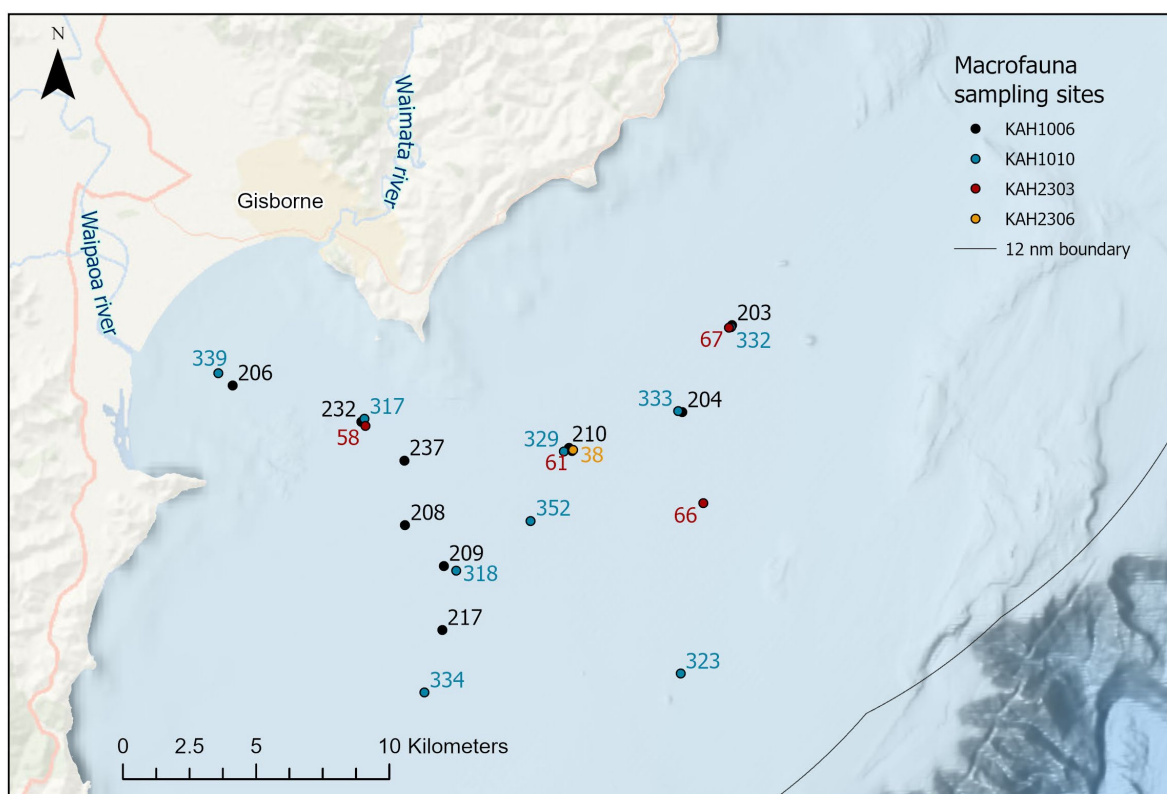
Figure 9: **Location of sites off Poverty Bay where macrofauna core samples were obtained in 2010 (RV *Kaharoa* surveys KAH1006 and KAH1010, black and blue filled circles, respectively) and 2023 (RV *Kaharoa* surveys KAH2303 and KAH2306, red and orange filled circles, respectively).**

When processing macrofauna cores from the June and October 2023 surveys, significant amounts of fine woody debris were retained on the 300 μm sieve along with the macrofauna organisms. This fine debris was removed using forceps under a dissecting microscope, air-dried in pre-weighed aluminium cups, then dried at 60 °C for 24 hours in an oven to determine the dry weight of this material in each macrofauna core sample.

For each macrofauna and meiofauna sample, we derived the following univariate metrics: total abundance (per core and per 0.01 m² area of seabed); species richness (i.e., total number of taxa per core); taxon evenness (Pielou's evenness index J′); and taxon diversity (Shannon diversity index H′10). The latter two metrics provide a measure of whether most taxa are present in similar densities or one or few taxa dominate the community. To investigate ecological patterns in these data we tested for correlations between univariate and multivariate community parameters and water depth, mud content, sediment total organic matter content, and sediment woody debris content at the corresponding sites (Appendix 3; see Section 2.3.3). No sediment data were available for the 2010 and October 2023 surveys, except for wood debris content data obtained from the macrofauna cores. Relationships between environmental parameters and community metrics were investigated using distance-based linear models (DistLMs) in PRIMER, a semi-parametric, permutation-based method that does not rely on the assumption of normally distributed data (Anderson et al. 2008). There was no strong correlation between predictor variables (i.e., no collinearity, $R^2 < 0.50$) (Quinn & Keough 2009). Similarity matrices of univariate response variables were built using Euclidean distance, whilst similarity of multivariate community data were built using the Bray-Curtis similarity measure (Anderson et al. 2008). Meiofauna abundance data were fourth root-transformed to decrease the influence of the highly abundant nematodes on multivariate analyses. Multivariate macrofauna abundance data were square root-transformed due to the more even distribution of taxa within the samples. P-values for individual predictor variables in marginal tests were obtained using 9999 permutations of raw data.

Macrofauna communities sampled before and after Cyclone Gabrielle off Poverty Bay were compared using data from the combined May and September 2010 surveys and 2023 surveys (see Table 4 and Figure 9). Both univariate and multivariate community structure were compared using a single factor (pre- vs. post-cyclone) permutational analysis of variance (PERMANOVA) in PRIMER v.7 (Clarke & Gorley 2015) with the PERMANOVA add-on (Anderson et al. 2008). Preliminary analyses showed a negative relationship between water depth and macrofauna abundance in both pre- and post-cyclone datasets; water depth was therefore included as a covariable in the analysis in order to control for this effect as part of the PERMANOVA (Anderson et al. 2008). Prior to analyses, the taxonomic resolution of the datasets was standardised by grouping crustacean and annelid species/morphospecies data in the June survey dataset, but leaving gastropod and bivalve mollusc species/morphospecies data which were available in both the 2010 and June 2023 datasets. A non-metric multi-dimensional scaling (nMDS) plot was used to visualise the relative dissimilarities between samples and treatment groups. As for the DistLM analyses, similarity matrices were built using the Bray-Curtis similarity measure of square root-transformed abundance data. The SIMPER routine in PRIMER was used to identify the taxa responsible for any significant differences in community structure between surveys uncovered in the PERMANOVA analysis.

Comparisons were conducted between a subset of sites where macrofauna samples were collected in both June and October 2023 surveys (7 sites from coring transects 1, 2, and 4) to describe potential temporal differences and recovery post Cyclone Gabrielle. Analyses were conducted as per the pre- and post-cyclone comparisons described above. Prior to analyses, the taxonomic resolution of the datasets was standardised by grouping annelid species/morphospecies data in the June survey dataset but leaving mollusc and crustacean species/morphospecies data which were available in both the June and October datasets.

2.3.5 Camera transects

A towed video camera system (CoastCam) was used to image the seafloor and its ecology (Figure 10, Figure 11, Figure 12). The system held two video cameras, one oriented down and the other facing slightly forward. Each had its own lighting and set of scaling lasers, and the camera feeds were sent to the surface in real time. The system was towed at 0.7–1.0 knots, with the track path logged with a GPS on board the survey vessel. Tow length ranged from a minimum target of 200 m, up to around 900 m, depending on the seafloor feature targets. During the October survey, a turbidity sensor (RBR Concerto logger equipped with a Seapoint TU sensor) was attached to the CoastCam to record high frequency measurements of turbidity (in nephelometer turbidity units, NTU) through the water column.

Wherever possible, the CoastCam was towed down depth profiles to best capture depth-related zonation patterns in the fauna and flora present, especially kelp which are heavily dependent on light levels. The forward angled camera feed was used to detect obstacles ahead of the system, with a remote-controlled winch used to raise and lower the system as needed. CoastCam was towed at a variable height above the seafloor depending on water visibility: in lower visibility conditions the unit was towed close to the seafloor, while in high visibility conditions the system was flown higher to provide a wider field of view (swept area). The upper limit was set by the need to retain sufficient fine resolution to identify taxa (nominally >2 cm in size).

Figure 10: The CoastCam system being deployed from RV *Kaharoa* during the October survey.
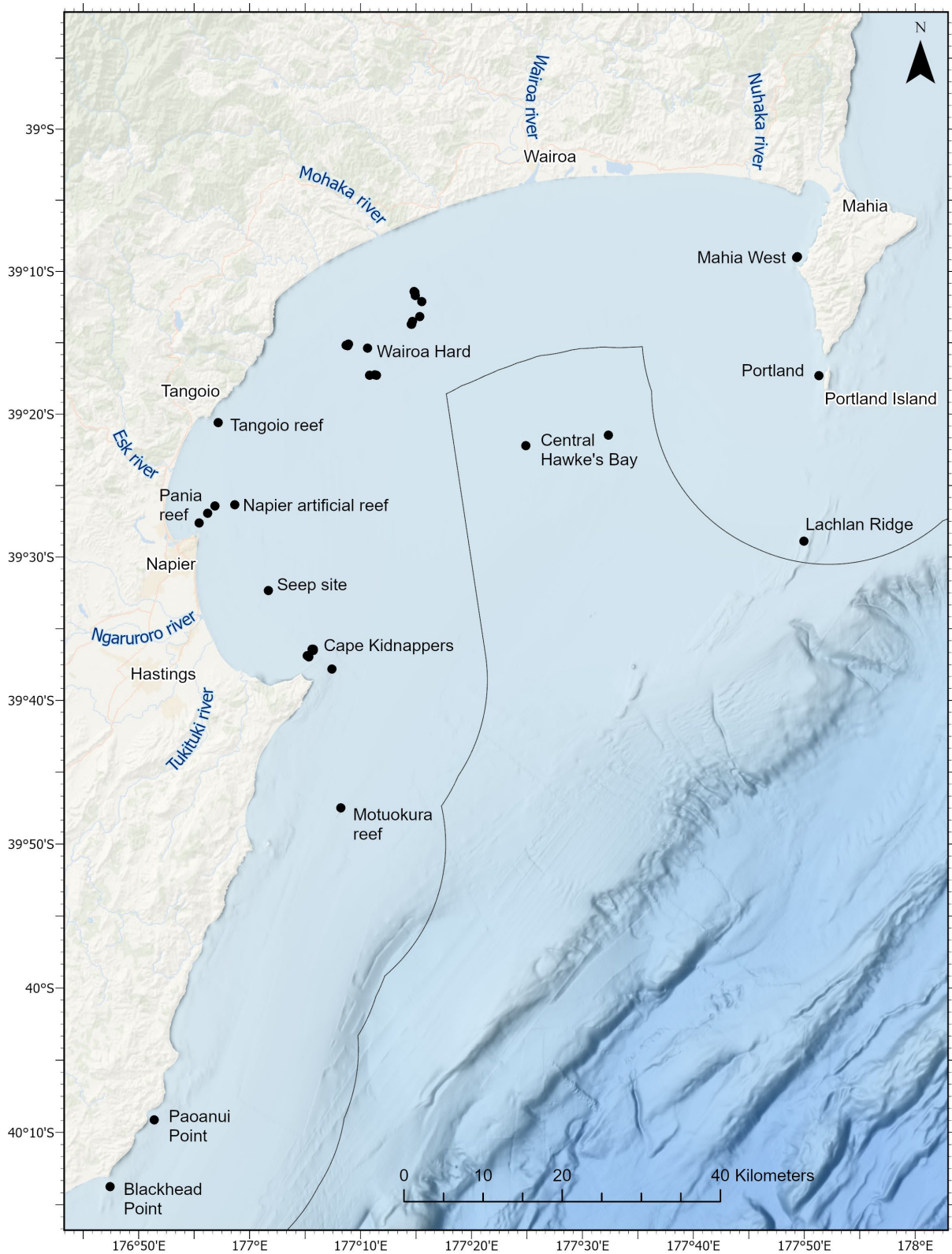
Figure 11: Location of CoastCam transects (black filled circles) conducted in June and October 2023 in Hawke Bay. Labels show names of features that were surveyed.
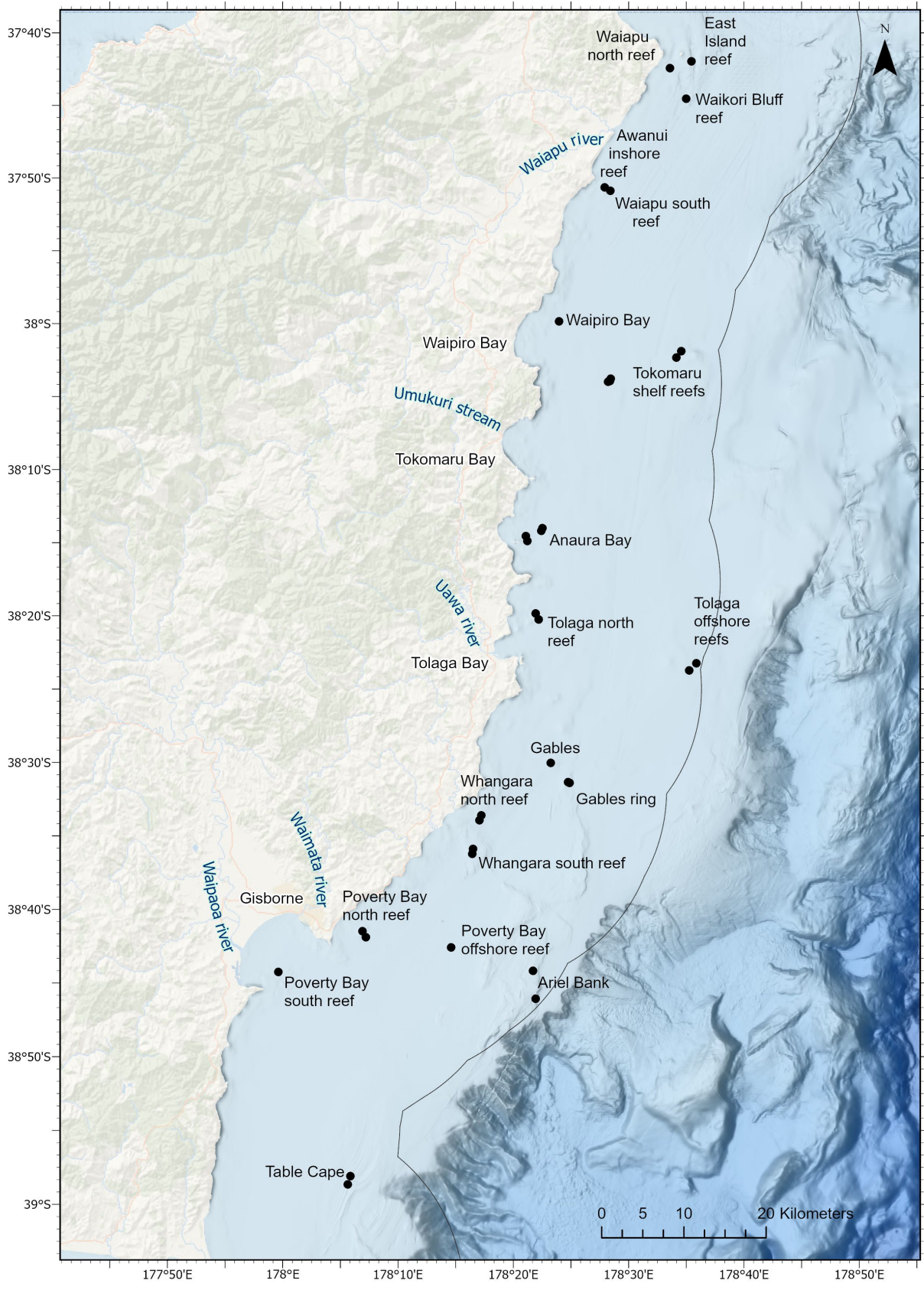
Figure 12: Location of CoastCam transects (black filled circles) conducted in June and October 2023 in the Gisborne region. Labels show names of features that were surveyed.

Following the first voyage, the video collected was viewed and screen grabs were taken of a range of taxa for identification by taxonomists. This information was used to create a list of taxa present in the video. The video processing software Ocean Floor Observation Protocol (OFOP) was used to spline the GPS records for each station to reduce the influence of GPS-error spikes. The video at each station was scored for the presence of the taxa identified, with the GPS track line used to assign each observation a spatial coordinate. Only larger discrete taxa were counted, where either an individual or a colony could be identified. Smaller encrusting and foliose taxa could not be counted but their presence and relative coverage were recorded.

Individual plants of common brown kelp *Ecklonia radiata* were counted and assigned to one of eight classes (new recruit no stalk, older recruit with stipe, adult plant holdfast only, adult plant stalk stipe, adult plant with rotting fronds, adult kelp plant with healed central thalli, adult plant healthy). Two of these classes were for new recruits, while adult plants were assigned a health class depending on damage seen (Figure 13). The proportions of these classes at a station were used to assess the health of the kelp forest/individuals.
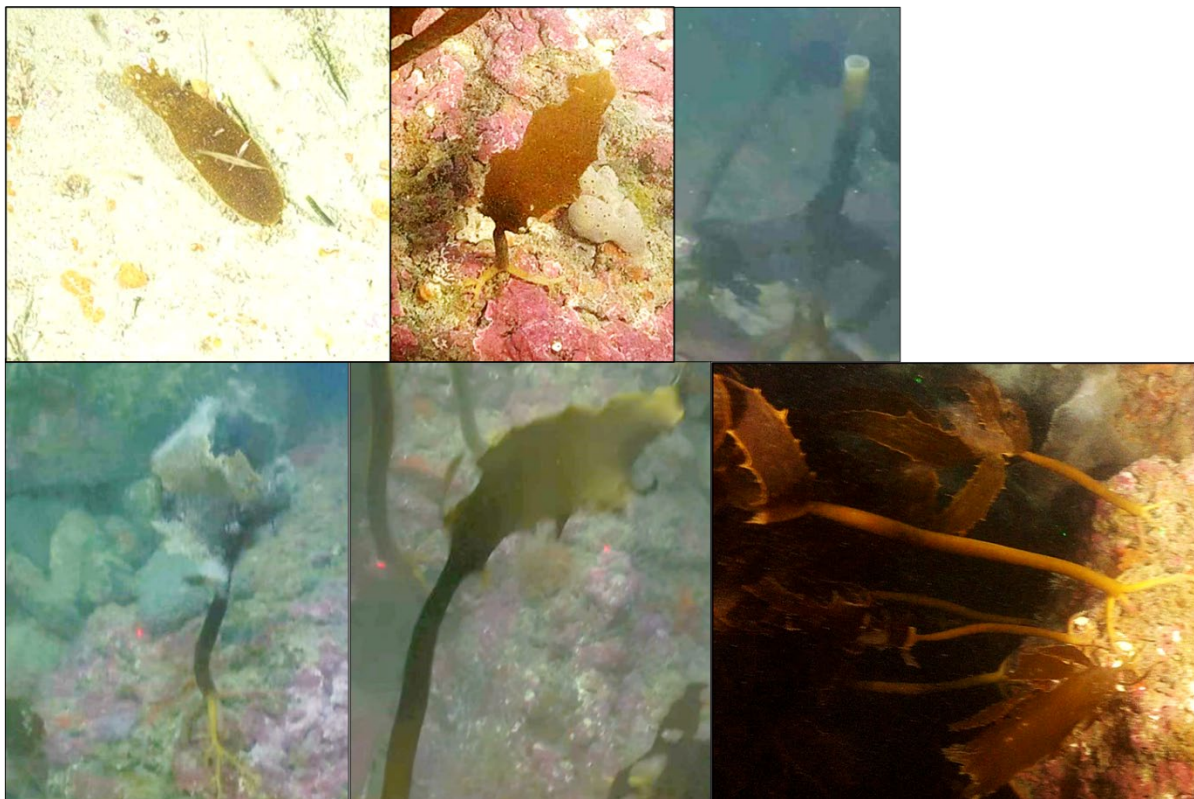
Figure 13: **Examples of kelp *Ecklonia radiata* health classes. From top left to lower right: new recruit no stalk, older recruit with stipe, adult plant stalk stipe, adult plant with rotting fronds, adult kelp plant with healed central thalli, adult plant healthy. Adult plant holdfast only health class is not shown.**

We focused our analyses on the following key taxa: *Ecklonia radiata*, finger sponges (all taxa combined), large sponges (>10 cm, all taxa combined), and glass sponges (one species only). These taxa were plotted as semi-quantitative data (counts per field of view) overlain on the multibeam sonar maps. In addition to these data, narratives describing key observations focusing on inshore sites and, in particular, inshore sites showing signs of potential sedimentation impacts, are provided. The narratives focus on taxa/observations that may indicate impacts of sediments on the reef assemblages, including:

- Macroalgae, including kelp (*Ecklonia radiata*), green algae (e.g., *Caulerpa* species), and red algae (including coralline algae)
- Three-dimensional mound, bowl, ridge, and finger sponges

- Black corals
- Mobile invertebrates and fish
- Spatial cover of low, grey-brown tubes on rock surfaces (possibly tube worms)
- Encrusting sponges and ascidians
- Low height epifaunal taxa, often as mixed assemblages (hydroids, soft bryozoans, calcified bryozoans, ascidians, brachiopods)
- Fine sediment dusting on sand ripple seafloor, small rock and cobbles, boulders, or bedrock
- Water clarity/turbidity.

The narratives focused on inshore areas in the vicinity of river mouths which are at higher risk of being impacted by sediments. Descriptions of offshore, clearly unimpacted sites are not included here.

2.4 Hydrodynamic and sediment transport modelling

2.4.1 Hydrodynamic model configuration

An implementation of the Regional Ocean Modelling System (ROMS), a free-surface, primitive equation hydrodynamic model (Haidvogel et al. 2008), was used to simulate the circulation in the Hawke's Bay and Gisborne regions for the period 1 January 2023 to 20 February 2023. The model grid spans the continental shelf of the eastern North Island of New Zealand extending from Cook Strait in the south to East Cape in the north (Figure 14). It has a horizontal resolution of ~2 km with 30 terrain-following depth levels. The model bathymetry was constructed from the following sources:

- the NIWA 250 m gridded bathymetry dataset
- a New Zealand land elevation digital terrain model at 200 m resolution,
- high-resolution coastline data from LINZ, and
- the General Bathymetric Chart of the Oceans (GEBCO; https://www.gebco.net/) gridded ocean bathymetry.

Figure 14: Model domain showing: a) bathymetry in metres and b) details of Hawke's Bay and Gisborne regions. The black dots represent rivers with annual mean discharge and cyan dots (named in right-hand panel) represent rivers with time-varying river discharge. The red diamond in right panel shows the location of the Hawke's Bay Water Quality information (HAWQi) buoy.

The model was initialised on 1 January 2023 with initial and open boundary conditions for the hydrodynamic variables (velocity, temperature, salinity, and sea surface height) derived from the

Operational Mercator global ocean analysis and forecast system[2]. This system, based on the "Nucleus for European Modelling of the Ocean" (NEMO, Madec et al. 2023), assimilates data from several sources, including satellite altimetry observations and satellite-measured surface temperature and vertical temperature and salinity profiles. The Mercator product used here provides daily mean fields of the 3-dimensional state of the global ocean on a 1/12° grid (~ 8 km).

The ROMS simulation was forced at the surface with heat, momentum, and freshwater fluxes derived from the New Zealand Convective Scale Model (NZCSM, Turner & Moore 2017). NZCSM covers all of New Zealand at a horizontal grid spacing of 1.5 km and provides hourly near-surface meteorology fields. Bulk formulae (Fairall et al. 1996) were used to compute freshwater momentum and heat fluxes from U and V wind momentum components, surface air temperature, air pressure, solar short- and long-wave radiation, and precipitation.

2.4.2 *Freshwater input*

The rivers draining into the ocean along the east coast of the North Island were represented in the model as point sources of freshwater. The input locations for each of the rivers were obtained from the New Zealand River Environment Classification (REC) (Biggs et al. 1990, Snelder et al. 2004) and then converted into model grid locations, with adjustments to ensure each freshwater input is located on the model's land-sea boundary.

An annual average discharge obtained from the REC was used for most rivers in the model domain. However, to simulate the impact of Cyclone Gabrielle on river plumes, time-varying river discharge was obtained for nine rivers along the Hawke's Bay and Gisborne coast. Daily river discharge for six rivers in Hawke's Bay and three rivers along the Gisborne coast were obtained for the period 1 January 2023–31 March 2023 from the Hawke's Bay Regional Council and the Gisborne District Council.

Data gaps exist in the daily discharge time series, but the portion of missing data tends to be small (<5%). The k-Nearest Neighbour (kNN) imputation algorithm which replaces missing values in a dataset with the weighted mean value from a number (k) of nearby data points, was used in order to get a complete time series for each of the nine time-varying rivers (Figure 15).

---

[2] https://data.marine.copernicus.eu/product/GLOBAL_ANALYSISFORECAST_PHY_001_024/description
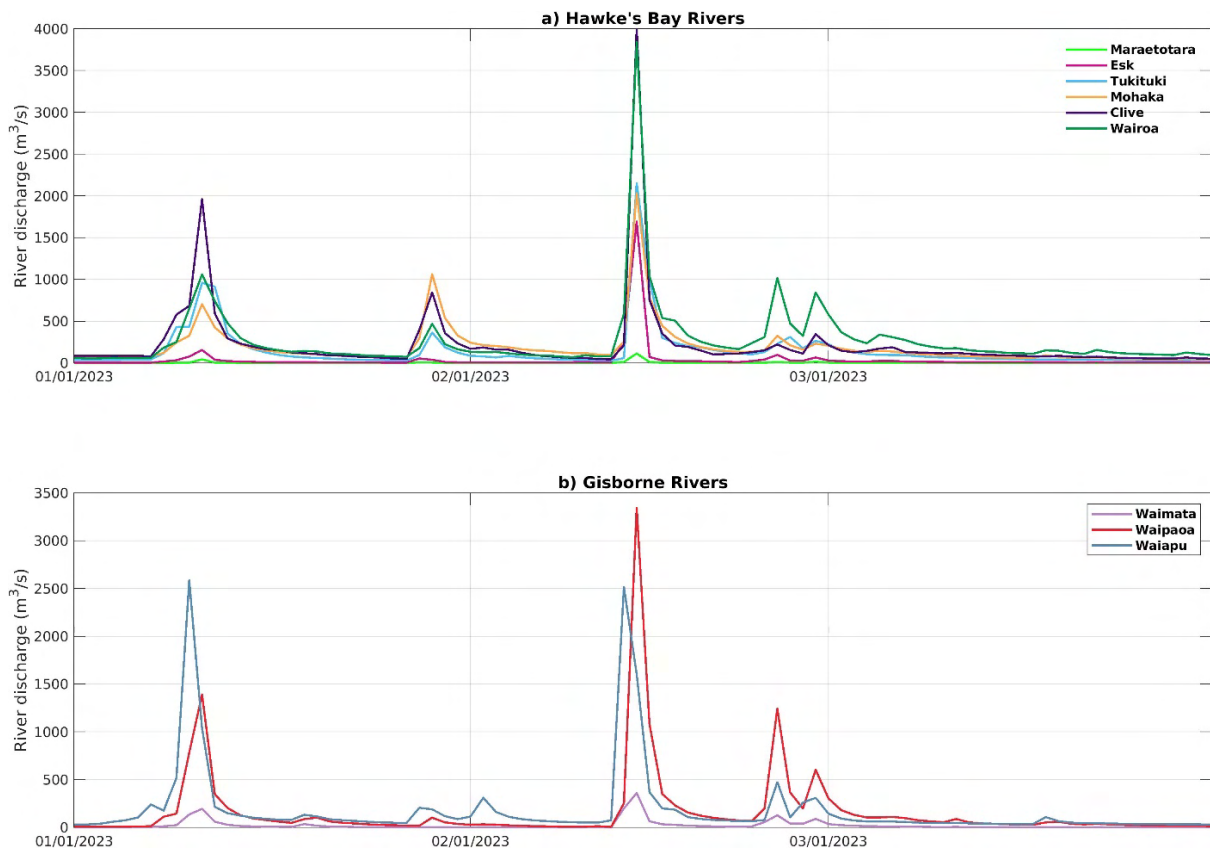
Figure 15: Time-varying river discharge for a) the six rivers discharging into Hawke Bay and b) the three rivers discharging along the Gisborne coast.

2.4.3 Dye tracer experiment

The passive tracer computational capabilities of ROMS were used to track the freshwater discharges from the nine rivers with time-varying discharge. To accomplish this, each river was tagged with a dye tracer (conservative passive tracer) which has a unit concentration (values ranging between 0 and 1) and represents the concentration of the corresponding river freshwater, i.e., if the dye has a value of 1 it means the water parcel is purely river water; if it has a value of 0 it means the water parcel contains no freshwater from that river. At the open boundaries, the dyes were nudged to the ocean water (dye is equal to zero) in the same manner as temperature and salinity.

2.4.4 Sediment model

The sediment model of Warner et al. (2008) was used to estimate the dispersal of riverine sediments and sediments resuspended off the ocean floor. The sediment model estimates sediment concentrations fractionated between different size classes. There were 4 size classes which represented sediments initialised in the seabed layer and 3 size classes which represented sediments coming into the domain from the rivers (Table 5).

Each size class was given properties such as median grain size, grain density, porosity (when in the sediment bed), settling velocity (when in suspension), and critical bed shear stress for erosion. These values were sourced from an existing model of the Hawke's Bay region (Moriarty et al. 2015) and are summarised in Table 5. Initial suspended sediment concentrations and lateral boundary and atmospheric boundary fluxes of sediments were set to zero.

Table 5:   Parameters used in the sediment model.

	Source	Diameter (mm)	Density (kg m^{-3})	Settling velocity (m/s)	Critical shear (N m^2)	Porosity (non-dimensional)
Class 1	Seabed	0.063	2 650	0.1	0.15	0.6
Class 2	Seabed	0.5	2 650	0.5	0.15	0.6
Class 3	Seabed	1.0	2 650	125	0.15	0.6
Class 4	Seabed	0.0126	2 650	0.15	0.15	0.6
Class 5	River	0.022	2 650	0.3	0.15	0.6
Class 6	River	0.03	2 650	0.5	0.15	0.6
Class 7	River	0.04	2 650	1.0	0.15	0.6

The model included a representation of the bottom sediment bed, including the process of sediment resuspension and deposition. In this bedform model there were eight vertical layers, and each layer comprised the seven sediment classes. The top bed layer exchanged sediments vertically with the lowest level in the water column and horizontally with its immediate neighbours (a process called bedload transport). The thickness of the bed layers was adjusted at each model time step according to the scheme described by Warner et al. (2008).

All seabed layers were initialised with sediments from sediment classes 1–3, distributed as 54% from class 1, 36% from class 2, and 10% from class 3. These percentages were calculated using an average of the initial sediment fraction used by Moriarty et al. (2015). Bottom stress was calculated with the Sherwood, Signell, and Warner bottom boundary layer formulation (Warner et al. 2008). This formulation requires data on the height, period, and direction of surface wind waves which was sourced from the NZWAVE wave forecasting model (http://EcoConnect.niwa.co.nz/).

2.4.5   River sediment concentrations

River suspended sediment yields for the nine rivers were estimated by developing rating curves between river discharge (Q) and suspended sediment concentration (SSC) or a proxy such as turbidity. Turbidity data for all nine rivers were obtained from Land, Air, Water Aotearoa (LAWA; https://www.lawa.org.nz/download-data/#river-water-quality) for the period 2004–2021. In addition, suspended sediment concentrations were also available for the Waipaoa River for the period 1950–2012 (Hicks et al. 2000). The available datasets did not contain many large riverine flow events such as those seen during Cyclone Gabrielle, and the errors associated with this large-scale event are unknown. Model experiments showed that these rating curves produced unrealistically large sediment depositions and the sediments coming in from the rivers were reduced by a factor of 100 to obtain realistic flows.

In keeping with international literature (e.g., see review by Hicks & Gomez 2016), a simple two-parameter 'power law' sediment rating curve model was adopted. The sediment rating curve model, SSC = aQ^b, was fitted to concurrent measurements of log-transformed SSC/turbidity and Q for each river. The model parameters a and b were estimated by fitting a traditional linear regression as well as a second order polynomial to the log-transformed data. The correlation coefficients for the linear regression and second order polynomial calculated for each of the nine rivers were very similar (R = 0.3–0.8) and thus the linear regression method was adopted. Where possible, the sediment yields calculated for the model period (1 January 2023–31 March 2023) were compared against observational data.

2.4.6   Model evaluation

The modelled hydrodynamics were assessed against satellite derived sea surface temperature and in situ temperature and salinity from a mooring in Hawke Bay. To ensure that the sediment model gives a realistic representation of the sediment dynamics in Hawke Bay and along the Gisborne coast, modelled surface sediment concentrations were compared against satellite derived total suspended material concentrations derived from the Ocean and Land Colour Instrument (OLCI) L2 datasets. OLCI L2 datasets overlapping the east coast region were directly downloaded from the European Organisation for the Exploitation of Meteorological Satellites (EUMETSAT) using the EUMETSAT Data Access

Client (EUMDAC). OLCI Level-2 Water Full Resolution (OL_2_WFR) 300 m pixels are in separate netcdf files from Sentinel-A and Sentinel-B overpasses. They contain a range of products, including a Neural Network atmospheric correction over coastal waters (Schroeder et al. 2022) for more accurate determination of products in turbid coastal waters (e.g., Total Suspended Matter (TSM, g m^{-3}). Reprojection (from satellite view to ground coordinates), subsetting (for products, masks, and east coast region of interest), and writing (netcdf files) were batch processed using the SeNtinel Applications Platform (SNAP 9.0.0). R software (RStudio Team 2022) was used to mosaic into daily products and mask extreme values. This identified the majority of cloud edge and shadow pixel and improved data near coastlines often excluded in SNAP cloud edge masking where coastline pixels are often misidentified as clouds.

The spatial variability of the modelled sea surface temperature (SST) for the model period was compared with the Multi-scale Ultra-high Resolution (MUR) SST dataset produced by the Group for High Resolution Sea Surface Temperature (GHRSST; https://podaac.jpl.nasa.gov/GHRSST?tab=mission-objectives&sections=about%2Bdata). This dataset uses a Multi-Resolution Variational Analysis (MRVA) method to produce daily, gap-free gridded SST estimates from the 1 km MODIS SST observations combined with Advanced Very-High-Resolution Radiometer (AVHRR), microwave, and in-situ SST (Chin et al. 2017).

Temperature and salinity from the HAWQi water quality buoy were obtained from the Hawke's Bay Regional Council (location shown in Figure 14). The HAWQi water quality buoy collects continuous temperature and conductivity measurements at four depths (0.5 m, 5 m, 10 m, 15 m). These data, available intermittently for the model period, were used to assess the model's ability to reproduce the observed temperature and salinity in Hawke Bay.

The skill of the model was assessed against the observational and satellite-derived data through statistical techniques such as the Pearson correlation coefficient and root-mean-square differences (RMSD). The RMSD and Pearson correlation coefficient were calculated using daily temperature and salinity data as follows:

$$RMSD = \left[\frac{1}{N} \sum (M - O)^2 \right]^{\frac{1}{2}}$$

$$Corr = \frac{1}{N} \sum \frac{(M - \mu_m)(O - \mu_O)}{\sigma_M \sigma_O}$$

where M and O are modelled and observed values of the variable, μ_m, μ_O, σ_M, σ_O are the averages and standard deviations and N is the number of data points.

The model skill was further assessed using the statistical method developed by Willmott (1981):

$$WS = 1 - \frac{\langle (M - O)^2 \rangle}{\langle (|M - \langle O \rangle| + |O - \langle O \rangle|)^2 \rangle}$$

where angle brackets denote the time average and vertical bars denote absolute values. The Willmott skill parameter is a simple measure of the agreement between two datasets with WS = 1 denoting a perfect match and WS = 0 denoting complete disagreement.

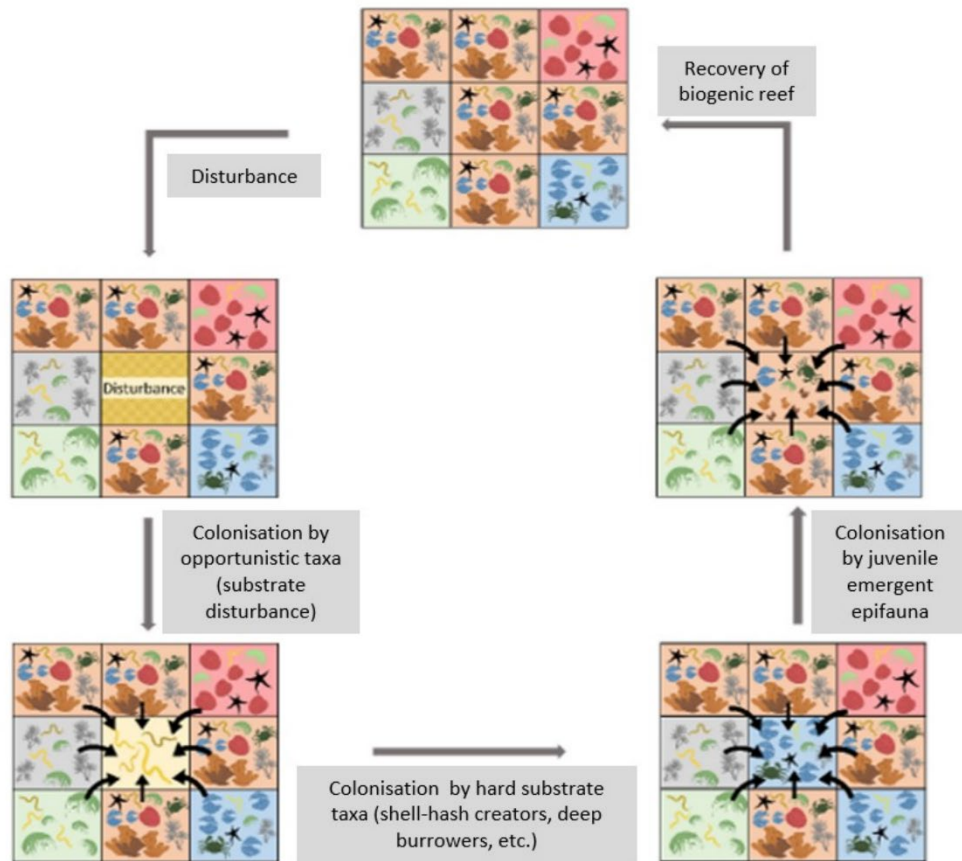## 2.4 Seafloor disturbance and recovery model

2.5.1 Seafloor model background

An existing model of seafloor disturbance and recovery dynamics (hereafter the 'Seafloor model') was adapted to explore the impacts of cyclone disturbance on seafloor communities (Lundquist et al. 2022a, 2022b, 2023). The Seafloor model was initially developed through funding to NIWA (Fisheries Ecosystem Effects, FRST Project C01X0212) (Thrush et al. 2005); further development has been funded by NIWA SSIF (Lundquist et al. 2010), Fisheries New Zealand (Project ZBD2009-25; Lundquist et al. 2013), and the Sustainable Seas National Science Challenge (Stephenson et al. 2019, Lundquist et al. 2022a, 2022b, 2023). The most recent application in the Hawke's Bay was funded by the Sustainable Seas National Science Challenge (MBIE Project no. C01X1901) with in-kind funding provided by Hawke's Bay Regional Council through its support of the Hawke's Bay Marine and Coastal Group. The Hawke's Bay case study explored responses of seafloor invertebrate communities to both bottom fishing impacts and land-based sediment inputs—and modelled scenarios that were developed by a participatory exercise with the Hawke's Bay Marine and Coastal Group (Lundquist et al. 2022a, 2022b, 2023).

The Seafloor model was developed to improve understanding of the scale and magnitude of the impact of different stressors on seafloor community dynamics, including both natural and human-induced disturbances that cause ecological responses at different spatial and temporal scales. Models such as the Seafloor model are often used to explore ecosystem responses under possible future scenarios when it is too difficult or too expensive to empirically test these scenarios at relevant temporal and spatial scales to inform decision-making. While models include many assumptions and are typically simplistic representations of complex systems, they can be useful in facilitating understanding of ecosystem dynamics under different management scenarios.

2.5.2 Seafloor model configuration

The Seafloor model is a spatially explicit model of seafloor benthic invertebrate community dynamics, coded in Matlab programing software. The model explores how the spatial extent and temporal frequency of seafloor disturbances impact on the dynamics of invertebrate seafloor communities. The model can explore scenarios to determine potential impacts and recovery due to bottom fishing (Lundquist et al. 2010, 2013) and sediment stressors on benthic invertebrate communities (Lundquist et al. 2022a). The model can be visualised as a grid of individual cells, each representing a patch of seafloor and the benthic invertebrates living within it (Figure 16). The model includes eight functional groups (FGs) of seafloor invertebrates that are commonly found in soft sediment seafloor ecosystems (Table 6). These eight groups were determined at expert workshops of NIWA inshore and offshore marine benthic ecologists as part of project ZBD2009-25 (Lundquist et al. 2013); individual species can be allocated to functional groups based on clusters of invertebrate functional traits (e.g., size, feeding modality, colonisation time, position in sediment). A representative life history for each group (i.e., age of reproductive maturity, post settlement or adult dispersal from source cell, reproductive seasonality, maximum lifespan) was determined by expert opinion along with published studies on representative taxa for each group, where available (Lundquist et al. 2013). The focal group for the Sustainable Seas Hawke's Bay case study was FG6, which includes epifaunal invertebrates that create biogenic habitat-structure such as sponge gardens and bryozoan reefs.

Figure 16: Visual depiction of the disturbance and recovery cycle and the eight functional groups of the Seafloor model. Each functional group is colour coded to show the transition from a disturbed community (yellow cells) dominated by opportunistic functional groups through colonisation, growth, and ageing to a mature community dominated by epifaunal biogenic-structure forming invertebrates (orange cells). Adapted from Lundquist et al. (2023).

Table 6: General description of invertebrate fauna classified under eight conceptual functional groups (FGs) for the Seafloor model based on key functional traits and life history characteristics. Adapted from Lundquist et al. (2013)

Functional group	Description	Typical taxa
FG 1	Opportunistic early colonists – limited substrate disturbance	Sedentary species (e.g., paraonid and spionid polychaetes)
FG 2	Opportunistic early colonists – considerable substrate disturbance	Mobile deposit feeders and small scavengers (e.g., phoxocephalid amphipods and other small crustaceans)
FG 3	Substrate stabilisers (tube-mat formers)	Tube-mat forming polychaetes (e.g., spionid, sabellid, and chaetopterid polychaetes) and tube-building amphipods (e.g., *Ampelisca* sp.)
FG 4	Substrate destabilisers	Spatangoid echinoids (e.g., *Echinocardium* sp.), holothurians, ophiuroids (e.g., *Amphiura* sp.)
FG 5	Shell hash-creating species	Bivalves, gastropods
FG 6	Late colonisers – emergent epifauna	Sponges, bryozoans, sea pens, sea whips, ascidians, gorgonians – primarily sedentary suspension feeders
FG 7	Late colonisers – burrowers	Shrimps, crabs, large burrowing polychaetes
FG 8	Predators and scavengers	starfish, crabs, hermit crabs, large-bodied predatory worms

At each time step in the model (seasonal, four time steps per year), disturbance events (e.g., bottom fishing, sedimentation), as well as natural ecological processes (e.g., growth, natural mortality, reproduction, predation, competition) occur in each cell (Figure 17). Dispersal between cells is restricted to larval recruits, and the potential dispersal distance into adjacent cells is parameterised based on empirically estimated distances for each of the eight functional groups (parameterisation described by Lundquist et al. 2013). The response to disturbance events (bottom fishing, sedimentation) of each of the eight FGs is based on empirically derived data representing the likelihood of mortality relative to the frequency or intensity of that stressor. Fishing responses are parameterised from data on global reviews of bottom fishing impacts (Sciberras et al. 2018), and sediment responses are parameterised from a compilation of empirical and laboratory data for New Zealand soft sediment invertebrates (Lundquist et al. 2022a, R. Bulmer pers. com).
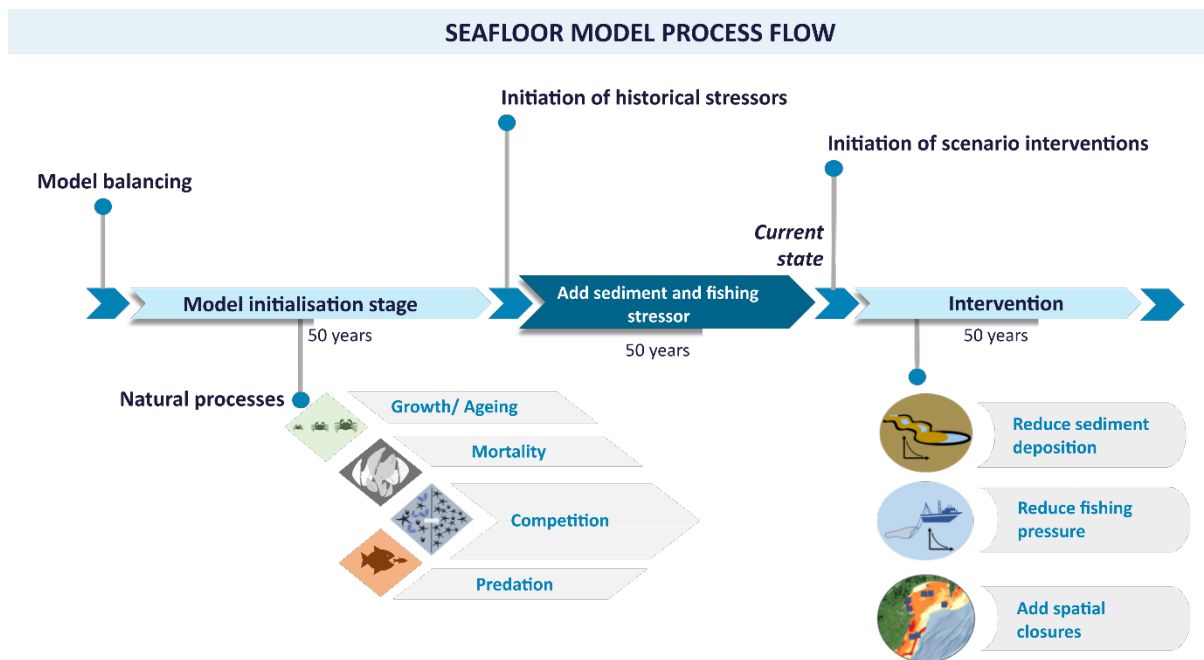
SEAFLOOR MODEL PROCESS FLOW

Initiation of historical stressors

Initiation of scenario interventions

Model balancing

Current state

Model initialisation stage — 50 years

Add sediment and fishing stressor — 50 years

Intervention — 50 years

Natural processes

Growth/ Ageing

Mortality

Competition

Predation

Reduce sediment deposition

Reduce fishing pressure

Add spatial closures

Figure 17: **Flowchart illustrating model flow and processes applied during a model scenario. Adapted from Lundquist et al. (2022a).**

2.5.3   *Sustainable Seas Hawke's Bay scenarios*

The objective of the Hawke's Bay modelling exercise was to explore potential management actions with regard to restoring the seafloor ecosystems in the bay, particularly those seafloor ecosystems represented by organisms creating habitat structure. The model was initialised for 200 time steps (50 years) without stressors, followed by a period of 50 years run with historical stressors to create a 'baseline' state, after which different scenarios were run to illustrate the potential changes following management interventions (Figure 17). The Hawke's Bay Marine and Coastal Group developed three scenarios (and a business-as-usual scenario) that included different combinations of mitigation of sediment inputs from land-based sources, reductions in fishing effort, and implementation of spatial closures (Lundquist et al. 2022a). Scenarios were co-developed through a participatory process and used to explore flow-on impacts of different management interventions on the broader social-ecological system (Connolly et al. 2020, 2022, Lundquist et al. 2022b).

A spatial layer representing grain size (percent mud content) on the seafloor surface was developed from datasets compiled for the Hawke's Bay marine and coastal review (Haggitt & Wade 2016) representing abiotic habitats (mud, sand, etc.) (Figure 18). Haggitt & Wade (2016) provided a map showcasing anecdotal distributions of abiotic habitats represented by sediment types. This map was converted into values representing the percent mud content at the seafloor using empirical data from point records of sediment grain size and multi-beam surveys from a variety of Hawke's Bay Regional Council sources (see Lundquist et al. 2022a for full list and map of point records).

Fisheries data were provided by Fisheries New Zealand and represented an annual average fishing footprint (converted from number of trawls per 25 km^2 to match model grid cell resolution; Figure 18). Differences in the footprint between 2007/08 and 2018/19 were explored, with analyses showing a reasonably consistent spatial footprint, and variation from -19.1% to 15.6% around the mean of aggregated swept area, -17.7% to 16.0% around the mean of annual number of trawls, and -15.3% to 11.4% around the mean of the annual footprint (Lundquist et al. 2022a); thus, the annual average footprint was deemed representative of historical fishing effort.

Existing spatial closures (e.g., Clive Hard, Mahia Peninsula, Wairoa Hard, Te Angiangi Marine Reserve) were determined to be adequately represented as closed areas within the fishing footprint, as

trawl counts were typically zero within these areas. Other seasonal spatial closures or voluntary fisheries closures were not included as closed areas, as these areas still experienced significant bottom fishing during some parts of the year. Fishing effort was modelled as the total number of vessels in the region, each allocated a total number of fishing events per time step; fishing events were distributed stochastically based on the spatial fishing footprint.
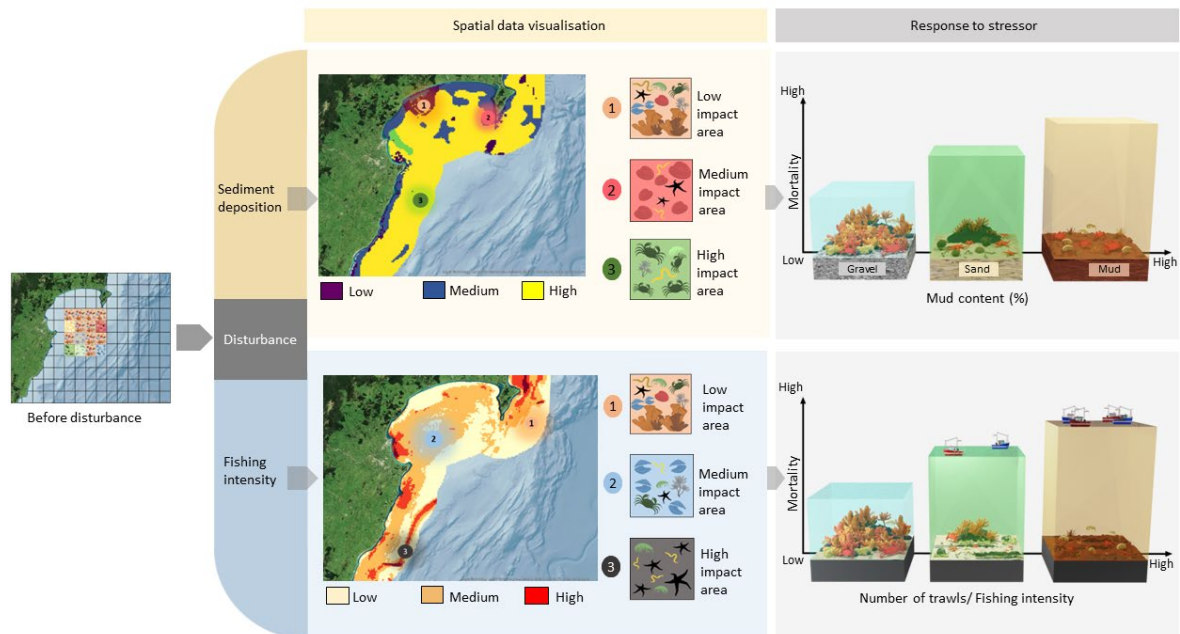

Figure 18: **Visual representation of spatial stressor layers and the relative change in seafloor invertebrate community assemblages across stressor gradients.**

Changes in sediment stressors in scenarios were implemented as a percent change per year for a set number of years; for example, expected reductions in sediment should catchment fencing and vegetation planting occur. Sediment inputs were modelled simply in this prior exercise, with any change in sediment inputs represented by an equally distributed change in sediment mud content throughout the model region. However, sediment riverine inputs are known to vary between the major catchments, and are available from the SedNet tool, which provides annual loading from each of the major rivers, as well as estimates of pre-human sediment loads (Dymond et al. 2016, Figure 19). During the Sustainable Seas exercise, high-resolution sediment transport information was not available to estimate patterns of sediment transport, deposition, and resuspension once sediments enter the bay. With the availability of the ROMS hydrodynamic model developed for this project (Section 2.4), spatially explicit sediment deposition could be included in the Seafloor model to estimate sediment plume dispersion and spatial distributions of sediment deposition from each river during the cyclone event. It is also notable that, during the Cyclone Gabrielle event, a number of catchments with typically low annual sediment loads far exceeded their annual average. The hydrodynamic model was also parameterised by river discharges, allowing estimation of sediment deposition from this particular event.

Changes in bottom fishing stressors in Sustainable Seas Hawke's Bay scenarios were implemented either through reductions in fishing effort or through implementation of spatial closures. To model changes in fishing intensity, the number of vessels, and thus total fishing events, was changed, but the spatial footprint of activity was kept constant, and events were distributed stochastically based on the spatial fishing footprint. To implement spatial closures, the spatial footprint was reduced but fishing intensity was not affected, and all fishing events were distributed within the modified spatial footprint.
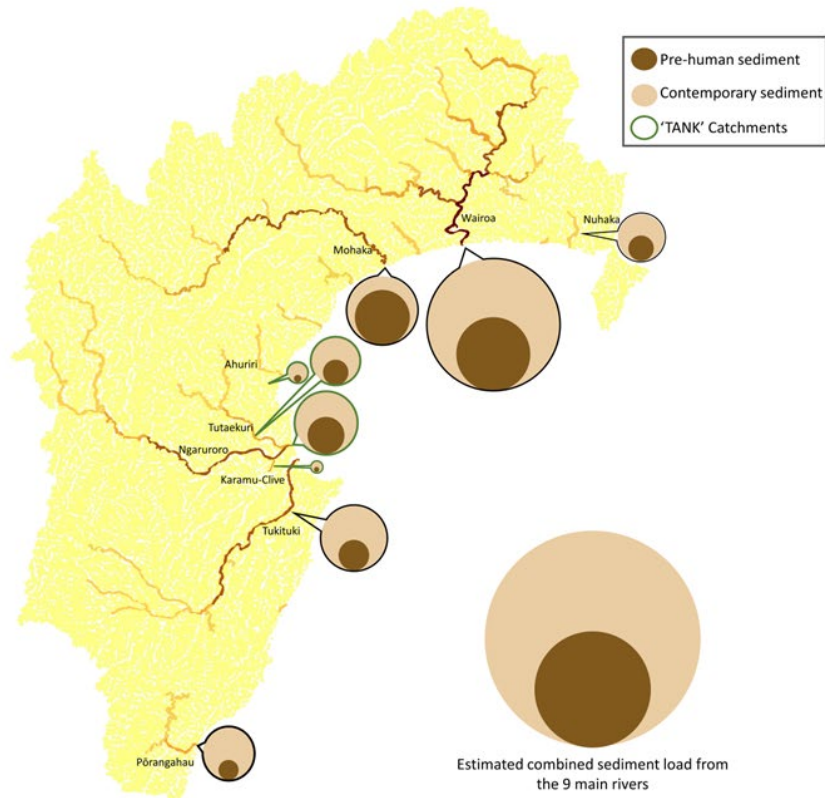
Figure 19: **Estimated sediment inputs from nine major catchments in the Hawke's Bay region, showcasing variability in sediment riverine inputs. As an indicator of scale, the Ngaruroro catchment pre-human sediment load is approximately 0.2 million t y^{-1}, whereas the Wairoa catchment contemporary sediment load is approximately 2.5 million t y^{-1}. The Karamu-Clive value was visually increased by an order of magnitude to allow it to be seen in the figure.**

2.5.4 Cyclone Gabrielle scenarios

Cyclone Gabrielle scenarios were initiated using a similar process to the Sustainable Seas Hawke's Bay scenarios, with initial baseline models resulting in predicted invertebrate communities based on the history of bottom trawl intensity and seafloor mud content. The Cyclone Gabrielle event was then simulated. The model was first extended to include two subareas, the prior Hawke's Bay regional model, and a second Gisborne regional model.

Sediment layers (percent mud content on the seafloor) were parameterised for the Hawke's Bay regional model using the Sustainable Seas sediment layer (Lundquist et al. 2022a). For the Gisborne regional model, baseline data on sediment grainsize was extracted from a national layer of the distribution of surficial sediments on the continental shelf (Bostock et al. 2019) and presented as percent mud content.

Fishing prior to the cyclone was assumed to be represented by the historical fishing footprint. Data were provided by Fisheries New Zealand in confidence to develop historical fishing footprint layers based on tow counts, updated to January 2023, for the Hawke's Bay and Gisborne regions. A second footprint was provided for February to July 2023, representing the changes in spatial footprint following cyclone impacts, resulting in some areas that were no longer accessible or suitable for bottom trawling.

Changes in sediment deposition following Cyclone Gabrielle were quantified based on the hydrodynamic model of sediment transport described in Section 2.4. Three combined metrics were used to parameterise spatial patterns of sediment deposition in the Seafloor model. First, model outputs of daily averages of suspended sediments in the upper water column were combined across eight sediment size classes, resulting in an estimated total suspended sediment concentration in the upper water column.

A similar metric was calculated for the near bottom model layer for combined suspended sediments across eight sediment size classes. A third metric was also quantified from daily hydrodynamic model output to estimate sediment deposition and erosion. This metric changes with time as sediments are deposited and eroded, and changes in total thickness provide a measure of deposition and erosion.

Finally, to contextualise the Cyclone Gabrielle event with respect to temporal patterns of storm events and associated suspended sediments, remote sensing data from SCENZ (described in Section 2.2) was used to estimate the size of the event relative to the intra-annual and interannual (seasonal) data to quantify the percent increase in sediment mud content, with the hydrodynamic model output used to distribute mud content within each of the model regions.

3. RESULTS

3.1 Remote sensing

Wairoa River flow began to rise from lowest basal flows on 12 February ($\sim$20 m^3 s^{-1}), peaked on 14 February ($\sim$3000 m^3 s^{-1}), then steadily declined until 23 February ($\sim$70 m^3 s^{-1}) when post-cyclone events began to influence river flows (Figure 20). For longer-term context, seasonal month boxplot statistics on average daily flow rates during 2023 are compared against those of the period January 2009 to August 2023 (Figure 20). Overall, seasonal patterns are evident, with high flows in mid-winter and peaking in July and low flows in summer (December to February). Besides Cyclone Gabrielle producing the largest daily flows overall, comparatively high river flows occur from January to June 2023. Flows during February 2023 were similar to highest seasonal flows typically observed in July.

On 18 February (four days after peak stormflows) most of the Hawke's Bay and Gisborne CMAs show modified water quality metrics relative to the pre-cyclone period, and by 20 February surface features have migrated further offshore in some regions as can be seen in maps of TSS concentrations (Figure 21) and HVIS (Figure 22). Some features extend beyond the CMAs, such as the eddies and south easterly progression off East Cape, a north easterly progression along the Wairarapa coast, and eddies and south easterly progression offshore from Mahia Peninsula and the Wairarapa Coast. Offshore features begin disappearing from the 22 February.
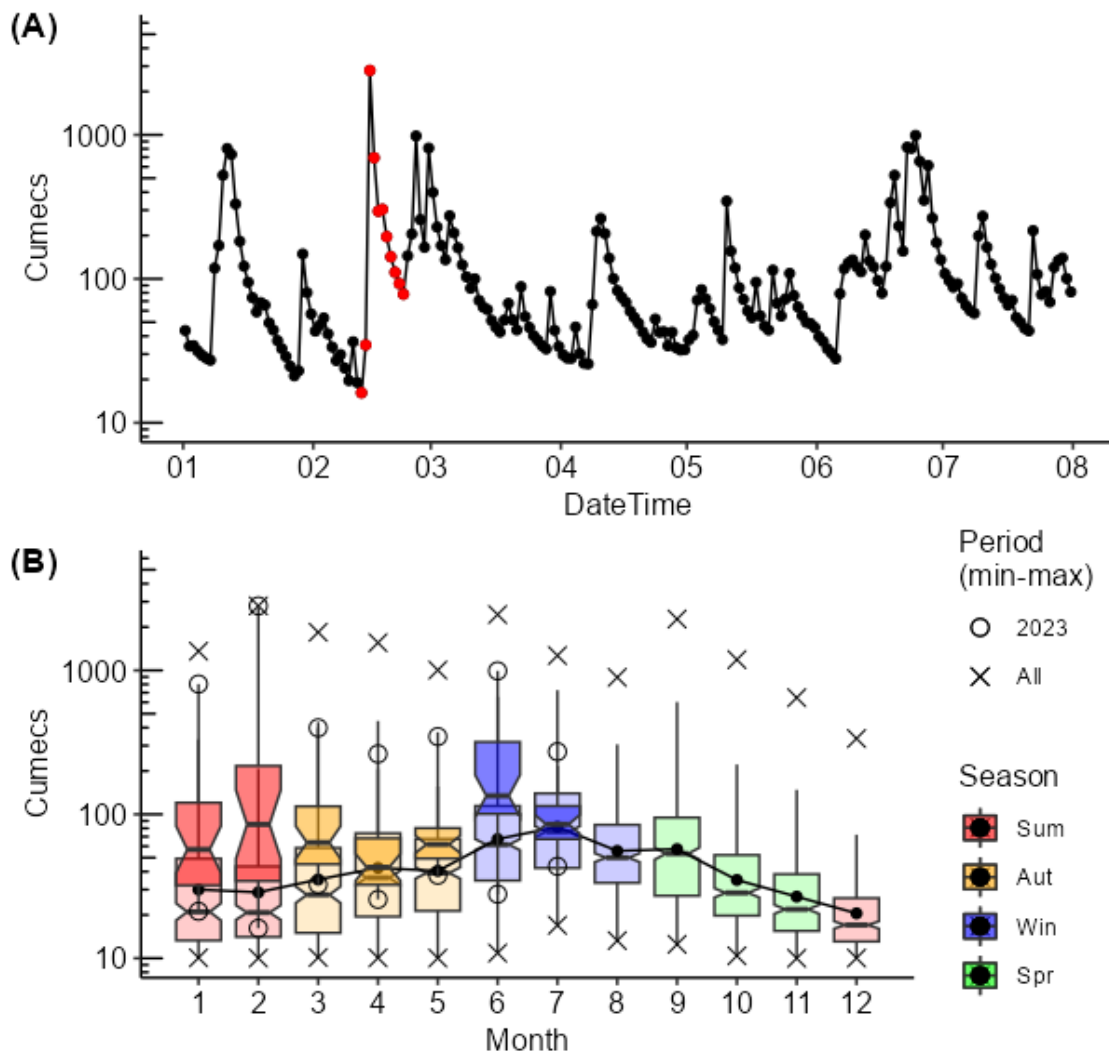
Figure 20: Wairoa River flows. (A) Average daily low rates from January to August 2023, with the influence of Cyclone Gabrielle shown by red filled circles. (B) Monthly flow rate boxplot statistics for the 2023 year against the January 2009 to August 2023 period. Light coloured boxplots show the median, and 25th and 75th percentile with standard error notches for the January 2009 to August 2023 period. Dark coloured boxplots show the same information for the 2023 year. Means for January 2009 to August 2023 are shown by black circles and black line. Minimum and maximum daily flows for each month are shown by 'X' symbols (January 2009 to August 2023) and empty circles (2023 only). Data were obtained from the Hawke's Bay Regional Council River Levels and Flows website (https://www.hbrc.govt.nz/environment/river-levels).

The boundary separating low offshore TSS values (~0.3 g m^{-3}) and high coastal TSS values (>1 g m^{-3}) gives an indication of the spatial extent of the sediment plume (Figure 21) and analysis of daily TSS from gap-free data in each CMA illustrates differences between Hawke's Bay and Gisborne regions in terms of timing and magnitude of response (Figure 23). Mean TSS across the Gisborne CMA peaked a few days earlier (15 February) than in the Hawke's Bay CMA (18 February). Distributions of TSS values are similar between the two CMAs, although the peak in mean TSS values is higher in Hawke's Bay than in Gisborne following the cyclone. Gap-free daily spatial maps of light energy at the seabed (EBED) are shown in Figure 24. Prior to the cyclone, mean EBED values in the Gisborne CMA were lower than in Hawke's Bay. Post-cyclone EBED values reached a minimum on 20 February in both regions, followed by a partial recovery. EBED values in Gisborne showed a smaller decrease post-cyclone than in Hawke's Bay.
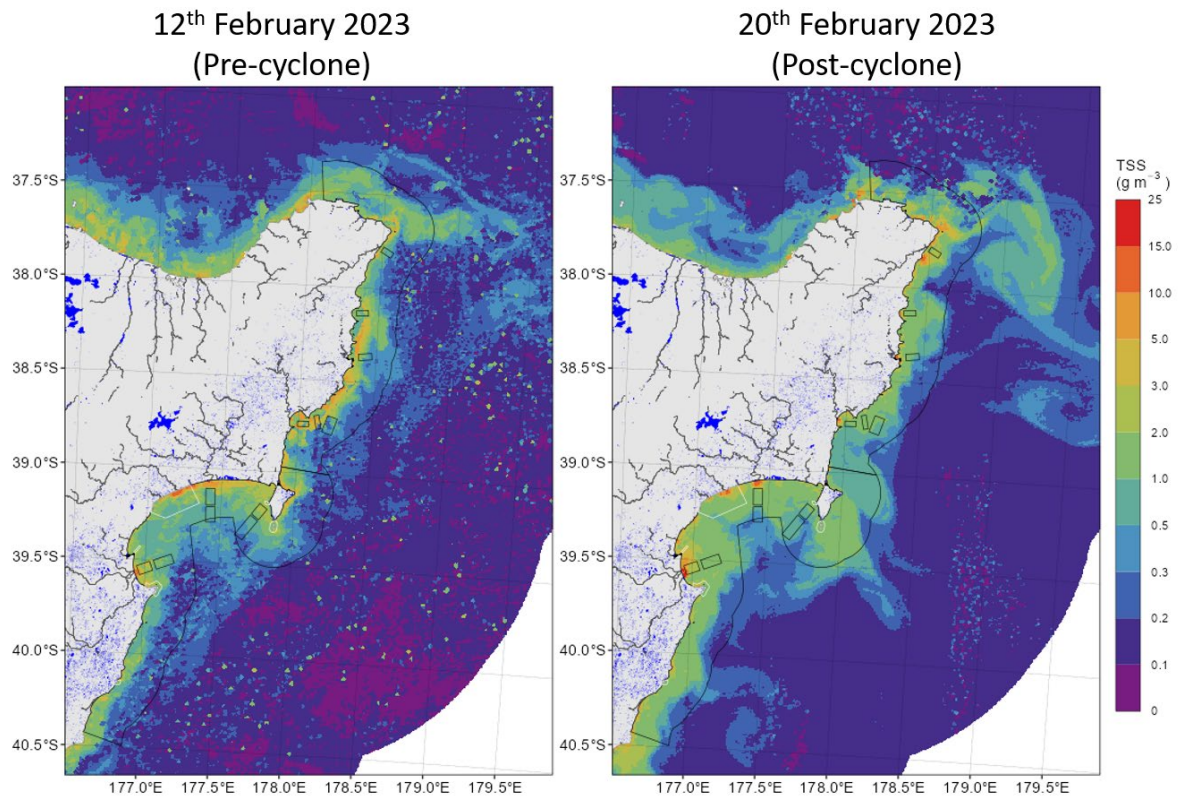
Figure 21: **Maps of total suspended solids concentrations (TSS, g m⁻³) pre- (12th February) and post-Cyclone Gabrielle (20th February 2023). The maps are gap-free, i.e., with missing pixels infilled using linear time interpolation between different daily maps. Black and white polygons show the boundaries of the Hawke's Bay and Gisborne CMAs, coring transects, and selected Significant Conservation Areas targeted as part of the RV *Kaharoa* voyages in June and October.**

12th February 2023
(Pre-cyclone)

20th February 2023
(Post-cyclone)
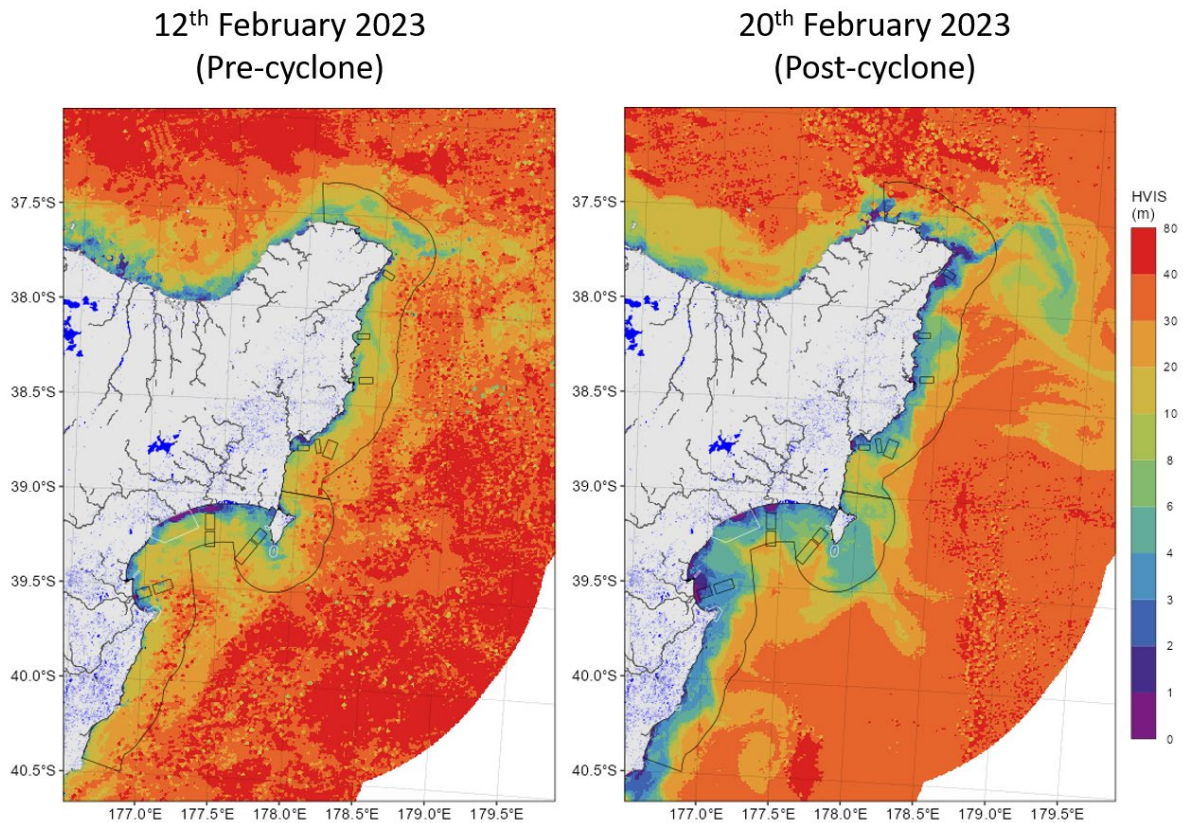
Figure 22: Maps of horizontal visibility distance (HVIS; metres) pre- (12th February) and post-Cyclone Gabrielle (20th February 2023). The maps are gap-free, i.e., with missing pixels infilled using linear time interpolation between different daily maps. Black and white polygons show the boundaries of the Hawke's Bay and Gisborne Coastal Marine Areas, coring transects, and selected Significant Conservation Areas targeted as part of the RV *Kaharoa* voyages in June and October.
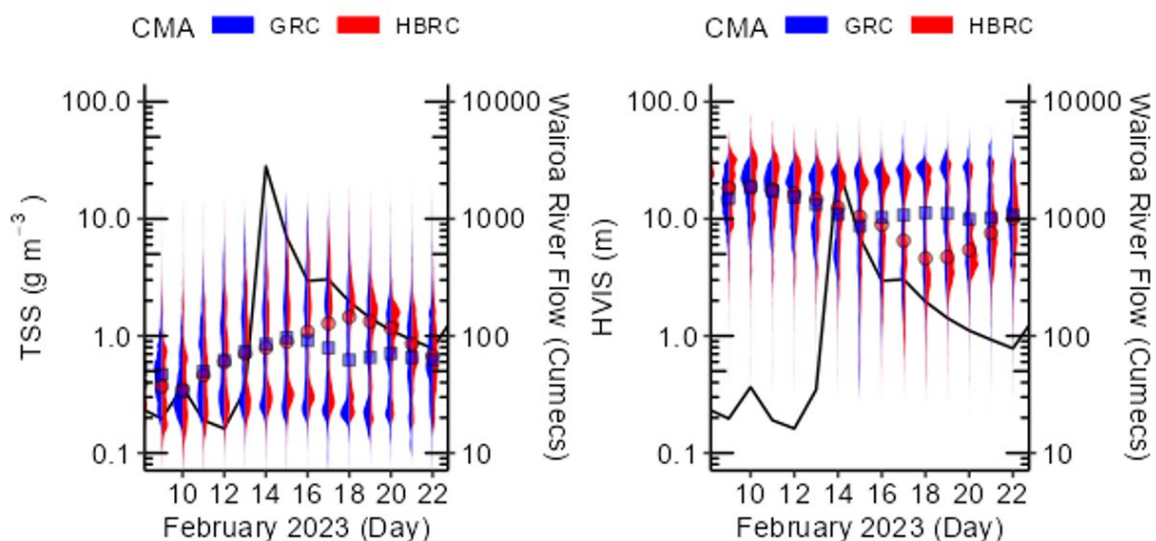
Figure 23: The distribution of daily gap-free surface water metrics within the HBRC and GDC CMAs for 9–22 February 2023. Left: TSS, g m^{-3}; right: HVIS, m. Vertical blue (GDC) and red (HBRC) shading show the distribution of TSS and HVIS values. Blue squares and red circles show average values for GDC and HBRC, respectively. Daily Wairoa River flow (cumecs) is shown for context by a black line. Gap-free data may underestimate TSS and overestimate HVIS due to exclusion of extreme values from cloud cover. Note logarithmic vertical scales.
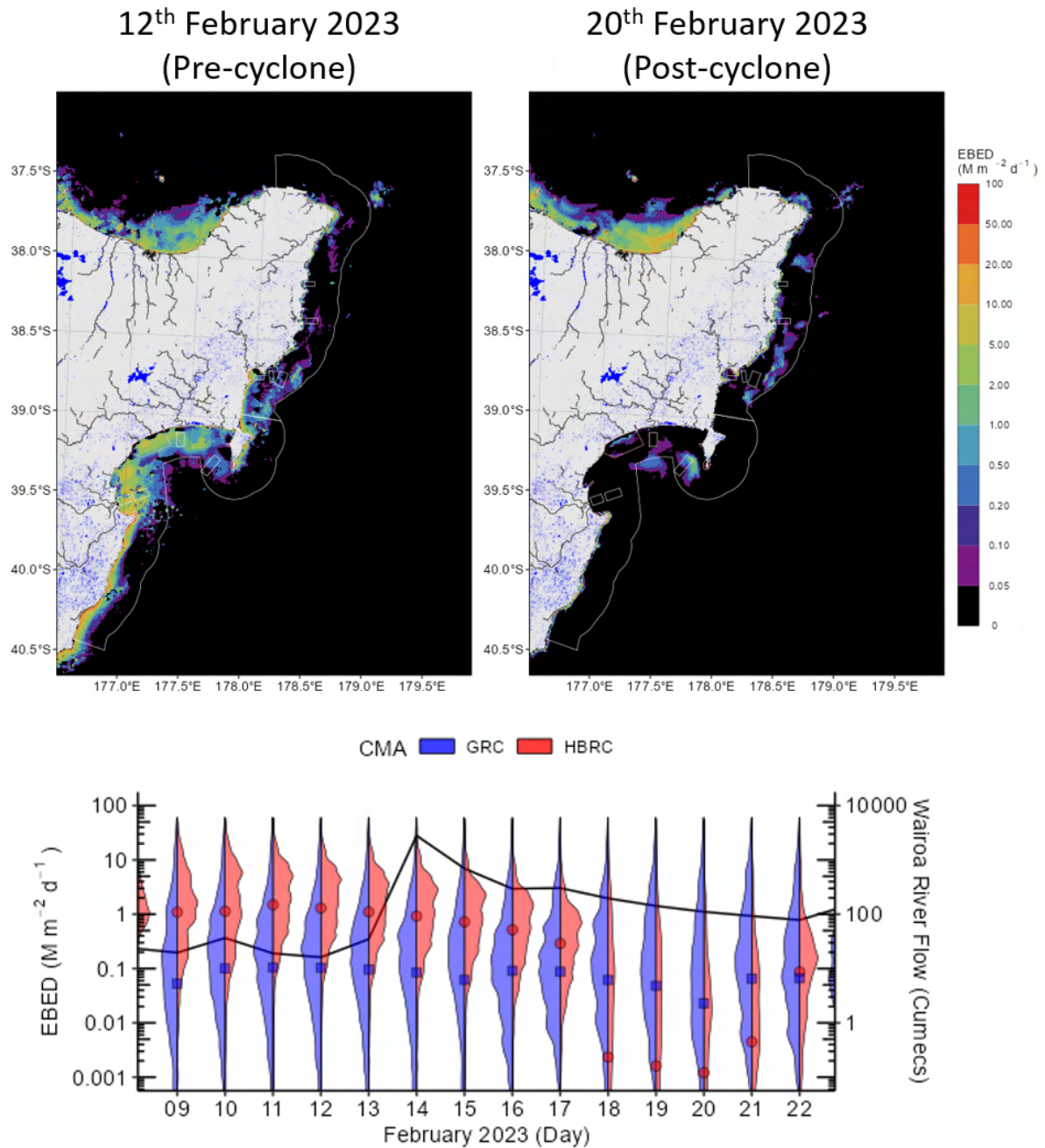
Figure 24: **Map of EBED (mol photons m^2 day^{-1}) pre- (12th February) and post-Cyclone Gabrielle (20th February 2023) (top); and distribution of daily gap-free surface EBED within the HBRC and GDC CMAs for 9–22 February 2023 (bottom). The maps are gap-free, i.e., with missing pixels infilled using linear time interpolation between different daily maps. White polygons show the boundaries of the Hawke's Bay and Gisborne CMAs, coring transects, and selected Significant Conservation Areas targeted as part of the RV *Kaharoa* voyages in June and October. Vertical blue (GDC) and red (HBRC) shading in bottom graph show the distribution of EBED values. Blue squares and red circles show average values for GDC and HBRC, respectively. Daily Wairoa River flow (cumecs) is shown for context by a black line. EBED is determined by the intensity of sunlight that day, light attenuation of the water column, and depth at each 500 × 500 m pixel. Note logarithmic vertical scales.**

A strong seasonal signal can be seen in time series plots of TSS, HVIS, EBED, and CHL for both the Hawke's Bay and Gisborne CMAs (Figure 25, Figure 26, Figure 27, Figure 28). On average, TSS values tend to be lowest in the summer months, increase in autumn, peaking in winter then decreasing in spring.

The opposite trend can be seen for HVIS and EBED, with the average value highest in summer and lowest in winter. The seasonal trend for CHL is similar to that of TSS but tends to peak in early-mid spring instead of winter.

Substantial variation in mean monthly TSS could be seen among years in addition to the seasonal variability (Figure 25). Overall, interannual variability in TSS is greater in the winter months than during the summer months. In 2023, the mean TSS value in January for both Hawke's Bay and Gisborne was higher than all previous years in the time series (2002–2023). The mean monthly TSS value then increased markedly in February, reaching a higher value than all previous years in both regions and remained elevated relative to previous years until May when it was well within the range of values for that month. Although the high February TSS values seen in 2023 were unusual for the month they were somewhat lower than the average TSS value seen in the winter months. The long-term February trend for TSS values in the Hawke's Bay and Gisborne CMAs is increasing but is not considered likely (McBride et al. 2014, McBride 2019).

There was no clear seasonal variation in interannual variability for HVIS or EBED (Figure 26 and Figure 27). In 2023, the mean HVIS and EBED values in January in both Hawke's Bay and Gisborne were lower than most or all previous years in the time series. The mean monthly HVIS and EBED values decreased markedly in February, reaching lower values than all previous years in both regions and remained low relative to most previous years until April-May in Hawke's Bay. HVIS values in Gisborne were within the range of previous years in March whereas low monthly EBED values persisted until June. The long-term February trend for HVIS and EBED values in the Hawke's Bay and Gisborne CMAs is decreasing but is not considered likely.

CHL in Hawke's Bay reached higher values than in Gisborne and showed a greater level of interannual variability (Figure 28). CHL values in January 2023 were more elevated than in of the previous years in the time series and reached extremely high values in February 2023 in both regions, exceeding all previous monthly averages in any month since 2002. The high CHL values may have been influenced by the elevated water turbidity, as it is not always possible to accurately tease apart the contributions of the main light attenuating components. This potential artefact cannot be verified without analyses of water samples from the field. CHL values decreased until May in both regions where they approached the long-term average, then increased again in June, remaining elevated in Hawke's Bay until August whilst decreasing more rapidly in Gisborne. The long-term February trend for CHL values in the Hawke's Bay and Gisborne CMAs is increasing but is not considered likely.

Figure 25: Seasonal and within month time series of TSS (g m⁻³) in the Hawke's Bay (top) and Gisborne (bottom) CMAs for the January 2002 to August 2023 period. Within each month, circular symbols show monthly mean values for the 2002 to 2022 years and square symbols with bold outline show the mean value for the 2023 year (up to August 2023). Interannual trends for each month are shown by solid lines, and the trend likelihood classification (following McBride et al. 2014 and McBride 2019) is shown by different colours.
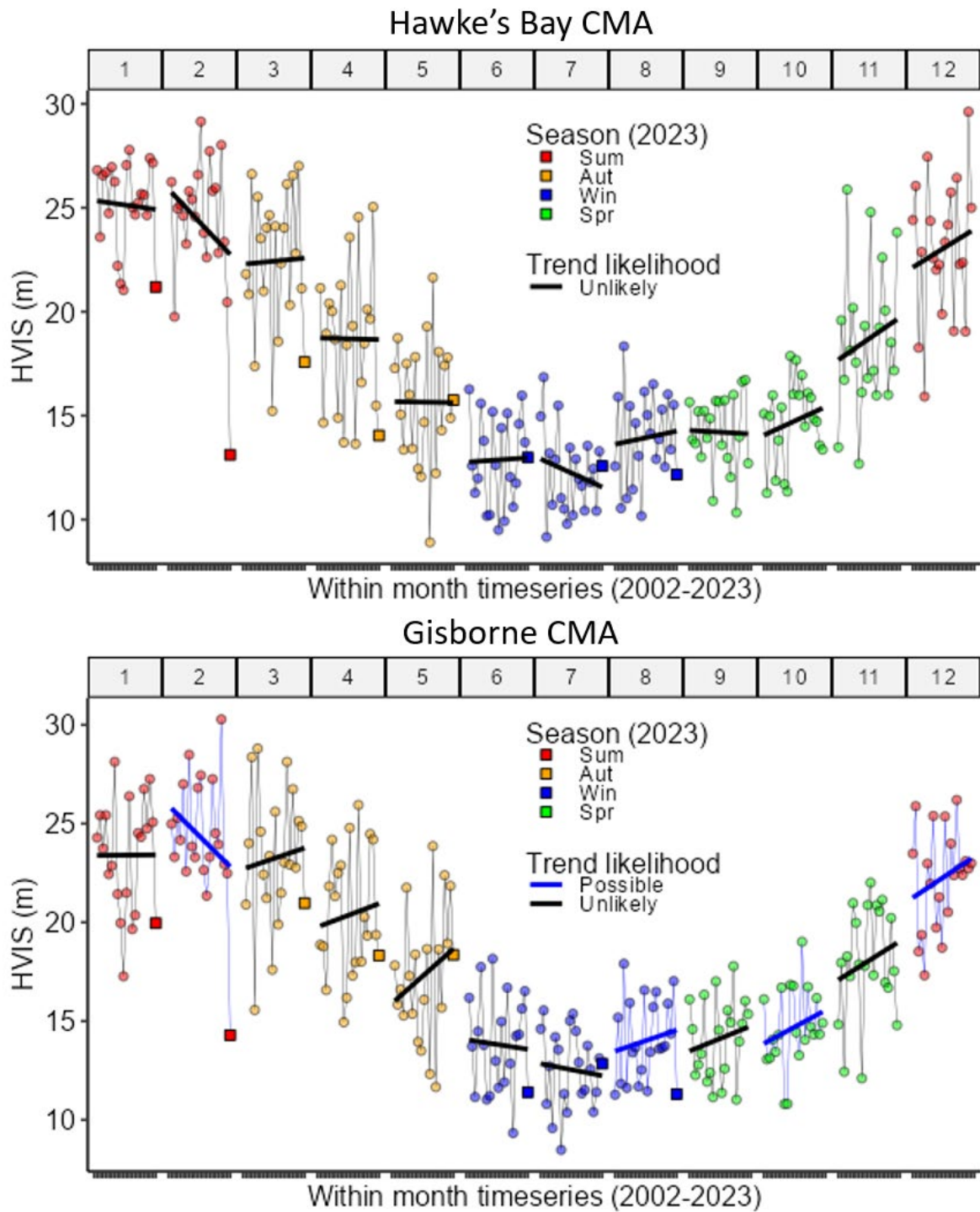
Figure 26: **Seasonal and within month time series of HVIS (m) in the Hawke's Bay (top) and Gisborne (bottom) CMAs for the January 2002 to August 2023 period. Within each month, circular symbols show monthly mean values for the 2002 to 2022 years and square symbols with bold outline show the mean value for the 2023 year (up to August 2023). Interannual trends for each month are shown by solid lines, and the trend likelihood classification (following McBride et al. 2014 and McBride 2019) is shown by different colours.**
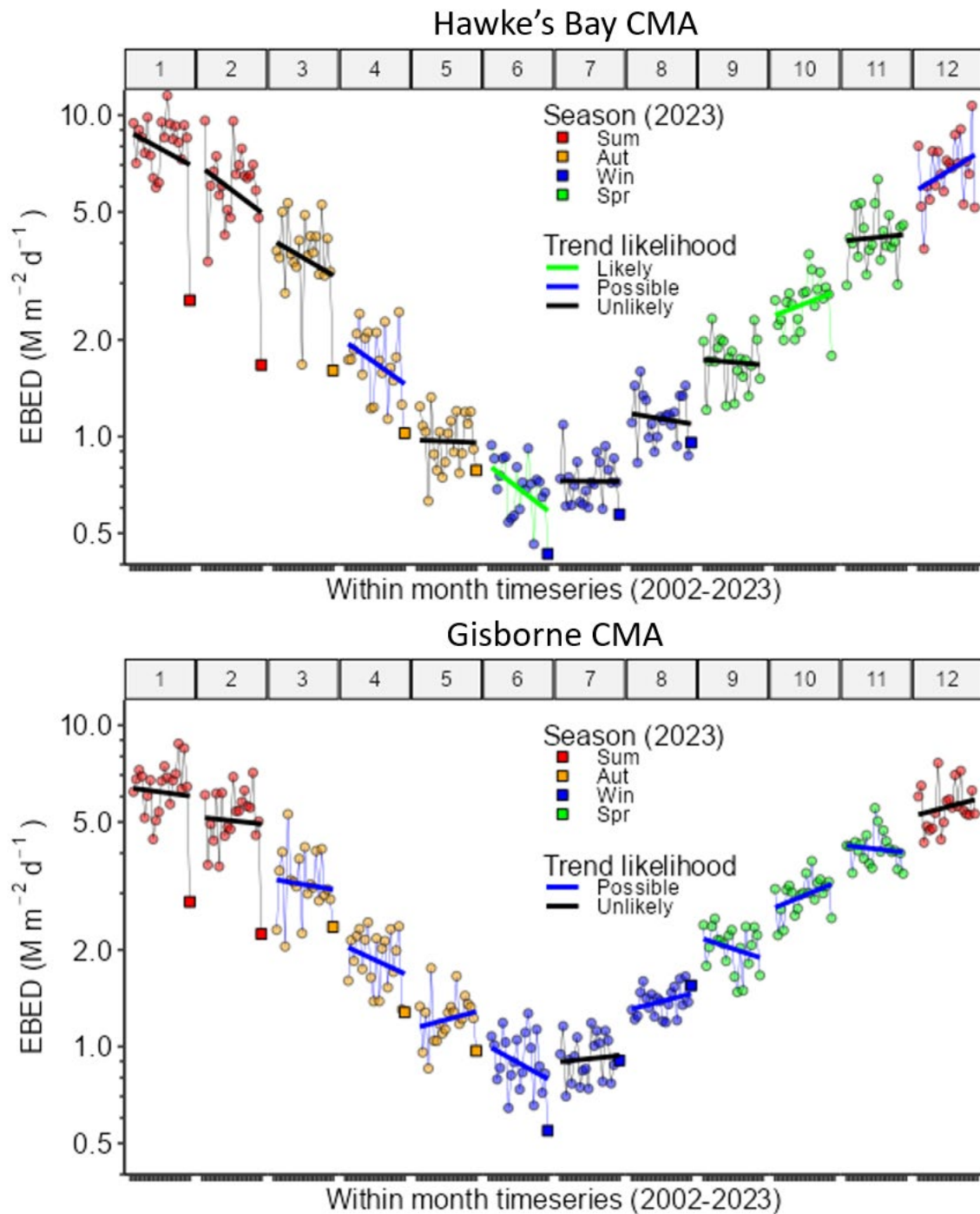
Figure 27: Seasonal and within month time series of EBED (mol photons m^{-2} day^{-1}) in the Hawke's Bay (top) and Gisborne (bottom) CMAs for the January 2002 to August 2023 period. Within each month, circular symbols show monthly mean values for the 2002 to 2022 years and square symbols with bold outline show the mean value for the 2023 year (up to August 2023). Interannual trends for each month are shown by solid lines, and the trend likelihood classification (following McBride et al. 2014 and McBride 2019) is shown by different colours.
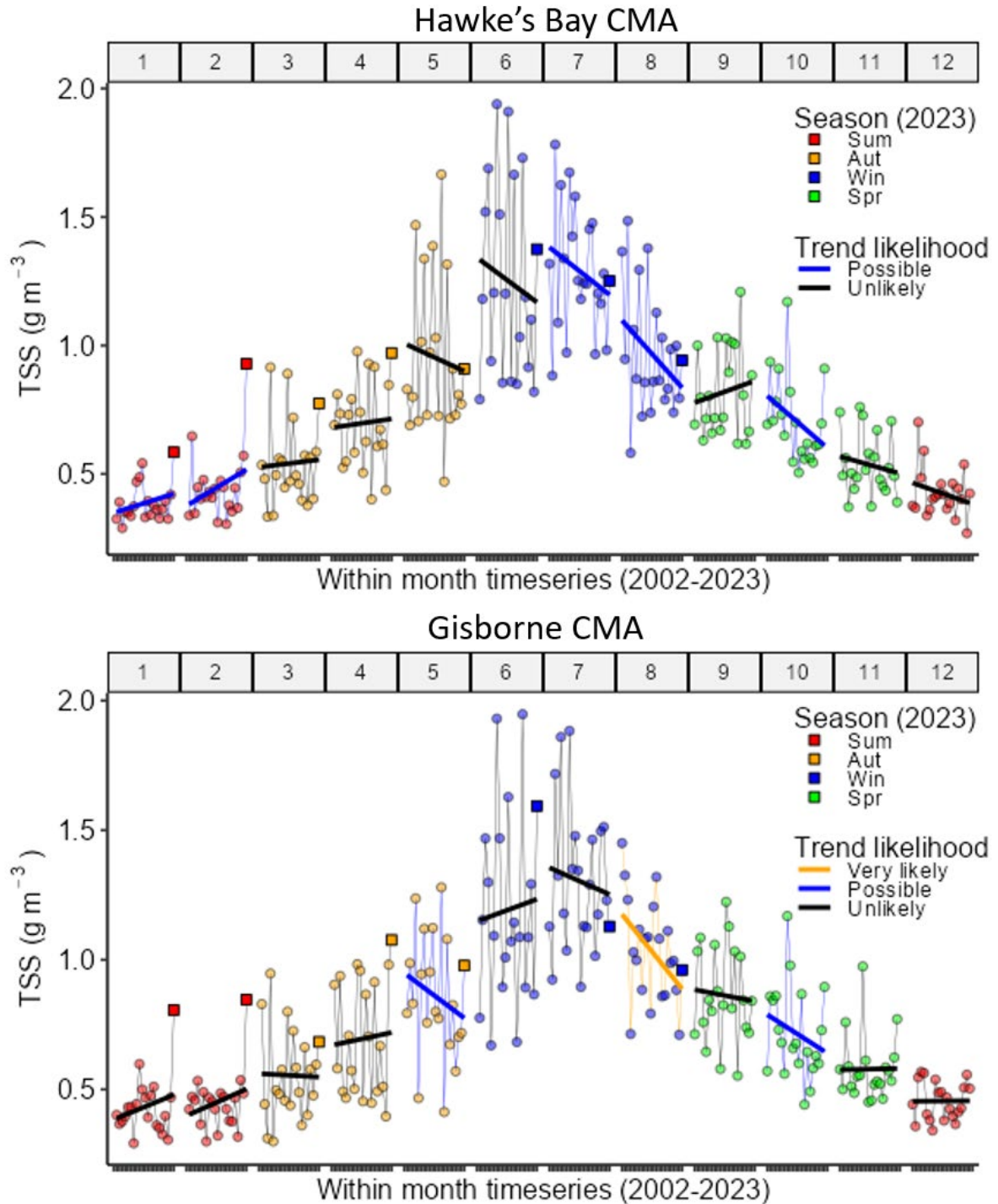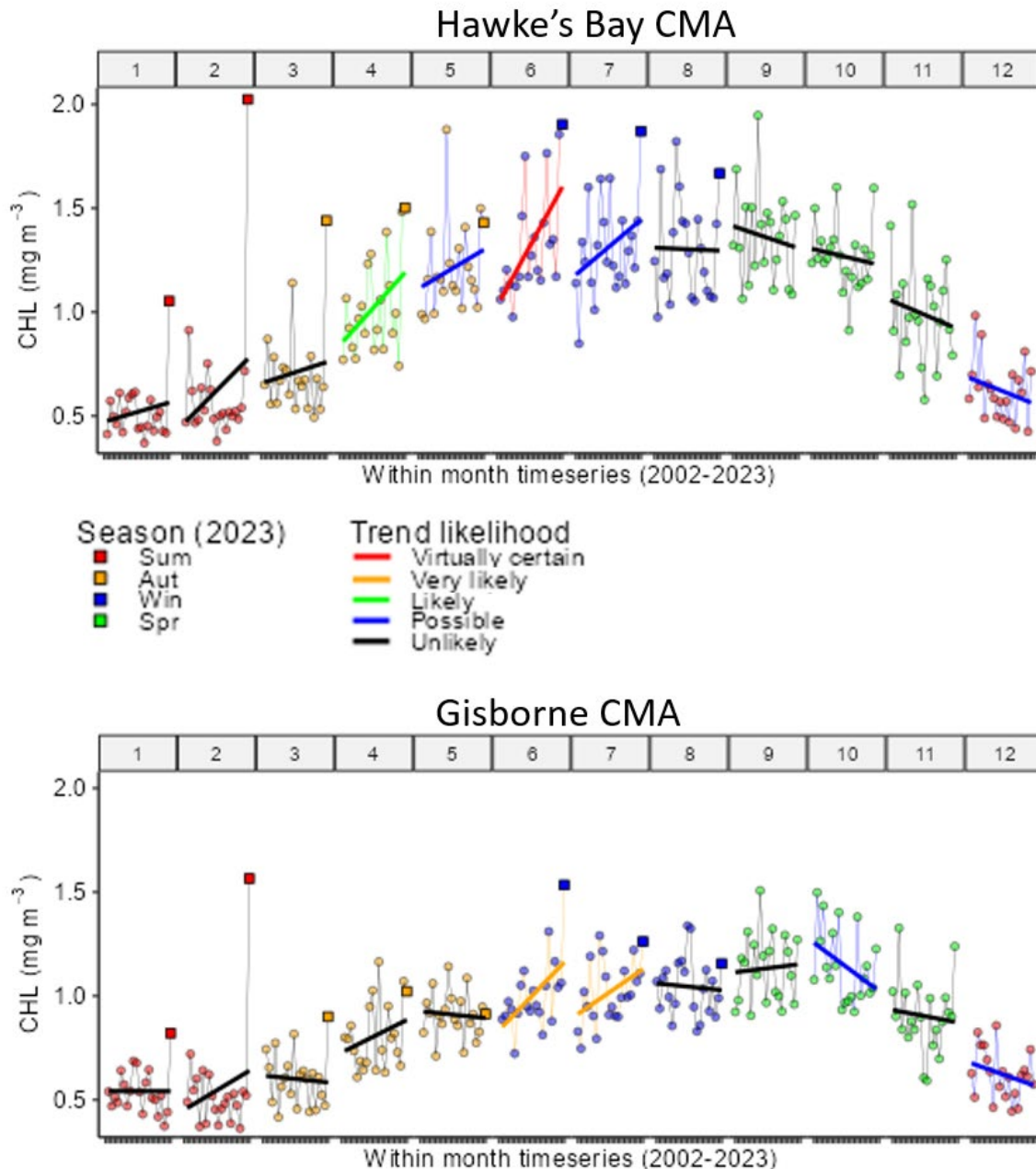
Figure 28: Seasonal and within month time series of CHL (mg m^{-3}) in the Hawke's Bay (top) and Gisborne (bottom) CMAs for the January 2002 to August 2023 period. Within each month, circular symbols show monthly mean values for the 2002 to 2022 years and square symbols with bold outline show the mean value for the 2023 year (up to August 2023). Interannual trends for each month are shown by solid lines, and the trend likelihood classification (following McBride et al. 2014 and McBride 2019) is shown by different colours.

Spatial patterns in long-term February trends of TSS, HVIS, EBED, and CHL and their likelihood are shown in Figure 29 and Figure 30. For TSS, we can see an overall increasing trend for the majority of the Hawke's Bay and Gisborne coast but which does not extend north of Waiapu River mouth. This trend is assessed as likely, very likely, or virtually certain in localised areas in Hawke's Bay (e.g., east of Cape Kidnappers, Wairoa Hard, and off the Wairoa and Nuhaka rivers) and Gisborne (south of Mahia Peninsula and offshore from Tolaga and Tokomaru bays). HVIS show the opposite spatial trend to TSS across the two regions, with similar patterns of trend likelihood. Trends in EBED have low likelihoods across the two regions, although the overall tendency is for a decrease in HVIS in Hawke's Bay and in the region between Tolaga Bay and East Cape, with increasing HVIS elsewhere. Trends in CHL also

have largely low likelihoods, but with increasing trends across most of the Hawke's Bay region and Gisborne region south of Waiapu River mouth.
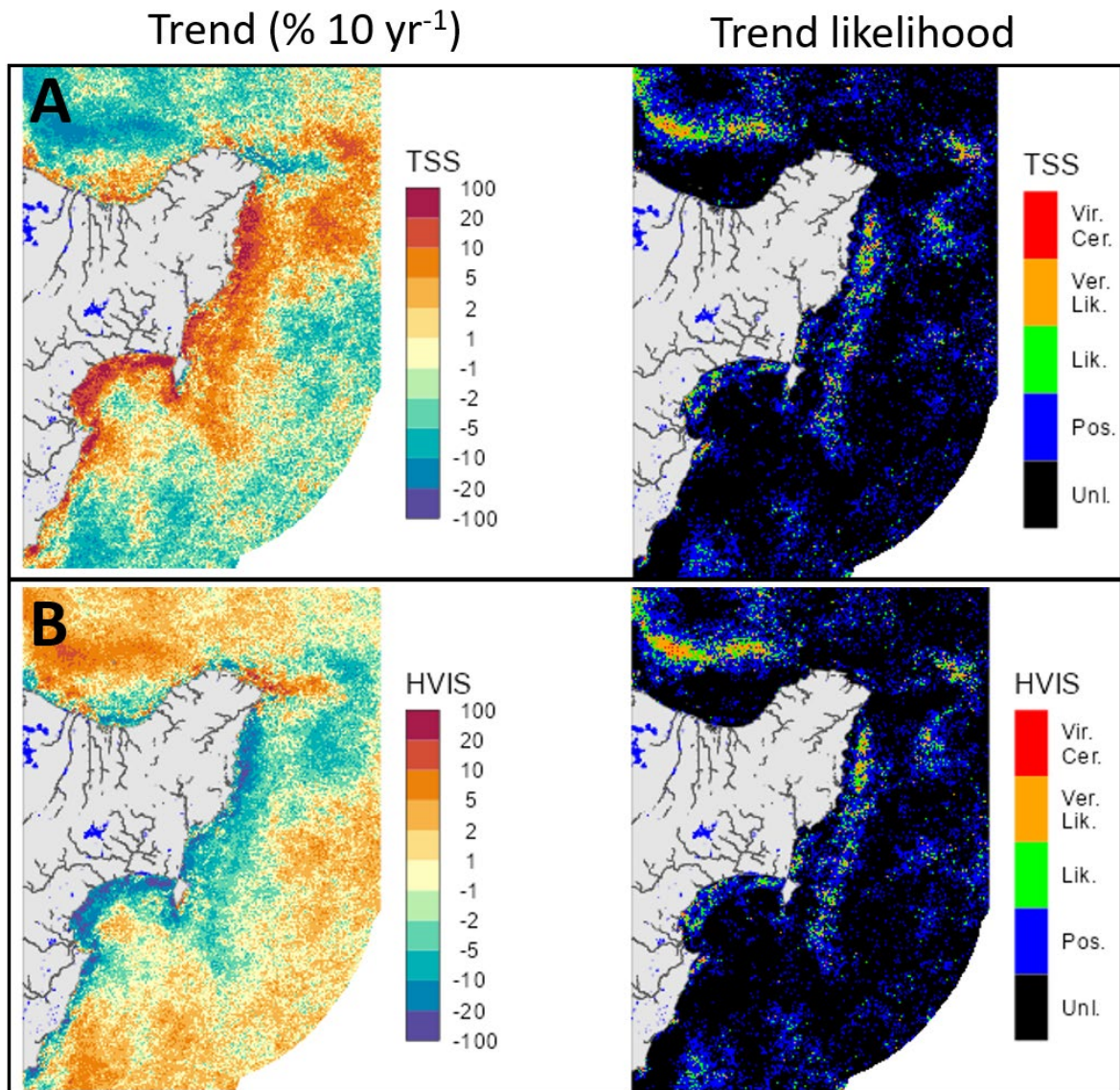
Figure 29: Long-term February relative linear trends (left; % 10 yr^{-1}) and trend slope likelihoods (right; following McBride (2019)) for the 2002–2023 period: (A) TSS (g m^{-3}) and (B) HVIS (m).
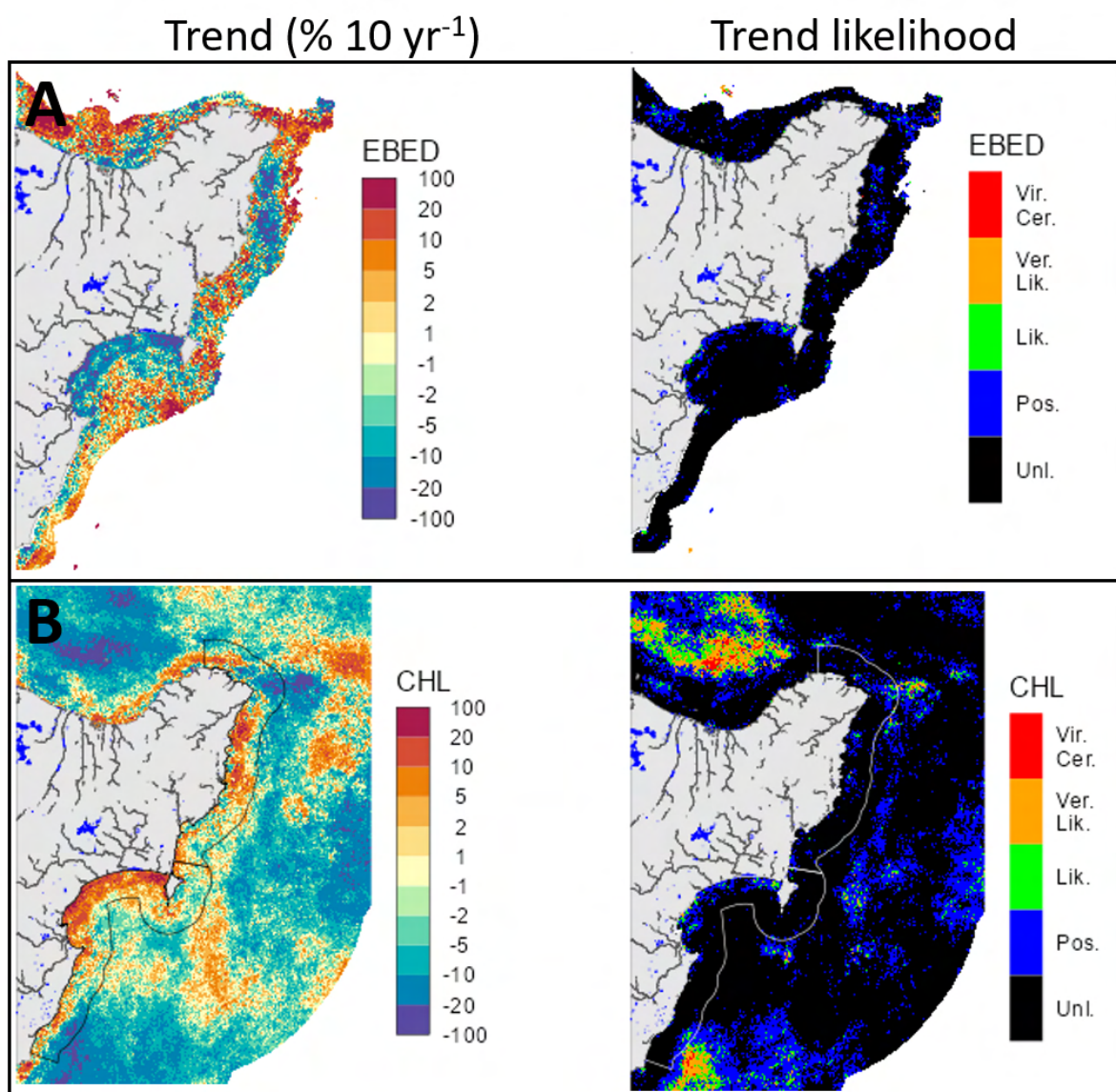
Figure 30: Long-term February relative linear trends (left; % 10 yr^{-1}) and trend slope likelihoods (right; following McBride 2019) for the 2002–2023 period: (A) EBED (mol photons m^2 day^{-1}); and (B) CHL (mg m^{-3}). EBED values only shown for pixels over less than 200 m water depth.

3.2 Research vessel surveys

3.2.1 Seafloor mapping

Multibeam mapping was conducted over 701.8 km^2 of seafloor over the three 2023 surveys, including transits (IKA2303, 119.8 km^2; KAH2303, 93.5 km^2; KAH2306, 488.5 km^2) (Appendix 4).

Areas of sediment deposition and erosion were detected at Pania Reef, Tangoio Reef, and Clive outfall area when comparing data obtained pre- and post-cyclone (Figure 7). At Pania Reef, substantial sediment accumulations of up to approximately 1 m in thickness and covering ~1.0 km^2 of seafloor were observed between the constriction points of the reef and fanning out at the northeastern edge of the reef (Figure 31). Areas along the northern edge of the reef showed a loss of up to ~1 m of sediment. At Tangoio Reef, two sediment linear deposition features ~650 m and ~350 m in length, covering ~0.2 km^2 of seafloor and up to ~1 m in height, were observed with some erosion of up to ~0.7 m of sediment seen in the northwestern corner of the mapped area (Figure 32). At the Clive outfall area, sediment deposition of up to approximately 0.9 m occurred through much of the mapped area except for an area of erosion offshore from the Clive River mouth (Figure 33).

Figure 31: Difference in seafloor bathymetry at Pania Reef (Hawke Bay) between pre- (2019) and post-cyclone (2023). Red colour shading indicates sediment accumulation, green colour shading indicates sediment erosion, and yellow shading indicates no change. Empty black circle shows location of multicorer deployment during June 2023 RV *Kaharoa* survey (KAH2023 station 29; see Section 2.3.3).

Figure 32: Difference in seafloor bathymetry at Tangoio Reef (Hawke Bay) between pre- (2022) and post-cyclone (2023). Red colour shading indicates sediment accumulation, green colour shading indicates sediment erosion, and yellow shading indicates no change. Empty black circle shows location of multicorer deployment during June 2023 RV *Kaharoa* survey (KAH2023 station 29; see Section 2.3.3).
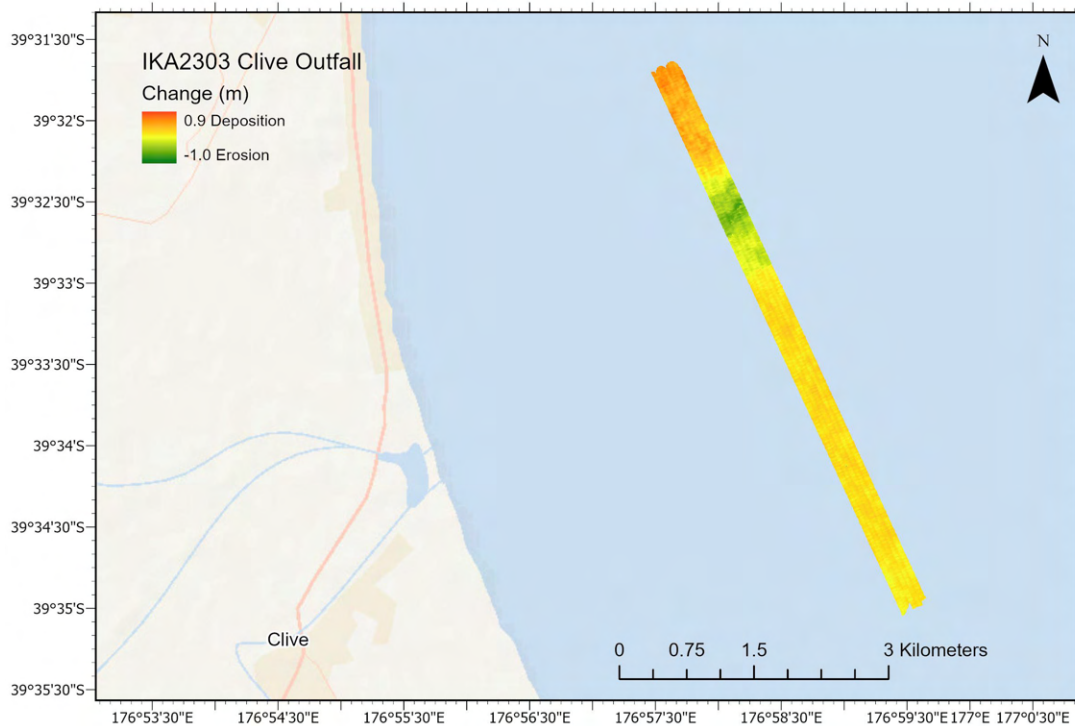
Figure 33: Difference in seafloor bathymetry at Clive outfall area (Hawke Bay) between pre- (2021) and post-cyclone (2023). Red colour shading indicates sediment accumulation, green colour shading indicates sediment erosion, and yellow shading indicates no change.

Minor patterns of deposition were noted at the Wairoa Hard survey area (Figure 34), concentrated along north-south trending linear features that are present in both the bathymetry and backscatter. The deposition features are of the same magnitude as artefacts in the data so are more difficult to delineate accurately. No notable areas of erosion or deposition are observed at Clive Hard (Figure 35).
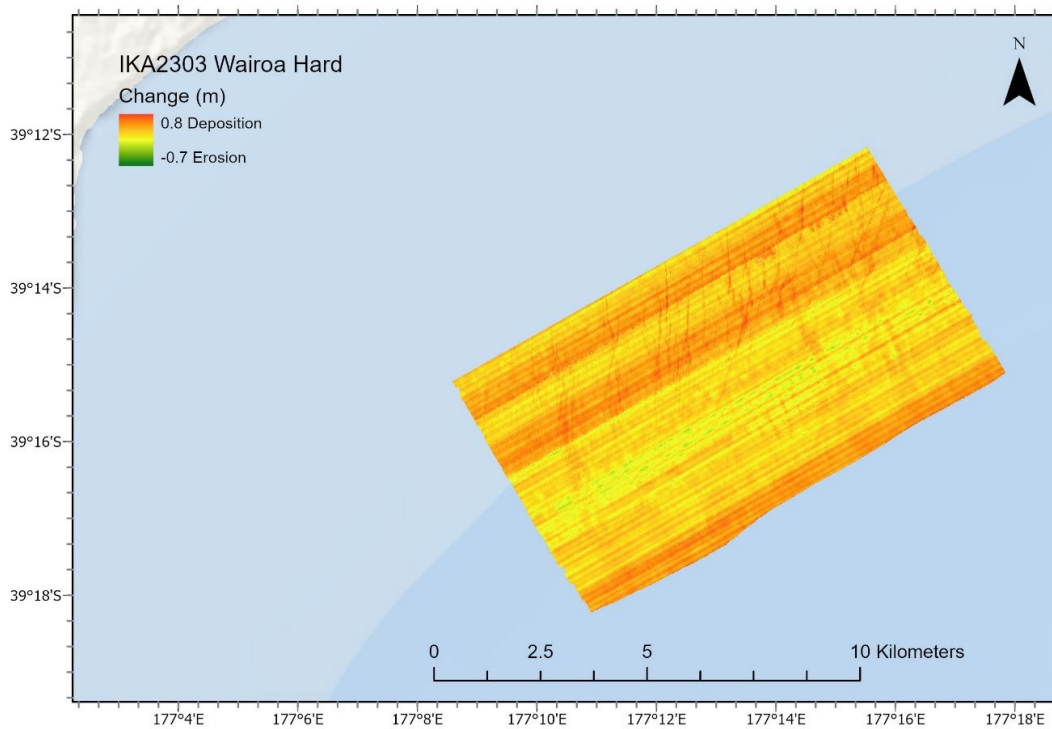
Figure 34: Difference in seafloor bathymetry at Wairoa Hard (Hawke Bay) between pre- (2018) and post-cyclone (2023). Red colour shading indicates sediment accumulation, green colour shading indicates sediment erosion, and yellow shading indicates no change. Lines parallel to the long axis of the Wairoa Hard polygon are data artefacts.

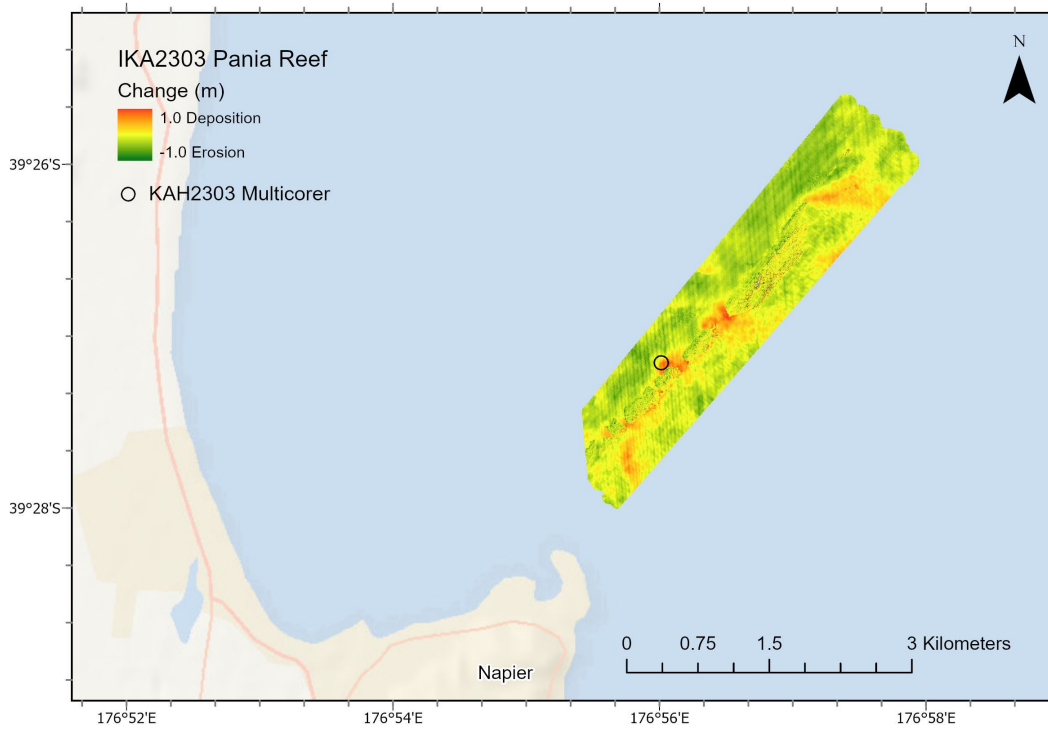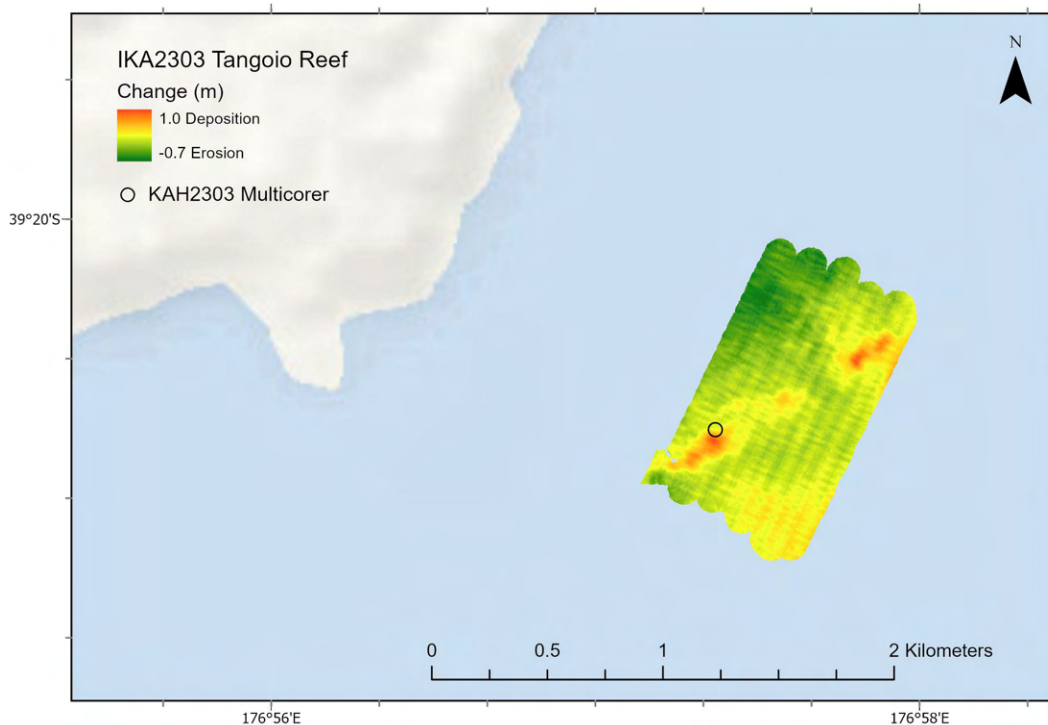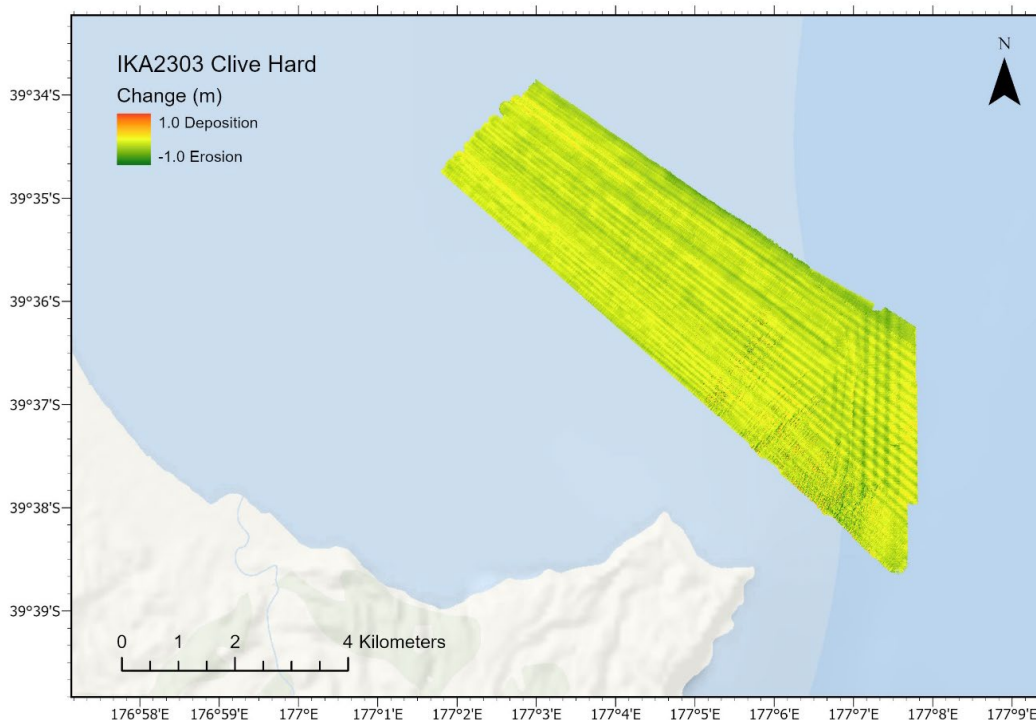

Figure 35: Difference in seafloor bathymetry at Clive Hard (Hawke Bay) between pre- (2019) and post-cyclone (2023). Red colour shading indicates sediment accumulation, green colour shading indicates sediment erosion, and yellow shading indicates no change. Lines parallel to the long axis of the Clive Hard polygon and north-south lines at the eastern edge of the polygon are data artefacts.

Prominent linear features were observed in the southwestern sector of Wairoa Hard, surrounded by a large cluster of pockmarks. These features vary in length from 5 to 13 m in length, ~0.4 to 0.5 m in height (Figure 36). Mosaics from backscatter snippets provided no further information. These dimensions of these features are consistent with the presence of large logs on the seafloor, which were observed in camera transects conducted in the area during the October survey (see Section 3.2.4).
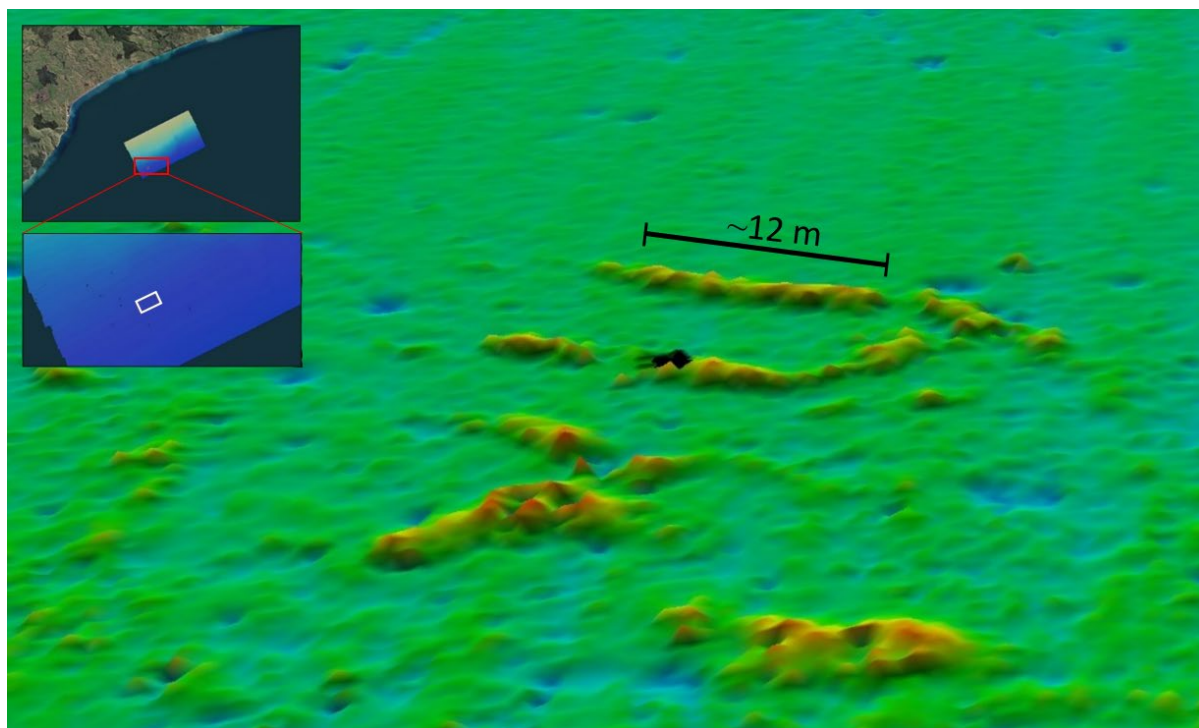
Figure 36: **Three-dimensional benthic-terrain model of linear features in the southwestern corner of the Wairoa Hard area mapped in April 2023. Top inset shows extent of area mapped; lower inset shows area where linear features were detected (white rectangle).**

3.2.2 Sediments

Thirty-four cores were recovered for sediment analyses from the June and October surveys (Table 7). A total of 26 multicore deployments returned 23 recoveries during the June survey, most of good to fair quality. The average core length was around 31 cm, but many deployments into soft substrate recovered cores in excess of 40 cm length, with the longest core being 55 cm. A total of 11 core sites were recovered during the October survey, with an average sediment core length of 37 cm and maximum length 60 cm.

Table 7: **Details of cores obtained during the June and October surveys (KAH2303 and KAH2306).**

Transect/Site	River/region	Depth range (m)	Number of cores: KAH2303, KAH2306
T1	Ngaruroro/Clive outfall	15–61	4, 3
T2	Wairoa	28–61	4, 4
T3	Nuhaka/Mahia West	35–76	5
T4	Waipaoa/Poverty Bay	27–54	4, 1
T5	Tokomaru	29–64	2, 1
T6	Waiapu/East Cape	21–146	2, 1
Targeted	Pania, Tangoio, Tolaga	16, 20, 49	2, 1
TOTAL			23, 11 (34 total)

Nearly all substrates were terrigenous silty muds, with varying amounts of very-fine and fine sand. The coastal transects consistently showed that cores at sites <27 m water depth encountered slightly muddy fine to very-fine sand, with poor substrate penetration and often disturbed (wash-out and cloudy

headspace in the tubes). The one exception was transect T1 off Ngaruroro River, where a core from 15 m water depth was muddy.

Identifying intact "event deposits" at the top of the cores was challenging in the field, albeit that the uppermost 2–5 cm was nearly always brown unconsolidated mud. Cores recovered from offshore of Ngaruroro River (transect 1) had very soft, muddy surface sediments, with some suggestion of stratified deposits visible as smeared colour bands through the wall of the multicore tube. Transect T2 off Wairoa River looked to preserve evidence of unconsolidated brown muddy tops overlying potentially laminated deposits. In Poverty Bay (transect T4) substrates were soft mud in water depths >35 m, most with visible bioturbation to tens of centimetres depth and some with open burrows. The core processing showed there were suggestions of broad stratification, with either firm sticky mud or slightly sandy deposits at the core base. Field observations will be tested and verified with laboratory sediment analysis, which will be included as part of Swales et al. (in prep.).

The two areas of sediment accumulation targeted at Pania Reef and Tangoio Reef during the June survey returned short cores of sand-dominated samples, suggesting that these putatively fine accumulated sediments had been dispersed in the two-month interval since being remapped in April, or that these accumulations originally consisted of sandy sediments (Figure 31 and Figure 32).

Repeat coring in October, at shelf sites where Cyclone Gabrielle event deposits were observed in cores collected in June, allowed an assessment of ongoing redistribution of benthic substrates. The hypothesis explored was whether further winter storms and swells might have resuspended and winnowed the seabed, and potentially moved muddy deposits. Preliminary field observations suggested that most of the core sites appear largely unchanged since June, with the exception of the shallowest site at T2, off Wairoa River (Figure 37).

A compilation of selected cores and regional sites captures some of the more compelling evidence for preservation of possible Cyclone Gabrielle event deposits (Figure 38). Some may already have undergone some modification from wave reworking and bioturbation in the months since the cyclone. The upcoming Fisheries New Zealand Aquatic Environment and Biodiversity Report for the SEA2022-13 Cyclone Gabrielle sediment analysis project will provide a comparison of visual observations on freshly collected sediment cores with x-ray computer tomography scans.

KAH2303
Station: 36
Site: T2 #1
Region: Wairoa

KAH2306
Station: 13
Site: T2 #1
Region: Wairoa

Figure 37: Contrasting sediment and substrate characteristics at site T2 #1 (28 m water depth) offshore of the Wairoa River. The core from site T2 #1 recovered in June (left; KAH2303 station 36) was largely very-fine sand with a variable overlying muddy layer up to a few centimetres in thickness. The sandy nature of the seabed resulted in relatively short core penetration into the substrate. The core from the same site recovered in October (right; KAH2306 station 13) shows a much thicker accumulation of stratified soft mud, visible as colour banding from brown and green-grey muds to dark grey sand at the core base.
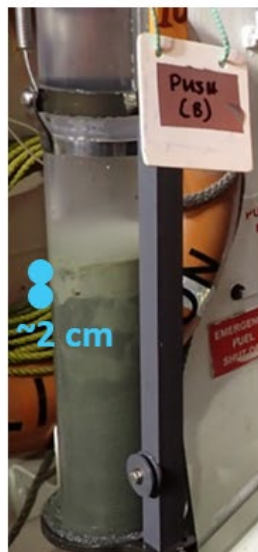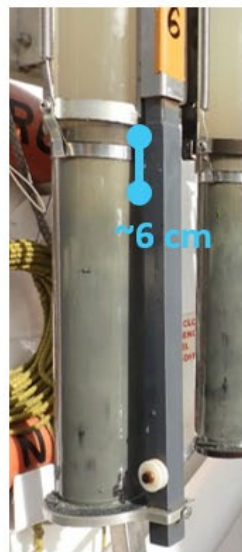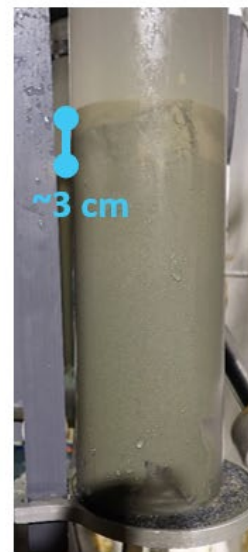
Figure 38: Field-based estimates of possible Cyclone Gabrielle event deposits in freshly collected core samples based on visual observations of sediment colour and texture (June and October 2023 surveys; KAH2303 and KAH2306, respectively).

3.2.3   Infauna

Woody debris

Woody debris was present in all the macrofauna samples we analysed from the Hawke's Bay and Gisborne regions, in both 2010 surveys (KAH1006 and KAH1010) and 2023 surveys (KAH2303 and KAH2306) (Appendix 5). Mean woody debris concentration across all the samples was 17.43 g m^{-2}. Values were highly variable both spatially and temporally. Wood debris concentrations were generally lower at inshore sites relative to offshore sites (Figure 39); however, the highest wood debris concentration (124.78 g m^{-2}) was recorded from a shallow site off Poverty Bay sampled in May 2010 (KAH1006 station 206, 18 m depth), while a sample collected at the same site in October of the same year had a much lower concentration of 3.82 g m^{-2}.
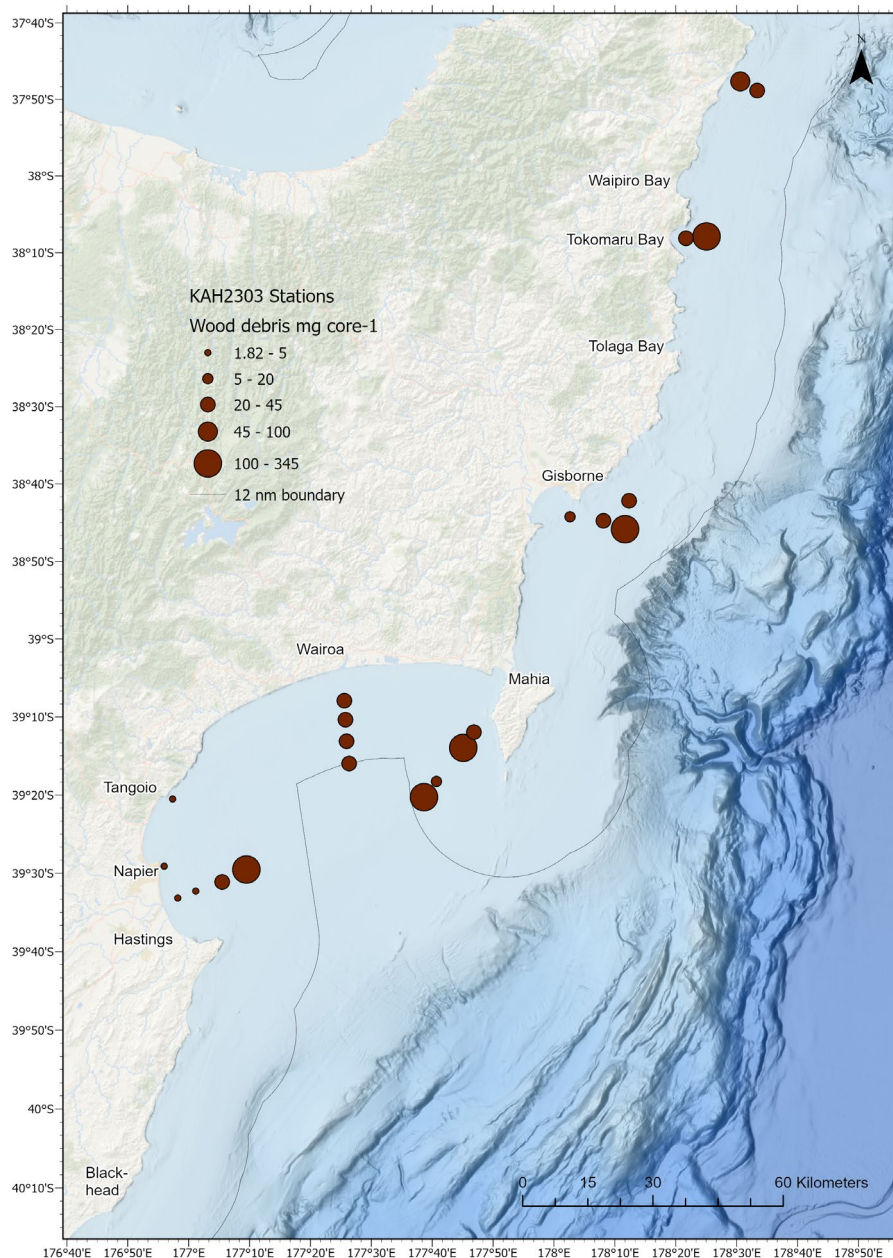
Figure 39:   Concentration of woody debris (mg core^{-1}) in macrofauna samples obtained in Hawke's Bay and Gisborne during the June 2023 RV *Kaharoa* survey KAH2303.

Meiofauna and macrofauna: June survey

Analyses of core samples obtained during the June survey showed that meiofauna abundance was highly variable across the Hawke's Bay and Gisborne regions, ranging from less than 100 individuals 10 cm^{-2} off the Waiapu River (21 m depth) to approximately 2500 individuals 10 cm^{-2} at two sites in Hawke Bay (40–47 m depth, Figure 40, Appendix 6). Average meiofauna density across all of the sites was 1014 individuals 10 cm^{-2}. Meiofauna abundance tended to be highest at intermediate depths in samples collected along the Hawke's Bay coring transects, and tended to increase with depth/distance from shore in the Gisborne coring transects.

A total of 16 meiofauna taxa were identified from the June survey samples (Appendix 7). An average of five taxa were present in each sample (range: 1–8 taxa per sample). Meiofauna communities were dominated by nematodes (94% of all individuals). Other relatively abundant taxa include harpacticoid copepods (2.4% of total), kinorhynchs (1.5%), and annelids (1.4%).

Meiofauna total abundance was significantly and positively correlated with mud content (DistLM, $P < 0.05$, $R^2 = 0.19$) but was not significantly correlated with any of the other environmental variables ($P > 0.05$) (Figure 41). Taxon richness, evenness, and diversity were significantly and positively correlated with water depth ($P < 0.05$, $R^2 = 0.19$–0.29) but not with any of the other predictor variables. Meiofauna community structure was significantly correlated with water depth and mud content ($P < 0.05$, $R^2 = 0.14$ and 0.16, respectively) but was not significantly correlated with sediment total organic matter content, wood debris content, or event layer thickness (DistLM, $P > 0.05$).
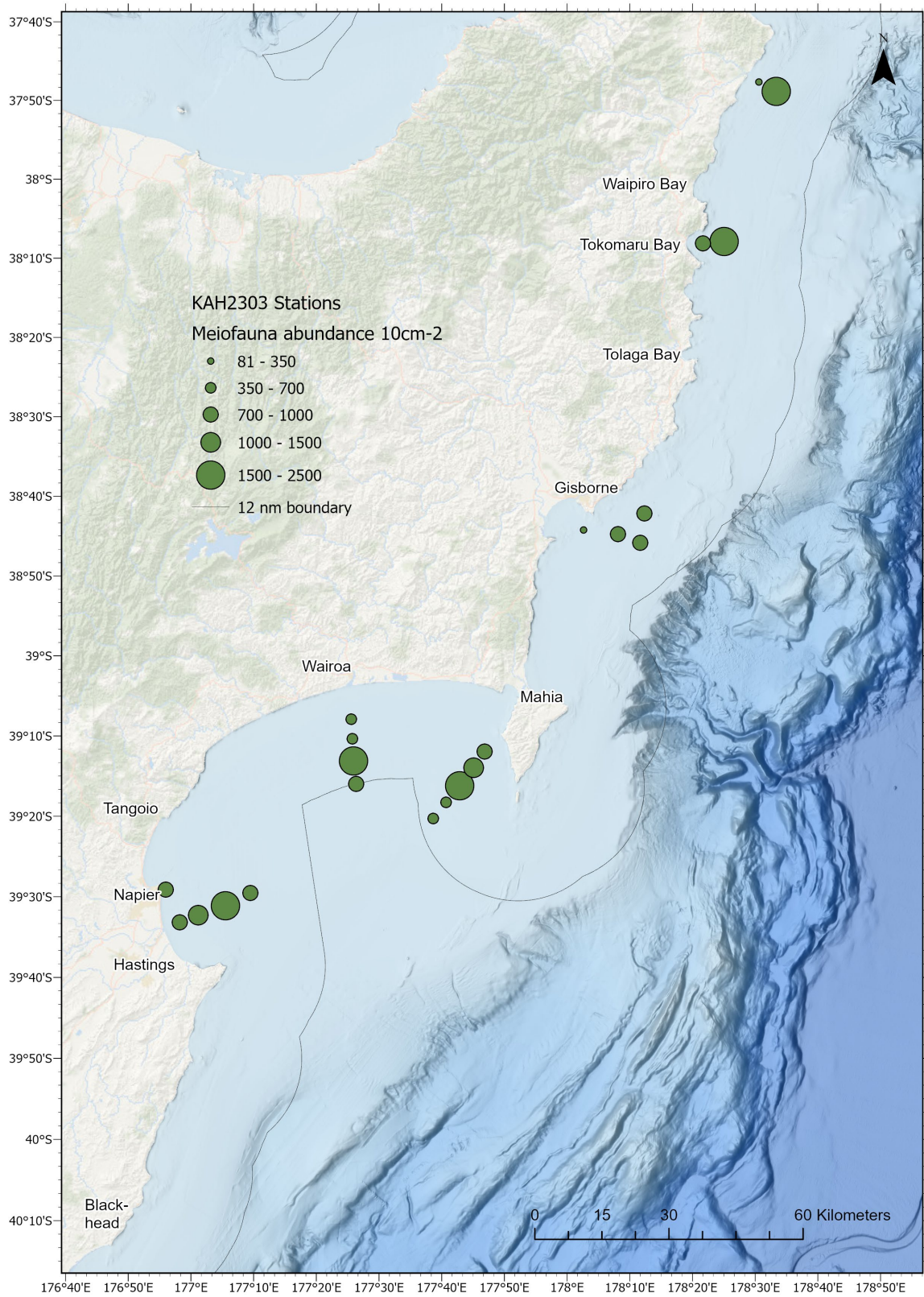
Figure 40: Meiofauna abundance (individuals per 10 cm²) in samples obtained in Hawke's Bay and Gisborne during the June 2023 RV *Kaharoa* survey KAH2303.
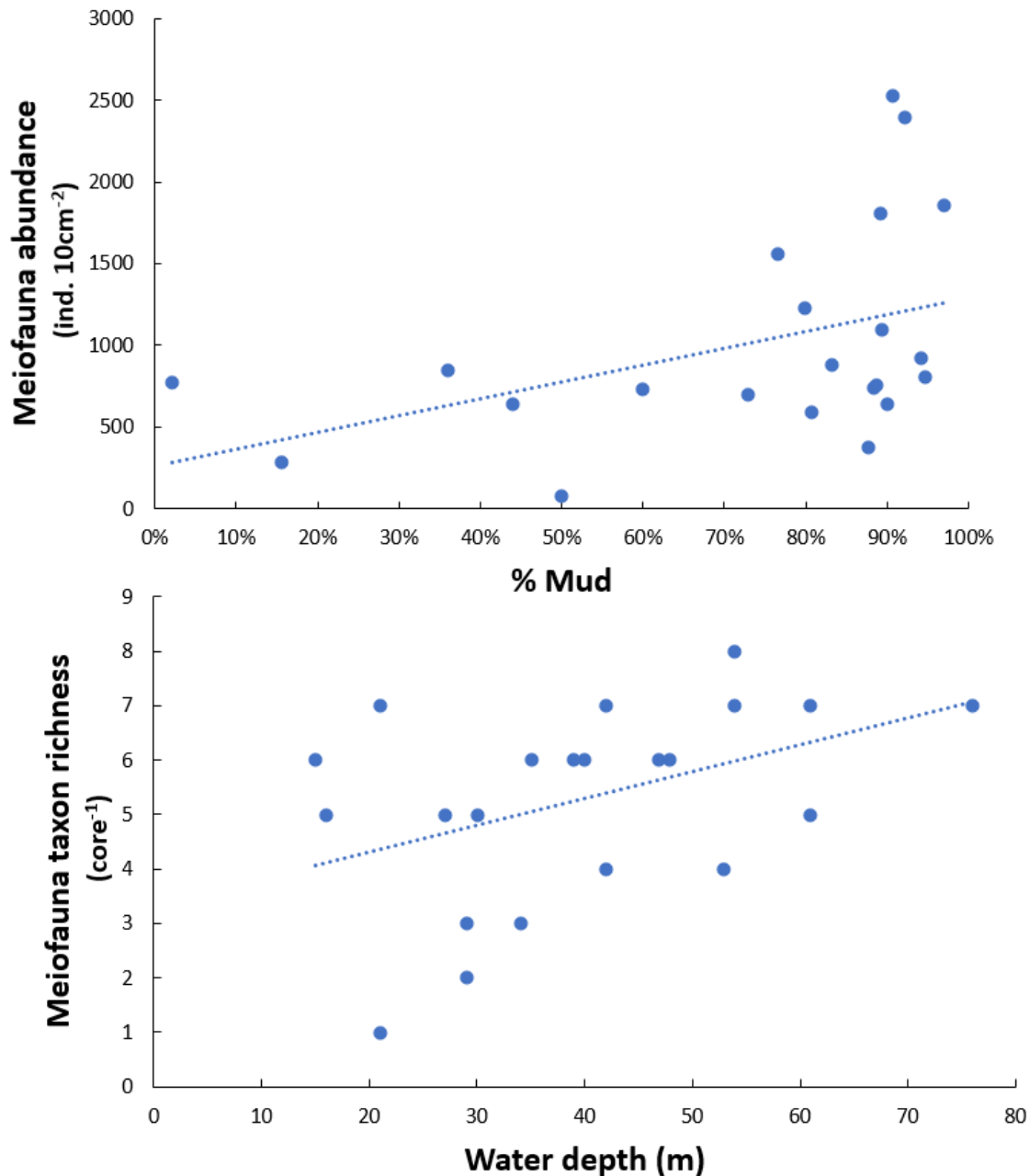
Figure 41: Relationship between sediment mud content and meiofauna abundance and between water depth and meiofauna taxon richness in samples obtained in Hawke's Bay and Gisborne during the June RV *Kaharoa* survey KAH2303.

Macrofauna abundance across the Hawke's Bay and Gisborne regions ranged from one individual in the core obtained from Tangoio Reef (1.4 ind. 0.01 m^{-2}, 31 m depth) to 68 individuals in a core obtained along the T3 transect off Nuhaka River (95.9 ind. 0.01 m^{-2}, 76 m depth; Figure 42, Appendix 8). Average macrofauna densities across all the sites was 41 individuals 0.01 m^{-2}. Macrofauna density tended to increase with distance from shore along all coring transects, except for transect T3 where the highest abundance was seen in the core collected furthest offshore but the lowest macrofauna abundance was in the middle of the transect.

A total of 84 macrofauna taxa were identified, with crustaceans (amphipods, cumaceans, and isopods), molluscs (gastropods and bivalves), and polychaetes identified to species/morphospecies by taxonomists. The most abundant taxon was the polychaete *Capitella* sp.1 (16% of all individuals). Other abundant taxa included the paranoid polychaete *Aricidea* sp. 1 (8% of total), the bivalve *Theora lubrica*

(6%), nematodes (5%), and the polychaetes *Syllis* sp. 1 and *Cossura consimilis* (each 4%) (Appendix 9). An average of ten taxa were present in each sample (range:1–23 taxa per sample).

Macrofauna total abundance was significantly and positively correlated with water depth and mud content (DistLM, $P < 0.05$, $R^2 = 0.43$ and 0.26, respectively) but was not significantly correlated with any of the other environmental variables ($P > 0.05$) (Figure 43). Taxon richness and diversity were significantly and positively correlated with water depth ($P < 0.05$, $R^2 = 0.47$ and 0.26, respectively) but not with any of the other predictor variables. No significant correlations were found for taxon evenness. Macrofauna community structure was significantly correlated with water depth and mud content ($P < 0.05$, $R^2 = 0.08$ and 0.07, respectively) but was not significantly correlated with sediment total organic matter content, wood debris content, or event layer thickness (DistLM, $P > 0.05$).

Figure 42: Macrofauna abundance (individuals per 0.01 m^2) in samples obtained in Hawke's Bay and Gisborne during the June 2023 RV *Kaharoa* survey KAH2303.

Figure 43: Relationship between water depth and macrofauna abundance and taxon richness in samples obtained in Hawke's Bay and Gisborne during the June RV *Kaharoa* survey KAH2303.

Macrofauna: pre- and post-cyclone comparisons off Poverty Bay

Macrofauna abundances in samples obtained in 2010 off Poverty Bay ranged from 17 to 181 individuals 0.01 m^{-2} (mean = 75 ind. 0.01 m^{-2}; Appendix 8). A total of 42 macrofauna taxa were identified from the 2010 samples, with gastropod and bivalve molluscs identified to species/morphospecies (Appendix 9). The most abundant taxon was polychaetes (49% of all individuals), followed by foraminiferans (16%), cumaceans (5%), ostracods, and amphipods (4% each). An average of ten taxa were present in each sample (range: 4–16 taxa per sample). There was no significant difference in macrofauna community structure between the May 2010 and October 2010 samples (PERMANOVA, P > 0.1).

Macrofauna total abundance and taxon richness were both significantly and positively correlated with water depth (DistLM, P < 0.01, R^2 = 0.79 and 0.66, respectively). Community structure was also significantly correlated with water depth (P < 0.01, R^2 = 0.24) (Figure 44). There were no significant correlations for taxon diversity or evenness.

PERMANOVA results show a significant difference in macrofauna abundance, taxon richness, and community structure between the 2010 and 2023 data off Poverty Bay (P < 0.05, with water depth as covariate). Macrofauna abundance in the 2023 samples was ~35–40 individuals 0.01 m^{-2} lower than macrofauna abundance in the 2010 samples across the 25–55 m water depth range. Macrofauna taxon richness in the 2023 samples was ~3–5 taxa $core^{-1}$ lower than macrofauna taxon richness in the 2010 samples across the same water depth range. Taxon evenness and diversity did not differ significantly between the two sampling years (P > 0.1).

The dissimilarity between the 2010 and 2023 surveys was 57.5% (SIMPER). SIMPER results show that eight taxa were responsible for at least 5% of overall dissimilarity between the 2010 and June 2023 communities (Table 8). Foraminiferans accounted for 11% of total dissimilarity and were slightly more abundant in the June 2023 samples than in the 2010 samples. Polychaetes accounted for 10% of total dissimilarity and showed the opposite pattern to foraminiferans; the bivalve *Nucula* sp., ophiuroids, amphipods, and ostracods were also more abundant in the 2010 samples than in the June 2023 samples. Like foraminiferans, nematodes were more abundant in the June 2023 samples than in the 2010 samples. The taxonomic resolution in the 2023 dataset had to be reduced by grouping polychaete and crustacean species/morphospecies to enable comparisons with the 2010 dataset. It is likely that the dissimilarity in macrofauna community structure between the 2010 and 2023 sampling years was underestimated as a result of this reduced taxonomic resolution.

Table 8: **SIMPER results* listing taxa responsible for differences in community structure between the 2010 (KAH2006 and KAH1010) and June 2023 surveys (KAH2303), based on square root-transformed data and the Bray-Curtis similarity measure. Only taxa contributing at least 5% to total dissimilarity between the survey years are shown.**

| Taxa | Average abundance $core^{-1}$ | | Av.Diss | Diss/SD | Contrib% | Cum.% |
	KAH2023	KAH1006 & KAH1010				
Foraminiferans	8.3	8.1	6.46	1.33	11.3	11.3
Polychaetes	22.0	25.3	6.17	1.38	10.7	22.0
Cumaceans	4.0	2.6	4.41	1.34	7.7	30.0
Nematodes	3.3	0.5	3.78	1.36	6.6	36.3
Nucula sp.	0	2.8	3.37	0.74	5.9	42.1
Ophiuroids	1.5	1.7	3.07	1.36	5.3	47.5
Amphipods	2.0	2.3	3.06	1.01	5.3	52.8
Ostracods	0.5	2.4	2.98	1.12	5.2	58.0

* Av.Diss: average dissimilarity; Diss.SD: dissimilarity to standard deviation ratio; Contrib%: percent contribution to total dissimilarity; Cum.%: percent cumulative dissimilarity.

The non-metric multi-dimensional scaling (nMDS) plot shows the relative dissimilarities between samples and sampling years (Figure 45). The two shallower macrofauna samples obtained in June 2023 (stations 58 and 61, 27 and 42 m water depth, respectively) are located away from most other samples on the nMDS plot and close to the two shallowest samples obtained in 2010 (stations 206 and 339, both 18 m water depth). In contrast, the deeper macrofauna samples obtained in June 2023 (stations 66 and 67, 54 and 53 m water depth, respectively) are placed in closer proximity to the 2010 samples.
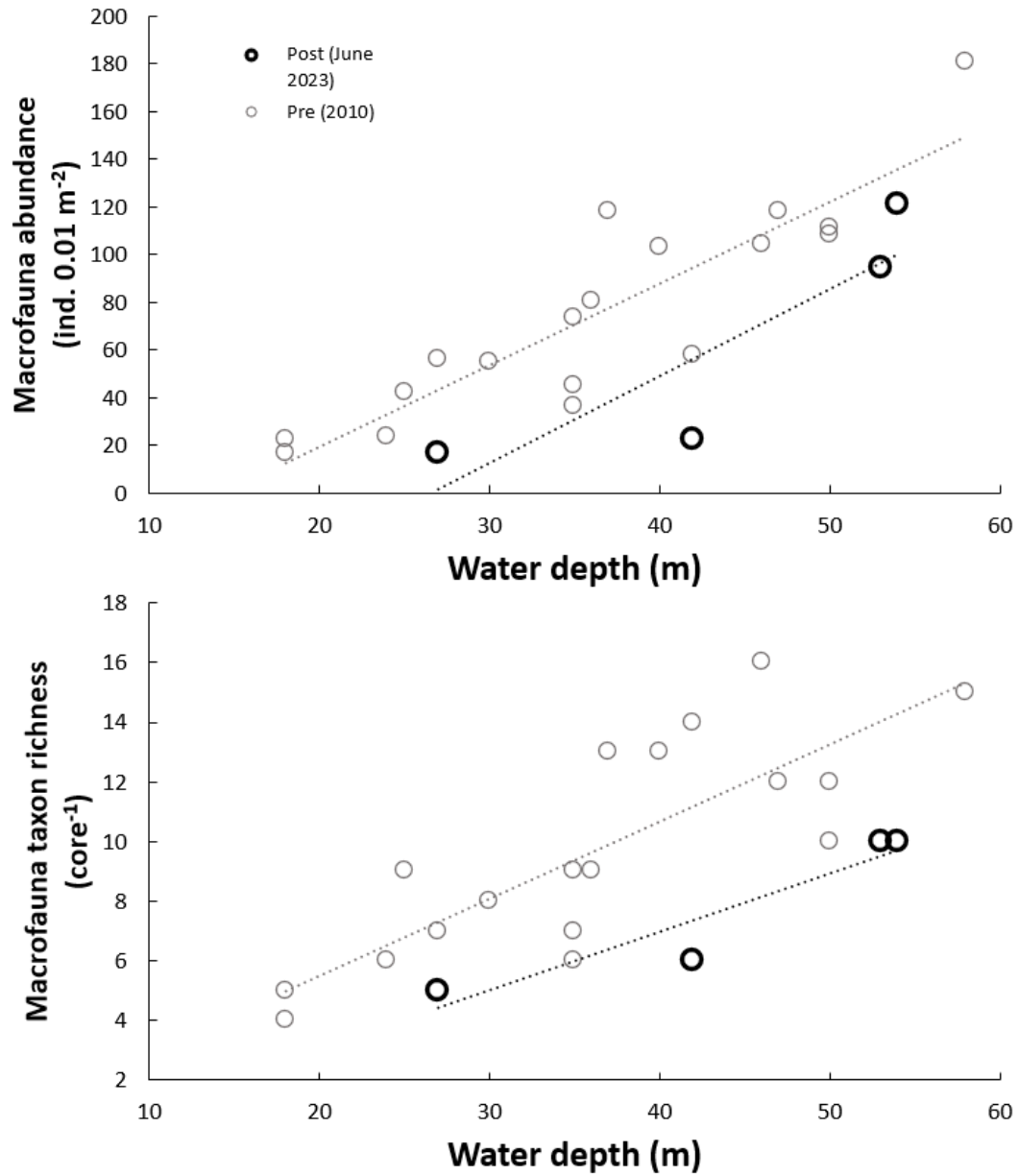
Figure 44: Relationship between water depth and macrofauna abundance and taxon richness in samples off Poverty Bay obtained in 2010 (grey circles) and 2023 (black circles).

Figure 45: Non-metric multi-dimensional scaling (nMDS) plot showing the relative dissimilarities between samples and sampling years, i.e., 2010 (light grey circles) and 2023 (black circles). Labels show station numbers. See Figure 3, Figure 4, and Figure 9 for location of samples.

Macrofauna: October vs June survey comparisons

Macrofauna abundance in the October survey samples ranged from 37 individuals $0.01\,m^{-2}$ in a sample obtained off Poverty Bay (T4 transect, 40 m water depth) to 218 individuals $0.01\,m^{-2}$ in a sample taken along the T2 transect off Wairoa River (61 m water depth) (Figure 46; Appendix 8). Average macrofauna densities across all the sites was 90 individuals $0.01\,m^{-2}$. Although fewer core samples were obtained than in the June survey, the trend of increasing macrofauna abundance moving further offshore along coring transect T2, and to a lesser extent coring transect T1, were similar to the trends observed in samples from the June survey (Figure 42).

A total of 49 macrofauna taxa were identified in the October survey samples, with crustaceans (amphipods, cumaceans, and isopods) and molluscs (gastropods and bivalves) identified to species/morphospecies by taxonomists (Appendix 9). The most abundant taxon were the polychaetes (49% of all individuals), followed by nematodes (10%), the amphipod *Photis brevicaudata* (5%), ostracods (4%), and foraminiferans (4%). An average of 12 taxa were present in each sample (range: 5–24 taxa per sample). The two samples with highest number of taxa were obtained along the T1 and T2 coring transects (both at 61 m water depth) in Hawke Bay.

Macrofauna total abundance was not significantly correlated with water depth (DistLM, $P > 0.05$) partly due to one deep sample with relatively low abundance (40 ind. $0.01\,m^{-2}$) obtained at 146 m water depth along the T6 transect off the Waiapu River (Figure 47). Omitting this sample resulted in a trend of increasing macrofauna abundance with water depth, but the relationship was not statistically significant ($P > 0.05$). A similar trend was observed for taxon richness; however, the removal of the same deep sample resulted in a positive, statistically significant relationship between water depth and taxon richness ($P < 0.05$). Macrofauna taxon diversity (H') was positively correlated with depth (all October 2023 samples included; $P < 0.05$) whereas there was no relationship for taxon evenness with or without the deep sample ($P > 0.05$).
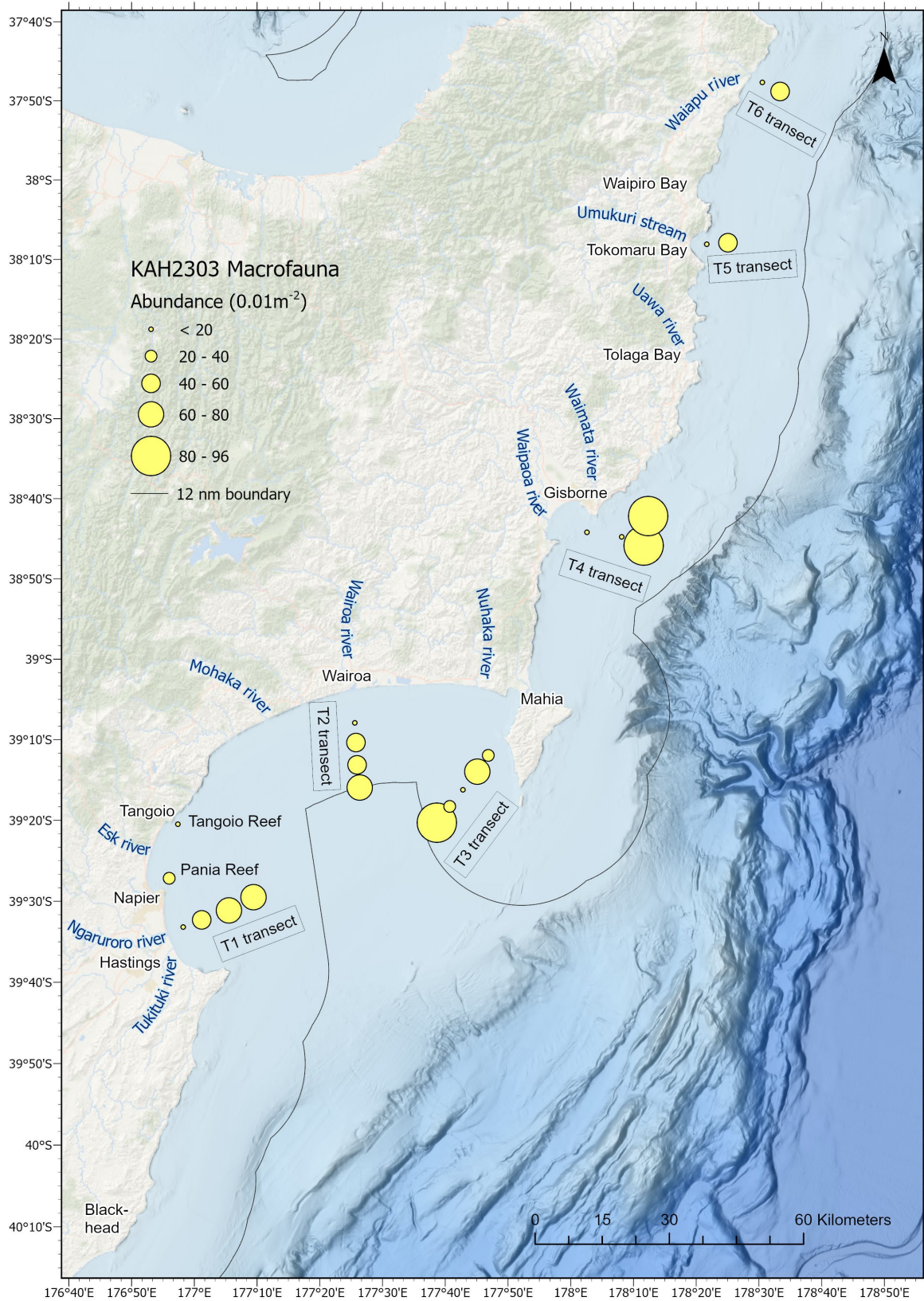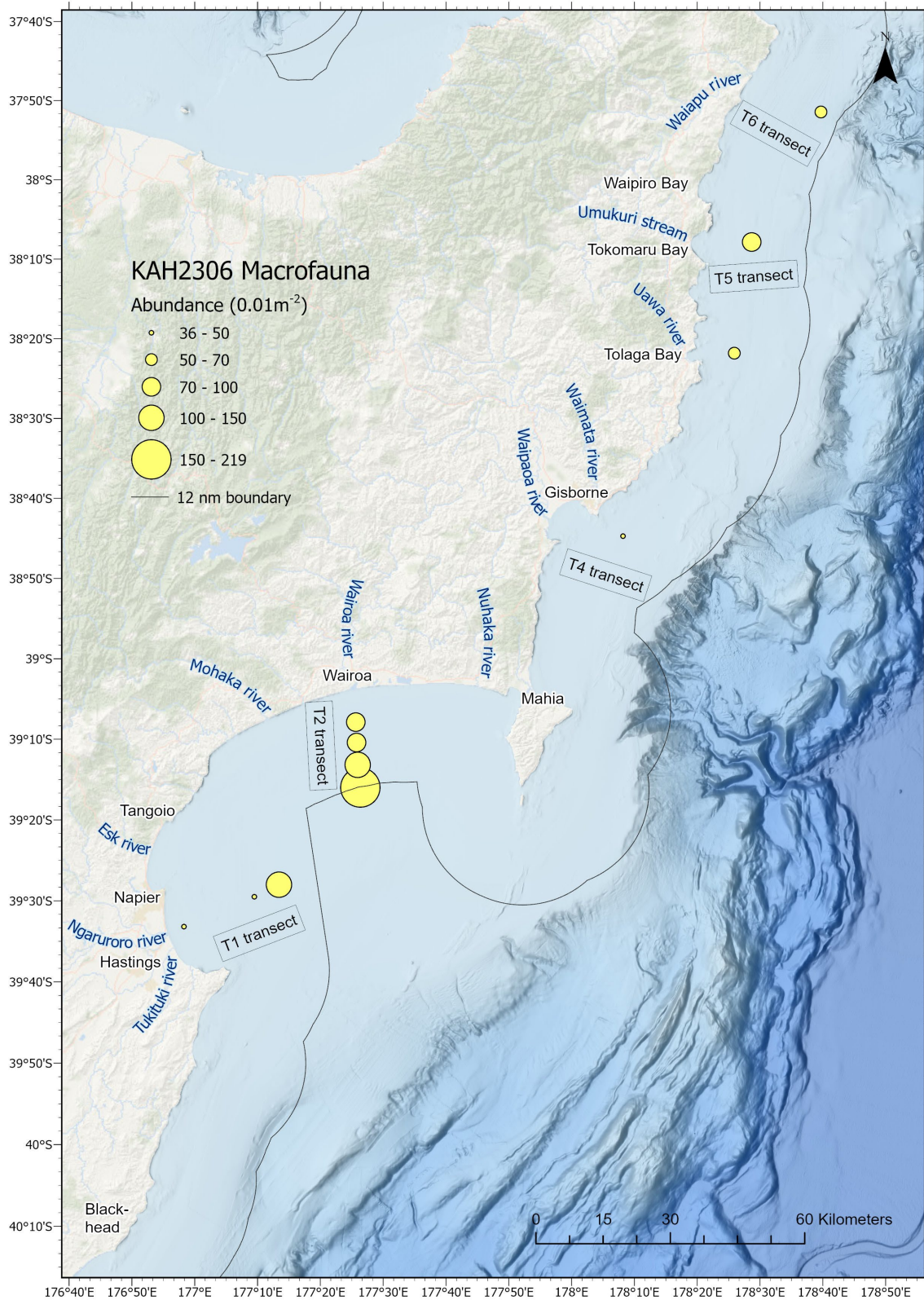
Figure 46: Macrofauna abundance (individuals per 0.01 m^2) in samples obtained in Hawke's Bay and Gisborne during the October 2023 RV *Kaharoa* survey KAH2306.
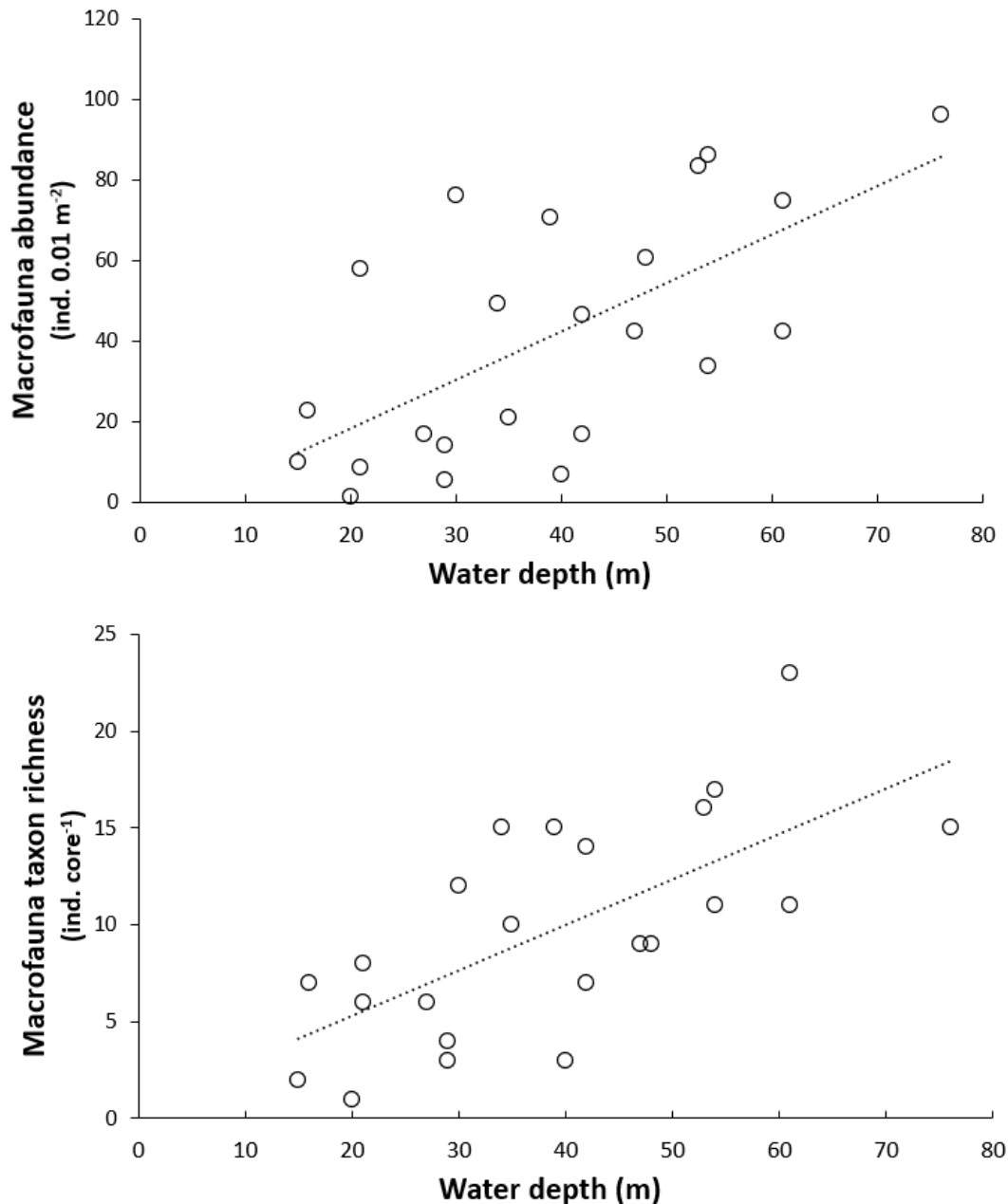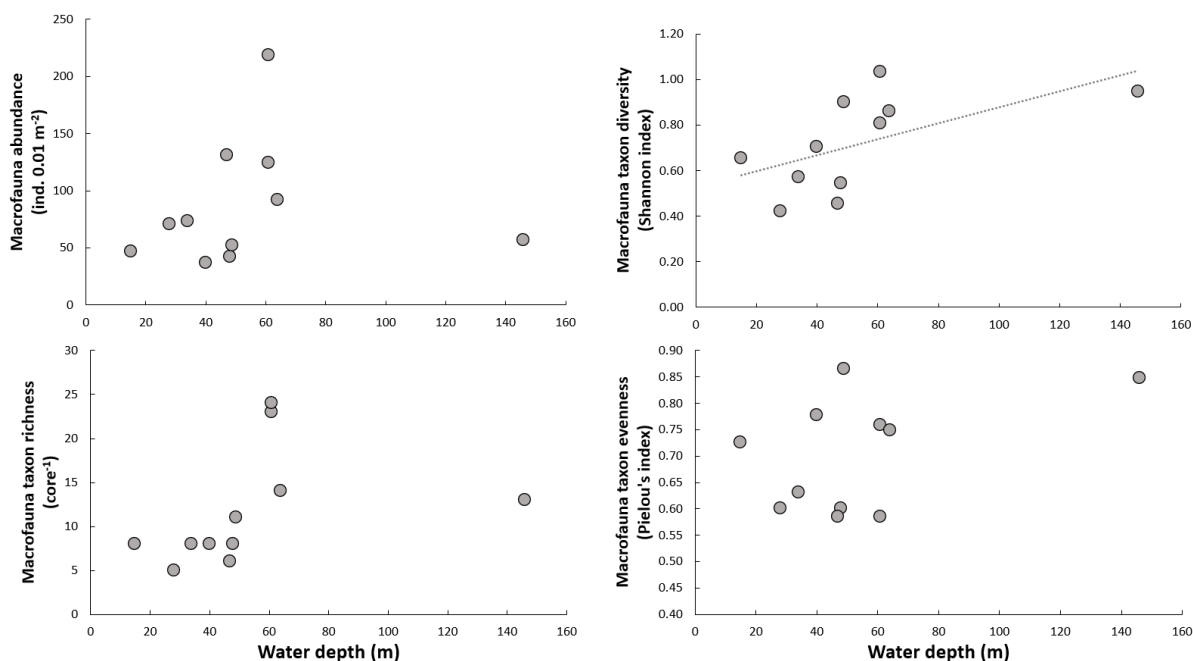
Figure 47: Relationship between water depth and macrofauna abundance, taxon richness, taxon diversity, and taxon evenness in samples obtained in the 2023 October survey (KAH2306) in the Hawke's Bay and Gisborne regions. The dotted line shows a statistically significant correlation (DistLM, P < 0.05).

PERMANOVA results comparing sites sampled in both June and October 2023 (n = 7) show a significant difference in macrofauna abundance and community structure between the surveys (P < 0.05, with water depth as covariate) (Figure 48). On average, macrofauna abundance in the October samples was 52 individuals 0.01 m⁻² greater than in the June samples; October values were consistently greater than in June when comparing individual sites, except for a site on the T1 coring transect (48 m depth) where the abundance in October was slightly lower than in June (42 vs. 51 individuals 0.01 m⁻²). Macrofauna taxon richness, diversity, and evenness did not vary significantly between the June and October surveys (P > 0.05).

The dissimilarity between the June and October 2023 surveys was 68.1%. SIMPER results show that four taxa were responsible for at least 5% of overall dissimilarity between the June and October 2023 communities (Table 9). Polychaetes, nematodes, and the amphipod *Photis brevicaudata* accounted for most of the dissimilarity between the two surveys and were all substantially more abundant in October than in June. The bivalve *Maorimactra ordinaria* also contributed to the dissimilarity between surveys but was more abundant in June than in October.
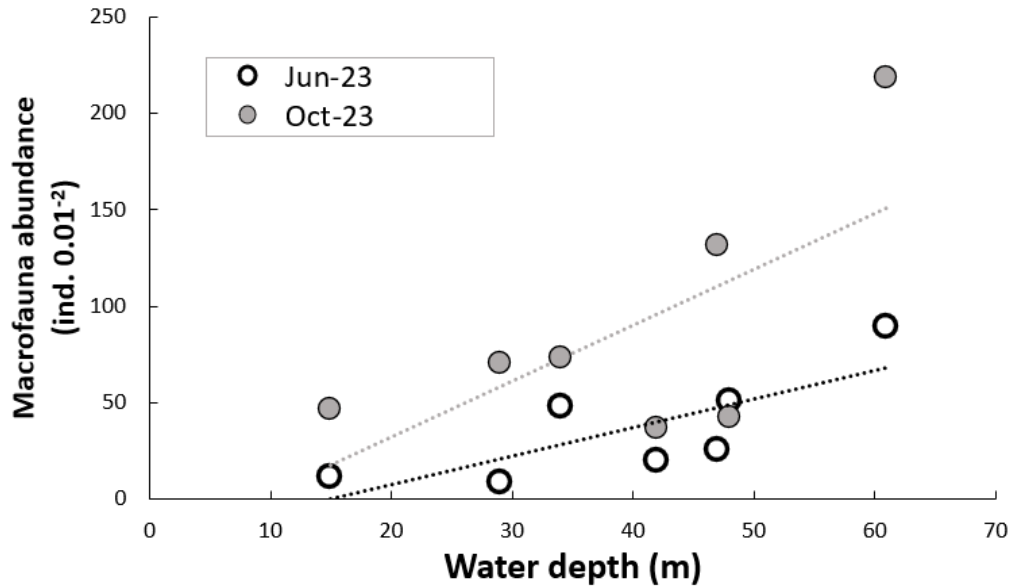
Figure 48: **Relationship between water depth and macrofauna abundance in the 2023 June and October surveys (KAH2303 and KAH2306, respectively) in the Hawke's Bay and Gisborne regions. The black dotted line shows a statistically significant correlation for the June data (DistLM, $P < 0.05$); grey dotted line shows non-significant trend for the October data ($P > 0.05$).**

Table 9: **SIMPER results* listing taxa responsible for differences in community structure between the June (KAH2023) and October 2023 surveys (KAH2306), based on square root-transformed data and the Bray-Curtis similarity measure. Only taxa contributing at least 5% to total dissimilarity between the survey years are shown.**

Taxa	Average abundance core^{-1}		Av.Diss	Diss/SD	Contrib%	Cum.%
	KAH2023	KAH2306				
Polychaetes	12.7	35.3	9.71	1.39	14.3	14.3
Nematodes	2.3	8.3	6.98	1.04	10.2	24.5
Photis brevicaudata	0.0	3.9	5.64	0.84	8.3	32.8
Maorimactra ordinaria	2.7	1.1	4.67	0.97	6.9	39.6

* Av.Diss: average dissimilarity; Diss.SD: dissimilarity to standard deviation ratio; Contrib%: percent contribution to total dissimilarity; Cum.%: percent cumulative dissimilarity.

The non-metric multi-dimensional scaling (nMDS) plot shows the relative dissimilarities between the June and October samples (Figure 49). Samples from the June survey form a largely separate cluster from samples obtained in the October survey. The only exception is station 43 from the June KAH2303 survey (T1 coring transect, 48 m water depth) which is located among the October survey samples and closest to the sample obtained at the same site in October (KAH2306 station 2). We note that this site was characterised by the thickest deposition of fine sediments (~15 cm) across the study region; this deposit was first observed in the June survey and was again observed during the October survey (see Section 3.2.2).
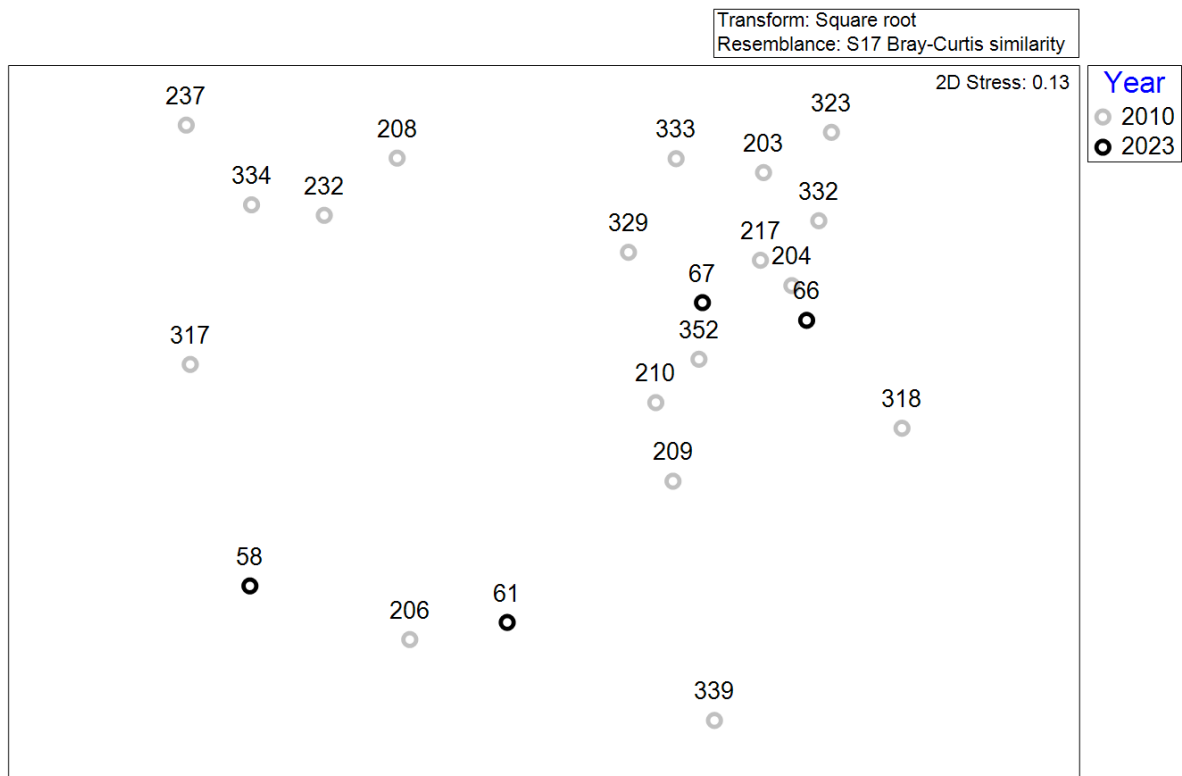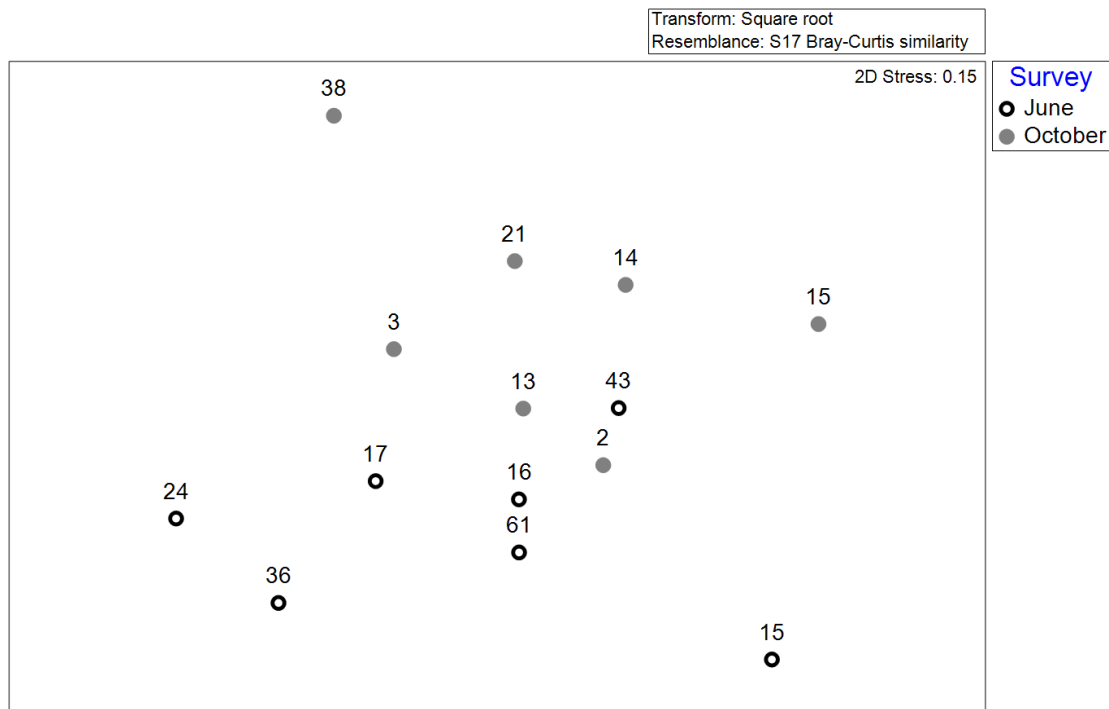
Figure 49: Non-metric multi-dimensional scaling (nMDS) plot showing the relative dissimilarities between sites sampled in June 2023, then revisited in October 2023 in the Hawke's Bay and Gisborne regions. Labels show station numbers.

3.2.4 Camera transects

The location of all towed camera transects conducted in Hawke's Bay and Gisborne regions during the June and October surveys are shown in Figure 50 and Figure 51, respectively.

The first RV *Kaharoa* voyage in June experienced very poor water visibility at the seafloor, along with large swells of 2–3 m in height. While most target sites were surveyed, none of those in less than 50 m water depth returned useable video footage due to extremely poor visibility. Those in deeper water had better seafloor visibility, but the effect of swells on the vessel was directly transmitted down the tow cable to the camera (CoastCam), resulting in poor coverage of the seafloor. The size of the field of view was also affected, along with the video resolution, making it impossible to calculate swept area. Conditions during the October survey were much improved with good underwater visibility and mostly calm seas. Results from both voyages are presented together, working from the south to the north.
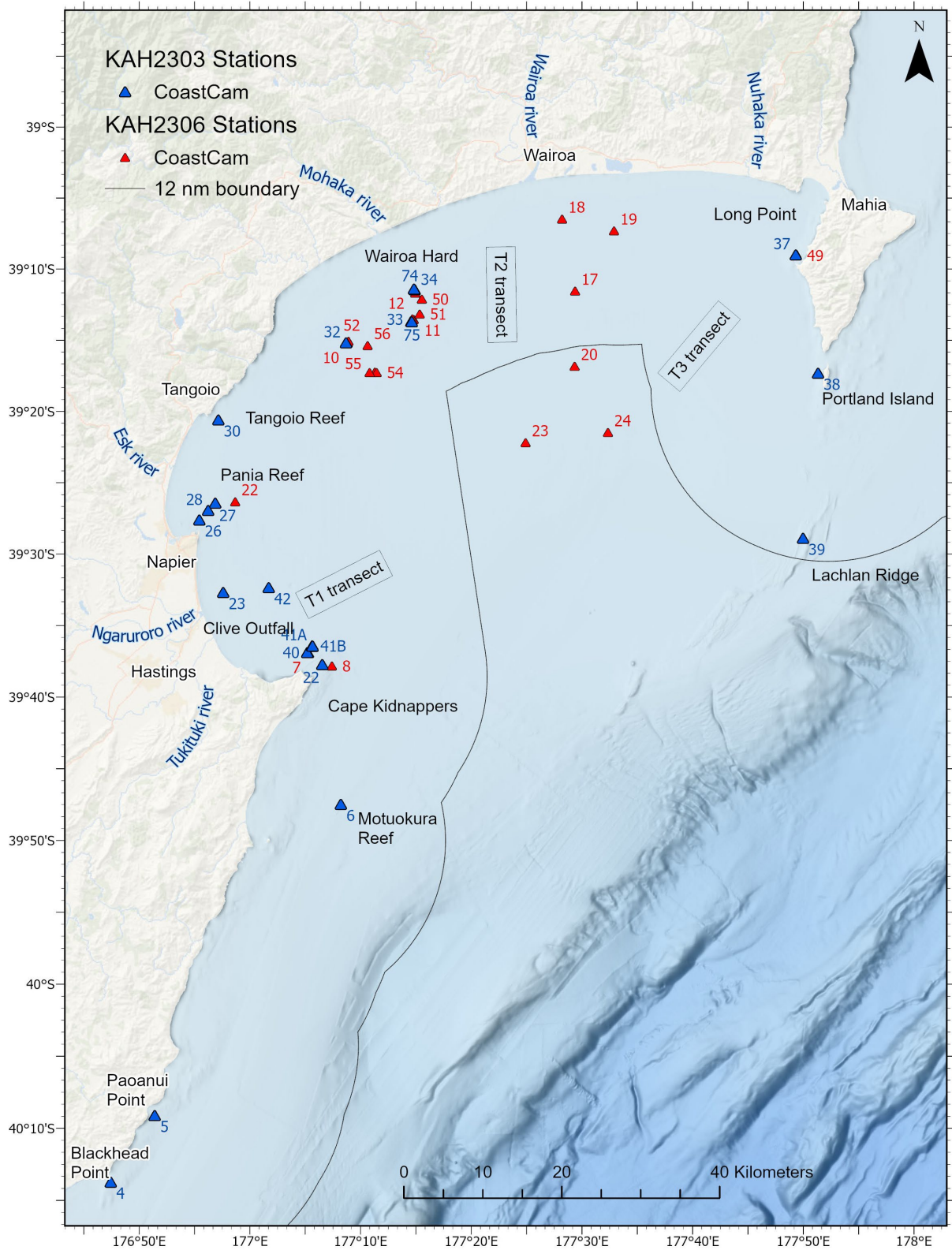
Figure 50: Location of all towed camera transects conducted in the Hawke's Bay region during the June and October RV *Kaharoa* surveys (KAH2303 and KAH2306, respectively).
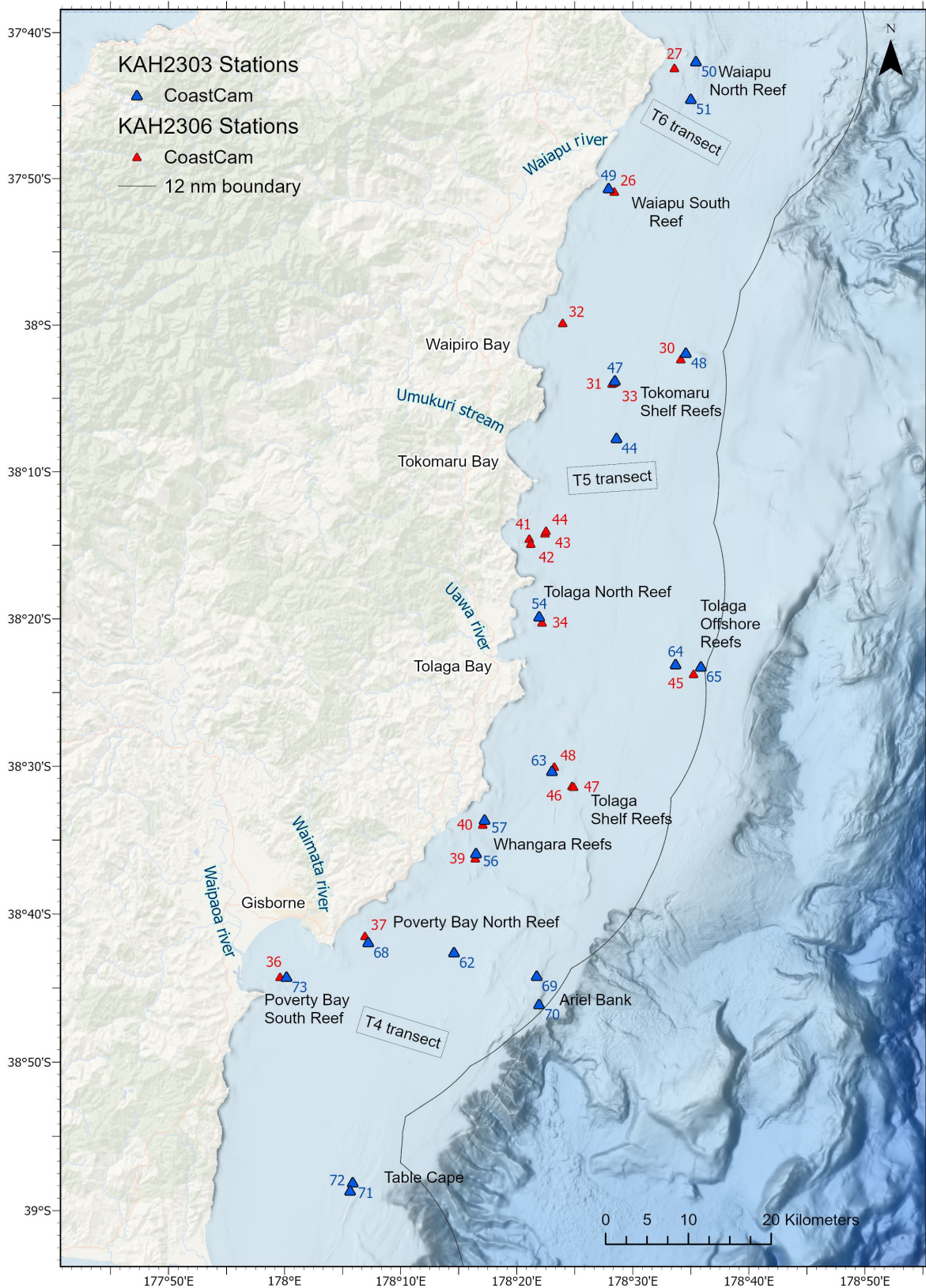
Figure 51: Location of all towed camera transects conducted in the Gisborne region during the June and October RV *Kaharoa* surveys (KAH2303 and KAH2306, respectively).

Near-bed turbidity

Near-bed turbidity values (~1–2 m above the seafloor) during the October survey are shown in Figure 52. Inshore stations had generally higher values than mid-shelf and outer shelf stations. The highest turbidity values occurred in Wairoa Hard offshore of the Mohaka River and offshore of the Wairoa River. The water column was stratified with highest turbidities within the benthic boundary layer. In Hawke Bay in particular, a turbid layer extended 2–5 m above bed, as evident with the very poor near-bed visibility in the benthic video footage from the central bay.
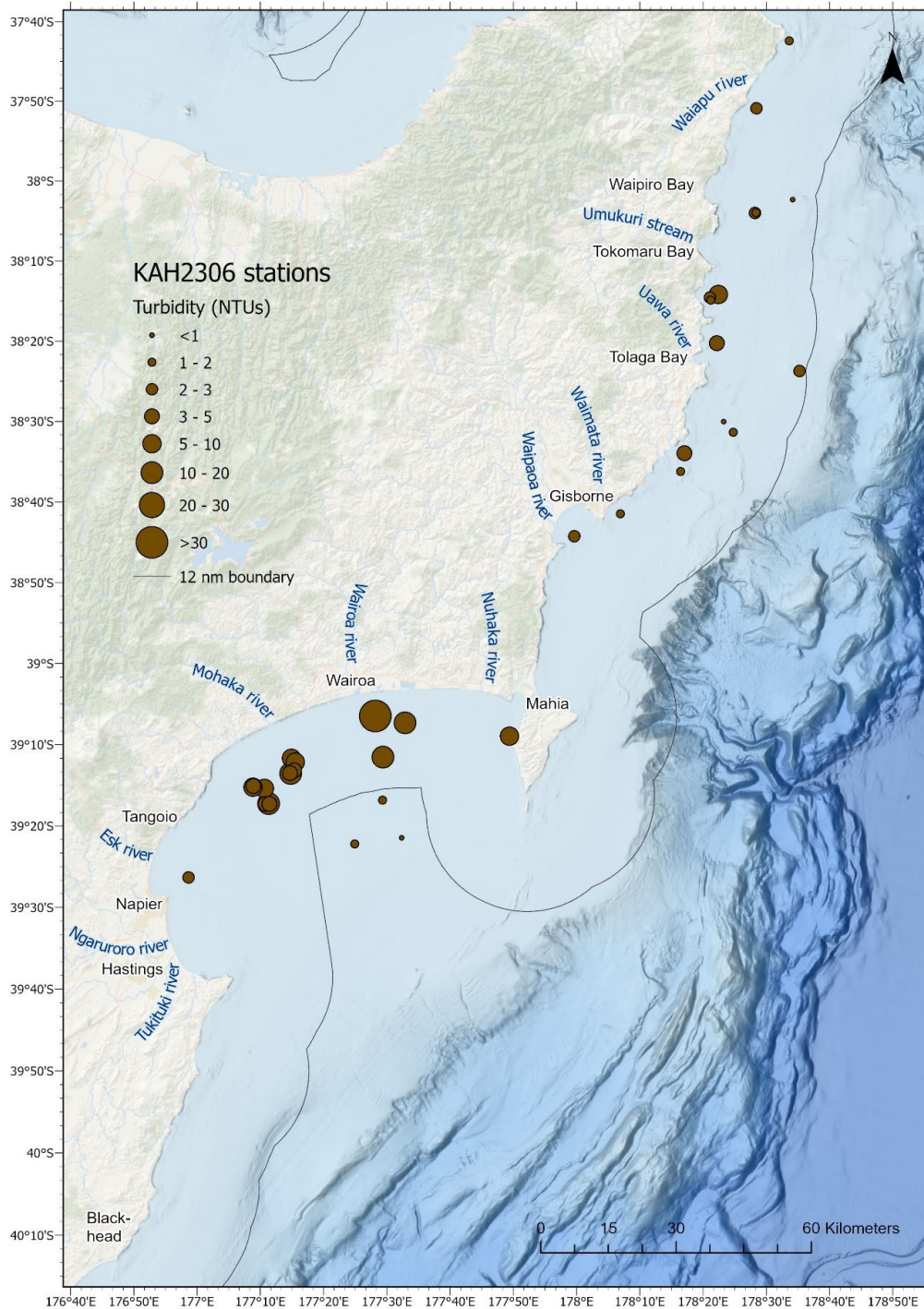
Figure 52: Turbidity values (Nephelometric Turbidity Units or NTUs) from the October RV *Kaharoa* survey KAH2306. No data were obtained near Cape Kidnappers due to instrument malfunction.

Health of kelp Ecklonia radiata

The number of kelp plants in each class for stations where kelp was present is shown in Table 10. Four locations were characterised by kelp at sufficiently high densities to constitute kelp forest (i.e., ~2 plants m^{-2} or more): Paoanui Point, Pania Reef, Poverty Bay North reef, and Gables reef. For the other sites, numbers were too low (Blackhead Point), or plants were too scattered (Arial Bank site B) to constitute kelp forests. The healthiest kelp populations were those of Hawke Bay, with healthy plants contributing 98 to 100% of all adults across four locations. The kelp populations around and offshore of Poverty Bay had lower proportions of healthy plants (88 to 94%, across three locations).

Table 10: **Classes of kelp *Ecklonia radiata* by location (southernmost on left, northernmost on right). Numbers are counts. Recruits may have been under-counted at Pania Reef and Mahia West due to low water visibility. See Figure 11 and Figure 12 for the details of locations.**

	Paoanui Point	Blackhead Point	Pania Reef	Mahia West	Table Cape	Ariel Bank	Poverty Bay north	Location Gables reef
Survey	June	June	October	October	October	October	October	October
Plant class								
New recruit	19	–	–		–	8	–	–
Stalked recruit	17	–	–	2	–	–	–	3
Adults:								
Holdfast only	9	–	–		–	1	–	1
Holdfast & stipe	–	–	1		1	1	–	15
Fronds rotting	–	–	–	3	–	2	88	13
Central thalli healed	–	–	–		–	–	6	8
Healthy	478	26	53	152	–	62	823	272
% Adults healthy	98%	100%	98%	98%	–	94%	90%	88%

Paoanui Point and Blackhead Point

Water clarity was good at both Paoanui Point and Blackhead Point in the southern Hawke's Bay coastal region when surveyed in June 2023 (see Figure 11). *Ecklonia radiata* kelp plants were largely healthy, and no evidence of fine sedimentation was seen on the reefs or the adjacent rippled sand. Collectively, the ecological assemblages at these locations were in line with what would be expected for an open coastal reef away from major sediment inputs, and there was no evidence of sediment impacts.

At Paoanui Point within the Te Angiangi Marine Reserve, extensive reef extended out from the shore, interspersed with patches of sand (Appendix 10). An *Ecklonia radiata* kelp forest was present across the main reef area (Figure 53). This forest occurred as patches, and was not continuous, occurring on both rock outcrops and on flat bedrock with a thin sand veneer. A small, foliose red alga was common, along with patches of remnant rhizomes of green alga *Caulerpa* sp. without blades (note that this alga was not the invasive exotic species *Caulerpa brachypus* or *Caulerpa parvifolia*). At least five other species of red macroalgae were also present, along with patches of the green alga *Codium* sp. Pink coralline algae were widespread as small patches. The soft bryozoan *Margaretta barbata* was common and widespread, as well as sponges, gastropods, sea cucumbers, and fish.

The Blackhead Point location held similar reef habitats as Paoanui Point (Figure 54, Appendix 10), although the kelp *Ecklonia radiata* was less abundant. The same red macroalgae as at Paoanui Point were present, along with pink coralline algae in the shallow reef areas. The soft bryozoan *Margaretta barbata* was more common and widespread than at Paoanui Point, often as a dominant seafloor cover, along with another species *Orthoscuticella innominata*. The most common sponge was again *Stelletta conulosa*, followed by golf ball sponges, while *Ecionemia (Ancorina) alata* was uncommon. Ascidians were more common, with multiple multi-coloured colonies of the small bobble-like *Hypsistozoa fasmeriana*. A milky/off-white ascidian was also common as both individuals and patches, along with *Cystodytes dellachiajei*, a smooth bright yellow lumpy species. The mix of other invertebrate species

was very similar to that at Paoanui Point, and fish included blue cod *Parapercis colias*, leatherjacket *Meuschenia scaber*, sea perch *Helicolenus* sp., red gurnard *Chelidonichthys kumu*, red moki *Cheilodactylus spectabilis*, butterfly perch *Caesioperca lepidoptera*, carpet shark *Cephaloscyllium isabella*, and pink maomao *Caprodon longimanus*. Two crayfish *Jasus edwardsii* were also counted.
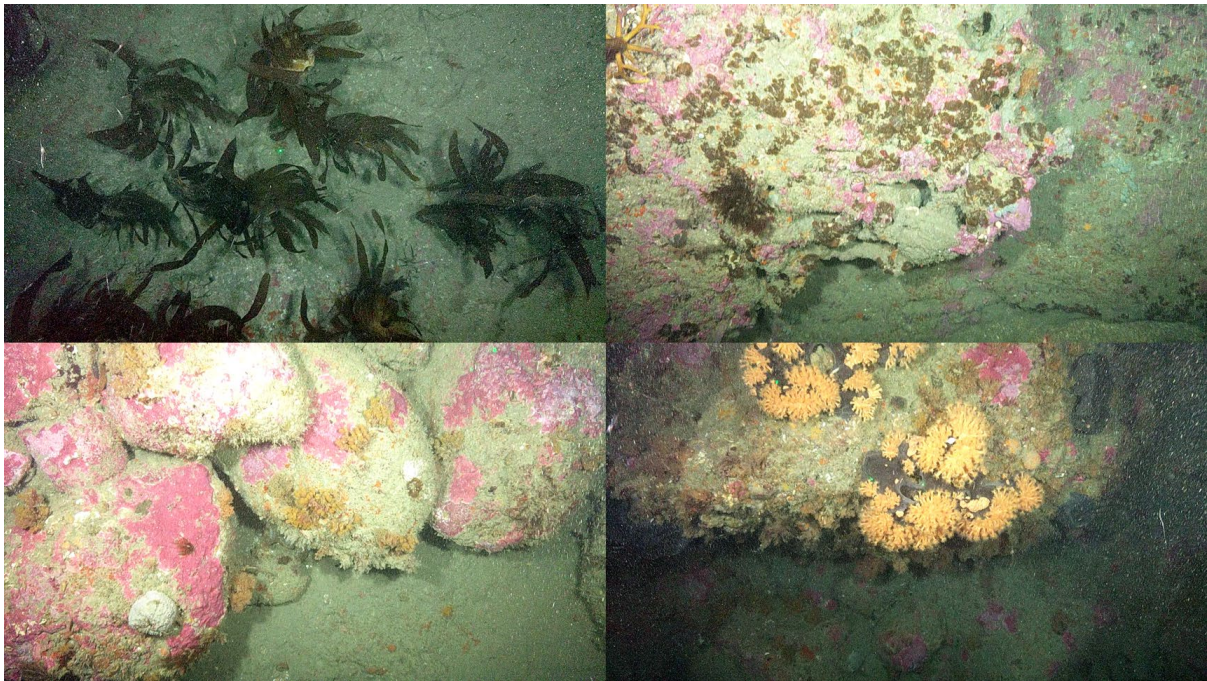
Figure 53: Paoanui Point seafloor imagery (June survey KAH2303 station 5). Top left: *Ecklonia radiata* kelp forest; top right: green macroalgae *Codium* sp. and coralline algae (pink); bottom left: boulder habitats with coralline algae and soft bryozoans (*Margaretta barbata*); bottom right: deeper reef with the sponge *Ecionemia alata* and the yellow zoanthid anemone *Epizoanthus* sp.
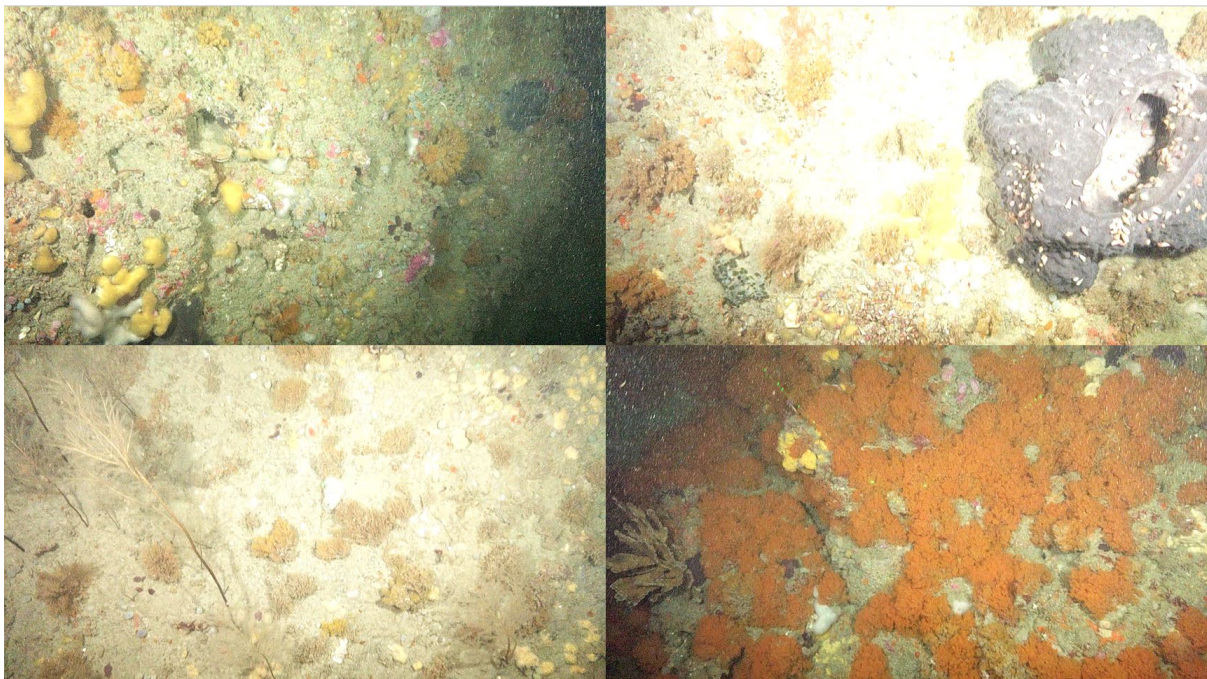
Figure 54: Blackhead Point seafloor imagery (June survey KAH2303 station 4). Top left: ascidians and soft bryozoans; top right: mound sponges, *Latrunculia* sp. sponge, and soft bryozoans; bottom left: hydroids and soft bryozoans; bottom right: soft bryozoans *Margaretta barbata*.

Motuokura offshore reef

There was no evidence of sedimentation at the Motuokura Reef on the mid-shelf offshore of Waimarama Beach and Motuokura Island, at ~110 metres water depth (KAH2303 station 6) (Appendix 10, Figure 55). Most of this feature was composed of fine sand, with occasional small oblong boulders and smaller irregular cobbles. The site was apparently too deep for macroalgae to grow. Sessile encrusting fauna dominated by finger sponges were present at low densities across the feature along with yellow encrusting sponges where rocky substrate was present. The fish present included jack mackerel *Trachurus* spp., sea perch, opalfish *Hemerocoetes* sp., yellow cod *Parapercis gilliesi*, butterfly perch, blue cod, sea dragons *Solegnathus spinosissimus*, red gurnard, eel, flatfish, and kingfish *Seriola lalandi* seen in the water column. Two carpet shark egg cases were also observed attached to rock.

Figure 55: Motuokura offshore reef seafloor imagery (June survey KAH2303 station 4). Top left: spiny sea dragon *Solegnathus spinosissimus*; top right: the ophiuroid *Ophiopsammus maculata*, and a carpet shark egg case; bottom left: the yellow tube mound sponge *Polymastia cf. echinus*; bottom right: the ophiuroid *Ophiopsammus maculata* and encrusting sponges.

Cape Kidnappers

No macroalgae were observed at this site despite its relatively shallow depth (~20–30 m). It is possible that light levels are too low to enable macroalgal growth due to the suspended sediment/particle loads. Some of the seafloor imagery shows a fine cover of sediments on the sessile epifauna. However, the surrounding flat seafloor consisting of fine sand, gravels, stones, and small cobbles appeared clean, with no fine sediment cover being present. It is possible that this area is impacted by the ongoing erosion of the adjacent coastline and cliffs, which are receding. Data from HBRC obtained pre-cyclone showed a complete absence of the kelp *Ecklonia radiata*. It is not clear whether Cyclone Gabrielle has impacted this ecosystem which apparently had some level of sedimentation occurring previously.

Previous multibeam mapping by NIWA and HBRC showed this area to include extensive sloping reefs, organised as rock platforms extending out to around 30 m depth, with fractures and ridges running north-east/south-west (Appendix 10). On its upper north extent, these change to numerous small slabs/outcrops/mounds ~3 m high and 5 m wide against a flat background. CoastCam transects targeted these mounds, whose exact nature was unknown prior to sampling, though suspected to be biogenic reef structures (Figure 56 and Figure 57). The five camera transects conducted during the June and October surveys spanned 22–33 m depth. The June survey transects were unsuccessful due to poor

visibility, but limited glimpses of the mound tops revealed them to be rock with attached epifauna, surrounded by seafloor of sand, small gravel, and cobbles. The October deployments were more successful, due to improved visibility, and confirmed the glimpses seen in the first voyage. Almost all fauna were restricted to the top of the rock mounds and, in some places, boulder piles. No macroalgae or coralline algae were present, with the fauna dominated by small foliose bryozoan and hydroid species, frequent large colonies of the ascidian *Hypsistozoa fasmeriana*, along with grey *Ecionemia alata* sponges, and occasional finger sponges (mainly *Trachycladus stylifer*). Crayfish were relatively common, with at least a dozen seen, both sheltering and out foraging on the surrounding flats at night. Fish seen included at least one blue moki *Latridopsis ciliaris*, although sampling around the mound bases where fish may have been sleeping was limited due the camera system being too high above the seafloor.

Figure 56: Cape Kidnappers seafloor imagery (October survey KAH2306 station 7). Top left: sand, gravels, and pebbles; top right: cluster of the ascidian *Hypsistozoa fasmeriana*; bottom left: the grey sponge *Ecionemia alata*, several ascidian species, and the finger sponge; bottom right: finger sponge *Callyspongia* sp., a yellow sponge, and the ascidian *Hypsistozoa fasmeriana*.
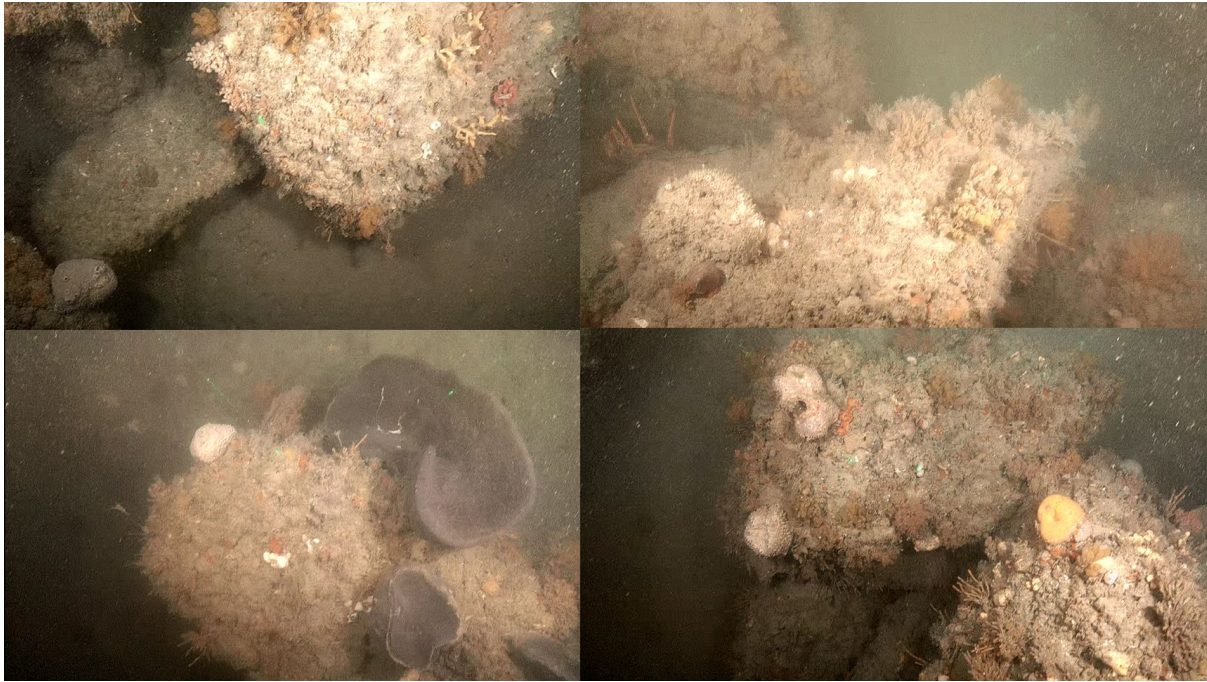
Figure 57: Cape Kidnappers seafloor imagery (October survey KAH2306 station 8). Top left: boulders with foliose soft and calcified bryozoans and the white round sponge *Psammocinia* sp.; top right: a sheltering crayfish and a gastropod (*Maurea* sp.); bottom left: pale sponge (*Psammocinia* sp.) and the grey sponge *Ecionemia alata*, several ascidian species, and the finger sponge *Trachycladus stylifer;* bottom right: sponge (*Psammocinia* sp.) and a yellow sponge. This station had better water visibility than the other three Cape Kidnappers stations.

Pania Reef

Pania Reef was fully mapped with multibeam sonar during the April 2023 RV *Ikatere* (IKA2303) survey (see Section 3.2.1, Appendix 10). Three CoastCam transects (KAH2303 stations 26, 27, and 28) were run across the reef, which rises to a maximum height of nine metres relative to the surrounding seafloor, during the June voyage, at locations where there was sufficient draft for the RV *Kaharoa*, and adjacent to or overlapping diver/video transects completed by the Cawthron Institute (based on figure 6 given by Kelly & Sim-Smith 2021). No positional or ecological data could be sourced from that work.

Water visibility was very poor, and only the most seaward transect allowed the reef to been seen, with CoastCam having to be towed close to the seafloor to see the reef. *Ecklonia radiata* kelp was present in low densities. Some red macroalgae, hydroids, and sponges including *Ecionemia elata* sponges were present.

Pania Reef is well known for having poor underwater visibility. However, no fine sediment accumulations were seen on the gravel, small rocks, and shell patches present. An ongoing ecological time survey series by Napier Port and Cawthron Institute will provide opportunities for pre- and post-cyclone comparisons in the future.

Wairoa Hard

This seafloor feature of cobbles and gravel, with scattered low rock outcrops, was a priority target for both surveys. Thought to be an important nursery ground for juvenile fish, especially small snapper *Chrysophrys auratus* (based on anecdotal accounts), it has been closed to commercial bulk fishing for a number of years. The HBRC requested a sampling focus on the offshore portion of the mapped area in the present project. The HBRC used a ROV (pre-cyclone) to complete a dropped camera grid survey of the entire Wairoa Hard area, with video for up to 10–20 m at each station. Initial observations included percentage cover of kelp and various types of macroalgae (Figure 58) as well as presence of

sponge and fish. These data were used to help guide our sampling efforts during the June and October surveys to enable pre- and post-cyclone comparisons.

Prior to the cyclone, *Ecklonia radiata* kelp was mainly confined to the 25–30 m depth range (Figure 58), with foliose macroalgae generally having a shallower depth distribution along the 25 m and 15 m contours but absent at intermediate depths. This dissected distribution may reflect different species environmental preferences. It is unclear whether the presence of suitable hard substrates for macroalgae to attach to helped drive these patterns. Two 0+ snapper (<1 year old, <90 mm length) were seen on one of the HBRC surveys, on a cobble seafloor (M. Morrison, NIWA, pers. obs.).

Five Wairoa Hard stations were surveyed during the June survey over a two-week duration, including one station (KAH2023 station 74) targeting the densest kelp forest seen in the HBRC survey. Unfortunately, visibility on these transects was close to zero or zero. On the last survey day, three fine-mesh research beam trawls were deployed on the Wairoa Hard. These tows returned varying amounts of wood, including roots, branches, and rotting bark strips (Figure 59). Mobile invertebrates were represented by saw shells and several heavy-shelled whelk species. The small fish assemblage was represented by six species across the three tows, of which only one was known to be structure-associated; bastard red cod *Pseudophycis breviusculus* are commonly caught in research beam trawls in northern New Zealand shallow waters in association with horse mussels and finger sponges (*Callyspongia* spp.) (M. Morrison pers. comm. 2024). In Wairoa Hard they may have been opportunistically associated with large wood debris. The remaining five species were all soft sediment-associated species: a sole species, opalfish *Hemerocoetes* sp., ahuru *Auchenoceros punctatus* (a small endemic morid cod), jack mackerel, a red gurnard, and a bumblebee squid *Sepioloidea pacifica.*

Visibility at Wairoa Hard was much improved during the October survey relative to the June survey, although it was still poor. Twelve camera tows were conducted, including three looking for a cluster of large logs ('linear features') seen during the April 2023 RV *Ikatere* multibeam survey (IKA2303). Visibility at those three stations was poor, and no wood debris was seen. The remaining stations found only muddy seafloor with the occasional small log or branch. Station 34, which ran over the densest kelp forest observed in the HBRC ROV survey, found no macroalgae at all. A single healthy *Ecklonia radiata* plant was observed at station 12, though it may have been detached and drifting. Station 10, situated on the far west side of Wairoa Hard, found a seafloor composed of small cobbles, gravel, shell, and stones. No live organisms were seen, and the rock surfaces appeared covered by a fine layer of sediment, although the video resolution made it difficult to be definitive.

Our assessment is that the Wairoa Hard appears to have been significantly impacted by Cyclone Gabrielle with kelp, macroalgae, and sponges almost completely or completely absent after the cyclone.
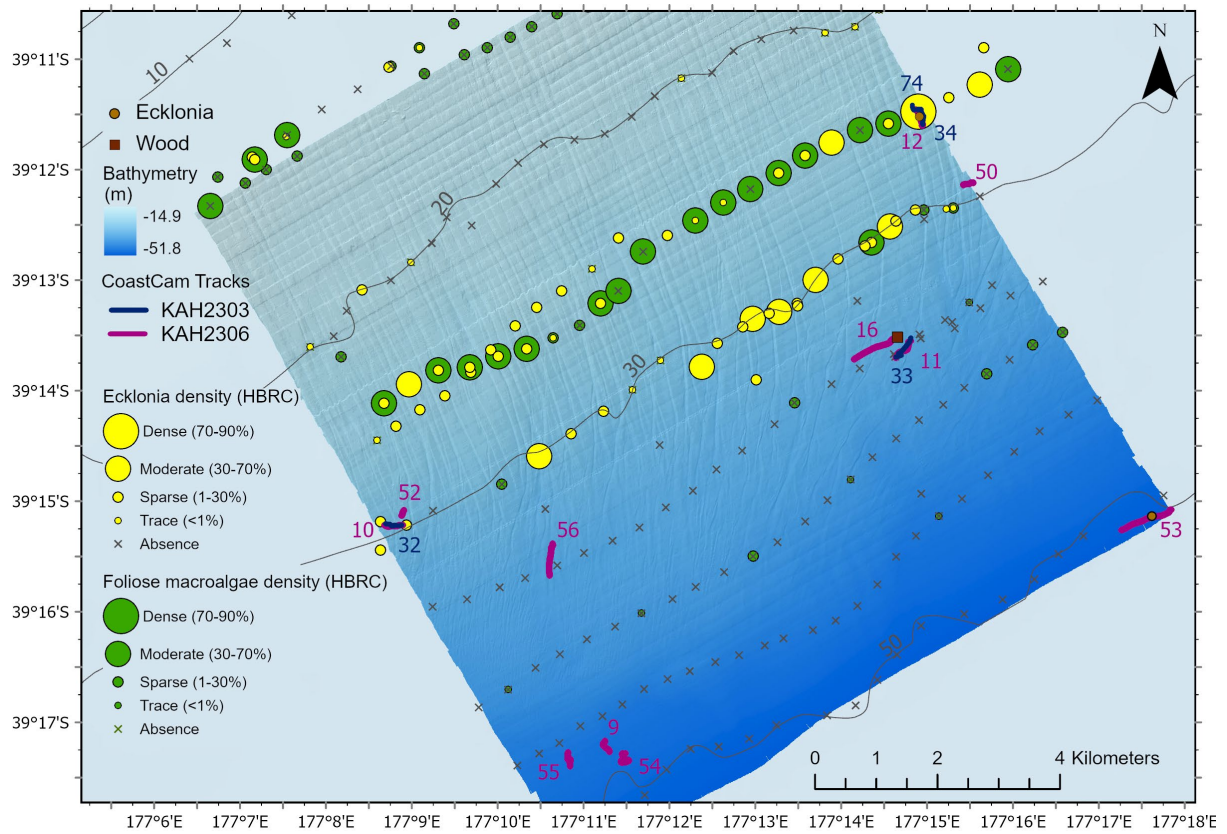
Figure 58: Wairoa Hard – seafloor bathymetry, path of towed camera transects labelled with station number (June and October surveys), and density of kelp *Ecklonia radiata* and foliose macroalgae from the pre-cyclone HBRC ROV survey.

Figure 59: **Wairoa Hard beam trawl catch from June RV *Kaharoa* survey KAH2303 station 76. Top: wood debris; middle: wood with large eggs attached (possibly from a large whelk); bottom: bastard red cod *Pseudophycis breviusculus*, sole, and opalfish *Hemerocoetes* sp. Gastropods include the saw shell *Astraea heliotropium* and several heavy-shelled whelk species that are hard surface-associated. Also present was a single foliose coralline alga, fragments of *Ecklonia radiata* kelp fronds, and several small crabs.**

Central Hawke's Bay

Two towed camera deployments were conducted during the October survey (KAH2306 stations 23 and 24) in the central Hawke's Bay over an area known to receive commercial trawling effort. A single multibeam sonar transect was mapped across the two stations but is not presented here. The water depth ranged from 73 to 83 m, with very clear waters, and a seafloor composed of well packed soft muds. Large burrows were common, but no epifauna or epiflora was present on the sediment surface. One small piece of wood debris and a few small eels were observed. We saw no obvious signs of sedimentation impacts at this site.

Mahia West

This site was composed of a large area of sloping reef and is part of the reef system running along most of the western side of Mahia Peninsula. Multibeam sonar mapping during the June survey extended the overall reef previously mapped further west (Appendix 10). The reef from 15 to 26 m depth and was bounded by soft sediment seafloor. The camera tow conducted in June (KAH2303 station 37) revealed poor water visibility, with only occasional glimpses of *Ecklonia radiata* kelp and the native green macroalga *Caulerpa flexilis*. Water visibility had considerably improved by October (KAH2306 station 49) but was still poor. Heathy *Ecklonia radiata* kelp was seen along much of the transect (noting that the seafloor was often obscured), as well as extensive *C. flexilis* cover, and some sponges (in particular the grey sponges *Stellata conulosa* and *Ecionemia alata*). Lower numbers of the finger sponge *Callyspongia* sp. and golf ball sponges (*Aaptos globosum, Tethya burtoni*) were also observed. One crayfish was seen, but no fish were encountered.

While the water visibility was poor, the dominant macroalgae species were healthy.

Poverty Bay south reef

An extensive shallow reef system was present on the south-eastern side of Poverty Bay (Appendix 10). Water clarity was zero when surveyed in June 2023 but had greatly improved by October (KAH2306 station 36). The reef was up to 6.5 metres in height and dissected by numerous open fractures, bounded by medium grain sand flats ranging from ~17–24 m water depth at the reef/sediment boundary. The seafloor was found to be largely devoid of any larger epifauna, aside from a few individuals of an unidentified oblong ascidian species and occasional small cup corals, and a number of grey *Stellata conulosa* sponges on the western side of the transect (Figure 60). A semi-continuous cover of small and low height tubes was present, which may be tubeworms. No mobile invertebrates or fish were observed.

There was clear evidence that this reef was impacted by sedimentation, with no macroalgae present despite the relatively shallow water depths, and only low numbers of larger sessile invertebrates. Whether this was due to Cyclone Gabrielle, or a more chronic ongoing issue caused by sediment inputs from the Waipaoa and Waimata rivers or erosion of the nearby extensive rock cliffs is unknown.
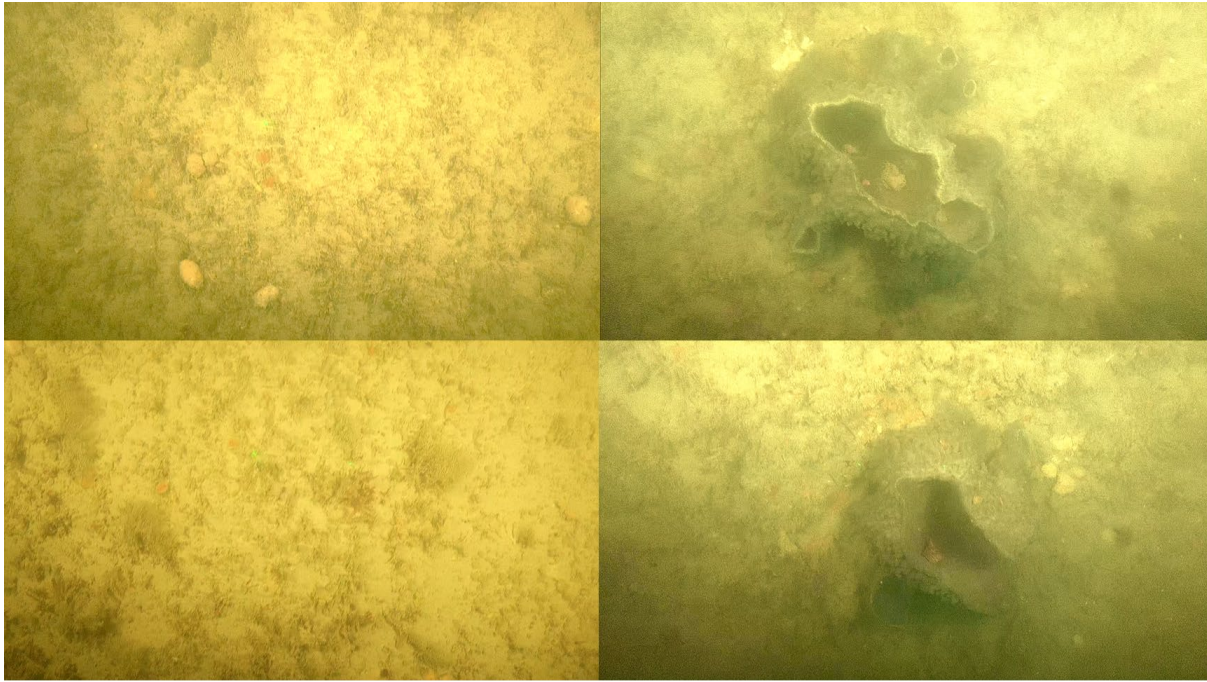
Figure 60: Poverty Bay south reef imagery (October survey KAH2306 station 46). Top left: small yellow oblong ascidians; top right and bottom right: larger grey sponges; bottom left: cup corals. Note layer of fine sediments covering substrate and some organisms.

Poverty Bay north reef

The coastal area just north of Gisborne held extensive reefs at 16–30 m deep (Appendix 10). Two stations surveyed during the June survey had poor visibility, although the kelp forest could be seen when the camera was closer to the seafloor. Water visibility had considerably improved by October, revealing extensive kelp forest, albeit with the lowest proportion of healthy adult plants for sites with kelp forest we surveyed (90%) (Figure 61). Large extensive patches of the native green macroalgae *Caulerpa brownii* were also widespread across the shallower reef area. The soft bryozoan *Margaretta barbata* was also abundant as patches, along with the encrusting orange sponge *Raspailia arbuscula/Tetrapocillon novaezelandiae*. Other widespread species included the grey sponges *Stellata conulosa* and *Ecionemia alata*, and yellow orange finger sponges *Callyspongia* sp. The cup sponges *Stelletta maori* and *Psammocinia hawere* were also relatively common and the yellow *Polymastia* sp. sponge was observed. Mobile invertebrates were uncommon, limited to a few gastropods and one crayfish. Fish observed included butterfly perch, red moki, leatherjacket, a sweep *Scorpis lineolata*, and a leatherjacket.

There was no evidence of adverse sediment impacts, aside from potentially the relatively higher proportion of unhealthy kelp plants. Overall, the reef assemblage was healthy and relatively diverse, though less so than the coastal reefs of Paoanui and Blackhead points. At the lower boundaries of the reef, there was evidence for the flatter reef areas being covered and exposed by the movement of coarser soft sediments, probably through the effects of storms and their associated swells. This included bare rock being exposed, as well as rock plane splits producing small irregular rock slabs in some areas.
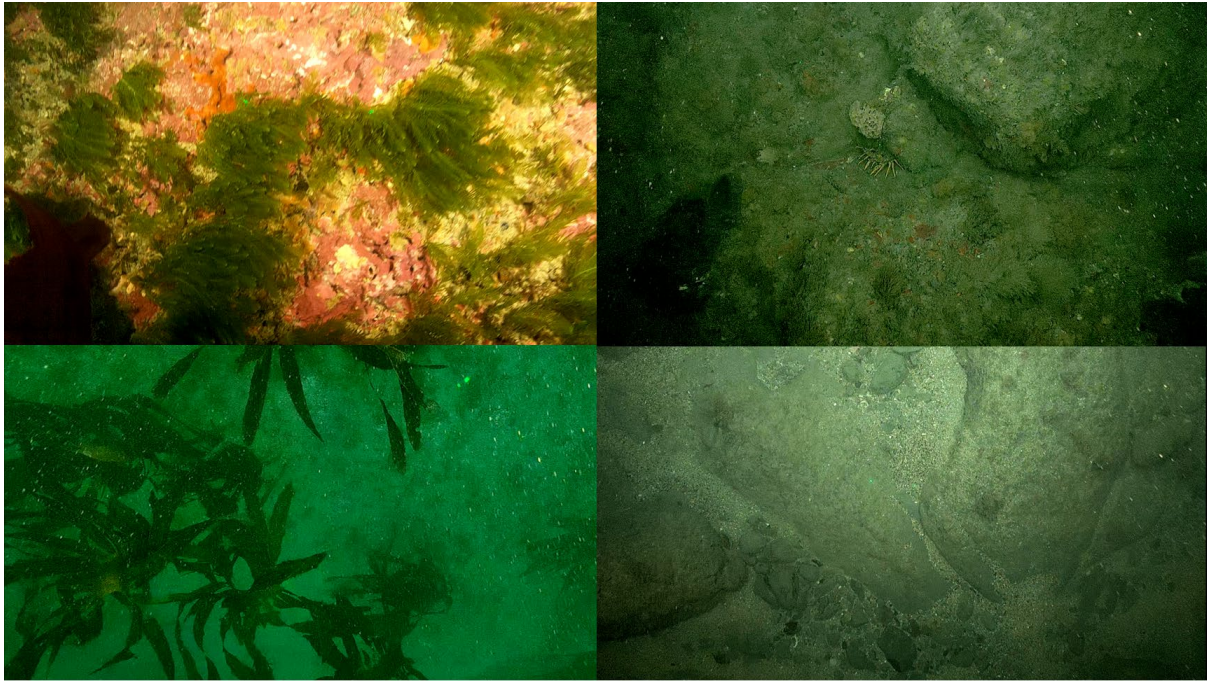
Figure 61: Poverty Bay north reef imagery (October survey KAH2306 station 37). Top left: green macroalgae and encrusting coralline algae; top right: rock with low foliose hydroids and calcified bryozoans, and a sheltering crayfish; bottom left: lower density *Ecklonia radiata* kelp forest on sand veneer over rock; bottom right: exposed bare rock at the bottom of the reef and small rock slabs.

Whangara south reef

A towed camera transect was run along the presumed reef edge during the June survey using the echosounder, but multibeam sonar mapping in October revealed the transect to have been too far east (Appendix 10). The water visibility in June at this location was relatively good; however, the large swell remained an issue. In October, the water visibility had improved (Figure 62) and the sea was relatively flat. The October transect revealed a seafloor mainly composed of small boulders on a cobble field with largely bare surfaces. Water depth ranged from 25 to 30 m, with the reef feature rising about four metres above the adjacent seafloor. Basement reef was largely restricted to the northern end of the transect. Encrusting and low foliose epifauna were only present on the upper surfaces of the large boulders, and included soft bryozoans (*Margaretta barbata*), encrusting orange (*Raspailia arbuscula/Tetrapocillon novaezelandiae*) and white (*Psammoclema* sp./*Thymosia* sp.) sponges, calcified 'cornflake' bryozoans, and a number of hydroid species. No macroalgae were seen. Two pink maomao, two unidentified fish, and one each of butterfly perch and sea perch were counted, along with two crayfish.

There was no evidence of sedimentation impacts at this location, aside from some finer sediment being present on some of the northernmost rock faces. The majority of the transect was covered by small boulders with epifauna on their top surfaces, surrounded by bare cobble field, with very clear water conditions. Some cobble patches were a lighter dull grey and very clean and looked to have been recently exposed. It appears that these cobbles move around during storms and associated heavy swells, grinding away any fauna that is attached to them and to the lower portion of the boulders.

Figure 62: **Whangara south reef imagery (October survey KAH2306 station 39). Top left: sessile fauna and a saw shell on a small, raised boulder surrounded by smaller, largely bare cobbles; dead dog cockle shells are also present; top right: sediment-covered reef wall towards the northern end of the transect; bottom left: boulder with coralline algae and soft bryozoans, adjacent to bare small cobbles; bottom right: white foliose hydroids, soft bryozoans, and a roughy sp generic sheltering below the ledge.**

Whangara north reef

This reef had close to zero visibility in June and was hard to locate without a multibeam map given its narrow shape (Appendix 10). In October, a towed camera transect was conducted along the reef, and revealed the reef to be quite complex, with walls, drop-offs, and overhangs, as well as extensive slopes (Figure 63). Sponges were notably abundant, more so than at any of the other inshore reef sites. Finger sponges dominated, including *Callyspongia* sp./*Dactylia varia* and *Trachycladus stylifer*. The yellow sponge *Polymastia croesus* was also widespread, often occurring in small groups. The encrusting orange sponge *Raspailia arbuscula/Tetrapocillon novaezelandiae* was also common, as were colonies of the ascidian *Hypsistozoa fasmeriana*. No macroalgae were seen. Fish included pink maomao, snapper, red moki, leatherjacket, and a juvenile blue cod.

Although the water was slightly murky, sponges were common, as well as smaller erect and encrusting sponges, hydroids, and soft bryozoans. No evidence of direct sediment effects was apparent.
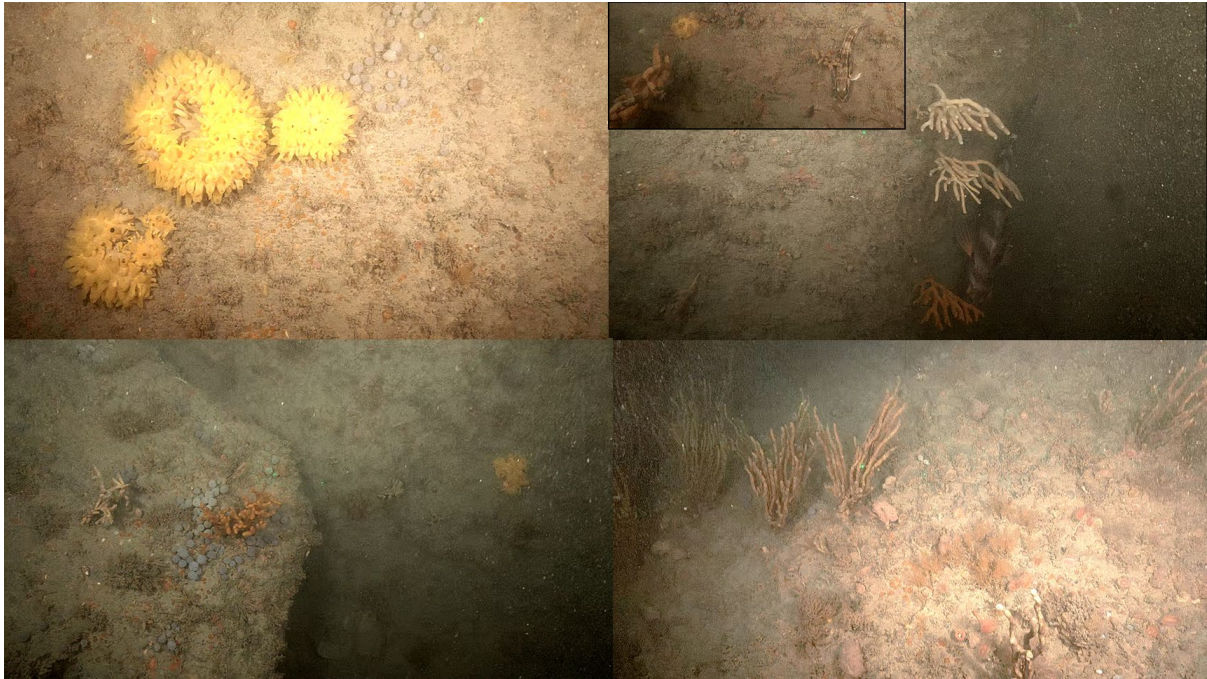
Figure 63: **Whangara north reef imagery (October survey KAH2306 station 40). Top left: yellow *Polymastia crocea* sponges; b) off-white finger sponges *Pararhaphoxya* sp. and a red moki - inset shows a juvenile blue cod; bottom left: finger sponges, bryozoans, hydroids, and colony of ascidian *Hypsistozoa fasmeriana*; d) patched of finger sponge *Dactylia varia*, soft bryozoans, and cup corals.**

Tolaga north reef

This location was mapped in October, but the multibeam data are yet to be processed (Appendix 10). The seafloor was composed of low height, variable strike ridges of rock. Water visibility was close to zero during the June voyage but had improved significantly by October. The video footage revealed a reef system with often steep slopes, and somewhat flat reef tops, with fine sediment accumulations on a subset of these reef tops together with unhealthy looking epifauna (Figure 64). Nevertheless, sponges were the dominant larger epifauna, including the finger sponge *Callyspongia* sp., *Stellata conulosa* and *Ecionemia alata*, and yellow *Polymastia croceus* sponges. The soft bryozoan *Margaretta barbata* was present, as was the orange encrusting sponge *Raspailia arbuscula/Tetrapocillon novaezelandiae*. No macroalgae were seen, nor mobile invertebrates or fish.

Wood debris, ranging from small sticks to branches ~10–15 cm in diameter, was relatively common lodged against the lower reef boundary, as well as further up the reef in soft sediment pockets, and wedged into narrow reef cracks. Overall, sediment impacts were apparent.

Figure 64: Tolaga north reef imagery (October survey KAH2306 station 34). Top left: rock with a narrow dividing channel holding coarse sediment and buried cobbles. Hydroids and soft bryozoans cover the upper left higher surface, while the rock slopes closer to the channel floor appear to have been scoured clean by sediment movement; top right: a sediment-covered reef slope covered in a layer of fine sediments and with unhealthy looking, small finger sponges (Callyspongiidae, *Pararhaphoxya* sp.), yellow sponge *Polymastia crocea*, and hydroids; bottom left: foliose bushy hydroids and soft bryozoan on a steep reef block; bottom right: rock slope on upper reef with the finger sponge *Dactylia varia* and small colonies of the ascidian *Hypsistozoa fasmeriana*, as well as colonies of a small unknown red/orange circle shaped species.

Waiapu south reef

This shallow reef system had very poor visibility in June, with the camera getting occasional glimpses of barren rock when close to the seafloor, along with cover of small epifauna dominated by hydroids and bryozoans. Mapping conducted in October revealed an elongated and narrow looking reef ridge, running north-west/south-east (Appendix 10). A towed camera transect conducted in October uncovered a reef composed of a mosaic of small elevated rock slabs and boulders, and occasional raised rock outcrops surrounded by small irregular cobbles. Much of the reef was devoid of fauna and was covered by a fine sediment layer (Figure 65). Live epifauna was restricted to the tops of boulders, large rock slabs, and locally elevated small rock outcrops. Attached fauna on the sides on these raised features appeared to be in poor health. The soft bryozoan *Margaretta barbata* was one of the dominant cover species (but in low abundance), along with the orange encrusting sponge *Raspailia arbuscula/ Tetrapocillon novaezelandiae* and to a lesser extent the white encrusting sponge *Psammoclema* sp./ *Thymosia* sp. Mobile invertebrates were absent, apart from two small crayfish. Some occasional small coralline algae patches were seen on raised rock outcrops. No foliose algae or kelp were seen except for probably dead stolon remains of the green alga *Caulerpa flexilis*. Red moki were the only fish seen.

This reef was heavily impacted by fine sediments, with the only refuges for epifauna being on raised rock surfaces that stood clear of the lower surrounding cobble field. This pattern was consistent along the entire transect. Large and smaller wood debris was present as localised drifts in several places, often in a pocket of soft sediment surrounded rock.
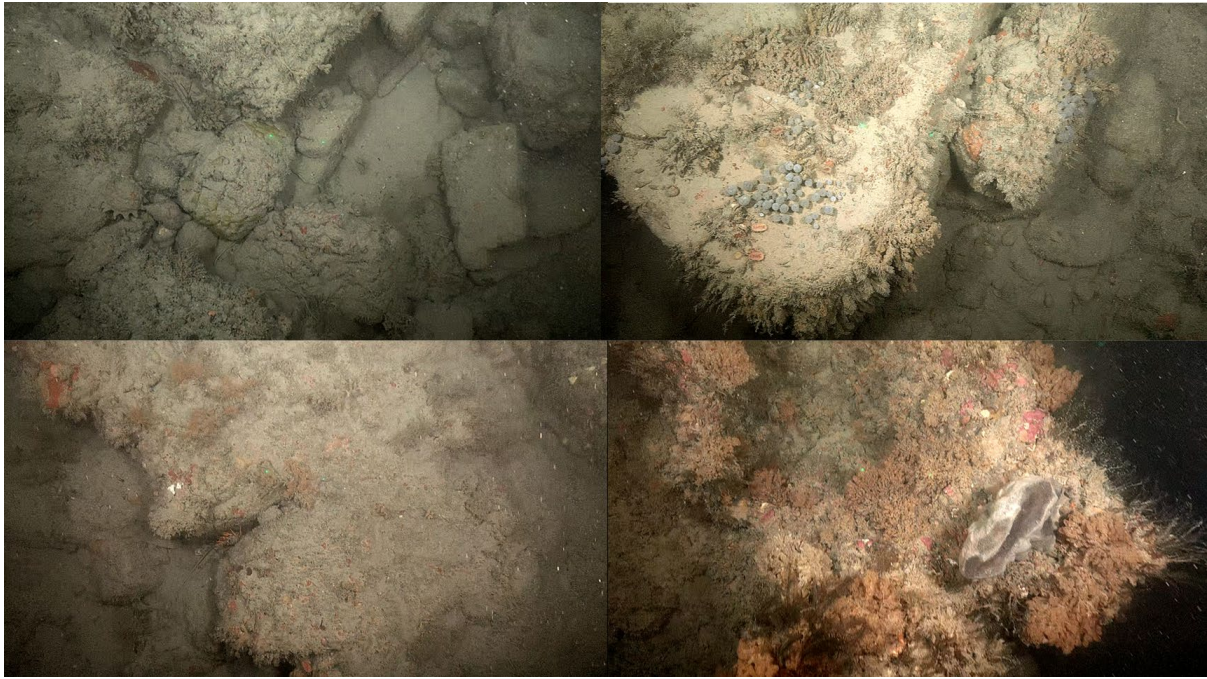
Figure 65: **Waiapu south reef imagery (October survey KAH2306 station 26). Top left: fine sediment-covered rock slabs and cobbles, with small hydroids (likely dead), the probable dead stolon remains of the green fleshy macroalgae *Caulerpa flexilis*, and given their spatial positioning, a likely dead individual saw shell and a large gastropod (possibly *Penion sulcatus*); top right: healthy looking small cup corals, and a colony of the ascidian *Hypsistozoa fasmeriana*, flanked by unhealthy looking soft bryozoans and hydroids on the side of the boulder. The boulders are surrounded by smaller irregular cobbles covered in fine sediment; bottom left: rock with fine sediment cover and unhealthy looking soft bryozoans, a sheltering crayfish is also present; bottom right: healthy looking epifauna on elevated rock surface, that comprised soft and calcified bryozoans, fine hydroids, a cup sponge, and pink coralline algae.**

Waiapu north reef

This shallow, 22–25 m deep reef was discovered during the October survey, rising to a maximum height of ~3.5 m above the surrounding seafloor (Appendix 10). Video from the towed camera revealed a complex of low reef blocks dissected by shallow channels filled with sand ripples. At the reef boundary, the rock substrate was often heavily colonised by boring taxa and appeared prone to breakage. The associated fauna was dominated by soft bryozoans and calcified colony formers which often seemed to be in poor health or damaged (Figure 66). Larger sized fauna were absent. Further into the reef system, the rock substrate was characterised by sessile fauna including ascidians, foliose hydroids, soft and calcified bryozoans, and small sponges. Hermit crabs were the only mobile invertebrates observed. No macroalgae were seen despite the relatively shallow depth. Fish included jack mackerel, red moki, sea perch, and sweep (*Scorpis lineolata*).

There was limited direct evidence of fine sediment impacts on this reef overall, although the edge of the reef was covered by a fine layer of sediment. The complete absence of macroalgae, despite the shallow water depths, could indicate that light levels may be too low to support plant growth and survival, perhaps due to elevated suspended sediment concentrations.
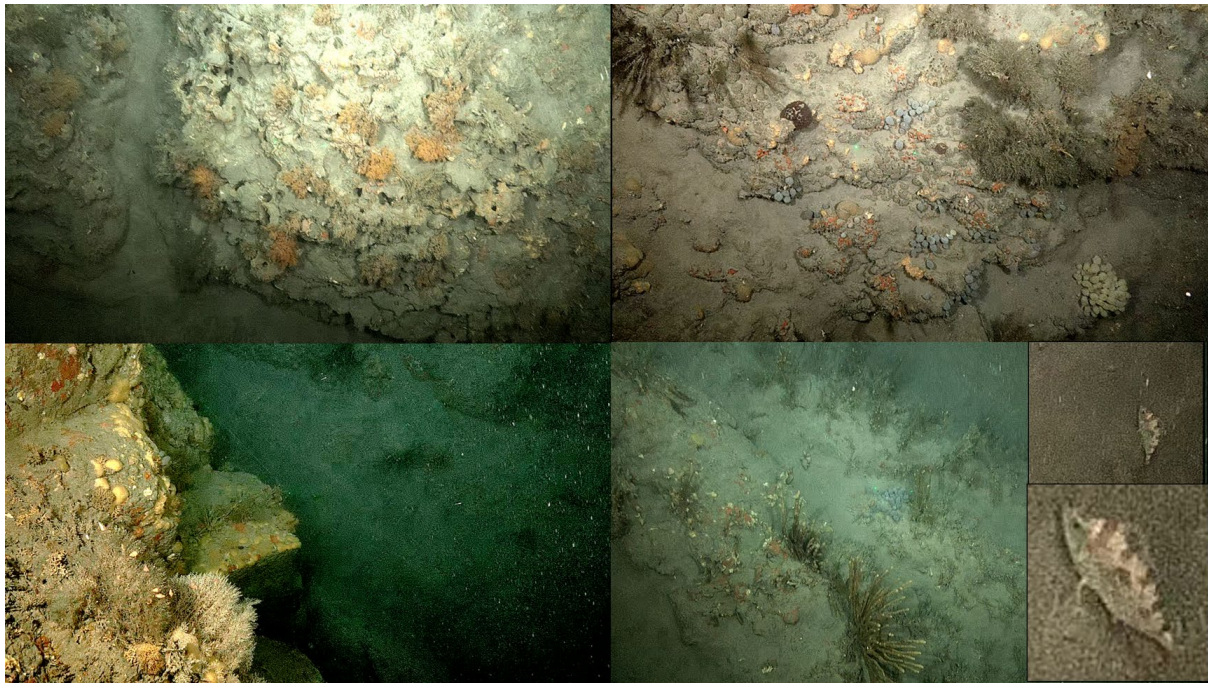
Figure 66: Waiapu north reef seafloor imagery. Top left: eroded rock near the lower boundary of the reef (possibly bored by burrowing bivalve), with soft and calcified bryozoans, which look to be in poor health; top right: more diverse epifaunal assemblages higher up the reef, with a small fish (likely a triplefin or blenny), sheltering against a *Hypsistozoa fasmeriana* ascidian; bottom left: ascidians, bushy hydroids, and encrusting sponge on the top part of an elevated low rock wall, flanked by coarse sand ripples; bottom right: a patch of the finger sponge *Dactylia varia*, on a stepped reef slope adjacent to sand-flats; Bottom right inserts: a likely small juvenile tarakihi *Nemadactylus macropterus* seen on flat sand patch within the reef system.

Assessment of potential sediment impacts

An assessment of the likelihood of sediment impact is shown in Table 11. Eleven reef and areas of hard substrate along the East Coast are assessed as having a high likelihood of sediment impacts (Figure 67). In contrast, nine areas are assessed as having a medium likelihood of sediment impacts. The remaining sixteen locations were assessed as having a low likelihood of sediment impact or no sediment impact. For most of these locations it is impossible to apportion some or all sediment impacts to Cyclone Gabrielle due to lack of pre-cyclone data, with the exception of the Wairoa Hard where sufficient pre-cyclone data on seafloor organisms existed that sediment impacts are more likely due to the cyclone.

Table 11: Assessment of the likelihood of sediment impact at Hawke's Bay and Gisborne locations surveyed using towed camera (sites and stations with poor or no visibility not included). Station numbers from the June survey (KAH2303) are underlined and the October survey (KAH2306) stations are not underlined. See Figure 11 and Figure 12 for details of locations.

Location	Station number	Likelihood of sediment impact
Anaura Bay	41, 42, 43, 44	High
Napier artificial reef	22	High
Poverty Bay offshore reef	62	High
Poverty Bay south reef	36	High
Table Cape	71, 72	High
Tolaga north reef	54, 34	High
Tolaga offshore reef	45, 65	High
Waiapu south reef	26	High
Waikori Bluff reef	51	High
Waipiro Bay inshore	32	High
Wairoa Hard	32, 33, 34, 74, 75, 65, 50, 51,53, 54, 55, 56	High
Ariel Bank (southernmost)	70	Medium
Awanui inshore reef	49	Medium
Cape Kidnappers	40, 41, 5, 6, 7, 8	Medium
East Island reef	50	Medium
Hawke's Bay seep	42	Medium
Pania Reef	26, 27, 28	Medium
Tangoio Reef	30	Medium
Waiapu north reef	27	Medium
Wairoa Hard	9, 10, 12, 16	Medium
Ariel Bank (northernmost)	69	Low
Mahia West	37, 49	Low
Poverty Bay north reef	68	Low
Tokomaru shelf reefs	47, 31, 33	Low
Whangara north reef	57, 40	Low
Blackhead Point	4	No impact
Gables	63, 46, 47, 48	No impact
Central Hawke's Bay	23, 24	No impact
Lachlan Ridge	39	No impact
Motuokura reef	6	No impact
Paoanui Point	5	No impact
Portland Island	38	No impact
Poverty Bay north reef	37	No impact
Tokomaru shelf reefs	30	No impact
Waipiro Bay	48	No impact
Whangara south reef	56, 39	No impact
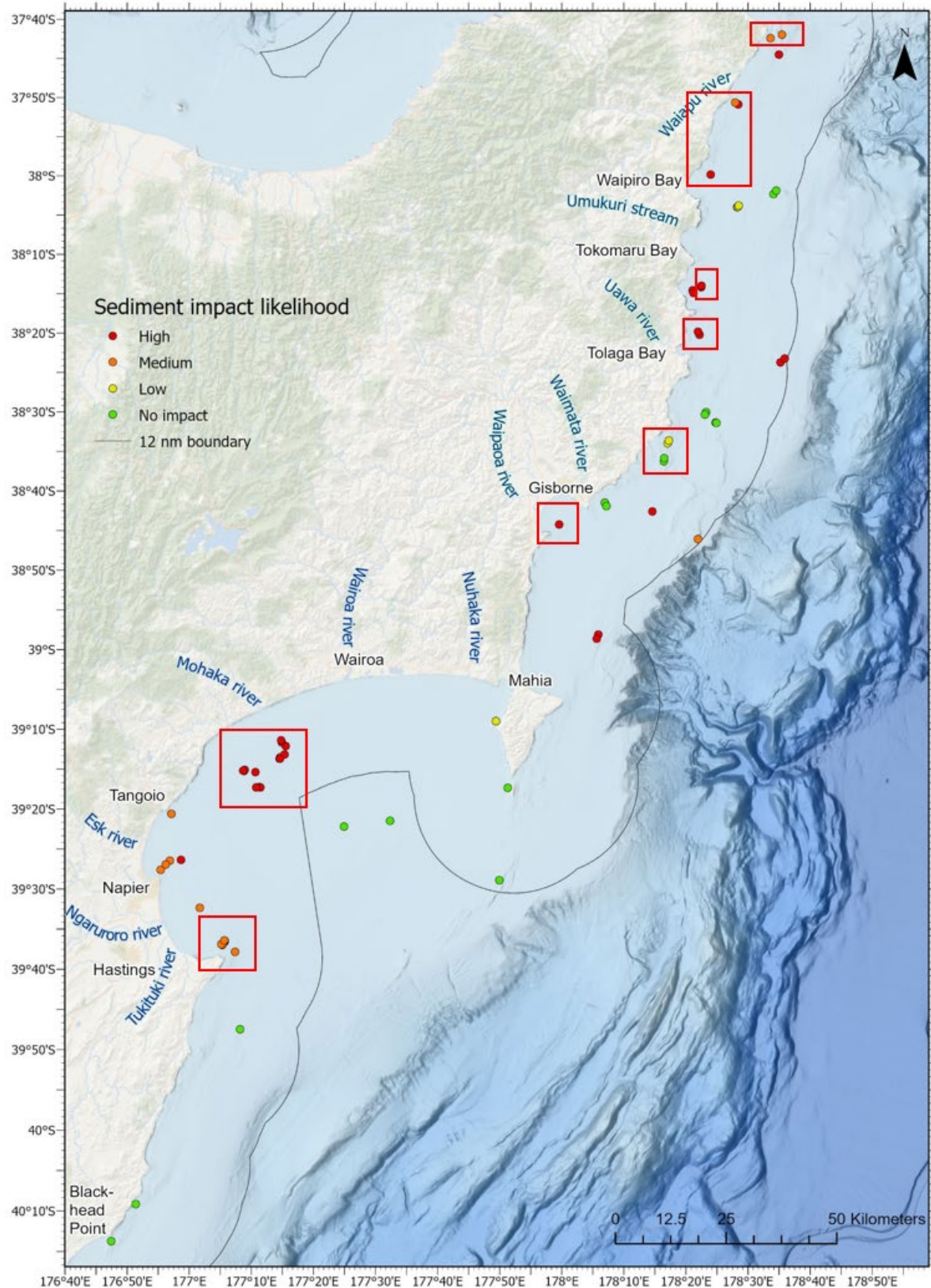
Figure 67: Likelihood of sediment impacts on seafloor ecosystems assessed through visual observations of the seafloor using towed camera transects. Shallow locations (<30 m depth) where kelp was not seen in the towed camera transects are shown by red rectangles.

3.3 Hydrodynamic and sediment transport modelling

3.3.1 Model validation

The hydrodynamic model reproduced the spatial variability of sea surface temperature (SST) well throughout the model domain, with good representation of the cross-shelf and along-shelf temperature gradients (Figure 68). Similar to the observations, colder temperatures occur in the southern part of the model domain with warmer temperatures to the north. In addition, the continental shelf is characterised by warmer temperatures in contrast with cooler temperatures offshore.

In general, the model underestimates SST throughout much of the model domain including in Hawke's Bay and along the Gisborne coast (Figure 68). Along the Wairarapa coast, however, the model overestimates SST. The magnitude of the model bias is similar to that of other hydrodynamic models of the New Zealand region (e.g., Behrens et al. 2020, Souza et al. 2023).

Regions of larger root-mean-squared-difference (RMSD) coincide with regions of high SST bias (Figure 68), in particular along the south coast of the North Island and along the Gisborne coast. These two regions are influenced by strong currents, the East Cape Current and D'Urville Current, transporting different water masses into the model domain. It is likely that the RMSD is related to differences in the strength, width, and location of these currents. In addition, biases in the temperature of the water masses transported by these currents are also likely to contribute to the larger RMSD.
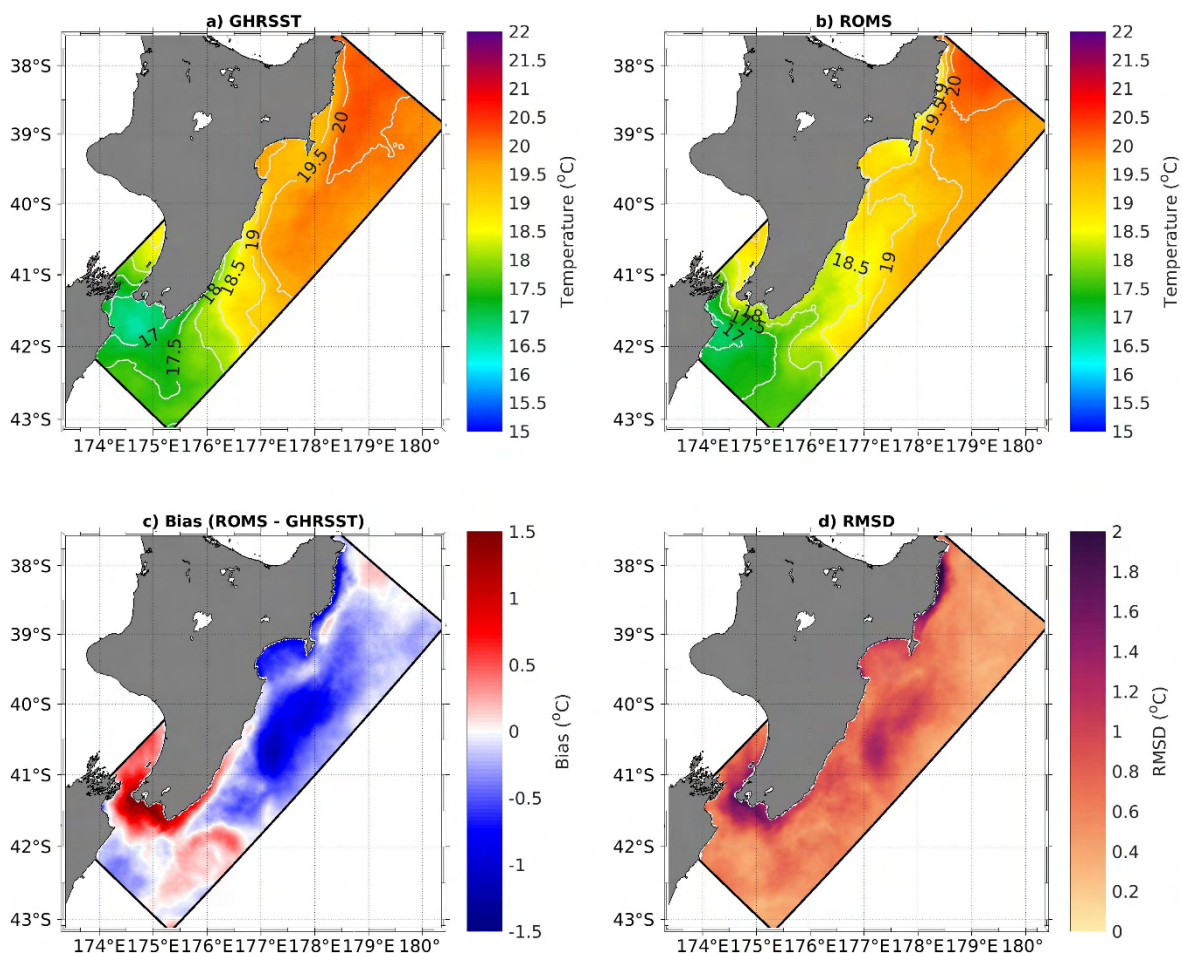
Figure 68: **Time-averaged (3 January 2023 – 15 March 2023) observational sea surface temperature (SST) product (a) and modelled SST (b). c) Bias (model – observations) and d) Root-mean-squared-difference (RMSD) of the modelled SST in comparison with the observational product.**

The comparison between model-simulated temperature and salinity and measurements from Hawke Bay indicate that the model simulates a reasonably realistic temperature and salinity field (Figure 69 and Figure 70). As with SST, the model tends to underestimate the near surface (0.5 m depth) temperature. Despite the underestimation of temperature at 0.5 m and 5 m, the model still has moderate predictive skill (Willmott Score > 0.5, Table 12) and simulates the overall trend reasonably well. At 15 m, the model underestimates temperature for the first two weeks of the modelling period whereafter it tends to overestimate temperature resulting in low correlation coefficient and relatively high RMSD (Table 12).

The comparison between model-simulated and observed salinity at 0.5 m and 5 m is less favourable than that for temperature as indicated by the lower skill scores and correlation coefficients (Table 12). The model overestimates salinity at these depths and, even though it captures some of the low salinity events, it underestimates the amplitude of these events (Figure 70). Surprisingly, the model is more skilful in representing subsurface salinity (15 m, Figure 70 and Table 12) as indicated by the low RMSD and higher correlation coefficient and Willmott skill score.
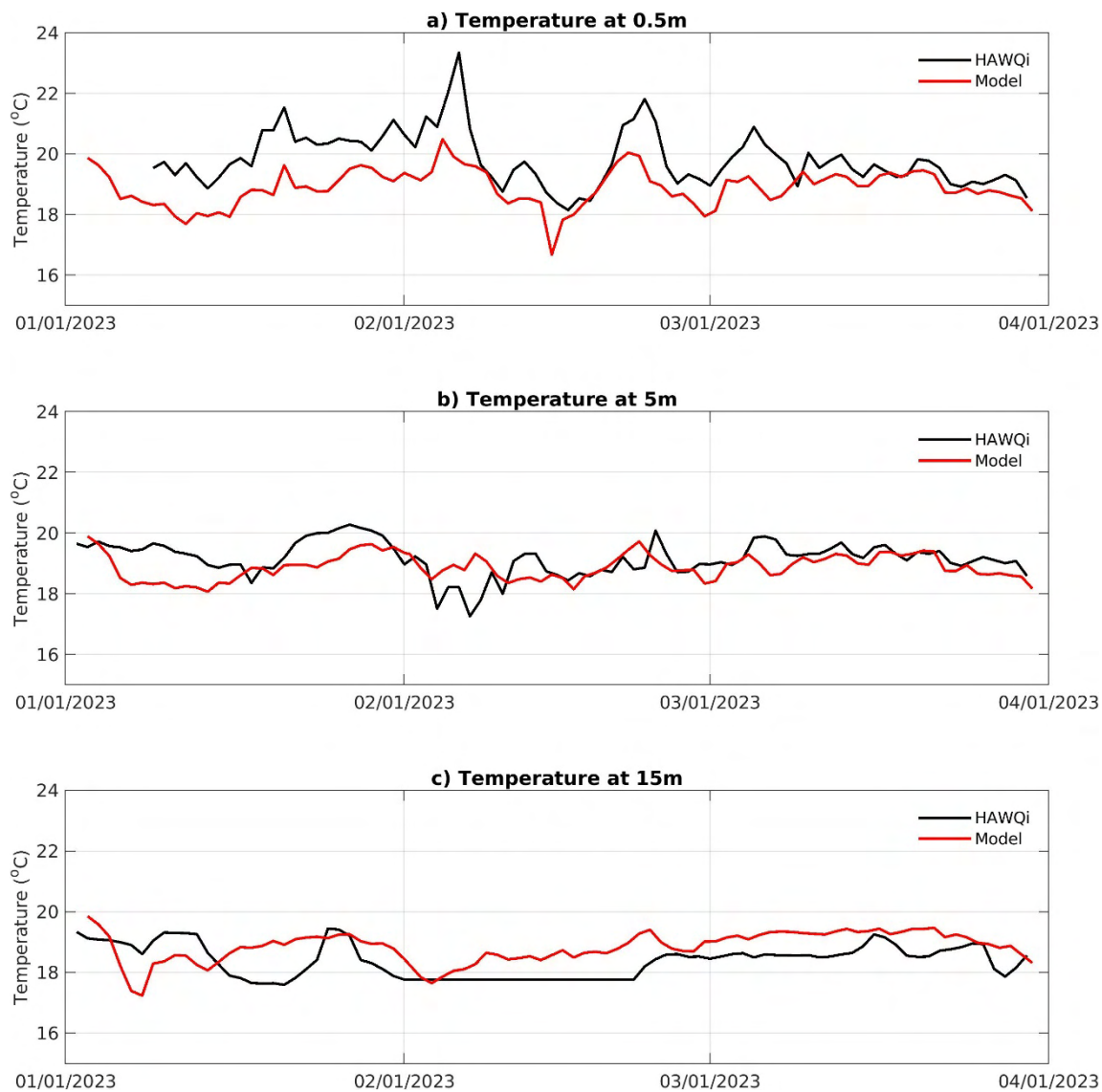
Figure 69: Modelled (red) and observed (black) temperature at a) 0.5 m, b) 5 m, and c) 15 m depth. The observed data are from the HAWQi buoy in Hawke Bay.
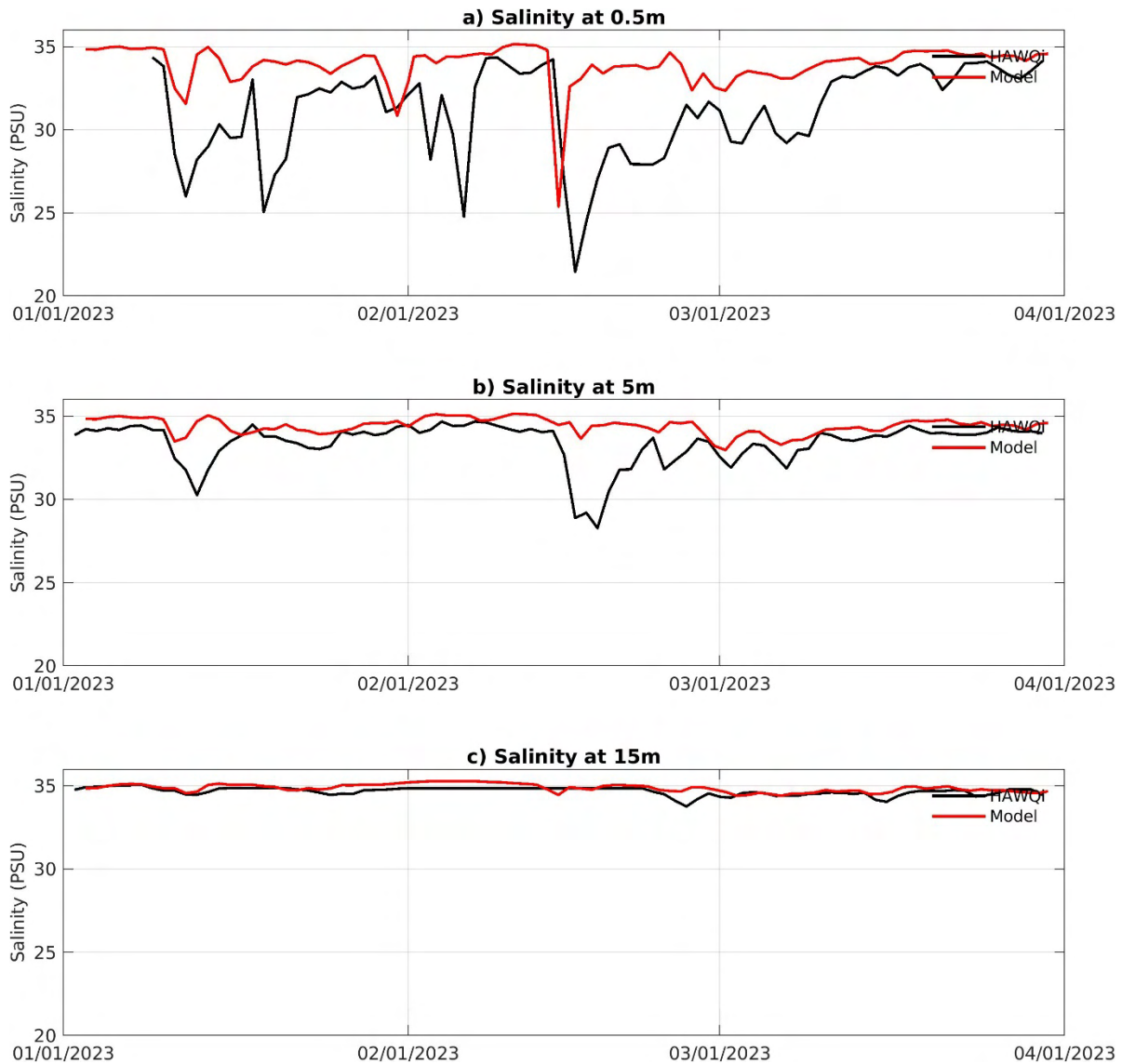
Figure 70: Modelled (red) and observed (black) salinity at a) 0.5 m, b) 5 m, and c) 15 m depth. The observed data are from the HAWQi buoy in Hawke Bay.

Table 12: Validation metrics calculated between the hydrodynamic model and HAWQi buoy temperature and salinity data. RMSD: root-mean-squared-difference; Corr: correlation; WS: Willmott Score.

	RMSD	Corr	WS
Temperature at 0.5 m	1.15	0.67	0.61
Temperature at 5 m	0.63	0.36	0.57
Temperature at 15 m	0.78	0.32	0.53
Salinity at 0.5 m	3.74	0.40	0.54
Salinity at 5 m	1.61	0.27	0.47
Salinity at 15 m	0.32	0.58	0.60

Compared with the satellite derived total suspended material concentrations, the model overestimates the surface sediment concentrations (Figure 71). It should be noted that both the model and satellite data were averaged over the same period (2 January–31 March 2023); however, within this period only ~50% of the data could be used because the rest were contaminated by cloud cover. Therefore, the

comparison of concentrations is influenced by the missing high sediment concentrations characteristic of storm events such as Cyclone Gabrielle and thus the time-averaged satellite derived concentrations are an underestimate.

Despite the discrepancy in sediment concentration values, the spatial variability of the time-averaged modelled surface suspended sediment compares relatively favourably to the satellite derived total suspended material. The model does reasonably well in predicting the sediment plume formation at the river mouths as well as the dispersal of riverine sediments. High sediment concentrations are associated with all the river mouths, except the Waiapu River. The lack of a clear sediment plume at the Waiapu River can be attributed to an excessive dampening of the sediment concentration load for this river, which had to be reduced to get realistic sediment loads across the modelled area.
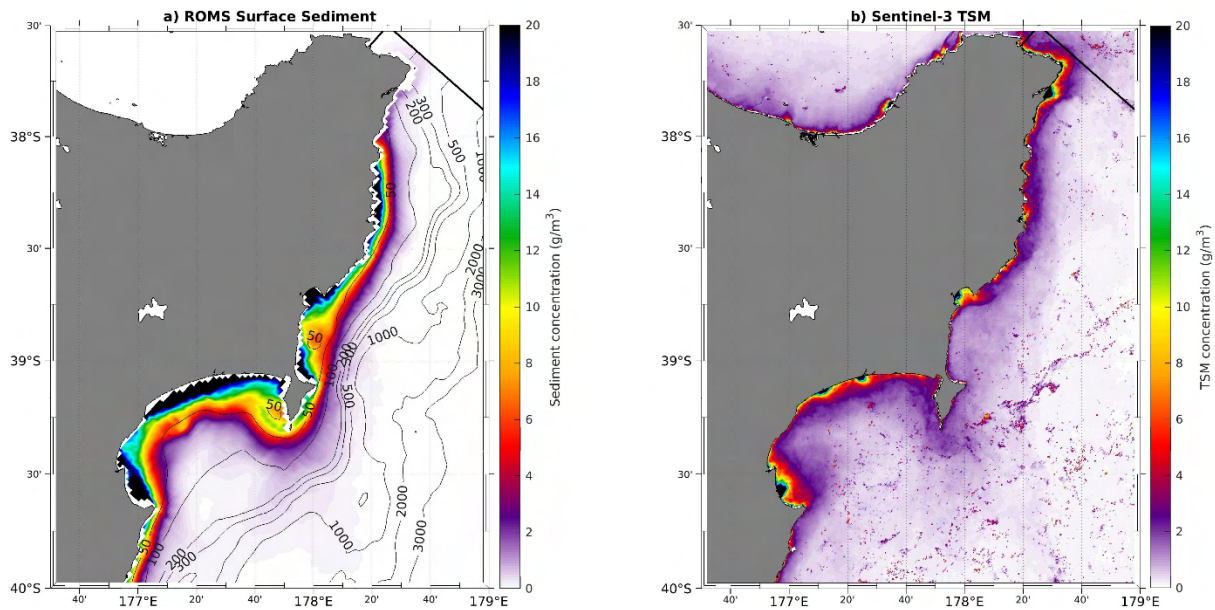
Figure 71:   Comparison of time-averaged (2 January 2023–31 March 2023) modelled surface suspended sediment concentration (left) and time-averaged (2 January 2023–31 March 2023) satellite derived total suspended matter.

3.3.2   Modelled river footprints

The concentration of riverine water before, during, and after the cyclone is shown in Figure 72 to Figure 75. Note the colour scale on these figures is logarithmic and blue indicates values of 0.1–1 kg m^{-3} (10–100% riverine waters), green indicates values of 0.01–0.1 kg m^{-3} (1–10% riverine waters), orange/yellow indicates values of 0.001–0.01 kg m^{-3} (0.1–1% riverine waters), and red/white indicates a value of <0.001 (<0.1% riverine waters).

Before the cyclone (on 11 February) only small amounts of riverine water were present in the Hawke's Bay region (Figure 72). The riverine waters from all rivers tended to disperse throughout Hawke Bay, but at very low concentrations (<0.1% riverine waters for most rivers for most of this region). The Wairoa and Mohaka rivers produced the largest concentrations of riverine waters which pooled in the northwestern corner of Hawke Bay, flowing out of Hawke Bay and northward. Large increases in riverine waters occurred from the 15 February due to the increase of waters from Cyclone Gabrielle. During and post Cyclone Gabrielle (Figure 72 and Figure 73), there were large plumes from the main rivers. These plumes were coastally attached and were transported clockwise (northerly) around the bay.
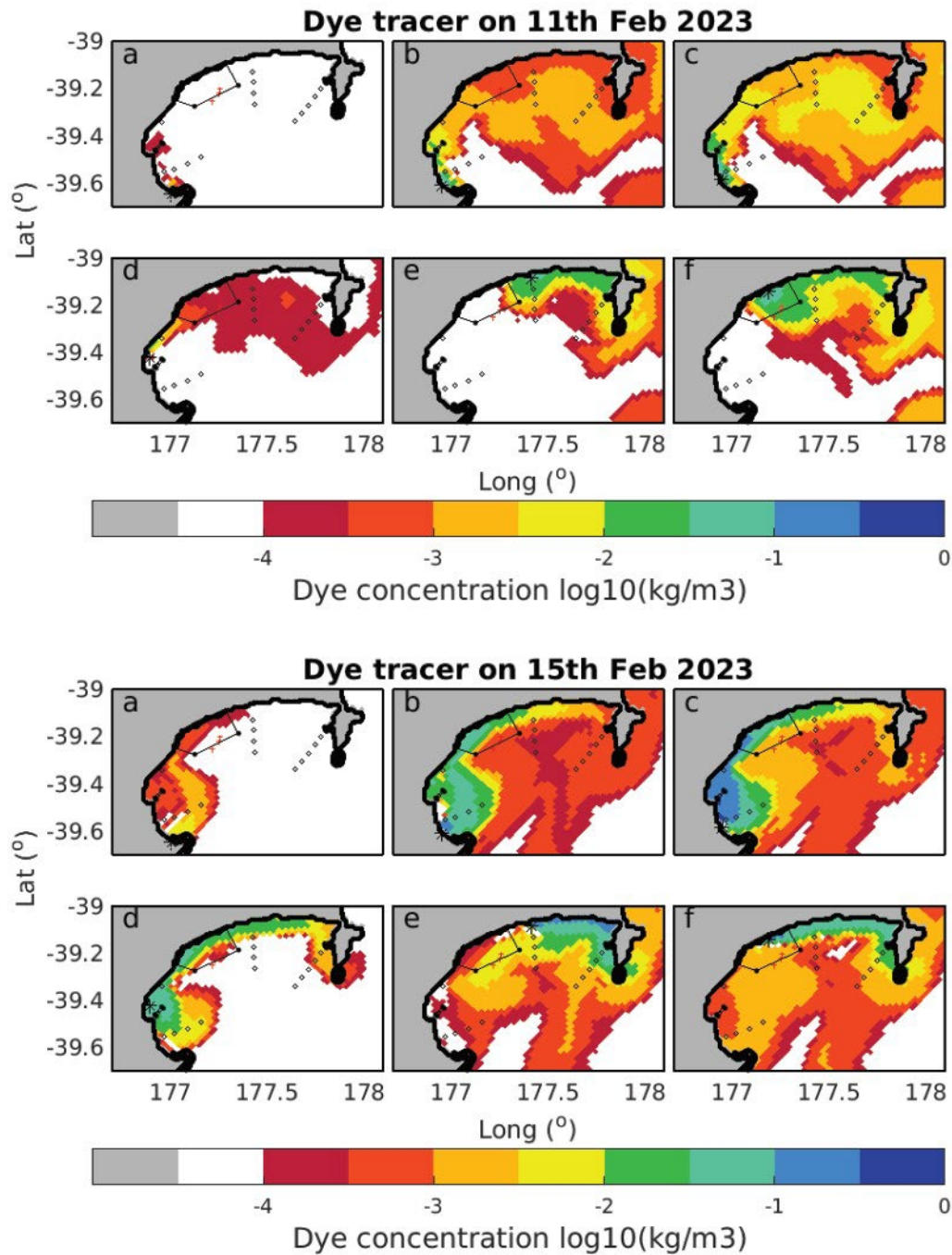
Figure 72: Concentration of dye released from major rivers on the 11th (pre-cyclone; top panel) and 15th of February (post-cyclone; lower panel) in the Hawke's Bay region. Each panel shows the concentration for dye released from a single river, with the location of each river marked with an asterisk. For reference, location of coring transect sites are marked with empty circles and location of beam trawl samples (June survey KAH2303) are shown by red crosses; the outline of Wairoa Hard is shown by a black line. a: Maraetotara River; b: Tukituki River; c: Clive/Ngaruroro River; d: Esk River; e: Wairoa River; f: Mohaka River.
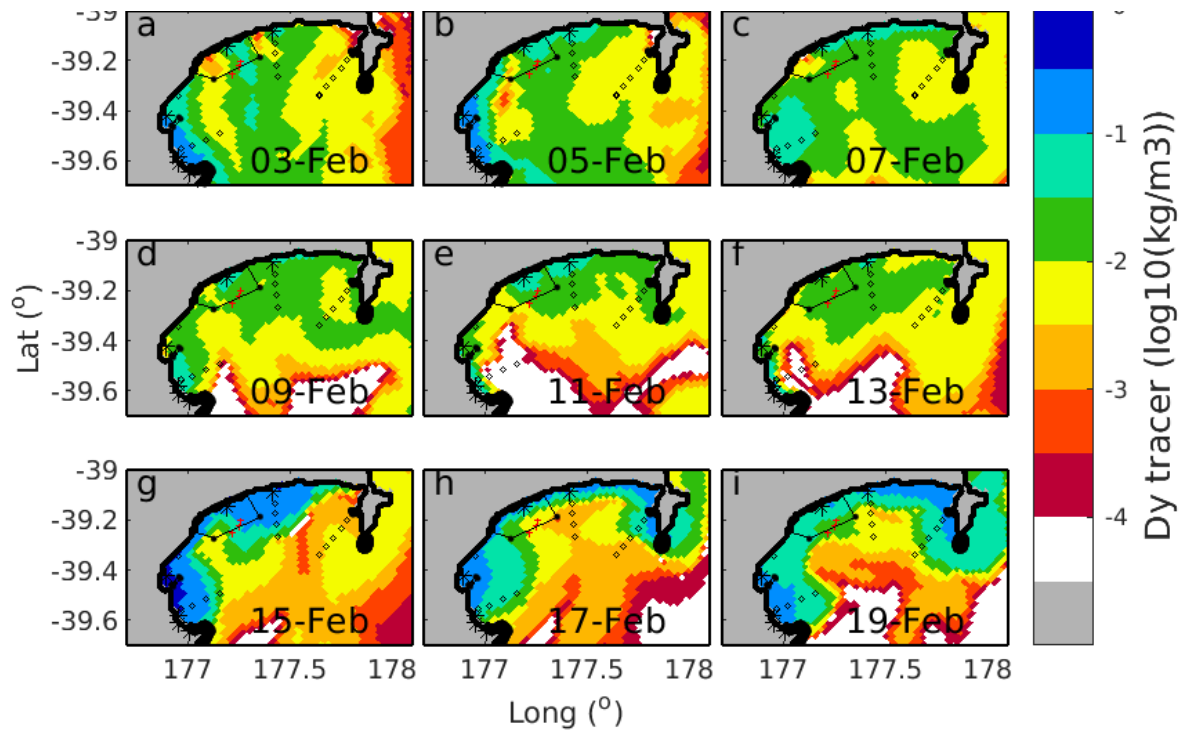
Figure 73: **Concentration of dye released from all major rivers combined (Maraetotara, Tukituki, Clive/Ngaruroro, Esk, Wairoa, and Mohaka rivers) from 3 February to 19 February 2023 in the Hawke's Bay region. For reference, location of coring transect sites are marked with empty circles and location of beam trawl samples (June survey KAH2303) are shown by red crosses; the outline of Wairoa Hard is shown by a black line.**

Pre-cyclone riverine concentrations were very low (<1%) throughout most of the Gisborne region (Figure 74), and elevated riverine concentrations near the Waimata and Waipaoa river mouths decreased steeply away from land. Post Cyclone Gabrielle, there was a large increase in riverine waters near the coast. This can be seen as a coastally attached plume which flows northeast along the coast. Water source from both the Waimata and the Waipaoa rivers had a similar footprint, but the Waipaoa River had much higher concentrations (by about an order of magnitude).

The time series showing river water concentrations immediately pre- and post-cyclone shows a plume entering the southern Gisborne region from the south from 9 February onwards (see green and yellow shading south of 38.5 °S latitude in Figure 75). The movement of this plume of riverine water, which preceded Cyclone Gabrielle, demonstrates how Hawke's Bay rivers can affect the Gisborne region through northward transport.
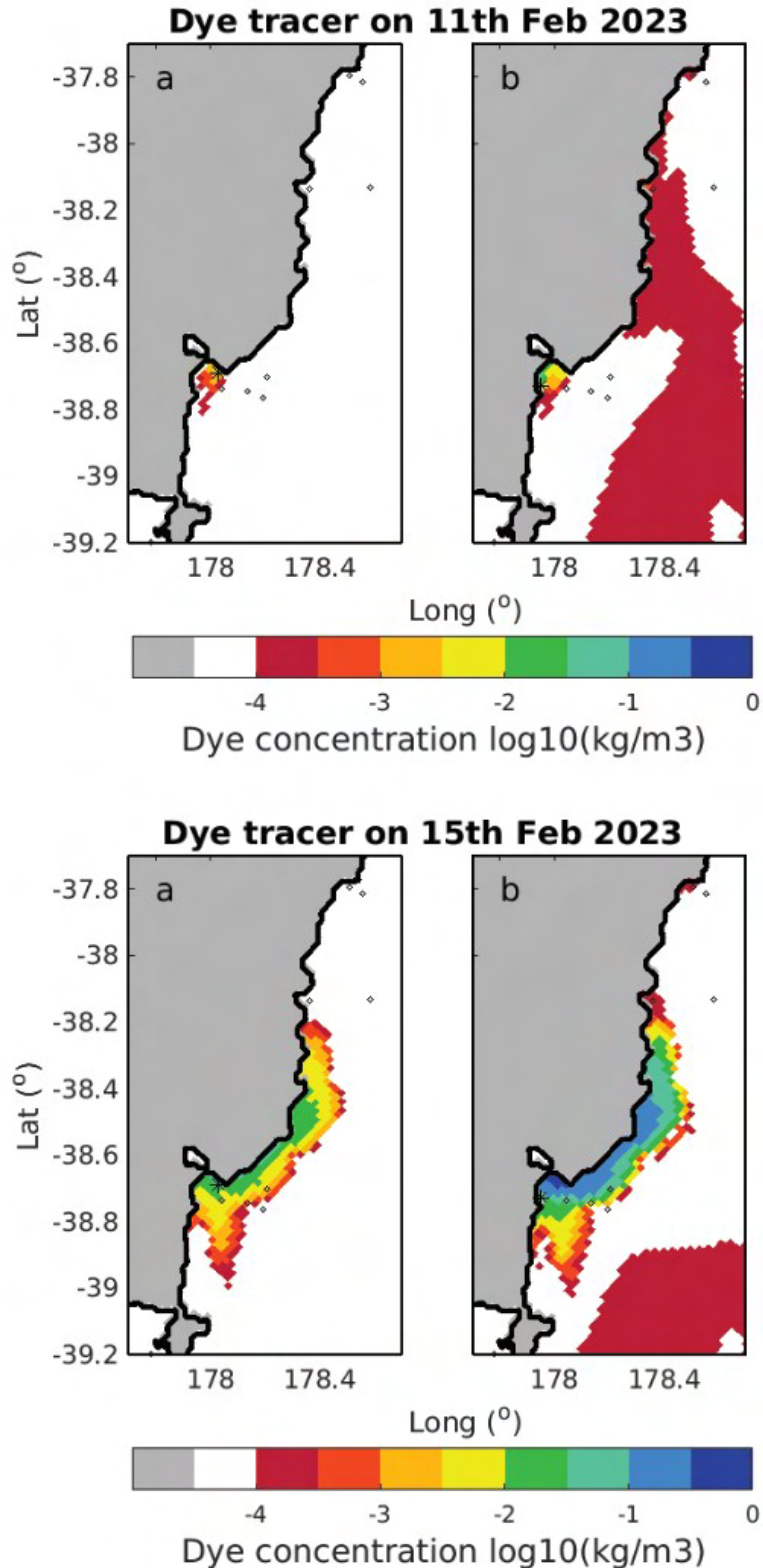
Figure 74: Concentration of dye released from the Waimata and Waipaoa rivers on the 11th (pre-cyclone; top panel) and 15th of February (post-cyclone; lower panel) in the Gisborne region. Each panel shows the concentration for dye released from a single river, with the location of each river marked with an asterisk. For reference, location of coring transect sites are marked with empty circles. a: Waimata River; b: Waipaoa River.
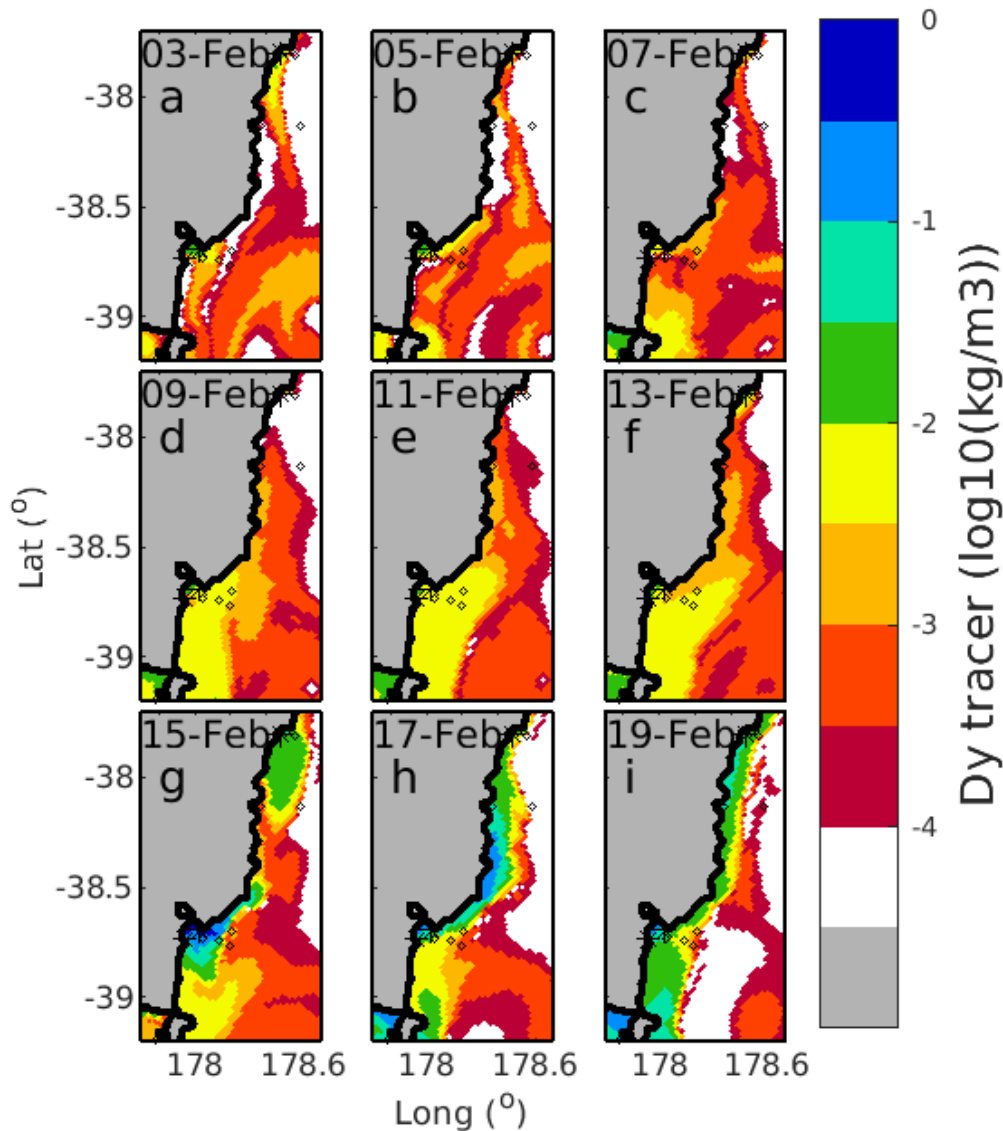
Figure 75: Concentration of dye released from the Waimata and Waipaoa rivers from 3 February to 19 February 2023 in the Gisborne region. For reference, location of coring transect sites are marked with empty circles.

3.3.3 Modelled surface and near-bed suspended sediment

Both riverine inputs and bottom sediment erosion were sources of suspended sediments in the model. In Hawke Bay, the modelled surface suspended sediment was generally concentrated near the coastal region. Pre-cyclone (3–11 February) the sediment concentrations were small and patchy with sediment concentrations mostly less that 1×10^{-4} kg m^{-3} (Figure 76). Sediment concentrations increased sharply between 11 and 13 February, covering the most of Hawke Bay with sediment concentrations 1×10^{-4} – 1×10^{-1} kg m^{-3}. Sediment concentrations started decreasing on 19 February but were still elevated compared with the original state on 3 February.

In general, the near-bed sediment concentrations in Hawke Bay were higher than at the surface (Figure 77). As with the surface sediments, there was a sudden increase in suspended sediment concentration during the period of Cyclone Gabrielle, with most of the near-bed in Hawke Bay containing sediments concentrations greater than 1×10^{-3} kg m^{-3}. The sediment concentrations dropped rapidly with distance from shore as these deeper waters experienced less resuspension from waves.
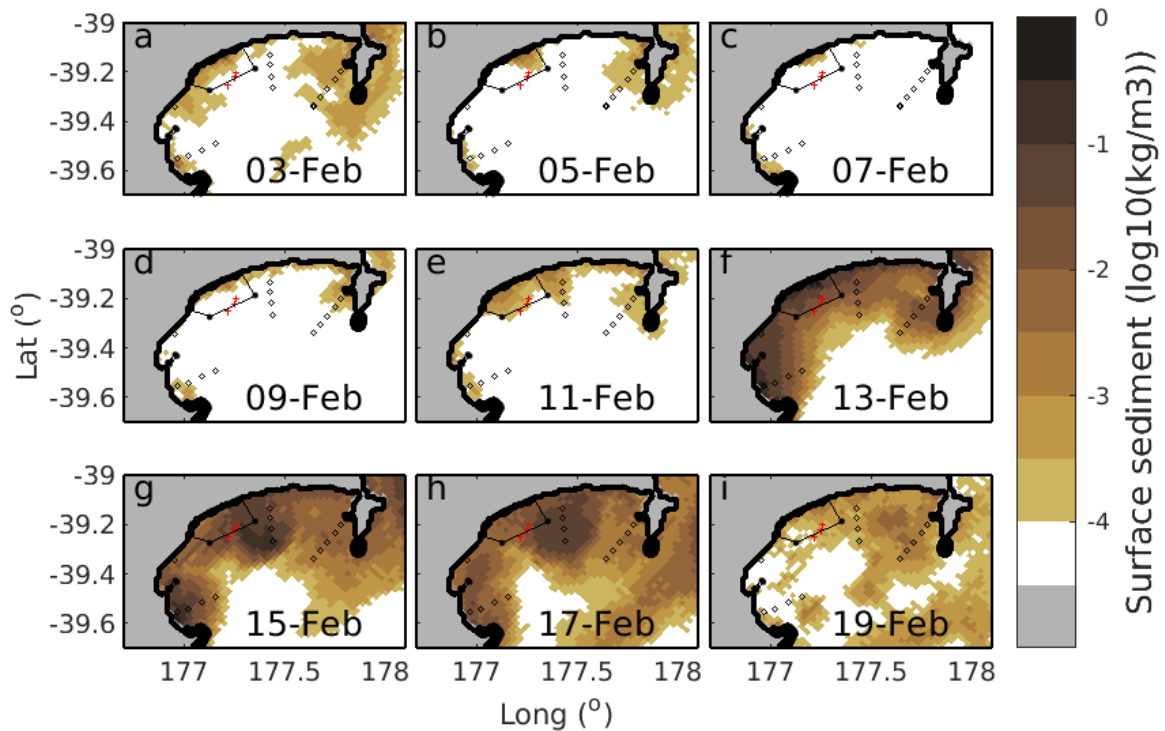
Figure 76: **Surface suspended sediment concentrations in the Hawke's Bay region (3–19 February 2023). Each panel shows the concentration of sediments for a given day. For reference, location of coring transect sites are marked with empty circles and location of beam trawl samples (June survey KAH2303) are shown by red crosses; the outline of Wairoa Hard is shown by a black line.**
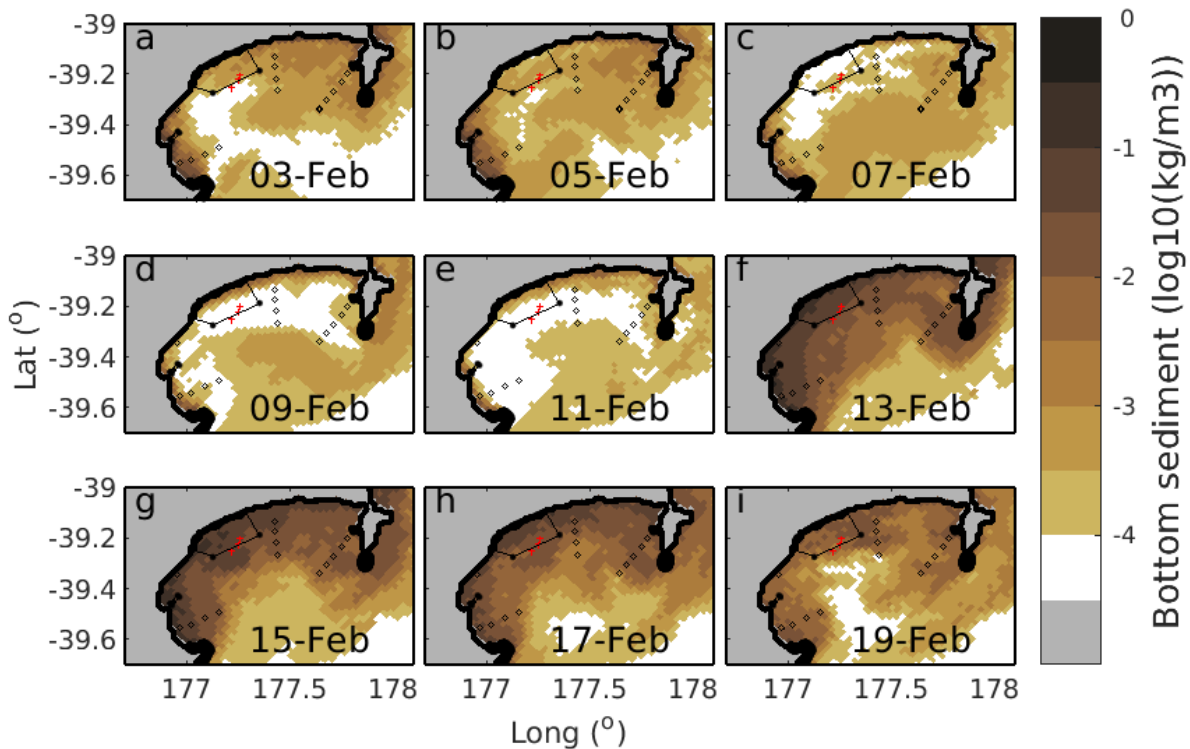
Figure 77: **Near-bed suspended sediment concentrations in the Hawke's Bay region (3–19 February 2023). Each panel shows the concentration of sediments for a given day. For reference, location of coring transect sites are marked with empty circles and location of beam trawl samples (June survey KAH2303) are shown by red crosses; the outline of Wairoa Hard is shown by a black line.**

On 3 February in the Gisborne region, there was a coastal plume of increased surface suspended sediment concentrations ranging between 1×10^{-4} and 1×10^{-2} kg m^{-3} (Figure 78). This concentration decreases with distance offshore due to a combination of the waning influence of riverine inputs with distance from the river mouths, together with reduced sediment resuspension from waves with increasing water depth. Throughout Cyclone Gabrielle (13–17 February), this near-shore sediment plume increased in concentration, persisting until 19 February. Near-bed suspended sediments were likely underestimated north of 38° S due to dampening of riverine inputs and boundary condition effects.

Near-bed suspended sediment concentrations were elevated across much of the Gisborne region from the start of February (Figure 79). Similarly, there was an increase in near-bed suspended sediment concentrations during and after Cyclone Gabrielle, but this was more pronounced in shallower regions where wave activity was strongest. Near-bed suspended sediment concentrations were generally more elevated in Gisborne than in Hawke's Bay.
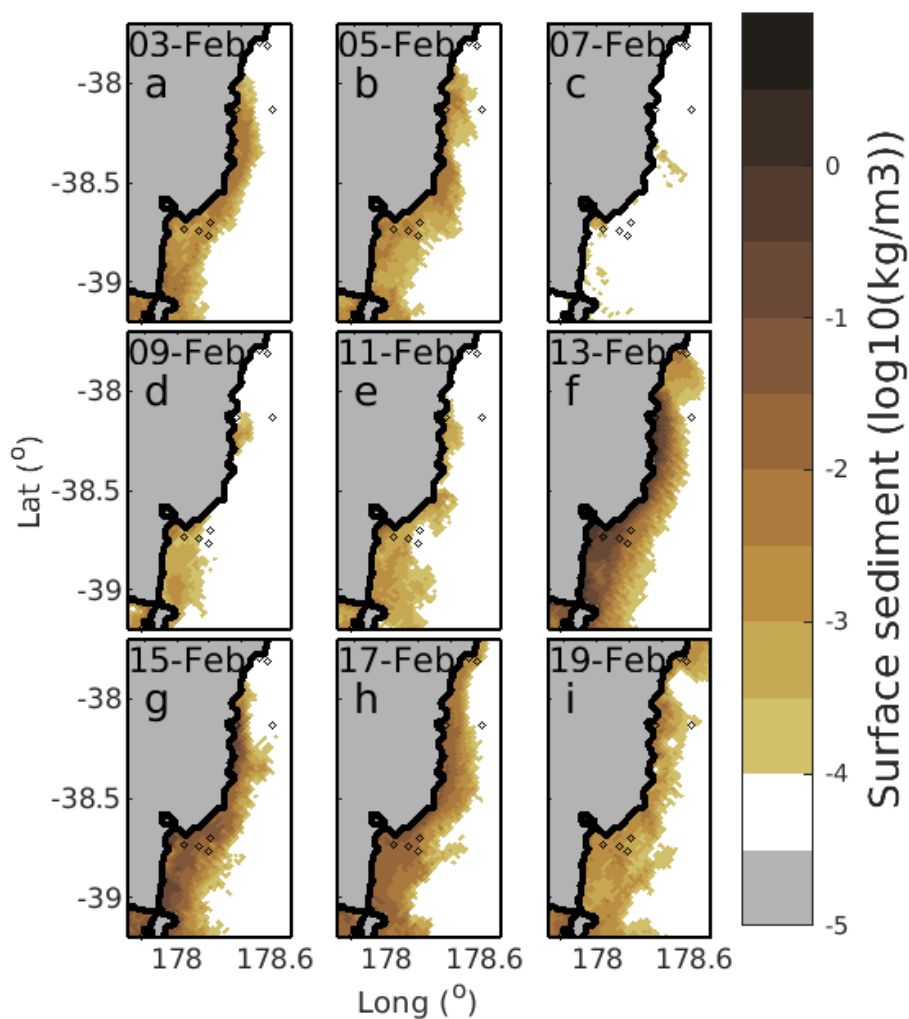
Figure 78: **Surface suspended sediment concentrations in the Gisborne region (3–19 February 2023). Each panel shows the concentration of sediments for a given day. For reference, location of coring transect sites are marked with empty circles.**
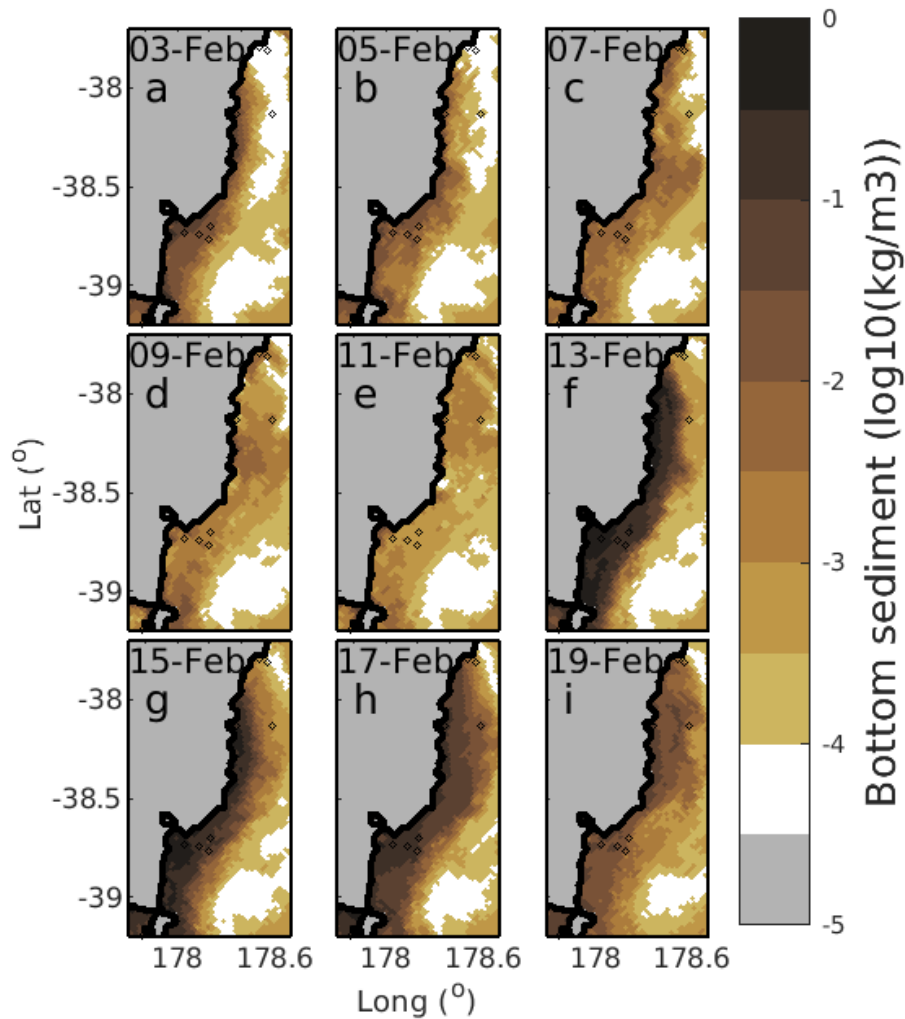
Figure 79: Near-bed suspended sediment concentrations in the Gisborne region (3–19 February 2023). Each panel shows the concentration of sediments for a given day. For reference, location of coring transect sites are marked with empty circles.

3.3.4 Modelled sediment deposition and erosion

Waves and currents cause resuspension, transport, and subsequent deposition, whilst riverine inputs create sediment deposition. These processes were amplified by Cyclone Gabrielle and the model captures both erosion and deposition associated with Cyclone Gabrielle storm event in the region. This deposition is shown as a change in bottom thickness from15 February, negative change indicating erosion, and a positive change indicating deposition (Figure 80).

Erosion occurred from the start of February off Cape Kidnappers and Mahia Peninsula in the Hawke's Bay region, increasing during the peak of Cyclone Gabrielle on the 15 February (Figure 80). These regions are more exposed to offshore currents and waves, making them more susceptible to erosion during normal and cyclonic conditions. Inshore, the model showed deposition of ~10 cm of sediments along the coast either side and offshore from Ngaruroro River mouth. This deposition persisted when riverine sediment inputs were removed from the model (not shown), indicating that deposition was at least partly driven by deposition of material resuspended by waves and currents, and not solely input from flood delivery. There was also significant deposition of up to ~0.5 m of sediment off the Mohaka River mouth, crossing the Wairoa Hard and fanning out offshore. This locus of deposition did not persist when riverine sediment inputs were removed from the model (not shown), confirming the contribution of riverine sediments at this location, and, more widely, the combination of drivers responsible for dispersal and the observed sediment distribution.
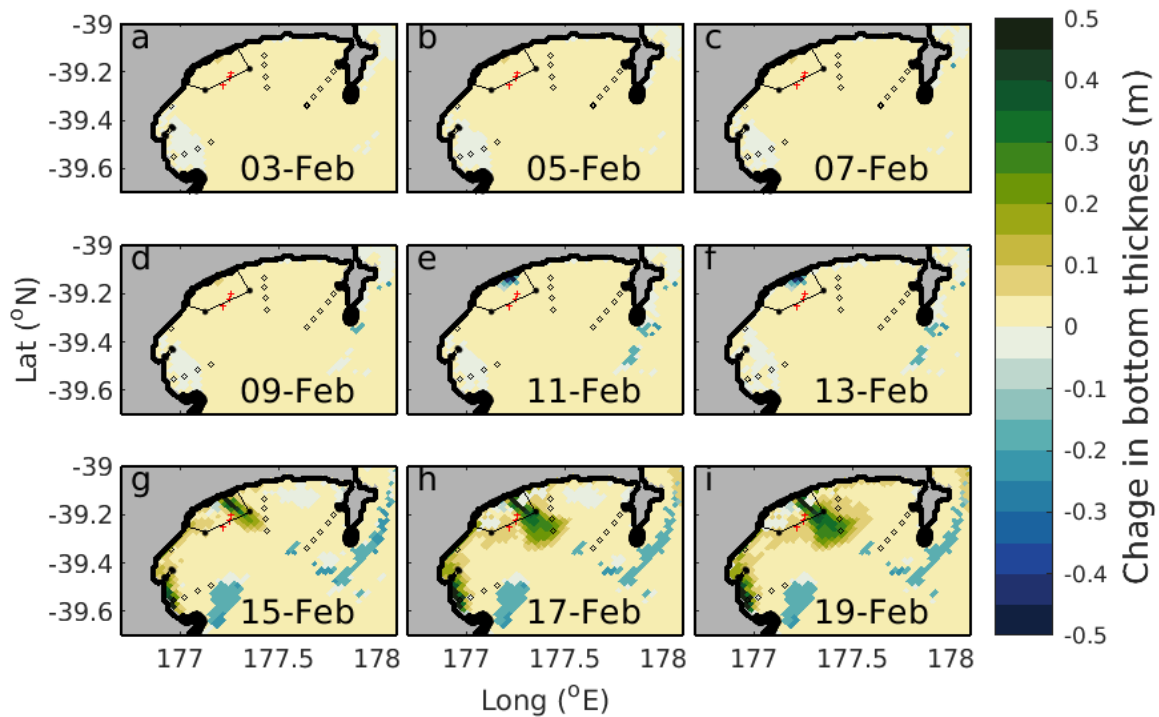
Figure 80: **Changes in seabed thickness in the Hawke's Bay region (3–19 February). Each panel shows the change in bottom thickness for a given day. For reference, location of coring transect sites are marked with empty circles and location of beam trawl samples (June survey KAH2303) are shown by red crosses; the outline of Wairoa Hard is shown by a black line.**

Over the simulation period there was erosion along the inner and inner-mid-shelf for most of the Gisborne region (Figure 81). This net erosion predated the cyclone and likely represents the backdrop of reworking of bottom substrates from prevailing waves and currents, rather than being an event-driven process. In the days following Cyclone Gabrielle, there was deposition of up to about 10 cm of sediments offshore of Poverty Bay and southwards. Sediment deposition also occurred along a narrow band of the coast to the north near Tokomaru and Tolaga bays. Sediment deposition was likely underestimated north of 38° S due to dampening of riverine inputs and boundary condition effects.
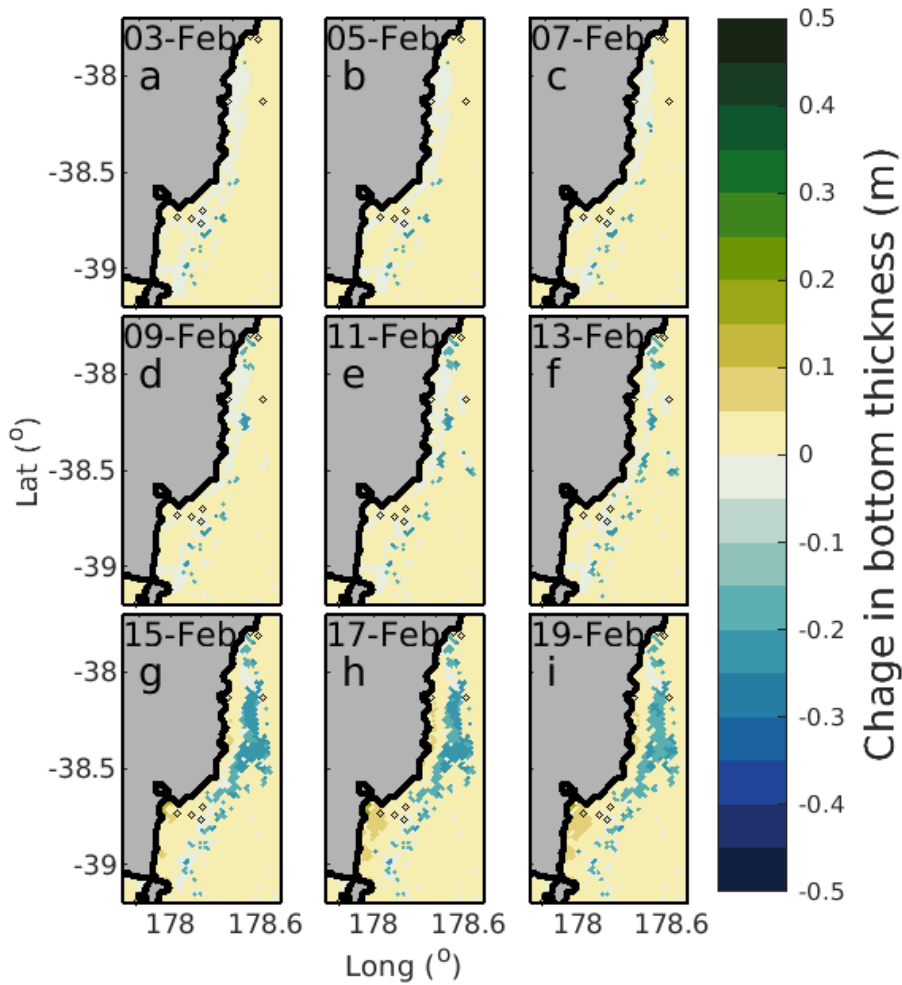
Figure 81: Changes in seabed thickness in the Gisborne region (3–19 February). Each panel shows the change in bottom thickness for a given day. For reference, location of coring transect sites are marked with empty circles.

3.4 Seafloor disturbance and recovery model

3.4.1 Seafloor model parameterisation

Sediment layers (representing percent mud content on the seafloor) were parameterised for the Hawke's Bay regional model using the Sustainable Seas sediment layer (Figure 82). A new data layer was prepared for the Gisborne regional model based on a national layer of the distribution of surficial sediments on the continental shelf and converted to percent mud content (Figure 83). Spatial fishing footprints were available for both regional models for both the pre-February 2023 historical fishing footprint, and for a post-February 2023 footprint (Figure 84).
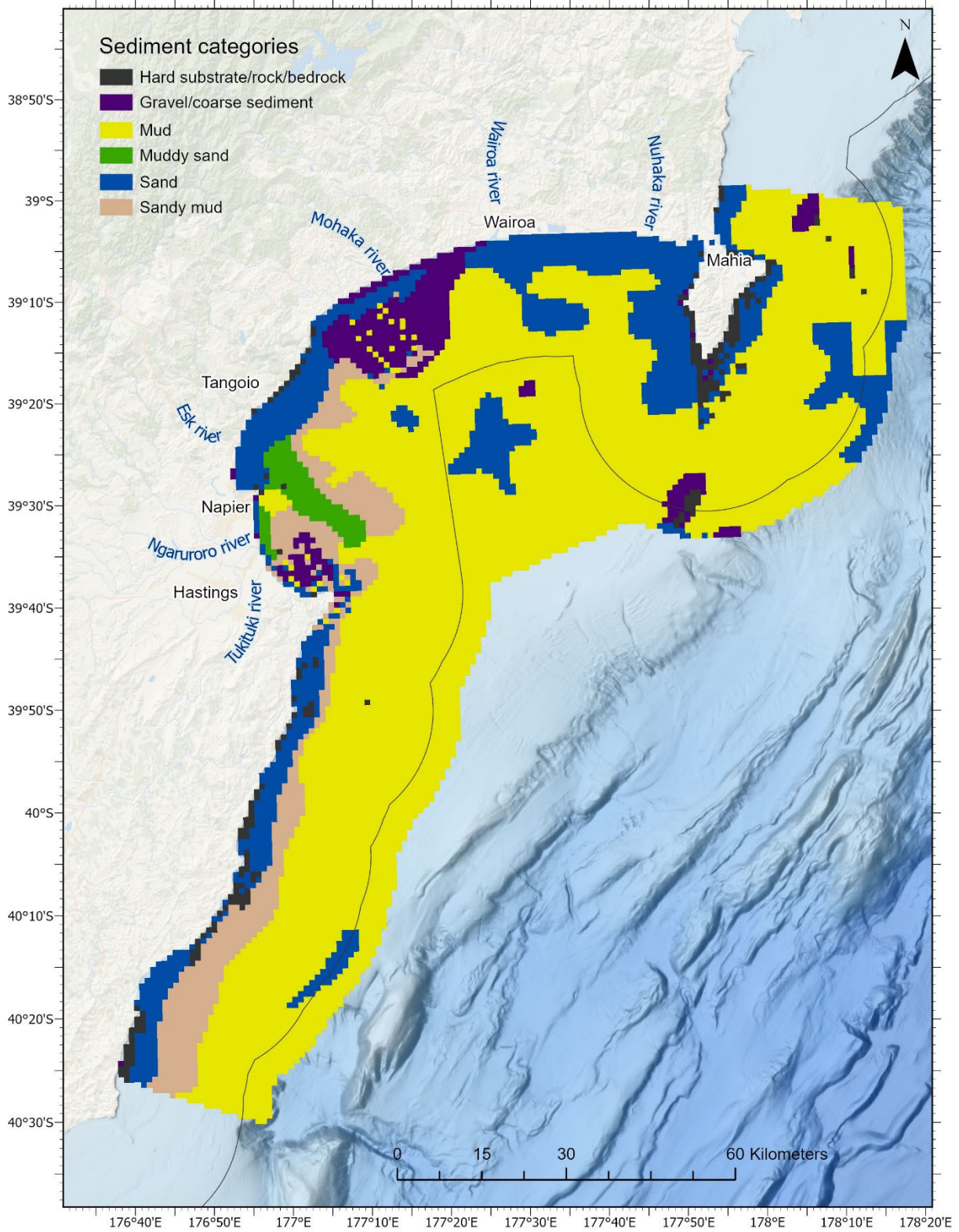
Figure 82: Spatial layer representing sediment mud content (the model indicator for the sedimentation stressor) in the Hawke's Bay region for the Seafloor model.
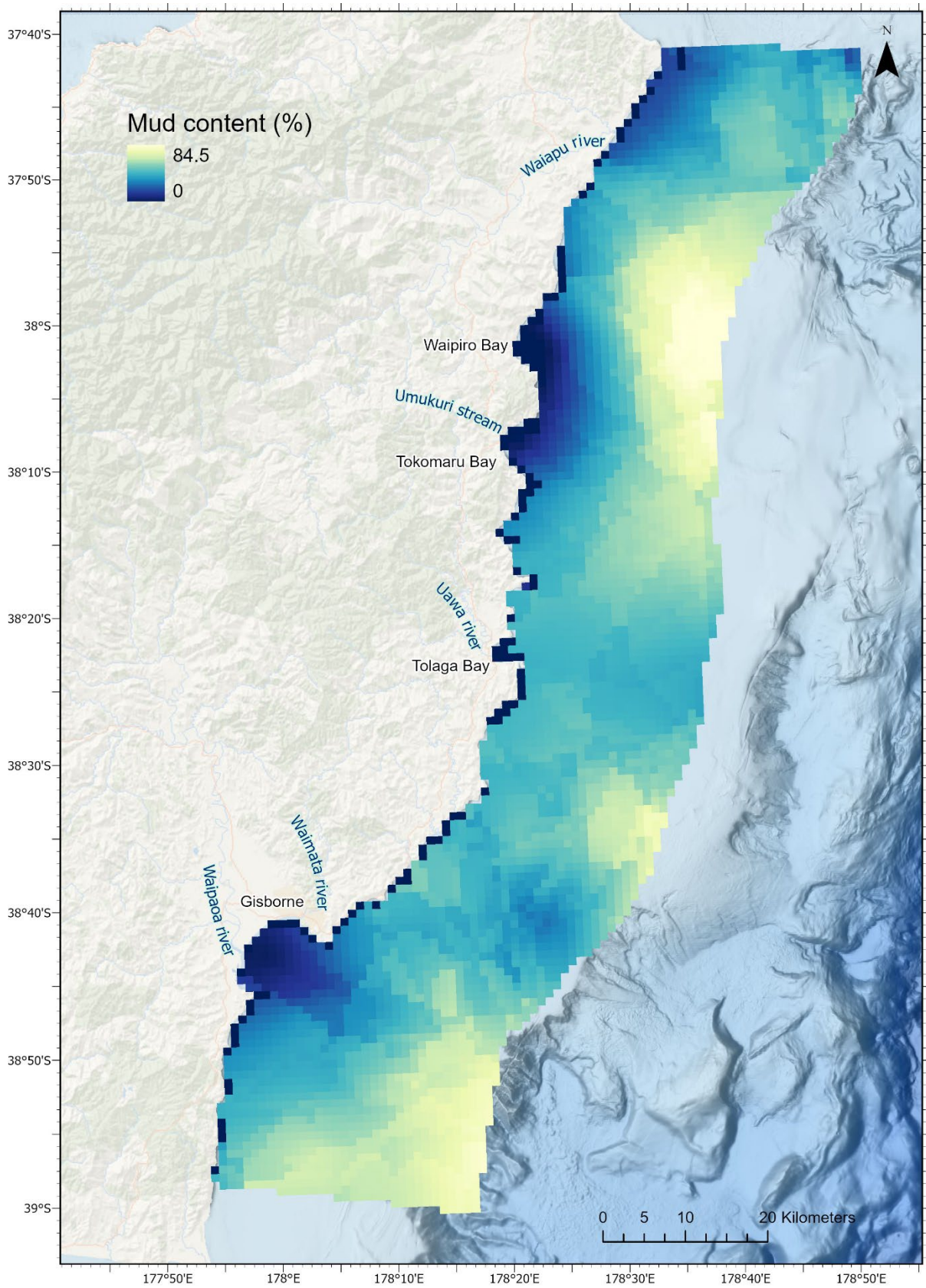
Figure 83: **Spatial layer representing sediment mud content (the model indicator for the sedimentation stressor) in the Gisborne region for the Seafloor model.**
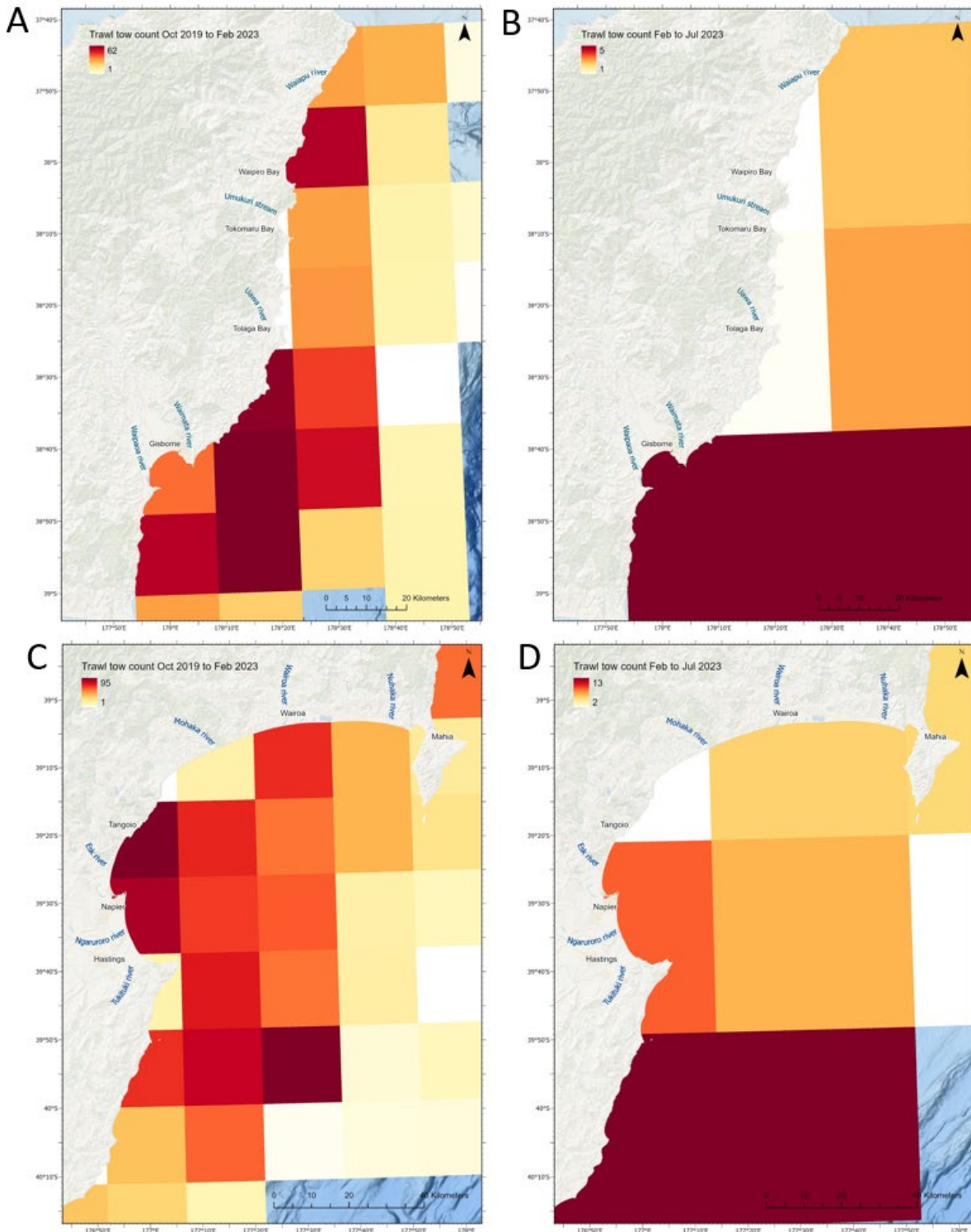
Figure 84: Spatial layers representing the spatial fishing footprint (number of tows per grid cell during given time period) for the Seafloor model. For the purpose of this report, spatial resolution of trawl count data was reduced to 0.2 (pre-cyclone) and 0.5 degree blocks (post-cyclone). Recent fishing footprint from 1 October 2019 to 13 January 2023 for the Gisborne region (A) and Hawke's Bay region (C). Post-cyclone fishing footprint based on data from 14 February 2023 to 31 July 2023 for the Gisborne region (B) and Hawke's Bay region (D). Note scales differ between figures and are not standardised to annual effort.

To quantify the rate of change in sediment mud content (the parameters used in the Seafloor model to represent mortality of functional groups due to sedimentation related processes), data from SCENZ

(Section 2.2) and the hydrodynamic model of sediment transport (Section 2.4) were interrogated to estimate the spatial pattern of sediment deposition and erosion on the seafloor.

Changes in sediment deposition following Cyclone Gabrielle were quantified based on the hydrodynamic model of sediment transport (described in Section 3.3). Three combined metrics were used to inform spatial patterns of sediment deposition in the Seafloor model: 1) daily averages of surface suspended sediment concentration (see Figure 76, Figure 78); 2) daily averages of near-bed suspended sediment concentration (see Figure 77, Figure 79); and changes in seabed thickness, showcasing areas of deposition and erosion (see Figure 80, Figure 81). The time series was explored, and layers representing spatial patterns of sediment deposition and erosion for the Seafloor model were developed assuming direct correlations between sediment deposition and changes in sediment mud content on the seafloor. Relationships between sediment deposition and percent mud content was parameterised based on existing data layers representing seafloor mud content, spatial differences in percent mud content from sediment cores (see Section 2.3.3), and expert knowledge of ecological impacts of sedimentation on seafloor invertebrates to approximate the rates of disturbance observed in the post-cyclone surveys of the region.

Patterns from SCENZ data suggested that suspended sediment concentrations from the cyclone event were within the range of typical winter events in terms of suspended sediment metrics such as TSS and EBED (see Section 3.1), and that the region is regularly impacted by events resulting in high levels of suspended sediments. Thus the sediment addition was modelled in the Seafloor model as a one-off addition of sediment mud content.

3.4.2 Cyclone event-based scenarios

To explore how the parameterisation of the cyclone event affected model predictions, scenarios were run varying the length of the sediment event (1 to 4 seasonal time steps) and the relationship between the hydrodynamic model predictions of sediment deposition and erosion with change in seafloor mud content. A key model development for this project was the inclusion of a spatially explicit layer of sediment deposition and erosion, which allowed for differential impacts across each model region. The prior model code (as used in the Hawke's Bay Sustainable Seas case study) included only a simple percent increase (or decrease) in sediment mud content that was applied equally across the active model region.

The scenarios presented here (Figure 85, Figure 86) use a length of one time step for cyclone related sedimentation selected for the final run for Gisborne, and two time steps for cyclone related sedimentation selected for Hawke's Bay. This difference was based on the expectation that sediment dispersed more rapidly in the Gisborne region than in Hawke's Bay, as suggested by the remote sensing, hydrodynamic modelling, and observations from the research vessel surveys. The scenarios presented for each region included a 200 time step (50 year) initialisation state, following by 200 time steps during which seafloor community assemblages stabilise (or in some cases, show declining trends) using pre-cyclone fishing effort (based on data from 1 October 2019 to 13 February 2023) to parameterise the bottom fishing stressor, and the seafloor mud content map prepared for each region to parameterise the sediment stressor, followed by addition of cyclone-related sediment deposition or erosion. Model results are presented as average proportion occupancy of adults of each functional group across the active model seascape, noting that average values may mask spatial variability in cyclone impact. Spatial differences were more apparent in the Hawke's Bay, and an example difference in spatial distribution of occurrence of functional group 6 (epifaunal biogenic structure-forming invertebrates) is illustrated in Figure 87 and Figure 88. The Seafloor model essentially shows a shrinking in the distribution of older age classes of epifaunal biogenic structure-forming invertebrates in Hawke's Bay during the Cyclone Gabrielle sedimentation event as a result of increased mortality at offshore locations.

Model behaviour differed slightly between the two model regions, primarily driven by how the seafloor sediment map was parameterised (Figure 85, Figure 86). The Hawke Bay seafloor sediment map included more areas defined as coarse sediments, which support different community assemblages than

muddier sediments due to the pre-defined model relationships between seafloor mud content and mortality of each of the functional groups. For example, some groups are more likely to occur in the Hawke's Bay region, likely due to these areas of coarse sediment (see e.g., Figure 82) which support higher abundance of functional group 3 (tube-forming invertebrates) and group 6 (epifaunal biogenic structure-forming invertebrates) in the Seafloor model. In contrast, the Gisborne region used a national layer representing seafloor mud content, which included generally higher mud content values for much of its model region (Figure 83).

Following the implementation of the cyclone sediment event, small declines are noted in most functional groups for Hawke Bay (Figure 85), though these declines are not substantial, as the pre-cyclone model state suggests the region is already impacted by decades of fishing and sediment stressors. The expected sediment inputs and seafloor deposition from the hydrodynamic and sediment transport model was predicted to be lower in Gisborne, resulting in lower percent increase in seafloor mud content in this regional scenario, and a more muted impact of the cyclone (Figure 86). Some groups showed either limited impact, or rapid recovery, post-cyclone; these were typically opportunistic groups (functional groups 1 and 2), predators/scavengers (functional group 8), and deep-burrowing invertebrates (functional group 7), which were parameterised as having a strong tolerance of high mud content. Each of these scenarios was presented with no fishing following the cyclone event to allow illustration of the cyclone event which was muted if the fishing stressor continued (Figure 85, Figure 86).
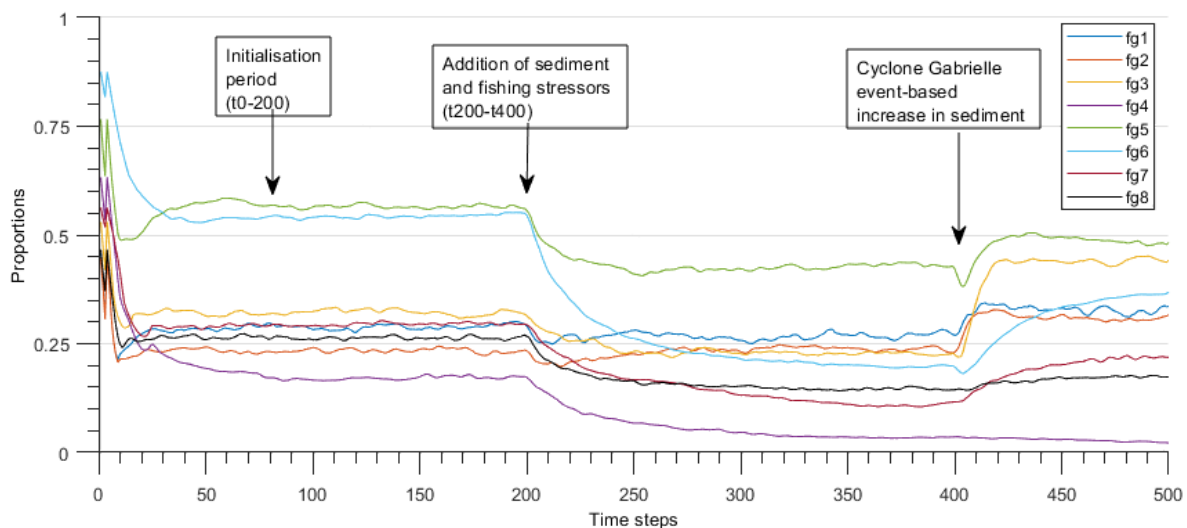
Figure 85: **Time series of the Seafloor model for the Hawke's Bay region, illustrating initialisation period (time steps 0-200), development of pre-cyclone seafloor community assemblage state (time steps 200–400), and addition of event-based stressor (400-401), followed by recovery. In this scenario, a full cessation of fishing activity is implemented following the cyclone event. The x-axis represents the proportion of cells in the active model region within which each functional group (fg) is present. The y-axis of time steps are seasons (4 seasons per year), and the full model simulation was for 125 years.**
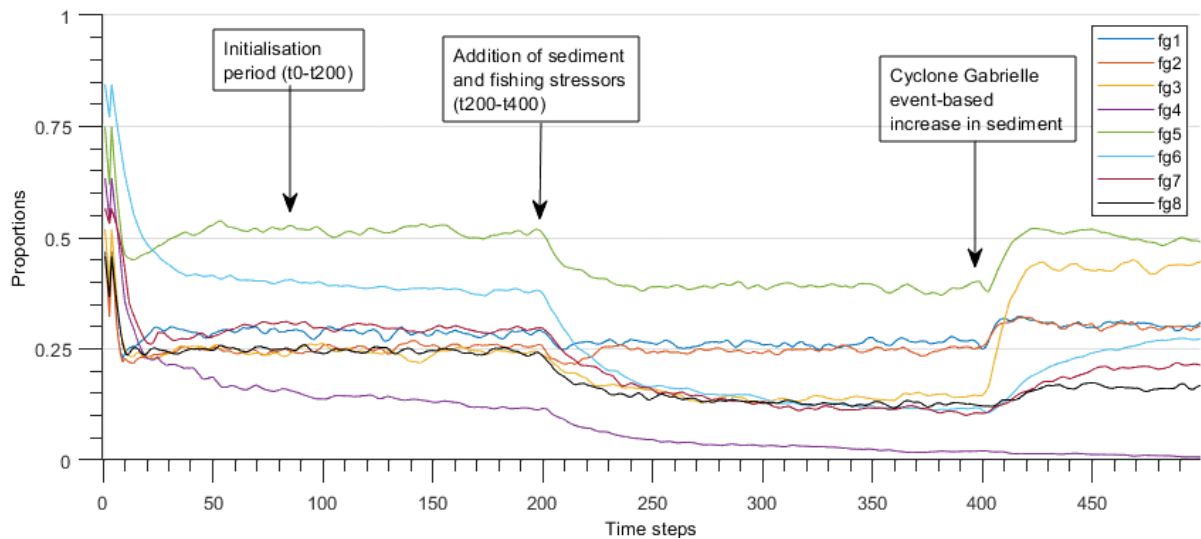
Figure 86: Time series of the Seafloor model for the Gisborne region, illustrating initialisation period (time steps 0-200), development of pre-cyclone seafloor community assemblage state (time steps 200-400), and addition of event-based stressor (t400-401), followed by recovery. In this scenario, a full cessation of fishing activity is implemented following the cyclone event. The x-axis represents the proportion of cells in the active model region within which each functional group (fg) is present. The y-axis of time steps are seasons (4 seasons per year), and the full model simulation was for 125 years.
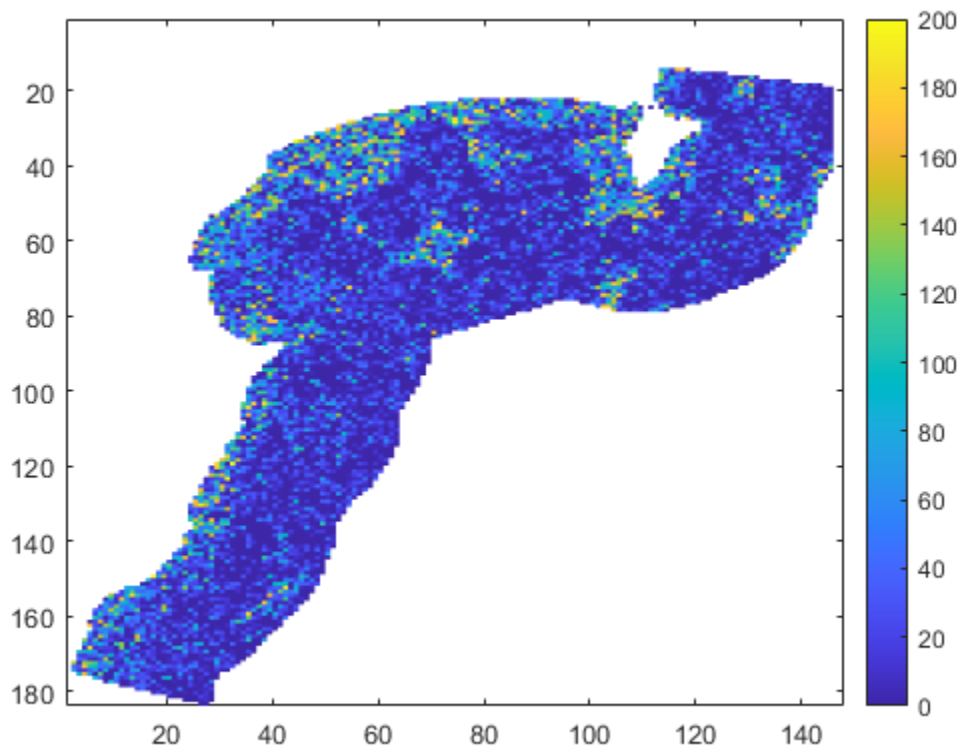
Figure 87: Spatial distribution of age classes of functional group 6 (epifaunal biogenic structure-forming invertebrate) prior to cyclone sedimentation event in the Hawke's Bay region in the Seafloor model. The colour legend represents maximum age of functional group 6 in each cell, with 0 representing an unoccupied cell, 1 representing a newly colonised cell, and increasing ages to a maximum age of ~200 seasonal time steps (50 years).
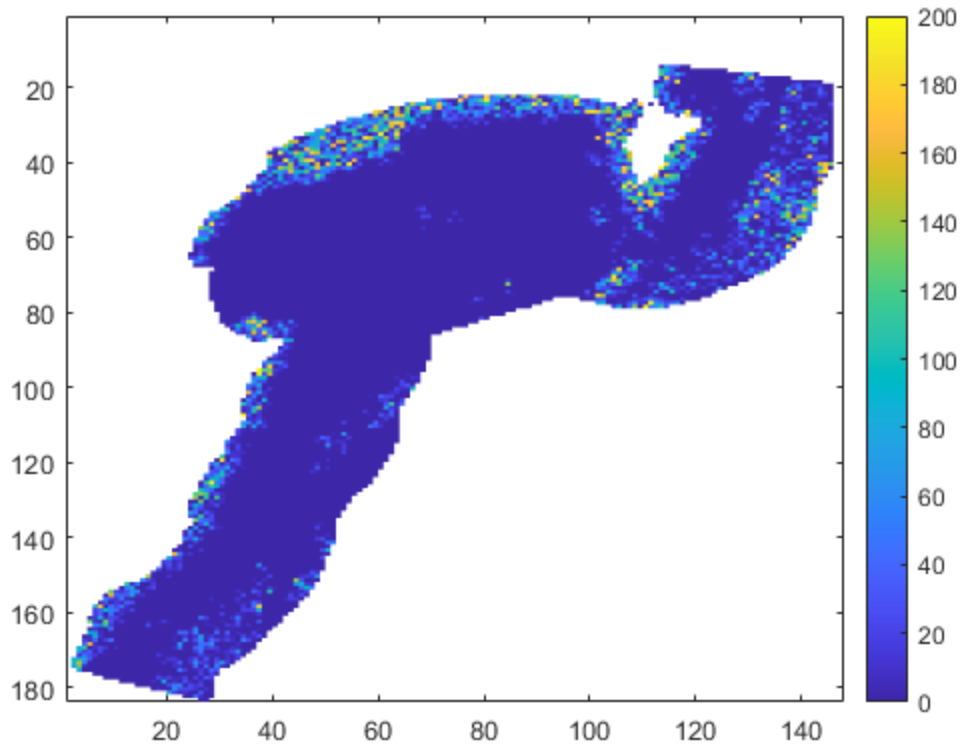
Figure 88: **Spatial distribution of age classes of functional group 6 (epifaunal biogenic structure-forming invertebrate) during the cyclone sedimentation event in the Hawke's Bay region in the Seafloor model. The colour legend represents maximum age of functional group 6 in each cell, with 0 representing an unoccupied cell, 1 representing a newly colonised cell, and increasing ages to a maximum age of ~200 seasonal time steps (50 years).**

Two recovery scenarios (Figure 89, Figure 90), run with 'hot starts' (i.e., pre-loaded with the time step 400 of the pre-cyclone conditions) showcased potential recovery trajectories with a modified fishing footprint. These scenarios were simulated to explore changes in seafloor invertebrate community recovery following modification of fisher behaviour to avoid high impact areas and woody debris in the inner Hawke Bay; changes in the fishing footprint in the Gisborne region were less apparent (Figure 84). Both scenarios show initial declines following the cyclone event, followed by some recovery (about 5% in the proportion of cells occupied for functional group 6) over the further 20 years (~80 seasonal time steps) of each model simulation. Recovery in these hot start scenarios is lower than for prior scenarios that included a full cessation of fishing activity in both regions (see e.g., Figure 85, Figure 86).
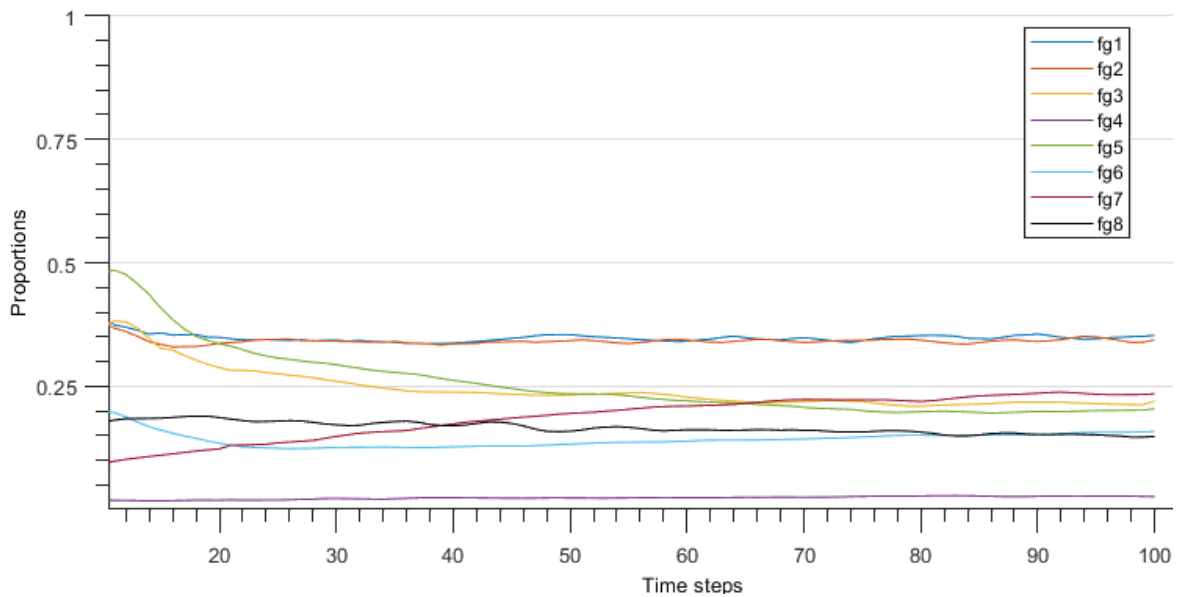
Figure 89: Time series of the Seafloor model for the Hawke's Bay region, illustrating a 'hot start' scenario with cyclone event occurring at time step 10, followed by implementation of modified post-cyclone fishing footprint. The y-axis of time steps are seasons (4 seasons per year), and the full model simulation was for 25 years.
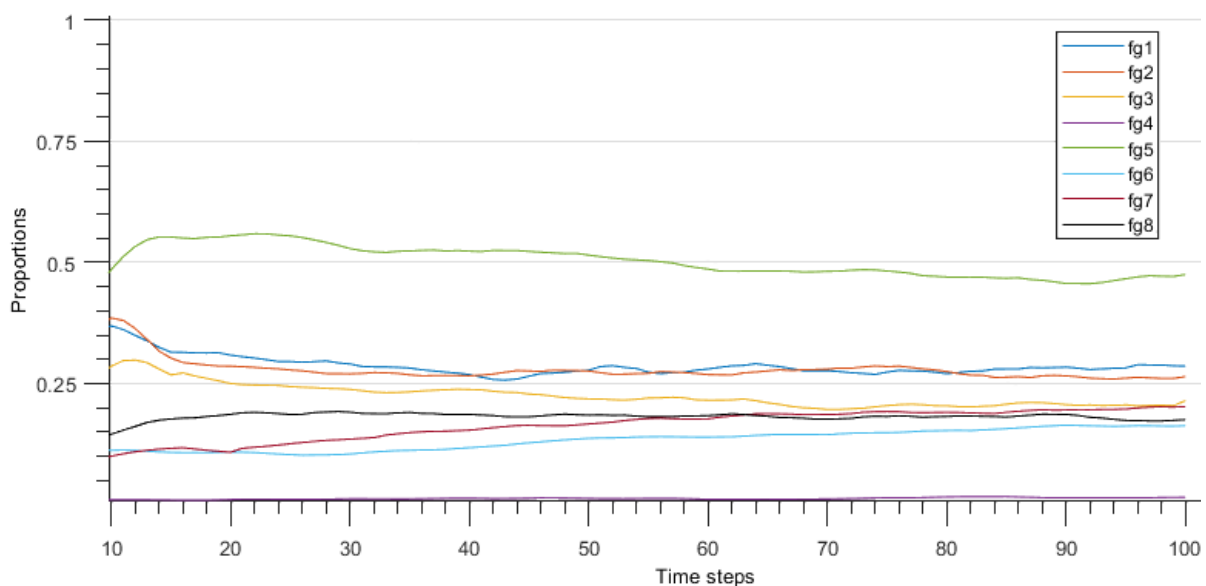
Figure 90: Time series of the Seafloor model for the Gisborne region, illustrating a 'hot start' scenario with cyclone event occurring at time step 10, followed by implementation of modified post-cyclone fishing footprint. The y-axis of time steps are seasons (4 seasons per year), and the full model simulation was for 25 years.

4. DISCUSSION

Remote sensing

This report provides data on a suite of satellite indicators to assess impacts and wider context of Cyclone Gabrielle on ocean health across a range of spatial and temporal scales. Companion web applications were built as part of this project to assist in exploring spatial patterns, climatologies, anomalies, and trends in the context of the cyclone using the NIWA-SCENZ mapping service. NIWA-SCENZ provides

a more accurate representation across clear open ocean to turbid coastal waters in a single product than from other sources of relevance to New Zealand conditions, at scales appropriate for coastal variability (500–1000 m; Aurin et al. 2013). More details on the use of remote sensing for monitoring suspended sediment and other ocean parameters, as well as the role of remote sensing in monitoring ocean health in New Zealand, are provided in recent reports (Pinkerton et al. 2022, 2023).

The limitations of satellite remote sensing of ocean colour in the New Zealand context are well documented and discussed elsewhere (Gall et al. 2022). Cloud cover during Cyclone Gabrielle, concealed observations during peak river flows, which is expected to lead to an underestimation of suspended sediment concentrations potentially propagating into temporal averaging. However, good viewing conditions occurred pre- and post-event, and, with linear time interpolation, a semi-quantitative view of the daily progression of changes provides the acute temporal and spatial context. Gap-free interpolation methods to handle missing data are being developed, with computationally efficient techniques showing promise in providing more accurate data (IOCCG 2019 and references therein).

Cyclone Gabrielle was preceded by Cyclone Hale earlier in January 2023, which brought significant rainfall across the Hawke's Bay and Gisborne regions. The influence of Cyclone Hale could be seen in elevated TSS and CHL values for the month of January relative to average values since 2002, and lower values for HVIS and EBED. It is likely that the magnitude of sediment erosion and transport from Cyclone Gabrielle would have been less pronounced without landscape conditioning (cf. Fuller & Marden 2010, Fuller et al. 2016) by Cyclone Hale, which likely exacerbated the speed with which rivers rose and the resulting number of landslides (Harrington et al. 2023). The impact of Cyclone Gabrielle on surface ocean parameters would also likely have been less pronounced.

Whilst oceanic mean-monthly total suspended sediment concentrations through February were significantly higher than mean values for the month, they did not exceed concentrations more typical of winter months. Similarly, the influence of the cyclone (as seen in elevated monthly values) persisted beyond the immediate impact of the flooding until about April, and thereafter were not evident by May. Thus, the influence of Cyclone Gabrielle on surface ocean parameters lasted approximately 2–3 months, at least at the scale of the Hawke's Bay and Gisborne CMAs. However, the duration of Cyclone Gabrielle effects at smaller spatial scales will likely have been more variable, depending on factors such as water depth, distance from major rivers, waves, and currents.

More pronounced short-term impacts on TSS, HVIS, and EBED were observed in Hawke's Bay relative to Gisborne in the days and weeks following the cyclone. This difference is likely due to differences in seabed topography and coastal morphology. As the largest bay along the eastern North Island, and with a broad and relatively shallow continental shelf, Hawke Bay is more likely to retain some sediment than the exposed and current-swept continental shelf at East Cape. A more pronounced, longer-term impact on light intensity at the seabed was also seen in Hawke Bay during February, March, and April than in Gisborne. This trend likely reflects the already low light intensity at the seafloor along most of the Gisborne coastline prior to the cyclone (which likely reflects its deeper seafloor) relative to Hawke Bay. Although the seabed topography and coastal morphology of Hawke Bay will tend to favour the retention of fine sediments for longer than in the Gisborne region, rivers in the latter region transport far greater amounts of sediments (Hicks et al. 2011). These factors may counteract each other to some degree, thus explaining why monthly trends in most ocean parameters did not differ more markedly between the two regions.

The extremely high chlorophyll concentrations observed in February in both regions are notable. These values were not only elevated for the month but also for the period since 2002. These high chlorophyll concentrations may have resulted from the pulse of nutrients produced from the fluvial export of sediment and soil to the ocean and greater vertical stratification in the water column resulting from freshwater input (Gall et al. 2024). Such a pulse in chlorophyll concentration was likely translated in elevated primary productivity, which may have had flow-on effects on the food web across the two regions and may have temporarily increased secondary productivity.

The spatial influence of Cyclone Gabrielle as observed using remote sensing extended well beyond the territorial sea (12 nautical miles). Spatial patterns in total suspended solids were influenced by the tidal forces and prevailing oceanic currents during and after the cyclone event. Key features broadly align with known oceanographic conditions of New Zealand shelf seas (Stevens et al. 2019), notably the large anti-clockwise East Cape Eddy located north of East Cape. This phenomenon induces alongshore currents, clockwise spinoffs, and a south easterly progression. Additionally, observable features include the influence of the Wairarapa Coastal Current and Eddy, demonstrating a north easterly progression along the Wairarapa coast. This is accompanied by currents both along and offshore, coupled with a south easterly progression off Mahia Peninsula.

Seafloor mapping and sediments
Repeat multibeam surveys revealed areas with modified bathymetry, suggesting sediment deposition and erosion at Pania Reef, Tangoio Reef, and the Clive outfall area. Because the pre-cyclone mapping surveys in some areas took place up to four years before Cyclone Gabrielle, attributing changes in bathymetry wholly to Cyclone Gabrielle will remain uncertain. Targeted sediment sampling from areas of sediment deposition at Pania Reef and Tangoio Reef consisted mostly of sandy sediments, indicating that either: (1) the original event deposit was sandy; or (2) the muddy fraction of the original Gabrielle event deposit has since been winnowed away by wave action and currents between the April and June surveys, leading to a coarser grained deposit. According to the physical habitat map of Haggit & Wade (2016), the seabed at Pania Reef and Tangoio Reef consists of sandy sediments, which is consistent with our findings. On balance, these areas are likely too shallow and exposed to oceanic reworking for fine sediment to settle for long periods. Accordingly, high near-bed turbidity is also sustained by the energetic ocean climate.

Macrofauna abundance in the Pania and Tangoio reef sediment deposit sites were low, particularly at Tangoio Reef, where only one individual was present in the core sample. These low abundances could be interpreted as evidence of a community impacted by the cyclone but more likely reflect a naturally depauperate macrofauna community resulting from an exposed environment with coarse sediments (McLachlan et al. 1984). The pattern of sediment deposition and erosion at the Clive outfall area suggests flood-related bottom flows on the innermost shelf eroded a channel seaward of the river mouth. Sediment deposits at this shallow location likely consist of sandy sediments (Haggit & Wade 2016).

It should be noted that whilst multibeam mapping can reliably determine sediment deposits ~0.5 m or more in thickness, potentially ecologically significant sediment drapes of a few to tens of centimetres are below the limit of detection for this method. Therefore, a lack of change in seabed geomorphology, as implied at the Wairoa Hard and Clive Hard multibeam data, does not necessarily imply that sediment deposition and/or resuspension did not take place.

A review of field observations during sediment coring and processing made during the June survey suggested the presence of fine sediment deposits, of variable thickness up to ~15 cm. These initial observations have recently been verified and advanced using X-ray computed tomography (CT) scans, the results of which will be made available as part of Swales et al. (in prep.). Most of these deposits were still present when a subset of the coring sites was revisited in October; however, without further age control from short-lived radionuclides collected immediately after Cyclone Gabrielle it is not clear whether these deposits were directly the result of Cyclone Gabrielle, and as such the origin of all the event deposits remains uncertain. For example, [7]Be, [234]Th, and ^{210}Pb were employed by Kniskern et al. (2014) to determine sediment dispersal across the shelf following a Waipaoa flood. Moreover, ocean storms, flood-sediment delivery, and combinations of these event drivers have been identified previously in the Poverty Bay shelf-sediment record (Hale et al. 2014).

Swell waves and oscillatory near-bed water motions were likely resuspending fine-grained substrates at inner shelf sites and winnowing the seabed, as was evident by the high near-bed turbidity seen on camera deployments during the June survey. However, some shallow (<30 m depth) sites off Ngaruroro and Wairoa rivers in Hawke Bay (coring transects T1 and T2, respectively) and off Tokomaru Bay and the Waiapu River (coring transects T5 and T6, respectively) in the Gisborne region consisted of fine

silty sediments which suggests retention of fines. However, contrasting core lithologies between the June and October voyages at coring transect T2 infers some remobilisation of fine sediments. At the shallowest site offshore of Wairoa (~30 m water depth), the uppermost deposit in October was significantly muddier, softer, and appeared to preserve more soft-sediment stratification than the previous core recovered in June.

Infauna

Infauna communities on continental shelves are influenced by a variety of factors including water depth, sediment grain size characteristics, food availability, and wave exposure (e.g., Martins et al. 2013). Significant seasonal and interannual variability can also be seen, with temperate soft bottom environments often exhibiting lowest macrofauna abundances in late winter/early spring and highest abundances in summer/early autumn due to seasonal recruitment patterns (Wheatcroft 2006).

Very little is known about the meiofauna communities on the New Zealand continental shelf. However, a recent study in the Kaikōura Canyon (~1000 m water depth) has shown meiofauna (and macrofauna) to be sensitive to benthic disturbance events (Bigham et al. submitted). Mean meiofauna abundance on the continental shelf of the west coast of the South Island was estimated at 1080 individuals 10 cm^{-2} by Probert (1986), similar to the mean abundance of 1014 individuals 10 cm^{-2} we observed. The overall abundance of the meiofauna community and the dominance of nematodes in samples from the continental shelf of Hawke's Bay and Gisborne are consistent with observations of communities in similar environments elsewhere (Giere 2009).

The macrofauna density observed across the Hawke's Bay and Gisborne regions during the June survey (41 individuals 0.01 m^{-2}), October survey (90 individuals 0.01 m^{-2}), and May and October 2010 surveys (75 individuals 0.01 m^{-2}) are comparable with macrofauna abundances on the continental shelf of the west coast of the South Island (Probert & Anderson 1986). In the latter study, macrofauna at inner shelf sites (23–31 m water depth) had a mean abundance of 80 individuals 0.01 m^2. Probert & Anderson (1986), however, used a coarser mesh than in the present study (1.0 mm *vs.* 0.3 mm) which will have led to a substantial underestimate of macrofauna abundances. Macrofauna abundance in sandy sediments north of Otago Harbour ranged from ~50 to 150 individuals 0.01m^{-2} at 15–26 water depth in a study by Paavo et al. (2011), which is comparable or slightly higher with the abundances observed in the Hawke's Bay and Gisborne regions. The Paavo et al. (2011) study also describes a trend of increasing abundance with depth across the 15–26 m depth range which was most marked at the Aramoana site where macrofauna patterns are likely the result of sediment disturbance. The latter study also showed slightly elevated macrofauna abundances and taxon richness in spring relative to autumn.

Most of the spatial variability in the infauna communities occurred along gradients of water depth and to a lesser extent sediment mud content. Sediment mud content varied widely among sites (2–97%) and tended to be greater at deeper sites, although a number of shallow sites also had elevated (>80%) mud content. Across the 2010 and 2023 surveys, we observed a trend of increasing macrofauna abundance with water depth, while no relationship was seen with sediment organic matter content (a proxy of food availability) or woody debris content. These findings could reflect the negative impact of wave-induced physical disturbance and/or riverine sediment discharges on macrofauna communities at shallow sites proximal to river mouths. There was a significant decrease in abundance (by almost 50%) and a shift in macrofauna community structure in June 2023 relative to May and October 2010 off Poverty Bay, followed by a significant increase in abundance (back to 2010 values) and shift in macrofauna community structure four months later in October 2023. This pattern could be interpreted as an impact on macrofauna communities caused by the deposition of riverine sediments during and immediately after the cyclone, followed by recovery later in the year, or may reflect natural seasonal and interannual variability. Macrofauna communities did not differ significantly between May and October 2010 however, which suggests that seasonal effects on macrofauna communities may be limited. If macrofauna communities were indeed impacted by the cyclone, the data gathered in October indicate that recovery likely occurred some eight months later, indicating that the infauna communities in the Hawke's Bay and Gisborne regions are adapted to benthic disturbance and can recover following extreme weather events. Time series data on the northern California shelf (70 m water depth) offshore

from the Eel River showed little evidence of impact on a macrofauna community following a historically significant flood that deposited 3–7 cm of fine sediments (Wheatcroft 2006).

Due to time constraints, not all major macrofauna taxa (i.e., annelids, molluscs, and arthropods) were identified beyond Phylum, Class, or Order level across all the 2010 and 2023 datasets. As a result, comparisons of macrofauna community structure between sampling years or months were conducted at relatively coarse taxonomic resolution for most taxa and changes in communities were likely missed (e.g., shifts in abundance of polychaete species). Variability in community structure was therefore likely underestimated in our analyses.

Although we were able to include pre-cyclone macrofauna samples from Poverty Bay in our analyses, the main impediment in evaluating the potential impacts of Cyclone Gabrielle on the infauna is the paucity of baseline information. Data from this study help provide a better understanding of spatial and temporal variability in the sediment fauna of Hawke's Bay and Gisborne, but more information is needed on seasonal and interannual variability to enable a better assessment of impacts from weather events in the future. Data on meiofauna are particularly scarce with only two other studies having been conducted on New Zealand continental shelf meiofauna to date (Probert 1986, Kamenev et al. 1993).

Towed camera transects
Over 70 towed camera transects were conducted at 36 sites along the Hawke's Bay and Gisborne CMAs to assess the likelihood of sediment impacts to benthic habitats. Key observational evidence includes: (1) fresh muddy deposits and sediment smothering of benthos; (2) organisms in poor condition; (3) absence of macroalgae at shallow depths. Using these qualitative measures, sediment impacts are highly likely to have occurred at 11 locations (see Table 11). However, for most of these locations demonstrating a direct link to Cyclone Gabrielle and drawing quantitative conclusions remains problematic without survey data prior to the event. One likely exception is Wairoa Hard, where comparison of pre- and post-cyclone data from imagery shows that while kelp, other macroalgae, and sponges were present before the cyclone, they were effectively absent after the cyclone. Whether this loss of biogenic habitat has led to reductions in associated fish populations cannot be determined due to lack of data on fish distributions, together with their potential association with the range of habitats regionally prior to the cyclone. Juvenile snapper are known to be strongly associated with subtidal seagrass meadows, horse mussel beds, and shallow muddy seafloors with extensive large multi-entranced crustacean burrows (Morrison et al. 2014a, b, c), as well shallow reef edges in estuaries (Campbell 2023). Juvenile snapper are affected by elevated suspended-sediment concentrations of 10–40 NTU through reduced foraging success, gill damage, and increased risk of infections (Lowe et al. 2015). Turbidity levels measured at Wairoa Hard during the October survey reached values of up to ~12 NTUs, which is at the lower end of the deleterious NTU range. However, the turbidity in October, some eight months after the cyclone, was lower than during the June survey based on our qualitative comparison of the poorer visibility encountered in June. Potential sediment impacts in the Hawke's Bay region might also have occurred at Cape Kidnappers, although observational data are less compelling. There, macroalgae are absent in both pre- and post-cyclone imagery, indicating that chronic sediment impacts may pre-date Cyclone Gabrielle. It is possible that this area is impacted by local erosion of the adjacent coastline and cliffs, or by ongoing sediment outputs from the nearby Ngaruroro River.

In the Gisborne region, several inshore reefs in Poverty Bay, Anaura Bay, Waipiro Bay, Whakariki Point, and Waikori Bluff were assessed as having a high likelihood of sediment impacts based on benthic observations. While the inshore Poverty Bay reef showed strong indications of impact, another inshore reef located just north of Poverty Bay showed no indication of being strongly impacted by sediment. Collectively, these observations suggest a range of benthic disturbance from river plumes that affect parts of the Gisborne coastline differently. Offshore reefs near the edge of the continental shelf off Poverty Bay and at Table Cape also showed signs of sediment impacts despite being located further seaward of riverine sources. Data from previous sediment dispersal studies off the Waipaoa and Waiapu sedimentary systems provide compelling evidence for the efficiency of hydrodynamic processes to transport riverine material across and along the continental shelf, amplified by climate and oceanic events (e.g., Kuehl et al. 2016). It is likely that most, if not all, of the locations impacted by sediments

are naturally exposed to high turbidity conditions near-bed, and periods of deposition. That said, the scale of Cyclone Gabrielle will likely have exacerbated suspended sediment loads in the region through an abundance of sediment supply. Evidence from coring suggests that inshore muddy deposits are still being reworked within Hawke Bay eight months after the cyclone, raising the possibility of ongoing chronic impacts to some habitats. Further observational data are needed to support a deeper understanding of long-term and residual impacts at specific sites.

Hydrodynamic/sediment modelling

Models of ocean currents and temperature used to predict the dye tracer movement are well developed for this region and tend to have few errors. The sediment model, however, is new for this region and was characterised by greater uncertainty due to lack of data to describe the sediment inputs and provide model calibration and by the short spin up time. The lack of data meant that the seabed sediments were not well described, and the bed layer was created from a small amount of data particularly in the Gisborne region. In the Hawke's Bay region, the model assumed that the sediments were composed completely of mud, but sediment data show that some of the shallower areas (e.g., Pania Reef, Clive outfall area) consist of mainly sandy sediments (Haggit & Wade 2016, present study).

Little information is available on the amount and nature of the sediments being transported to the ocean by rivers. For most of the rivers, rating curves were calculated from turbidity data, but these did not contain many large riverine flow events such as those seen during Cyclone Gabrielle and the errors associated with this large-scale event are unknown. Model experiments showed that these rating curves produced unrealistically large sediment deposits and the sediments coming in from the rivers had to be reduced by a factor of 100 to get realistic sediment inputs. Improvements could be made to the existing model by calibrating the sediment size classes coming in from the rivers.

Some areas of erosion in the model coincide with regions characterised by hard substrates, such as Lachlan Ridge and off Portland Island in Hawke's Bay and Table Cape in Gisborne, indicating that erosional forces may be acting over these features over the long term. The relatively large areas of erosion seen in the wake of the cyclone in both study regions, however, occur over areas of soft sediments. This sediment will have been resuspended and transported elsewhere, adding to the already elevated near-bed suspended sediment loads from river flows. This is exemplified by the sedimentation in western Hawke Bay in the vicinity of Ngaruroro River mouth, which persisted in the model when riverine sediment inputs were removed, indicating that this deposition was at least partly due to deposition of material resuspended by waves and currents from elsewhere in the region. Thus the sedimentation-related impacts of the cyclone were not solely due to sediment inputs from rivers, but also the erosion and resuspension of the seafloor by increased swell and wave action. This process can also be seen in maps of near-bed suspended sediments, which show that most of the seafloor in the Hawke's Bay and Gisborne regions lies under highly turbid water with elevated sediment concentrations in the days following the cyclone. Our own observations during the June survey showed very low visibility throughout much of the shallower parts (<40–50 m depth) of Hawke's Bay and Gisborne, which shows that these conditions are not unusual in normal conditions.

The model predictions of sediment deposition in the central and western parts of Hawke Bay are consistent with our observations from sediment core samples in the region. The thickness of recent sediment deposition layers were most elevated along coring transects T1 and T2 in western and central Hawke Bay, respectively, while thinner deposits were seen in cores from coring transect T3 on the eastern side of Hawke Bay, where the model describes limited sediment deposition (or erosion). Recent sediment deposits in cores from coring transect T4 off Poverty Bay were broadly consistent with sediment deposition patterns from the model. The model performed less well near East Cape and the Waiapu River where sediment deposition was likely underestimated due to dampening of riverine inputs and boundary condition effects.

Seafloor model

The Seafloor model was used to explore different scenarios of cyclone impact and recovery, as well as allowing exploration of how different parameterisations of sedimentation influenced the likelihood of recovery. The Seafloor model illustrated the challenge of the limited baseline data within the Hawke's Bay and Gisborne regions, both in terms of seafloor sediment mud content and also in baseline knowledge of seafloor invertebrate community assemblages. The Hawke Bay seafloor sediment map was likely more accurate, based on local knowledge of habitat features, whereas the Gisborne map was based on national scale sediment analyses with few samples in the region extrapolated to create a continuous sediment layer. No coarse sediment features were present in the Gisborne national sediment model, though these features are known to occur (e.g., Ariel Bank), similar to those known and mapped by local fishers in Hawke Bay.

The Seafloor model was initially parameterised for cumulative sediment impacts, experienced primarily through changes in mud content at the seafloor, and was not developed to model event-based sediment deposition such as that of Cyclone Gabrielle. A number of assumptions were taken into account to create this cyclone-based event scenario. First, the relationship between sediment mud content and hydrodynamic model changes in sediment bed level were modelled in a linear fashion, which could be either an over- or an under-estimate of sediment impacts. Limited sediment cores were available to estimate mud content and how this varied across the impacted region to validate the modelled relationship. Increases in sediment mud content resulted in increased mortality rates for most groups (especially epifaunal invertebrates) in the model (i.e., increasing mortality to reflect impacts of sediment). However, the model is not parameterised to allow for rapid burial impacts. Inputs of woody debris were documented in surveys but not included in the Seafloor model; inclusion of this additional impact could further inform understanding of cyclone impact and recovery.

Further, little information was available to describe the post-cyclone sediment resuspension and erosion. The Seafloor model assumes minimal sediment erosion; rather, it subjects seafloor invertebrate communities to ongoing and cumulative impacts of sediment that has been deposited. Sediment erosion and offshore transport of sediments could be included in the model, and the Sustainable Seas Hawke's Bay case study presented scenarios that modified sediment inputs with expectation of reduction in seafloor mud content (Lundquist et al. 2022a, b). However, as rates and spatial patterns in erosion and offshore transport of sediments are unknown, they were not included in model scenarios, but further information could allow for this additional complexity.

Fishing effort was modified in some scenarios to account for changes in the footprint due to observed changes in fisher behaviour. Scenarios included both a full cessation of fishing as well as the modified fishing footprint. Both showcase recovery following the cyclone, though recovery is slower with fishing than without. It is unknown how long the modified fishing footprints will continue, and the Seafloor model allows testing of different options to explore how spatial changes in fishing effort could enhance recovery following the cyclone event. Scenarios could also explore a time series of sedimentation events, such as Cyclone Hale in January 2023, and other events in recent and past decades that have resulted in significant sediment inputs into the Hawke's Bay and Gisborne regions.

Overall, the Seafloor model shows small declines in most functional groups for Hawke Bay following Cyclone Gabrielle. These declines were not substantial, most likely because the pre-cyclone model state suggests the region is already impacted by decades of fishing and sediment stressors. This degraded state reflects perceptions of the Hawke's Bay Marine and Coastal Group and is in part why this group was founded (Lundquist et al. 2022a); historical habitat degradation is also reflected in fisheries management measures such as closure of the Wairoa Hard to enhance recovery of this important nursery ground. Nevertheless, the Seafloor model showed a shrinking in the distribution older age classes of epifaunal biogenic structure-forming invertebrates in Hawke Bay during the Cyclone Gabrielle sedimentation event as a result of increased mortality at offshore locations.

The expected sediment inputs and seafloor deposition from the hydrodynamic and sediment transport model were predicted to be lower in Gisborne than in Hawke's Bay, resulting in a more muted impact

of the cyclone on seafloor communities. This difference between the regions is also likely to be partly due to an underestimation of the extent of hard substrates (and their associated communities) in the Gisborne region due to fewer data being available. The modelling suggests that seafloor communities in the Gisborne region show signs of pre-cyclone impacts from increased sedimentation and fishing, as seen in the Hawke's Bay modelling.

Concluding remarks

A major impediment in assessing the potential impacts of Cyclone Gabrielle on seabed ecosystems of Hawke's Bay and Gisborne was the paucity of baseline information, particularly for inshore reefs in the Gisborne region where virtually no data were available. Without information on the spatial and temporal distribution of seabed organisms, it is challenging to quantify the magnitude of any potential cyclone effects. Data collected and described herein, including data on sediment infauna from core samples and visual observations of habitat-forming organisms, now form a valuable baseline dataset that will inform future impact assessments in the region. With extreme storms forecast to increase with global warming, the relevance of similar baseline data will only increase, informing quantitative assessments of benthic disturbance, ecological impact, and recovery.

One critical limitation with current methodologies is the use of towed cameras to survey benthic communities. High near-bed turbidity was a constant challenge for towed camera deployments in Hawke Bay and along the Gisborne coast during the June survey, and visibility remained limited in parts of Hawke Bay during the October survey. The habitats and organisms most likely to be impacted by sedimentation cannot be visually assessed for extended periods (8 months in the case of Cyclone Gabrielle) following extreme weather events, preventing a rapid assessment of impacts. Whilst habitat-forming species such as kelp and sponges may survive sediment deposition and extended period of elevated turbidity, high levels of near-bed suspended sediments may reduce the extent to which these ecosystems are used by commercially and recreationally harvested species. Potential flow-on effects on fisheries (e.g., from low recruitment) will likely not be felt for a number of years. With this limitation in mind, a precautionary approach could be warranted in the period following an extreme weather event until key habitats and ecosystems can be surveyed, while fish stocks and catch levels are carefully monitored in the years following the event.

Sediment transport modelling is a promising tool for rapidly identifying areas most at risk from sedimentation following extreme weather events such as Cyclone Gabrielle. The model developed for the east coast of the North Island provided a realistic picture of surface and near-bed suspended sediments as well as sedimentation levels as assessed through comparisons with satellite data products and samples and observations obtained in the field. This model could be improved by obtaining data on the concentration and grain size distribution size of suspended river sediments both under normal conditions and during extreme weather events, turbidity, and suspended sediment concentrations in coastal and offshore waters in the wake of an event, and with more detailed spatial information on seafloor substrate characteristics. There are time-critical dependencies at scales of days to weeks after an event for collection of some data and samples. Thus, rapid response field sampling following an event should concentrate on obtaining a range of water and sediment parameters that will provide valuable data to calibrate sediment transport models. Sediment core sampling can also provide valuable samples for analyses of the short-term response of sediment infauna, thickness of deposited sediment layer, and radionuclides for identification of terrestrial inputs.

The Seafloor model could be improved with the inclusion of better information on the spatial distribution of seafloor substrates (including sediment grain size and extent of hard substrates), particularly in the Gisborne region, as well as seafloor communities. The model suggests that the seafloor communities in the Hawke's Bay and Gisborne regions are already impacted by the effects of increased sedimentation and bottom trawling, and that continued trawling may slow down recovery at the CMA scale following an event such as Cyclone Gabrielle. The Seafloor model could be used to explore how spatial changes in fishing effort could enhance recovery following extreme weather events.

Findings from this project show that the impacts of Cyclone Gabrielle on the marine environment are not just related to increased sediment inputs from rivers in the immediate wake of events. Sediments have accumulated along the coast and shelf of Hawke's Bay and Gisborne at an increasing rate for decades due to deforestation and land use change. During an extreme weather event, the impacts of increased river flows are compounded by the remobilisation and suspension, by the action of waves and swell, of fine sediments accumulated over long periods. Addressing the long-term issue of sedimentation in marine ecosystems as well as the impact of extreme weather events will require addressing the factors that have made New Zealand's catchments more prone to erosion.

5. FULFILLMENT OF BROADER OUTCOMES

5.1 Remote sensing, acoustic, and oceanographic data

A range of data and data products were derived from this project, including:

- Ocean colour satellite data from NASA's MODIS-Aqua satellite (now integrated in the NIWA-SCENZ portal and publicly available from January 2024)
- Multibeam mapping data covering 582 km^2 of seafloor (KAH2303: 93.5 km^2; KAH2306: 488.5 km^2). These data are archived in the acoustic database held by NIWA.
- Conductivity Temperature Depth (CTD) data were collected during towed camera deployments (June and October surveys). These data are stored in the CTD database held by NIWA.

5.2 Building capacity and capability in the research sector

- Sediment core samples and data obtained from multicorer deployments, which will feed directly into the SEA2022-13 Cyclone Gabrielle sediment analyses project.
- Data on sediment infauna (macrofauna and meiofauna) from 52 core samples, including identification to species/morphospecies of polychaetes, and selected mollusc and crustacean taxa.
- Curation into the NIWA Invertebrate Collection and data entry (*niwainvert* database) of all identified polychaete, crustacean, and mollusc taxa identified from the macrofauna samples.
- Video, images, and associated data of seafloor communities from 81 towed camera transects.
- Creation and calibration of a coupled hydrodynamic and sediment transport model for the east coast of the North Island.
- Adaptation of a model of seafloor disturbance impacts encompassing Hawke's Bay and Gisborne, informed and calibrated by new data obtained as part of this project (listed above).
- Provision of nematode specimens for taxonomic work and species descriptions.
- We communicated our findings to the research community via a keynote presentation at the Geosciences Society of New Zealand Annual Conference 2023 on 16 November in Wellington (Alan Orpin; Title: "Cyclone Gabrielle impacts on seabed ecosystems off Te Matau a Māui/Hawke's Bay and Tairāwhiti/Gisborne regions").
- We presented projects findings in Seaweek's Nga Korero webinar on extreme weather and ocean warming, 9 November (Daniel Leduc; Title: "Cyclone Gabrielle's impacts on seabed ecosystems"). An overview and recoding of the webinar is available here: https://seaweek.org.nz/news/extreme-weather-and-warming-nga-korero-webinar-recap.

5.3 Working collaboratively with Māori, stakeholders, and industry

We are committed to ensuring this project benefits Māori and stakeholders. We began engaging with Hawke's Bay and Tairāwhiti iwi/hapū from the start of the project in May 2023, initially via conference calls and email. These early discussions resulted in the participation of Justin Tibble (Ngāti Porou) in the June RV *Kaharoa* survey.

Engagement and discussions with iwi and hapu partners during the project were coordinated by Joshu Mountjoy and members of NIWA's Te Kuwaha team (April Nepia-Su'a and Niketi Toataua). Joshu Mountjoy presented an overview of the project and some preliminary findings from the June survey at the Fish Hook Summit in Napier in July. A small team from the project attended workshops in Gisborne and Tokomaru Bay in August and September, respectively, to discuss early findings and identify priority areas for the following survey in October. An engagement day and RV *Kaharoa* port call was organised halfway through the October survey at Napier port. This provided an opportunity for participants to visit the vessel, interact with some of the scientists involved in the project, and discuss findings. A port call was also originally planned for Gisborne but could not go ahead due to health and safety concerns.

We actively engaged with Hawke's Bay Regional Council and Gisborne District Council from the beginning of the project. These early discussions enabled us to target areas of interest to the councils as well as share available information on marine ecosystems in these regions. The fishing industry also identified areas of interest which we were able to target during the RV *Kaharoa* surveys.

6. ACKNOWLEDGEMENTS

7. REFERENCES

Alexander, C.R.; Walsh, J.P.; Orpin, A.R. (2010). Modern sediment dispersal and accumulation on the outer Poverty continental margin. *Marine Geology 270*: 213–226.

Anderson, M.; Clarke, K.; Gorley, R. (2008). *PERMANOVA+ for Primer. Guide to Software and Statistical Methods*. University of Auckland and PRIMER-E Ltd, Plymouth.

Aurin, D.; Mannino, A.; Franz, B. (2013). Spatially resolving ocean color and sediment dispersion in river plumes, coastal systems, and continental shelf waters. *Remote Sensing of Environment 137*: 212–225. <http://dx.doi.org/10.1016/j.rse.2013.06.018.

Behrens, E.; Williams, J.; Morgenstern, O.; Sutton, P.; Rickard, G.; Williams, M.J. (2020). Local grid refinement in New Zealand's earth system model: Tasman Sea ocean circulation improvements and super-gyre circulation implications. *Journal of Advances in Modeling Earth Systems 12(7)*: 2019MS001996.

Berryman, K.B.; Marden, M.; Eden, D.; Mazengarb, C.; Ota, Y.; Moriya, I. (2000). Tectonic and paleoclimatic significance of Quaternary river terraces of the Waipaoa River, east coast, North Island, New Zealand. *The New Zealand Journal of Geology and Geophysics 43*: 229–245.

Biggs, B.J.F.; Duncan, M.J.; Jowett, I.G.; Quinn, J.M.; Hickey, C.W.; Davies-Colley, R.J., Close, M.E. (1990). Ecological characterisation, classification, and modelling of New Zealand rivers: An introduction and synthesis. *New Zealand Journal of Marine and Freshwater Research 24(3):* 277–304.

Bigham, K.T.; Rowden, A.A.; Leduc, D.; Bowden, D.A.; Nodder, S.D.; Orpin, A.O.; Halliday, J. (2023). Deep-sea macrofauna community recovery in Kaikōura Canyon following an earthquake-triggered turbidity flow. *Deep-Sea Research Part I 202*: 104192.

Bigham, K.T.; Leduc, D.; Rowden, A.A.; Bowden, D.A.; Nodder, S.N.; Orpin, A.O. (submitted) Recovery of deep-sea meiofauna community in Kaikoura Canyon following and earthquake-triggered turbidity flow. PeerJ.

Blott, S.J. (2020). GRADISTAT 9.1: A grain size distribution and statistics package for the analysis of unconsolidated sediments by sieving or laser granulometer.

Blott, S.J.; Pye, K. (2001). GRADISTAT: a grain size distribution and statistics package for the analysis of unconsolidated sediments. *Earth Surface Processes and Landforms 26(11):* 1237–1248.

Bostock, H.; Jenkins, C.; Mackay, K.; Carter, L.; Nodder, S.; Orpin, A.; Pallentin, A.; Wysoczanski, R. (2019). Distribution of surficial sediments in the ocean around New Zealand/Aotearoa. Part B: continental shelf. *New Zealand Journal of Geology and Geophysics 62(1)*: 24–45.

Campbell, J. (2023). The habitat use, diet and behaviour of juvenile snapper (*Chrysophrys auratus*). Unpublished PhD thesis, University of Auckland. 235 p.

Chin, T.M.; Vazquez-Cuervo, J.; Armstrong, E.M. (2017). A multi-scale high-resolution analysis of global sea surface temperature. *Remote sensing of Environment 200*: 154–169.

Clarke, K.R.; Gorley, R.N. (2015). *PRIMER v7: User Manual/Tutorial*. PRIMER-E, Plymouth.

Collins, C.; Plew, D. (2020). Modelling the effect of river inputs on coastal water quality in Hawke's Bay. *Hawke's Bay Regional Council Publication No. 5469*. 42 p.

Connolly, J.; Lundquist, C.J.; Madarasz-Smith, A.; Shanahan, B. (2020). Hawke's Bay EBM case study - Part 1: System mapping to understand increased sedimentation and loss of benthic structure in the Hawke's Bay. Deliberate, Hamilton, New Zealand. 94 p.

Connolly, J.; Lundquist, C.J.; Shanahan, B.; Madarasz-Smith, A. (2022). Hawke's Bay EBM case study - Part 2: Applying Analogue Simulation - A qualitative process to explore the socio-ecological flow-on impacts in a system in response to modelled biophysical changes. Deliberate, Hamilton, New Zealand. 20 p. plus appendices.

Dickey, T.; Lewis, M.; Chang, G. (2006). Optical oceanography: recent advances and future directions using global remote sensing and in situ observations. *Reviews of Geophysics 44*: 1–39.

Dunbar, G.B.; Barrett, P.J. (2005). Estimating palaeobathymetry of wave-graded continental shelves from sediment texture. *Sedimentology:* 1–17.

Dymond, J. R.; Herzig, A.; Basher, L.; Betts, H. D.; Marden, M.; Phillips, C.J.; Ausseil, A.-G.E.; Palmer, D. J.; Clark, M.; Roygard J. (2016). Development of a New Zealand SedNet model for assessment of catchment-wide soil-conservation works. *Geomorphology 257*: 85–93.

Fairall, C.W.; Bradley, E.F.; Rogers, D.P.; Edson, J.B.; Young, G.S. (1996). Bulk parameterization of air–sea fluxes for TOGA COARE. *Journal of Geophysical Research 101*: 3747–64.

Foster, G.; Carter, L.; (1997). Mud sedimentation on the continental shelf at an accretionary margin - Poverty Bay, New Zealand. *New Zealand Journal Geology and Geophysics 40(2)*: 157–173.

Fuller, I.C.; Marden, M. (2010). Rapid channel response to variability in sediment supply: cutting and filling of the Tarndale Fan, Waipaoa catchment, New Zealand. *Marine Geology 270*: 45–54.

Fuller, I.C.; Riedler, R.A.; Bell, R.; Marden, M.; Glade, T. (2016). Landslide-driven erosion and slope–channel coupling in steep, forested terrain, Ruahine Ranges, New Zealand, 1946–2011. *Catena 142*: 252–268. <http://dx.doi.org/10.1016/j.catena.2016.03.019

Funnell, G.A.; Hancock, N.; Williston, T; Drury, J. (2005). Tuingara to Blackhead Point habitat mapping. NIWA Client Report HAM2004-094 prepared for the Department of Conservation. https://www.doc.govt.nz/globalassets/documents/conservation/marine-and-coastal/marine-protected-areas/mcu11.pdf

Gall, M.P.; Pinkerton, M.H.; Steinmetz, T.; Wood, S. (2022). Satellite remote sensing of coastal water quality in New Zealand. *New Zealand Journal of Marine and Freshwater Research 56(3)*: 585–616. http://dx.doi: 10.1080/00288330.2022.2113410

Gall, M.; Zeldis, J.; Safi, K.; Wood, S.; Pinkerton, M. (2024). Vertical stratification of phytoplankton biomass in a deep estuary site: implications for satellite-based net primary productivity. *Frontiers in Marine Science 10*: 1250322. http://dx.doi.org/10.3389/fmars.2023.1250322

Giere, O. (2009). *Meiobenthology: the microscopic motile fauna of aquatic sediments*. Springer, Berlin.

Gomez, B.; Cui, Y.; Kettner, A.J.; Peacock, D.H.; Syvitski, J.P.M. (2009). Simulating changes to the sediment transport regime of the Waipaoa River, New Zealand, driven by climate change in the twenty-first century. *Global and Planetary Change 67*: 153–166.

Haggitt, T.; Wade, O. (2016). Hawke's Bay Marine Information: Review and Research Strategy. Client report prepared for Hawke's Bay Regional Council. eCoast Marine Consulting and Research. HBRC publication 4806. Report No. RM16-21. 121 p.

Haidvogel, D.B.; Arango, H.; Budgell, W.P.; Cornuelle, B.D.; Curchitser, E.; Di Lorenzo, E. et al. (2008). Ocean forecasting in terrain-following coordinates: Formulation and skill assessment of the Regional Ocean Modeling System. *Journal of Computational Physics 227(7)*: 3595–3624. https://doi.org/10.1016/j.jcp.2007.06.016

Hale, R.P.; Ogston, A.S.; Walsh, J.P.; Orpin, A.R. (2014). Sediment transport and event deposition on the Waipaoa River Shelf, New Zealand. *Continental Shelf Research 86*: 52–65.

Harrington, L.J.; Dean, S.M.; Awatere, S.; Rosier, S.; Queen, L.; Gibson, P.B.; Barnes, C.; Zachariah, M.; Philip, S.; Kew, S.; Koren, G.; Pinto, I.; Grieco, M.; Vahlberg, M.; Snigh, R.; Heinrich, D.; Thalheimer, L.; Li, S.; Stone, D.; Yang, W.; Vecchi, G.A.; Frame, D.J.; Otto, F.E.L. (2023). The role of climate change in extreme rainfall associated with Cyclone Gabrielle over Aotearoa New Zealand's East Coast. World Weather Attribution Initiative Scientific Report. http://dx.doi.org/ 10.25561/102624

Hicks, D.M.; Gomez, B.; Trustrum, N.A. (2000). Erosion thresholds and suspended sediment yields, Waipaoa River Basin, New Zealand. *Water Research 36(4):* 1129–1142.

Hicks, D.M.; Shankar, U. (2003). Sediment yield from New Zealand rivers. NIWA Chart Miscellaneous Series No. 79. NIWA, Wellington. https://niwa.co.nz/freshwater/management-tools/new-zealand-river-maps

Hicks, D.M.; Gomez, B.; Trustrum, N.A.; (2004). Event suspended sediment characteristics and the generation of hyperpycnal plumes at river mouths: East Coast Continental Margin, North Island, New Zealand. *Journal of Geology 112(4)*: 471–485.

Hicks, D.M.; Shankar, U.; McKerchar, A.I.; Basher, L.; Lynn, I.; Page, M.; Jessen, M. (2011). Suspended sediment yields from New Zealand rivers. *Journal of Hydrology 50*: 81–142.

Hicks, D.M.; Gomez, B. (2016). Sediment Transport. *In*: Kondolf, G.M.; Piégay, H. (Eds), pp. 324–356. *Tools in Fluvial Geomorphology*. 2nd Edition, John Wiley and Sons, Ltd.

Hijmans, R.J.; Bivand, R.; Forner, K.; Ooms, J.; Pebesma, E.; Sumner, M.D. (2022). Package 'terra'. https://cran.r-project.org/web/packages/. Maintainer: Vienna, Austria.

Hipel, K.W.; McLeod, A.I. (1994). Time series modelling of water resources and environmental systems. *Developments in Water Science 45*. Elsevier.

IOCCG (2019). Uncertainties in ocean colour remote sensing. Mélin, F. (Ed.). *IOCCG Report Series, No. 18*. Reports and Monographs of the International Ocean Colour Coordinating Group. (Dartmouth, Canada: IOCCG). 164 p.

Jones, E.G.; Morrison, M.A.; Davey, N.; Mills, S.; Pallentin, A.; George, S.; Kelly, M.; Tuck, I. (2018). Biogenic habitats on New Zealand's continental shelf. Part II: National field survey and analysis. *New Zealand Aquatic Environment and Biodiversity Report No. 202*. 261 p.

Kamenev, G.M.; Fadeev, V.I.; Selin, N.I; Tarasov, V.G. (1993). Composition and distribution of macro- and meiobenthos around sublittoral hydrothermal vents in the Bay of Plenty, New Zealand. *New Zealand Journal of Marine and Freshwater Research 27*: 407–418

Kelly, S.; Sim-Smith, C. (2021). Hawke's Bay Coastal Hazards Ecological effects of mitigation measures: Phase 1 Gap Analysis. *Hawke's Bay Regional Council Publication No. 5562.*

Kendall, M.G. (1948). *Rank correlation methods.* Charles Griffin and Co. Ltd., London. 160 p.

Kniskern, T.A.; Kuehl, S.A.; Harris, C.K.; Carter, L. (2010). Sediment accumulation patterns and fine-scale strata formation on the Waiapu River shelf, New Zealand. *Marine Geology 270(1-4)*: 188–201.

Kniskern, T.A.; Mitra, S.; Orpin, A.R.; Harris, C.K.; Walsh, J.P.; Corbett, D.R. (2014). Characterization of a flood-associated deposit on the Waipaoa River shelf using radioisotopes and terrigenous organic matter abundance and composition. *Continental Shelf Research 86*: 66–84.

Kuehl, S.A.; Alexander, C.R.; Blair, N.E.; Harris, C.K. et al. (2016) A source-to-sink perspective of the Waipaoa River margin. *Earth-Science Reviews 153*: 301–334.

Larned, S.; Snelder, T.; Unwin, M.; McBride, G. (2016). Water quality in New Zealand rivers: current state and trends. *New Zealand Journal of Marine and Freshwater Research 50(3):* 389–417.

Lowe, M.L.; Morrison, M.A.; Taylor, R.B. (2015). Harmful effects of sediment-induced turbidity on juvenile fish in estuaries. *Marine Ecology Progress Series 539*: 241–254.

Lundquist, C.; Bulmer, R.; Yogesh, N. (2023). *Using the Seafloor Disturbance Model to understand the dynamics of seafloor disturbance and recovery.* Summary report prepared for the Sustainable Seas National Science Challenge. Hamilton, New Zealand: NIWA. 5 p.

Lundquist, C.; Bulmer, R.; Yogesh, N.; Allison, A.; Leunissen, E.; Brough, T. (2022a). *Development of a seafloor model of disturbance impacts on benthic structure in the Hawke's Bay.* Report prepared for the Sustainable Seas National Science Challenge. Hamilton, New Zealand: NIWA. 30 p. August 2022.

Lundquist, C.; Watson, S.; McCartain, L.; Stephenson, F. (2020). Key Ecological Areas of the Hawke's Bay Coastal Marine Area. *Hawke's Bay Regional Council Publication No. 5479.* 92 p.

Lundquist, C.J.; Connolly, J.; Shanahan, B.; Madarasz-Smith A. (2022b). Enabling Ecosystem- Based Management in the Hawke's Bay: Overview of Stages 1 and 2 of the case study process. Report prepared for the Sustainable Seas National Science Challenge. NIWA Hamilton, New Zealand. 24 p. https://docs.niwa.co.nz/library/public/LunCJEnab.pdf

Lundquist, C.J.; Pritchard, M.; Thrush, S.F.; Hewitt, J.E.; Greenfield, B.L.; Halliday, J. Lohrer, A.M. (2013). Bottom disturbance and seafloor community dynamics: Development of a model of disturbance and recovery dynamics for marine benthic ecosystems. *New Zealand Aquatic Environment and Biodiversity Report No. 118.* 58 p.

Lundquist, C.J.; Thrush, S.F.; Coco, G.; Hewitt, J.E. (2010). Interactions between disturbance and dispersal reduce persistence thresholds in a benthic community. *Marine Ecology Progress Series 413:* 217–228.

Ma, Y.; Friedrichs, C.T.; Harris, C.K.; Wright, L.D. (2010). Deposition by seasonal wave- and current-supported sediment gravity flows interacting with spatially varying bathymetry: Waiapu shelf, New Zealand. *Marine Geology 275*: 199–211.

Ma, Y.; Wright, L.D.; Friedrichs, C.T. (2008). Observations of sediment transport on the continental shelf off the mouth of the Waiapu River, New Zealand: evidence for current-supported gravity flows. *Continental Shelf Research 28(4):* 516–532.

McBride, G.; Cole, R.G.; Westbrooke, I.; Jowett, I. (2014). Assessing environmentally significant effects: a better strength-of-evidence than a single P value? *Environmental Monitoring and Assessment 186*: 2729–2740.

McBride, G.B. (2019). Has water quality improved or been maintained? A quantitative assessment procedure. *Journal of Environmental Quality 48(2)*: 412–420. http://dx.doi.org/10.2134/jeq2018.03.0101

MacDiarmid, A; McKenzie, A; Sturman, J; Beaumont, J; Mikaloff-Fletcher, S; Dunne, J (2012). Assessment of anthropogenic threats to New Zealand marine habitats. *New Zealand Aquatic Environment and Biodiversity Report No.93.* 255 p.

MacMillan, A.; Dymond, J.; Jolly, B.; Shepherd, J.; Sutherland, A. (2023). Rapid assessment of land damage – Cyclone Gabrielle. Manaaki Whenua Landcare Research Report prepared for Ministry for the Environment, LC4292. 34 p.

Madec, G.; NEMO System Team. (2023). *NEMO Ocean Engine Reference Manual*, Zenodo, https://doi.org/10.5281/zenodo.8167700

Mann, H.B. (1945). Nonparametric tests against trend. *Econometrica: Journal of the Econometric Society*: 245–259.

Martins R.; Quintino, V.; Rodrigues, A.M. (2013) Diversity and spatial distribution patterns of the soft-bottom macrofauna communities on the Portuguese continental shelf. *Journal of Sea Research 83*: 173–186.

McLachlan, A.; Cockcroft, A.C.; Malan, D.E. (1984) Benthic faunal response to a high energy gradient. *Marine Ecology Progress Series 16*: 51–63.

Miller, A.J.; Kuehl, S.A. (2010). Shelf sedimentation on a tectonically active margin: a modern sediment budget for Poverty continental shelf, New Zealand. *Marine Geology 270(1)*: 175–187.

Moriarty, J.M.; Harris, C.K.; Hadfield, M.G. (2014). A hydrodynamic and sediment transport model for the Waipaoa shelf, New Zealand: Sensitivity of fluxes to spatially-varying erodibility and model nesting. *Journal of Marine Science and Engineering 2*: 336–369.

Moriarty, J.M.; Harris, C.K.; Hadfield, M.G. (2015) Event-to-seasonal sediment dispersal on the Waipaoa River Shelf, New Zealand: A numerical modeling study. *Continental Shelf Research 110*: 108–123

Morrison, M.A.; Jones, E.G.; Parsons, D.M.; Grant, C.M. (2014b). Habitats and areas of particular significance for coastal finfish management in New Zealand: A review of concepts and life history knowledge, and suggestions for future research. *New Zealand Aquatic Environment and Biodiversity Report No. 125*. 202 p.

Morrison, M.A.; Lowe, M.L.; Grant, C.M.; Smith, P.J.; Carbines, G.; Reed, J.; Bury, S.J.; Brown, J. (2014c). Seagrass meadows as biodiversity and productivity hotspots. *New Zealand Aquatic Environment and Biodiversity Report No. 137*. 147 p.

Morrison, M.A.; Lowe, M.L.; Jones, E.G.; Makey, L.; Shankar, U.; Usmar, N..; Miller, A.; Smith, M.; Middleton, C. (2014a). Habitats of particular significance for fisheries management: the Kaipara Harbour. *New Zealand Aquatic Environment and Biodiversity Report No. 129*. 169 p.

Morrison, M.A.; Lowe, M.L.; Parsons, D.M.; Usmar, N.R.; McLeod, I.M. (2009). A review of land-based effects on coastal fisheries and supporting biodiversity in New Zealand. *New Zealand Aquatic Environment and Biodiversity Report No. 37*. 100 p.

Paavo, B.; Jonker, R.; Thrush, S.; Probert, P.K. (2011). Macrofaunal community patterns of adjacent coastal sediments with wave-reflecting or wave-dissipating characteristics. *Journal of Coastal Research 27:* 515–528.

Pinkerton, M.; May, K.; Lundquist, C.; Stephenson, F.; Watson, S. (2020). Baseline data report in support of application under Marine and Coastal Area (Takutai Moana) Act 2011. NIWA Client Report No. WN202035. 140 p.

Pinkerton, M.; Gall, M.; O'Callaghan, J.; Thoral, F.; Swales, A. (2022). Monitoring suspended sediment in Aotearoa/New Zealand: utility of satellite remote sensing. (NIWA Client Report No. 2022106WN, prepared for the Department of Conservation.) 113 p.

Pinkerton, M.; Gall, M.; Thoral, F.; Sutton, P.; Wood, S. (2023). Monitoring ocean health: 2023 update on satellite indicators for surface temperature, productivity and suspended solids. (NIWA Client Report No. WN2023217, Wellington, NIWA.)

Probert, P.K. (1986). Energy transfer through the shelf benthos off the west coast of South Island, New Zealand. *New Zealand Journal of Marine and Freshwater Research 20*: 407–417.

Probert, P.K.; Anderson, P.W. (1986) Quantitative distribution of benthic macrofauna off New Zealand, with a particular reference to the west coast of the South Island. *New Zealand Journal of Marine and Freshwater Research 20*: 281–290.

Quinn, P.Q.; Keough, M.J. (2009). *Experimental Design and Data Analysis for Biologists*. Cambridge University Press, Cambridge.

Rose, L.E.; Kuehl, S.A. (2010). Recent sedimentation patterns and facies distribution on the Poverty Shelf, New Zealand. *Marine Geology* 270 (1-4): 160–174.

RStudio Team (2022). RStudio: Integrated Development for R. RStudio, PBC, Boston, MA.

Schroeder, T.; Schaale, M.; Lovell, J.; Blondeau-Patissier, D. (2022). An ensemble neural network atmospheric correction for Sentinel-3 OLCI over coastal waters providing inherent model uncertainty estimation and sensor noise propagation. *Remote Sensing of Environment 270*: 112848.

Sciberras, M.; Hiddink, J.G.; Jennings, S.; Szostek, C.L.; Hughes, K.M.; Kneafsey, B.; Clarke, L.J.; Ellis, N.; Rijnsdorp, A.D.; McConnaughey, R.A.; Hilborn, R.; Collie, J.S.; Pitcher, C.R.; Amoroso, R.O.; Parma, A.M.; Suuronen, P.; Kaiser, M.J. (2018). Response of benthic fauna to experimental bottom fishing: A global meta-analysis. *Fish and Fisheries 19*: 698–715.

Sen, P.K. (1968). Estimates of the regression coefficient based on Kendall's tau. *Journal of the American Statistical Association 63(324)*: 1379–1389.

Snelder, T.H.; Biggs, B.; Weatherhead, M.A. (2004). *New Zealand River Environment Classification User Guide*. (Updated in 2010. Ministry for the Environment publication ME 1026.)

Somerfield, P.; Warwick, R.M. (1996). *Meiofauna in Marine Pollution Monitoring Programmes: A Laboratory Manual.* Ministry of Agriculture, Fisheries, and Food, Lowestoft.

Souza, J.M.A.C.; Suanda, S.H.; Couto, P.P.; Smith, R.O.; Kerry, C.; Roughan, M. (2023). Moana Ocean Hindcast–a > 25-year simulation for New Zealand waters using the Regional Ocean Modeling System (ROMS) v3. 9 model. *Geoscientific Model Development 16(1):* 211–231.

Stephenson, F.; Bulmer, R. H.; Meredyth-Young, M.; Meysick, L.; Hewitt, J. E.; Lundquist. C.J. (2019). Effects of benthic protection extent on recovery dynamics of a conceptual seafloor community. *Frontiers in Marine Science 6:* 607.

Stevens, C.L.; O'Callaghan, J.M.; Chiswell, S.M.; Hadfield, M.G. (2019). Physical oceanography of New Zealand/Aotearoa shelf seas–a review. *New Zealand Journal of Marine and Freshwater Research 55(1):* 6–45.

Swales, A.; Haddadchi, A.; Olsen, G.; Orpin, A.; Bind, J.; Bilewitch, J.; Hayden, M.; Mountjoy, J.; Bury, S.; Jung, R.; Frontin-Rollet, G.; Smith, L.; Brooks, A. (in prep.) Cyclone Gabrielle: tracing sediment source contributions to river and marine sedimentation. New Zealand Aquatic Environment and Biodiversity Report.

Swales, A.; Ovenden, R.; Budd, R.; Hawken, J.; McGlone, M.S.; Hermanspahn, N.; Okey, M.J. (2005). Whaingaroa (Raglan) Harbour: Sedimentation and the effects of historical catchment landcover changes. *Environment Waikato Technical Report 2005/36*. Lincoln, Christchurch, NIWA, Landcare Research ltd, National Radiation Laboratory prepared for Environment Waikato. 67 p.

Swales, A.; Williamson, B.; Van Dam, L.F.; Stroud, M. (2002). Reconstruction of urban stormwater contamination of an estuary using catchment history and sediment profile dating. *Estuaries 25(1)*: 43–56.

Thrush, S.F.; Lundquist, C.J.; Hewitt J. (2005). Spatial and temporal scales of disturbance to the seafloor: a generalised framework for active habitat management. *American Fisheries Society Symposium 41:* 639–649.

Turner, R.; Moore, S. (2017). An analysis of three years of Convective Scale Numerical Model diagnosed gusts over New Zealand. 9th Asia-Pacific Conference on Wind Engineering, Auckland, New Zealand.

Udden, J.A. (1914). Mechanical composition of clastic sediments. *Bulletin of the Geological Society of America 25:* 655–744.

Walling, D.E.; Webb, B.W. (1996). Erosion and sediment yield: a global overview. *IAHS Publications 236*: 3–19.

Walsh, J.P.; Corbett, D.R.; Kiker, J.M.; Orpin, A.O.; Hale, R.P.; Ogston, A.S. (2014). Spatial and temporal variability in sediment deposition and seabed character on the Waipaoa River margin, New Zealand. *Continental Shelf Research 86*: 85–102.

Warner, J.C.; Sherwood, C.R., Signell, R.P.; Harris, C.K.; Arango, H.G. (2008). Development of a three-dimensional, regional, coupled wave, current, and sediment-transport model. *Computers & Geosciences 34*: 1284–1306.

Wentworth, C.K. (1922). A scale of grade and class terms for clastic sediments. *Journal of Geology 30*: 377–392.

Wheatcroft, R.A. (2006) Time-series measurements of macrobenthos abundance and sediment bioturbation intensity on a flood-dominated shelf. *Progress in Oceanography 71*: 88–122.

Willmott, C.J. (1981). On the validation of models. *Physical Geography 2(2):* 184–194.

Yue, S.; Wang, C. (2004). The Mann-Kendall test modified by effective sample size to detect trend in serially correlated hydrological series. *Water Resources Management 18(3):* 201–218.

APPENDIX 1 – SATELLITE PRODUCTS METHODS

Light attenuating components

Chlorophyll *a* concentration (CHL; mg m^{-3}) was estimated using the MODIS-default (open ocean - Case 1) algorithm from NASA (R2018.0) which is likely to be accurate and robust away from the coast but typically biased in some coastal (Case 2) waters (IOCCG 2000, Pinkerton et al. 2006, and Zeldis et al. 2013). For Case 2 we used the Quasi Analytical Algorithm (QAA v5) from Lee et al. (2002) and Lee et al. (2009) for Case 2 waters. QAA was first used to estimate phytoplankton absorption at 488 nm [aph488, m^{-1}]. Phytoplankton absorption was converted to chlorophyll *a* concentration (mg m^{-3}) assuming a Chlorophyll specific absorption coefficient (aka "absorption cross-section") at 488 nm (aph*488, m^2 mg^{-1}). The value of aph*488 can vary seasonally and spatially, depending on different phytoplankton species (with varying cell physiology and pigments), cell sizes, and the light environment (Kirk 2011). Here, we used an average (0.084 m^2 mg^{-1}) between oceanic (~0.04 m^2 mg^{-1}) phytoplankton (Bricaud et al. 1995, Bissett et al. 1997) and measurements in the lower reaches of New Zealand rivers and estuaries (~0.12 m^2 mg^{-1}, Pinkerton 2017). Particulate backscatter at 555 nm (BBP, m^{-1}) was also estimated using QAA. BBP was used for logistic scaling to blend Case 1 and Case 2 products into a single product (i.e., ADET, CHL, KPAR and EBED).

Total Suspended Solids (TSS; g m^{-3}) was derived from an empirical non-linear scaling of the backscattering of particulates at 555 nm product (BBP - b_{bp}555, m^{-1}, QAA v5), using relationships to *in situ* measurements from the Firth of Thames, Marlborough Sounds, and the National River Water Quality Network water samples (Pinkerton 2017): TSS = 49.4(b_{bp}555$^{0.8701}$). The relationship was based on a Standardized Major Axis regression between measurements of backscatter at 660 nm (b_{bp}660, ECOtriplet, Seabird Inc.) and laboratory measurements of TSS (n=367, r^2= 0.928, p< 0.001). We assume that BBP (b_{bp}555) is equivalent to b_{bp}660 based on relatively flat backscattering spectra reported for relatively large colloidal particles >0.4–1.0 um (Stramski & Woźniak 2005), about the lower limit of particle capture on glass fiber filters.

Absorption of detritus at 443 nm (ADET; m^{-1}) was estimated using the MODIS-default (open ocean - Case 1) product from NASA (R2018.0) and using a QAA v5 and BBP blending.

Water clarity

Secchi disk depth (SEC; m) was estimated from methods outlined by Hou et al. (2007), following Preisendorfer (1986) and Davies-Colley & Vant (1988). Preisendorfer (1986) showed from theory an approximation similar for yBD based on photopic properties: zSD (SEC, m) = Γ /(Kd550 +c550), where Γ~6. As Γ is known to vary with photopic reflectance, synthetic Secchi depth was generated where Γ was modelled from photopic reflectance (Davies-Colley & Vant 1988) using the CIE 2008 luminosity function (quanta, 10°). This provided a spectrally resolved simulation to build an improved empirical regression:

$$z_{SD} = e^{(-0.04458x^2 - 0.9708x^1 + 1.991)}, \text{where } x = \ln(K_d 550 + c550)$$

Horizontal visibility (HVIS, m), also known as black disc visibility, was estimated using a robust empirical relationship to the "*photopic*" eye-centered (green, 550 nm) beam attenuation coefficient (c550, m^{-1}) y_{BD} (HVIS, m) = 4.8/c550 (Davies-Colley 1988, Zaneveld & Pegau 2003). QAA was used first to estimate absorption and back-scattering coefficients at 550 nm (a550 and b_{bp}550). A total-scattering to back-scattering ratio (b550/b_{bp}550) of 0.0176 from the scattering phase function of Petzold (1972) was then used to estimate total scattering (b550) which includes the pure water scattering coefficient (bw550, 0.00191 m^{-1} from Morel (1974) for calculation of c550 (m^{-1}) = a550 + b550.

The diffuse downwelling light attenuation coefficient of PAR (KPAR, m^{-1}) was estimated in clear ocean waters (Case 1) from the attenuation at 490 nm, which is more accurate when estimated using the default MODIS band-ratio algorithm (Clark 1997) and converted to KPAR using an empirical relationship assuming a layer thickness of twice the optical depth (Morel et al. 2007). In optically complex (Case 2)

coastal waters, the QAA v5 is more accurate. The spectral absorption and scattering coefficients are estimated first and then their spectral diffuse attenuation coefficients (Lee et al. 2005). KPAR was then calculated by accounting for the variation of light (converted to quanta) with depth (Pinkerton 2017). An iterative method was used when applying Lee et al. (2005) to determine the appropriate depth over which to estimate KPAR.

Light (Energy from photosynthetically active radiation - PAR) at the seabed (EBED, mol photons m^2 day^{-1}) was estimated by combining incident irradiance at the sea surface (MODIS-Aqua PAR product, Frouin et al. 2012), diffuse downwelling irradiance attenuation (KPAR – see below) and bathymetric depth (Mitchell et al. 2012). The MODIS PAR product is a daily-integrated, broadband, incident irradiance at the sea-surface based on day length, solar elevation, and top-of-atmosphere conditions. Bathymetric depth in the New Zealand region (NZVD2016; McCubbine et al. 2018) was interpolated from various sources, including multi-beam and single-beam echo sounders, and satellite observations.

References

Bissett, W.P.; Patch, J.S.; Carder, K.L.; and Lee, Z.P. (1997). Pigment packaging and Chl a-specific absorption in high-light oceanic waters. *Limnology and Oceanography 42(5)*: 961–968.

Bricaud, A.; Babin, M.; Morel, A.; Claustre, H. (1995). Variability in the chlorophyll-specific absorption coefficients of natural phytoplankton: Analysis and parameterization. *Journal of geophysical Research 100(C7)*: 13321–13332.

Clark, D. (1997). Bio-optical algorithms—Case 1 waters. MODIS Algorithm Theoretical Basis Document (MOD-ATBD-18), National Oceanic and Atmospheric Administration, National Environmental Satellite Service, Washington DC.

Davies-Colley, R.; Vant, W. (1988). Estimation of optical properties of water from secchi disk depths 1. *JAWRA Journal of the American Water Resources Association 24(6)*: 1329–1335.

Frouin, R.; McPherson, J.; Ueyoshi, K.; Franz, B.A. (2012). A time series of photosynthetically available radiation at the ocean surface from SeaWiFS and MODIS data. *In*: *Remote Sensing of the Marine Environment II*: International Society for Optics and Photonics, pp. 234–245.

Hou, W.; Lee, Z.; Weidemann, A.D. (2007). Why does the Secchi disk disappear? An imaging perspective. *Optics Express 15*: 2791–2802.

IOCCG (2000). Remote sensing of ocean colour in coastal, and other optically-complex, waters. *In Reports of the International Ocean-Colour Coordinating Group,* ed. S. Sathyendranath. (Dartmouth, Canada: IOCCG.) 140 p.

Kirk, J.T.O. (2011). *Light and Photosynthesis in Aquatic Ecosystems.* Cambridge University Press.

Lee, Z.P.; Carder, K.L.; Arnone, R.A. (2002). Deriving inherent optical properties from water color: a multiband quasi-analytical algorithm for optically deep waters. *Applied optics 41(27)*: 5755–5772.

Lee, Z.P.; Darecki, M.; Carder, K.L.; Davis, C.O.; Stramski, D.; Rhea, W.J. (2005). Diffuse attenuation coefficient of downwelling irradiance: An evaluation of remote sensing methods. *Journal of Geophysical Research-Oceans 110(C2)*: 1–9.

Lee, Z.P.; Lubac, B.; Werdell, J.; Arnone, R. (2009). An update of the quasi-analytical algorithm (QAA_v5). *International Ocean Color Group Software Report*.

McCubbine, J.; Amos, M.; Tontini, F.; Smith, E.; Winefied, R.; Stagpoole, V. et al. (2018). The New Zealand gravimetric quasigeoid model 2017 that incorporates nationwide airborne gravimetry. *Journal of Geodesy 92*: 923–937.

Mitchell, J.S.; Mackay, K.A.; Neil, H.L.; Macklay, E.J.; Pallentin, A.; Notman, P. (2012). Undersea New Zealand, 1:5,000,000. *NIWA Chart, Miscellaneous Series No. 92*.

Morel, A. (1974). Optical properties of pure water and pure sea water. *In*: *Optical Aspects of Oceanography,* eds. N.G. Jerlov & E. Steeman. Academic, London, 1–24.

Morel, A.; Gentili, B.; Claustre, H.; Babin, M.; Bricaud, A.; Ras, J.; Tièche. F. (2007). Optical properties of the "clearest" natural waters. *Limnology and Oceanography 52*: 217–229.

Petzold, T. (1972). Volume Scattering Functions for Selected Ocean Waters. SCRIPPS Institution of Oceanography La Jolla CA Visibility Lab.

Pinkerton, M.H.: Moore, G.F.: Lavender, S.J.: Gall, M.P.: Oubelkheir, K.: Richardson, K.M.: Boyd, P.W.; Aiken, J. (2006). A method for estimating inherent optical properties of New Zealand continental shelf waters from satellite ocean colour measurements. *New Zealand Journal of Marine and Freshwater Research 40(2)*: 227–247.

Pinkerton, M. (2017). Satellite remote sensing of water qualtiy and temperature in Manukau Harbour. Wellington, NIWA.

Preisendorfer, R.W. (1986). Secchi disk science: Visual optics of natural waters. *Limnology and Oceanography 31(5)*: 909–926.

Stramski, D.; Woźniak, S.B. (2005). On the role of colloidal particles in light scattering in the ocean. *Limnology and oceanography 50(5)*: 1581–1591.

Zaneveld, J.; Pegau, W. (2003). Robust underwater visibility parameter. *Optics Express 11(23)*: 2997–3009.

Zeldis, J.; Hadfield, M.; Booker, D. (2013). Influence of climate on Pelorus Sound mussel aquaculture yields: predictive models and underlying mechanisms. *Aquaculture Environment Interactions 4(1)*: 1–15.

APPENDIX 2 – KAH2303 & KAH2306 STATIONS

Station details of June RV *Kaharoa* voyage KAH2303 to the Hawke's Bay and Gisborne regions. BT: Beam trawl; CCAM: CoastCam; MUC: Multicorer; SVP: Sound velocity profiler.

Station	Date NZST	Time on bottom NZDT	Latitude S	Longitude E	Depth (m)	Site	Gear	Pre-cyclone data?	Pre-cyclone reference
1	2-Jun-23	13:37	41 27.47	174 51.60	102	Cook Strait	SVP	N/A	N/A
2	2-Jun-23	15:42	41 26.64	174 53.42	63	Cook Strait	CCAM	N/A	N/A
3	3-Jun-23	12:33	40 03.15	176 54.96	20	Paoanui Point	SVP	N/A	N/A
4	3-Jun-23	18:11	40 13.74	176 47.43	20	Blackhead Point	CCAM	Camera drops	DOC
5	3-Jun-23	19:58	40 09.12	176 51.40	18	Paoanui Point	CCAM	Sidescan sonar, camera drops	Funnell et al. (2005)
6	4-Jun-23	0:31	39 47.49	177 08.22	93	Motuokura Reef	CCAM	Sidescan sonar, camera drops	Funnell et al. (2005)
7	4-Jun-23	8:01	39 30.12	177 51.45	135	Lachlan Ridge	SVP	N/A	N/A
8	4-Jun-23	16:01	39 20.34	177 38.61	75	T3 #5	MUC	N/A	N/A
9	4-Jun-23	16:35	39 20.302	177 38.651	76	T3 #5	MUC	N/A	N/A
10	4-Jun-23	18:05	39 18.263	177 40.700	54	T3 #4	MUC	N/A	N/A
11	4-Jun-23	20:10	39 16.229	177 42.842	40	T3 #3	MUC	N/A	N/A
12	4-Jun-23	21:10	39 13.969	177 45.082	39	T3 #2	MUC	N/A	N/A
13	4-Jun-23	22:46	39 11.955	177 46.868	35	T3 #1	MUC	N/A	N/A
14	4-Jun-23	2:13	39 09.41	177 48.50	28	Mahia West	SVP	N/A	N/A
15	5-Jun-23	13:58	39 15.95	177 26.37	61	T2 #4	MUC	N/A	N/A
16	5-Jun-23	15:40	39 13.113	177 25.924	47	T2 #3	MUC	N/A	N/A
17	5-Jun-23	17:25	39 10.356	177 25.778	34	T2 #2	MUC	N/A	N/A
18	6-Jun-23	7:57	39 35.09	176 59.49	15	Clive outfall	SVP	N/A	N/A
19	6-Jun-23	11:51	39 31.53	176 57.19	15	Hawke's Bay	SVP	N/A	N/A
20	6-Jun-23	14:43	39 38.303	177 01.182	21	T1 #2	MUC	N/A	N/A
21	6-Jun-23	16:17	39 31.115	177 05.496	30	T1 #3	MUC	N/A	N/A
22	6-Jun-23	19:30	39 37.73	177 06.54	21	Cape Kidnappers	CCAM	Camera drop	HBRC unpubl. data
23	6-Jun-23	21:10	38 32.69	176 57.59	16	T1 #1	CCAM	N/A	N/A

24	6-Jun-23	22:00	39 33.179	176 58.204	15	T1 #1	MUC	N/A	N/A
25	7-Jun-23	8:55	39 25.66	176 57.34	18	Pania Reef	SVP	N/A	N/A
26	7-Jun-23	14:46	39 27.618	176 55.434	11	Pania Reef #8	CCAM	N/A	N/A
27	7-Jun-23	15:26	39 26.436	176 56.874	19	Pania Reef north	CCAM	N/A	N/A
28	7-Jun-23	16:01	39 26.945	176 56.231	17	Pania Reef mid	CCAM	N/A	N/A
29	7-Jun-23	16:50	39 27.155	176 56.013	16	Pania Reef	MUC	N/A	N/A
30	7-Jun-23	19:35	39 20.601	176 57.153	19	Tangoio Reef	CCAM	N/A	N/A
31	7-Jun-23	20:37	39 20.503	176 57.370	20	Tangoio Reef	MUC	N/A	N/A
32	7-Jun-23	22:43	39 15.189	177 08.687	32	Wairoa Hard #1	CCAM	N/A	N/A
33	7-Jun-23	23:47	39 13.693	177 14.584	37	Wairoa Hard #2	CCAM	N/A	N/A
34	8-Jun-23	0:39	39 11.459	177 14.885	25	Wairoa Hard #3	CCAM	N/A	N/A
35	8-Jun-23	3:17	39 12.79	177 15.99	35	Wairoa Hard	SVP	N/A	N/A
36	8-Jun-23	13:32	39 07.902	177 25.569	29	T2 #1	MUC	N/A	N/A
37	8-Jun-23	16:39	39 09.007	177 49.316	20	Mahia West	CCAM	N/A	N/A
38	8-Jun-23	19:36	39 17.321	177 51.334	27	Portland Island	CCAM	N/A	N/A
39	8-Jun-23	22:24	39 28.897	177 49.977	97	Lachlan Ridge #1	CCAM	N/A	N/A
40	9-Jun-23	14:14	39 36.895	177 05.185	21	Cape Kidnappers #1	CCAM	Camera drop	HBRC unpubl. data
41A	9-Jun-23	15:26	39 36.423	177 05.630	24	Cape Kidnappers #2A	CCAM	Camera drop	HBRC unpubl. data
41B	9-Jun-23	15:49	39 36.442	177 05.662	25	Cape Kidnappers #2B	CCAM	Camera drop	HBRC unpubl. data
42	9-Jun-23	16:59	39 32.350	177 01.702	21	Seep site	CCAM	N/A	N/A
43	10-Jun-23	18:51	39 29.518	177 09.461	48	T1 #4	MUC	N/A	N/A
44	11-Jun-23	15:05	38 07.697	178 28.593	64	T5 #3	CCAM	N/A	N/A
45	11-Jun-23	16:34	38 07.896	178 35.035	42	T5 #2	MUC	N/A	N/A
46	11-Jun-23	19:20	38 08.101	178 21.693	29	T5 #1	MUC	N/A	N/A
47	11-Jun-23	22:10	38 03.777	178 28.462	59	Tokomaru shelf reef	CCAM	N/A	N/A
48	11-Jun-23	23:55	38 01.887	178 34.572	86	Tokomaru shelf reef	CCAM	N/A	N/A
49	12-Jun-23	10:12	37 50.647	178 27.918	22	Awanui inshore reef	CCAM	N/A	N/A
50	12-Jun-23	12:37	37 41.959	178 35.440	23	East Island reef	CCAM	N/A	N/A
51	12-Jun-23	13:28	37 44.535	178 35.002	52	Waikori Bluff reef	CCAM	N/A	N/A
52	12-Jun-23	16:34	37 48.832	178 33.385	61	T6 #2	MUC	Sediment cores	Ma et al. 2010

53	12-Jun-23	18:58	37 47.645	178 30.563	21	T6 #1	MUC	Sediment cores	Ma et al. 2010
54	14-Jun-23	9:54	38 19.828	178 21.934	25	Tolaga north reef	CCAM	N/A	N/A
56	14-Jun-23	16:41	38 35.877	178 16.494	32	Whangara south reef	CCAM	N/A	N/A
57	14-Jun-23	18:59	38 33.611	178 17.232	34	Whangara north reef	CCAM	N/A	N/A
58	15-Jun-23	10:22	38 44.216	178 02.612	27	T4 #2	MUC	Sediment cores	Kniskern et al. 2014; Walsh et al. 2014
59	15-Jun-23	12:31	38 44.655	178 08.133	40	T4 #3	MUC	Sediment cores	Kniskern et al. 2014; Walsh et al. 2014
60	15-Jun-23	12:50	38 44.769	178 08.108	42	T4 #3	MUC	Sediment cores	Kniskern et al. 2014; Walsh et al. 2014
61	15-Jun-23	13:00	38 44.748	178 08.132	42	T4 #3	MUC	Sediment cores	Kniskern et al. 2014; Walsh et al. 2014
62	15-Jun-23	15:14	38 42.578	178 14.599	61	Poverty Bay offshore reef	CCAM	N/A	N/A
63	15-Jun-23	17:22	38 30.312	178 23.035	48	Gables	CCAM	N/A	N/A
64	15-Jun-23	20:10	38 23.070	178 33.688	76	Tolaga offshore reef	CCAM	N/A	N/A
65	15-Jun-23	21:27	38 23.225	178 35.873	104	Tolaga offshore reef	CCAM	N/A	N/A
66	16-Jun-23	10:15	38 45.845	178 11.649	54	T4 #4	MUC	Sediment cores	Kniskern et al. 2014; Walsh et al. 2014
67	16-Jun-23	11:43	38 42.153	178 12.340	53	T4 #5	MUC	Sediment cores	Kniskern et al. 2014; Walsh et al. 2014
68	16-Jun-23	14:37	38 41.897	178 07.209	33	Wainui Beach reef	CCAM	N/A	N/A
69	16-Jun-23	17:33	38 44.170	178 21.720	51	Ariel Bank (northernmost)	CCAM	Multibeam, towed camera	Jones et al. (2018)
70	16-Jun-23	18:45	38 46.082	178 21.926	77	Ariel Bank #3 (southernmost)	CCAM	Multibeam, towed camera	Jones et al. (2018)
71	16-Jun-23	21:32	38 58.096	178 05.869	46	Table Cape #1	CCAM	Multibeam, towed camera	Jones et al. (2018)
72	16-Jun-23	22:15	38 58.650	178 05.648	49	Table Cape #2	CCAM	Multibeam, towed camera	Jones et al. (2018)
73	17-Jun-23	10:24	38 44.235	178 00.167	21	Poverty Bay south reef	CCAM	N/A	N/A
74	18-Jun-23	12:30	39 11.409	177 14.825	24	Wairoa Hard A	CCAM	Camera drop	HBRC unpubl. data
75	18-Jun-23	13:02	39 13.708	177 14.626	37	Wairoa Hard B	CCAM	Camera drop	HBRC unpubl. data
76	18-Jun-23	14:33	39 13.310	177 15.240	38	Wairoa Hard #1	BT	Camera drop	HBRC unpubl. data
77	18-Jun-23	15:28	39 12.136	177 15.369	33	Wairoa Hard #2	BT	Camera drop	HBRC unpubl. data
78	18-Jun-23	16:25	39 15.169	177 08:808	31	Wairoa Hard #2	BT	Camera drop	HBRC unpubl. data

Station details of October RV *Kaharoa* voyage KAH2306 to the Hawke's Bay and Gisborne regions. CCAM: CoastCam; MUC: Multicorer; SVP: Sound velocity profiler.

Station	Date NZST	Time on bottom NZDT	Latitude S	Longitude E	Depth (m)	Site	Gear	Repeat site? (KAH2303 station)
1	13-Oct-23	16:38	39 28.01	177 13.43	61	T1 #5	MUC	No
2	13-Oct-23	19:15	39 29.510	177 09.47	48	T1 #4	MUC	Yes (43)
3	13-Oct-23	20:33	39 33.20	176 58.30	15	T1 #1	MUC	Yes (24)
4	13-Oct-23		39 36.61	177 06.03	27	Hawke's Bay	SVP	N/A
5	13-Oct-23	23:29	39 36.530	177 05.751	26	Cape Kidnappers 1	CCAM	No
6	13-Oct-23	23:58	39 36.441	177 05.745	24	Cape Kidnappers 2	CCAM	No
7	14-Oct-23	0:26	39 36.956	177 05.356	21	Cape Kidnappers 3	CCAM	No
8	14-Oct-23	1:15	39 37.827	177 07.410	41	Cape Kidnappers 4	CCAM	No
9	14-Oct-23	14:38	39 17.248	177 11.293	47	Wairoa Hard log target	CCAM	No
10	14-Oct-23	15:38	39 15.22	177 08.84	32	Wairoa Hard #1 Repeat	CCAM	Yes (32)
11	14-Oct-23	16:32	39 13.554	177 14.807	37	Wairoa Hard SE	CCAM	Yes (75)
12	14-Oct-23	17:10	39 11.694	177 14.946	27	Wairoa Hard NE	CCAM	Yes (74)
13	14-Oct-23	19:04	39 07.89	177 25.63	28	T2 #1	MUC	Yes (36)
14	14-Oct-23	20:18	39 13.18	177 25.96	47	T2 #3	MUC	Yes (16)
15	14-Oct-23	22:26	39 15.97	177 26.36	61	T2 #4	MUC	Yes (15)
16	14-Oct-23	23:58	39 13.506	177 14.675	36	Wairoa SE	CCAM	Yes (75)
17	15-Oct-23	14:22	39 11.55	177 29.38	32	T2 #2	CCAM	Yes (17)
18	15-Oct-23	15:26	39 06.488	177 28.204	24	East of T2 #1	CCAM	No
19	15-Oct-23	16:29	39 07.314	177 32.899	24	Wairoa NE	CCAM	No
20	15-Oct-23	19:45	39 16.834	177 29.338	67	Wairoa outer	CCAM	No
21	15-Oct-23	21:05	39 10.40	177 25.75	34	T2 #2	MUC	Yes (17)
22	16-Oct-23	17:49	39 26.343	176 58.675	23	Pania Reef	CCAM	No
23	16-Oct-23	20:46	39 22.199	177 24.911	72	Central Hawke's Bay 1	CCAM	No
24	16-Oct-23	22:02	39 21.481	177 32.351	83	Central Hawke's Bay 2	CCAM	No
25	17-Oct-23	16:13	38 07.83	178 28.67	64	T5 #3	MUC	No
26	17-Oct-23	18:39	37 50.884	178 28.412	27	Whakariki Point	CCAM	Yes (49)
27	17-Oct-23	21:27	37 42.425	178 33.590	24	Waiapu north reef	CCAM	No

28	17-Oct-23	23:35	37 51.42	178 39.69	146	T6 #4	MUC	No
29	18-Oct-23	1:17	37 50.50	178 32.55	57		SVP	N/A
30	18-Oct-23	14:13	38 02.326	178 34.137	69	Tokomaru shelf reef	CCAM	Yes (48)
31	18-Oct-23	16:21	38 03.987	178 28.214	56	Tokomaru shelf reef	CCAM	No
32	18-Oct-23	19:24	37 59.855	178 23.963	38	Waipiro Bay	CCAM	No
33	18-Oct-23	21:02	38 03.937	178 28.379	57	Tokomaru shelf reef	CCAM	Yes (47)
34	18-Oct-23	23:44	38 20.245	178 22.184	28	Tolaga north reef	CCAM	Yes (54)
35	19-Oct-23	1:09	38 21.83	178 25.88	49	Tolaga	MUC	No
36	19-Oct-23	13:47	38 44.25	177 59.610	17	Poverty Bay south reef	CCAM	Yes (73)
37	19-Oct-23	15:46	38 41.483	178 06.926	13	Poverty Bay north reef	CCAM	No
38	19-Oct-23	17:38	38 44.72	178 08.17	40	T4 #3	MUC	Yes (59-61)
39	19-Oct-23	19:47	38 36.23	178 16.43	31	Whangara south reef	CCAM	Yes (56)
40	19-Oct-23	21:25	38 33.948	178 17.075	35	Whangara north reef	CCAM	Yes (57)
41	20-Oct-23	15:50	38 14.553	178 21.085	18	Anaura Bay inshore 1 north (W to E)	CCAM	No
42	20-Oct-23	16:31	38 14.893	178 21.208	24	Anaura Bay inshore 2 south (W to E)	CCAM	No
43	20-Oct-23	17:11	38 14.184	178 22.438	33	Anaura patch reefs 1 (south)	CCAM	No
44	20-Oct-23	17:39	38 14.015	178 22.527	33	Anaura patch reefs 2 (north)	CCAM	No
45	20-Oct-23	20:32	38 23.738	178 35.240	97	Tolaga offshore reef	CCAM	Yes (65)
46	20-Oct-23	22:49	38 31.336	178 24.764	60	Gables ring 1	CCAM	Yes (63)
47	20-Oct-23	23:08	38 31.388	178 24.898	60	Gables ring 2	CCAM	Yes (63)
48	21-Oct-23	0:07	38 30.025	178 23.237	44	Gables 2	CCAM	No
49	21-Oct-23	12:32	39 08.963	177 49.387	21	Mahia West	CCAM	Yes (37)
50	21-Oct-23	17:19	39 12.120	177 15.538	31	Wairoa Hard-M	CCAM	No
51	21-Oct-23	19:07	39 13.165	177 15.344	36	Wairoa Hard-N	CCAM	No
52	21-Oct-23	20:16	39 15.078	177 08.909	31	Wairoa Hard-O	CCAM	Yes (32)
53	21-Oct-23	20:36	39 15.087	177 08.904	31	Wairoa Hard-O_2	CCAM	Yes (32)
54	21-Oct-23	22:35	39 17.278	177 11.451	49	Wairoa Hard log site	CCAM	No
55	21-Oct-23	23:07	39 17.278	177 10.814	50	Wairoa Hard-P	CCAM	No
56	21-Oct-23	23:46	39 15.384	177 10.637	38	Wairoa Hard-Q	CCAM	No

APPENDIX 3 – ENVIRONMENTAL VARIABLES

Environmental variables for sites sampled during the June KAH2303 RV *Kaharoa* survey. Sediment parameters (except event thickness) were based on analyses of top 5 cm of sediments. Details of methods used in deriving these parameters will be available in an upcoming AEBR of project *SEA2022-13 Cyclone Gabrielle sediment analyses* to be published in 2024. TOM = total sediment organic matter content.

KAH2303 station	Site	Water depth (m)	Sediment wood debris content (mg core^{-1})	%TOM	Mud content	Event thickness (mm)
9	T3 #5	76	193.55	3.17	90%	8.8
10	T3 #4	54	9.52	1.28	81%	15.2
11	T3 #3	40	345.32	3.60	91%	10.4
12	T3 #2	39	244.58	1.92	80%	44.8
13	T3 #1	35	34.53	1.51	36%	13.6
15	T2 #4	61	20.47	6.29	95%	45.2
16	T2 #3	47	31.42	7.00	92%	66.4
17	T2 #2	34	43.04	1.20	44%	18.8
20	T1 #2	21	2.520	2.25	89%	53.2
21	T1 #3	30	28.75	2.88	89%	10.4
24	T1 #1	15	3.75	3.52	73%	69.2
29	Pania Reef	16	2.47	1.03	2%	0
31	Tangoio Reef	20	1.82	0.52	8%	0
36	T2 #1	29	44.19	3.52	88%	64
43	T1 #4	48	205.72	9.40	88%	141.2
45	T5 #2	42	181.70	1.76	77%	23.8
46	T5 #1	29	33.30	1.93	60%	28.0
52	T6 #2	61	41.61	2.69	97%	100.0
53	T6 #1	21	122.48	0.72	50%	1.6
58	T4 #2	27	11.77	1.12	16%	15.6
61	T4 #3	42	37.62	3.51	89%	59.6
66	T4 #4	54	103.52	2.78	83%	9.2
67	T4 #5	53	28.29	4.07	94%	24

APPENDIX 4 – BATHYMETRY MAPS

Bathymetry maps of selected areas in the Hawke's Bay and Gisborne regions surveyed during the June and October RV *Kaharoa* surveys (KAH2303 and KAH2306, respectively).

KAH2303 Mahia West

Bathymetry (m)

-11.2

-36.2

KAH2306 Tolaga North Reef

Bathymetry (m)

-13.0

-58.1

KAH2306 Tolaga Offshore Reefs

Bathymetry (m)

-53.8
-118.2

KAH2306 Tolaga Shelf Reefs

Bathymetry (m)

-20.8

-112.0
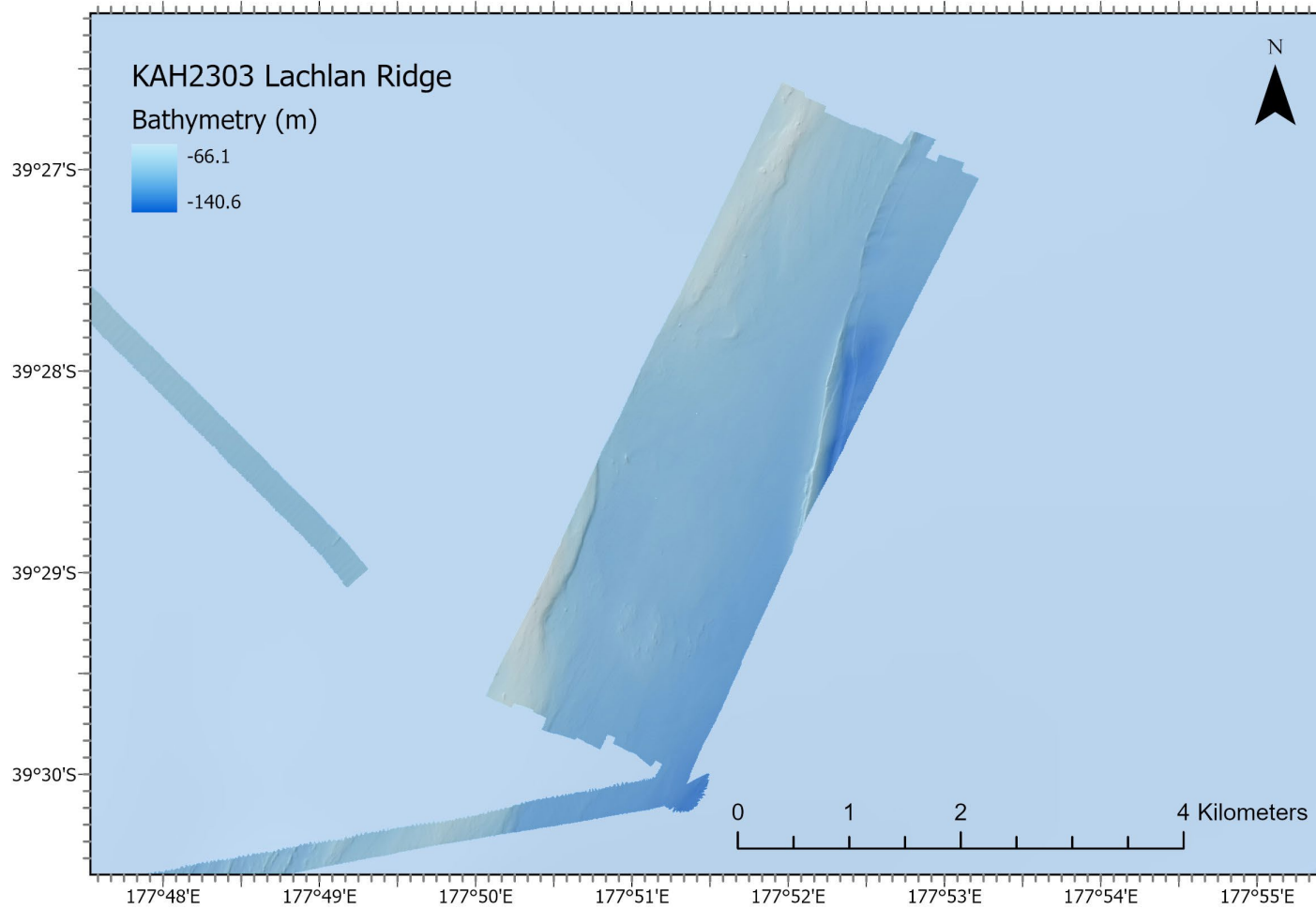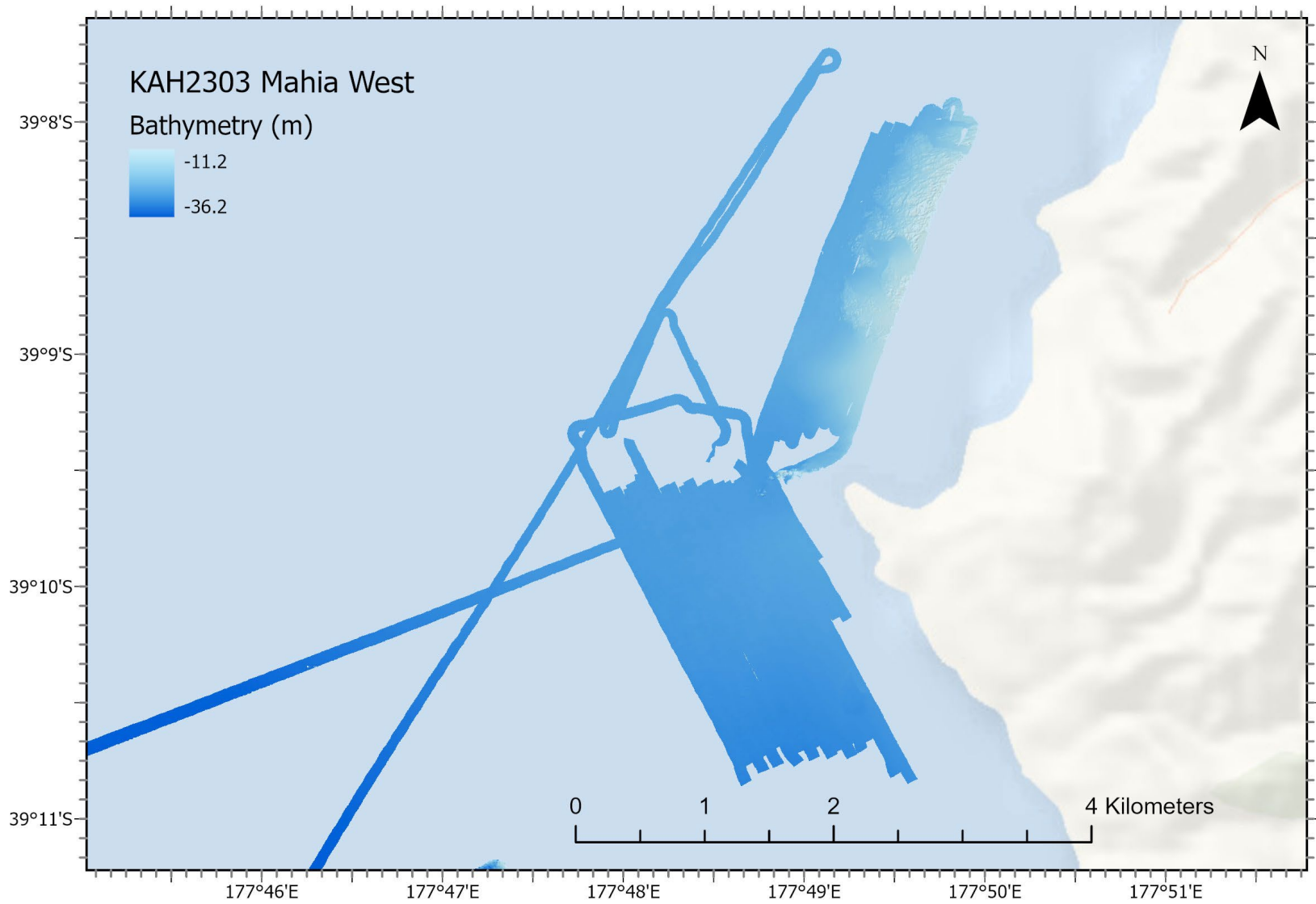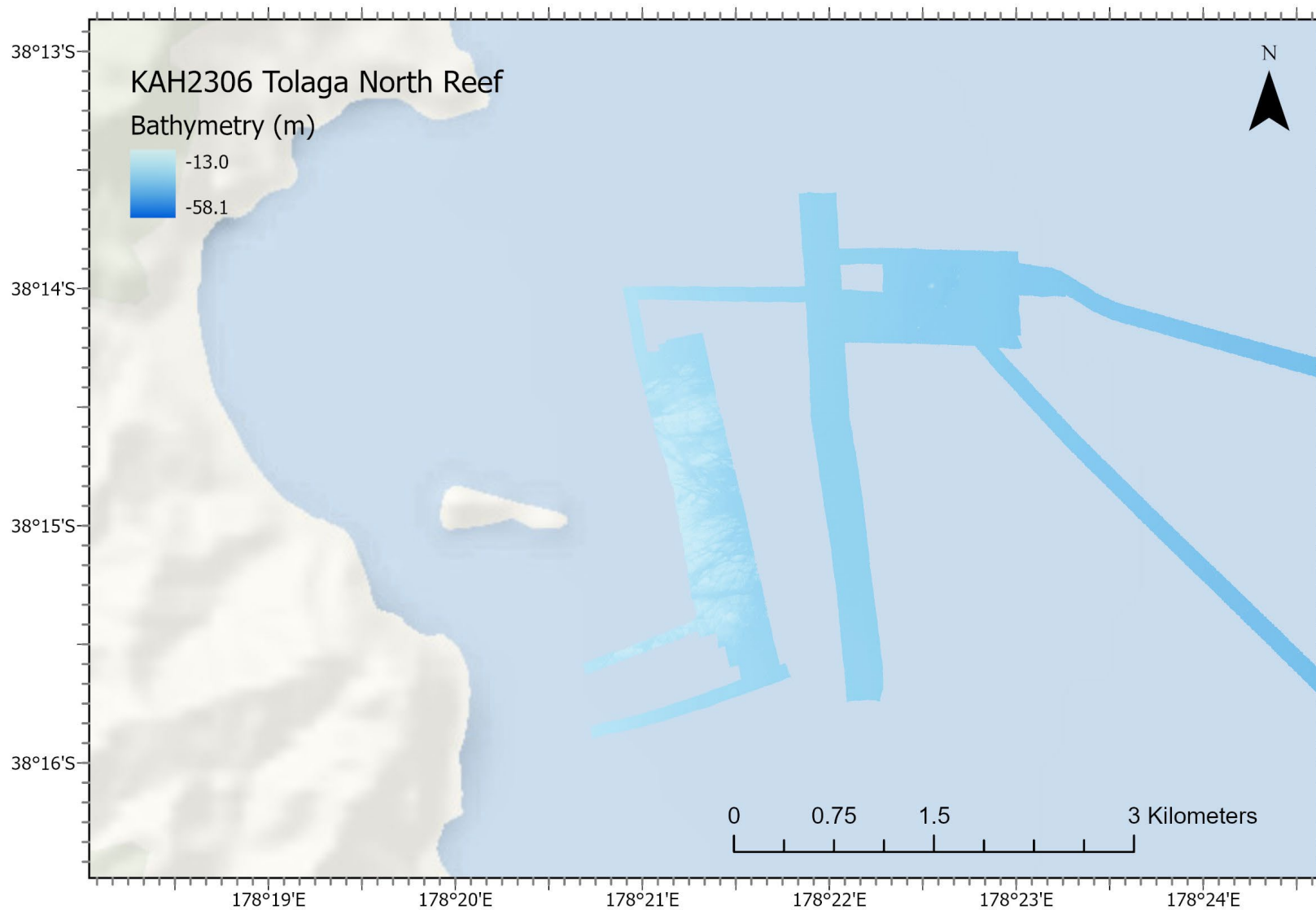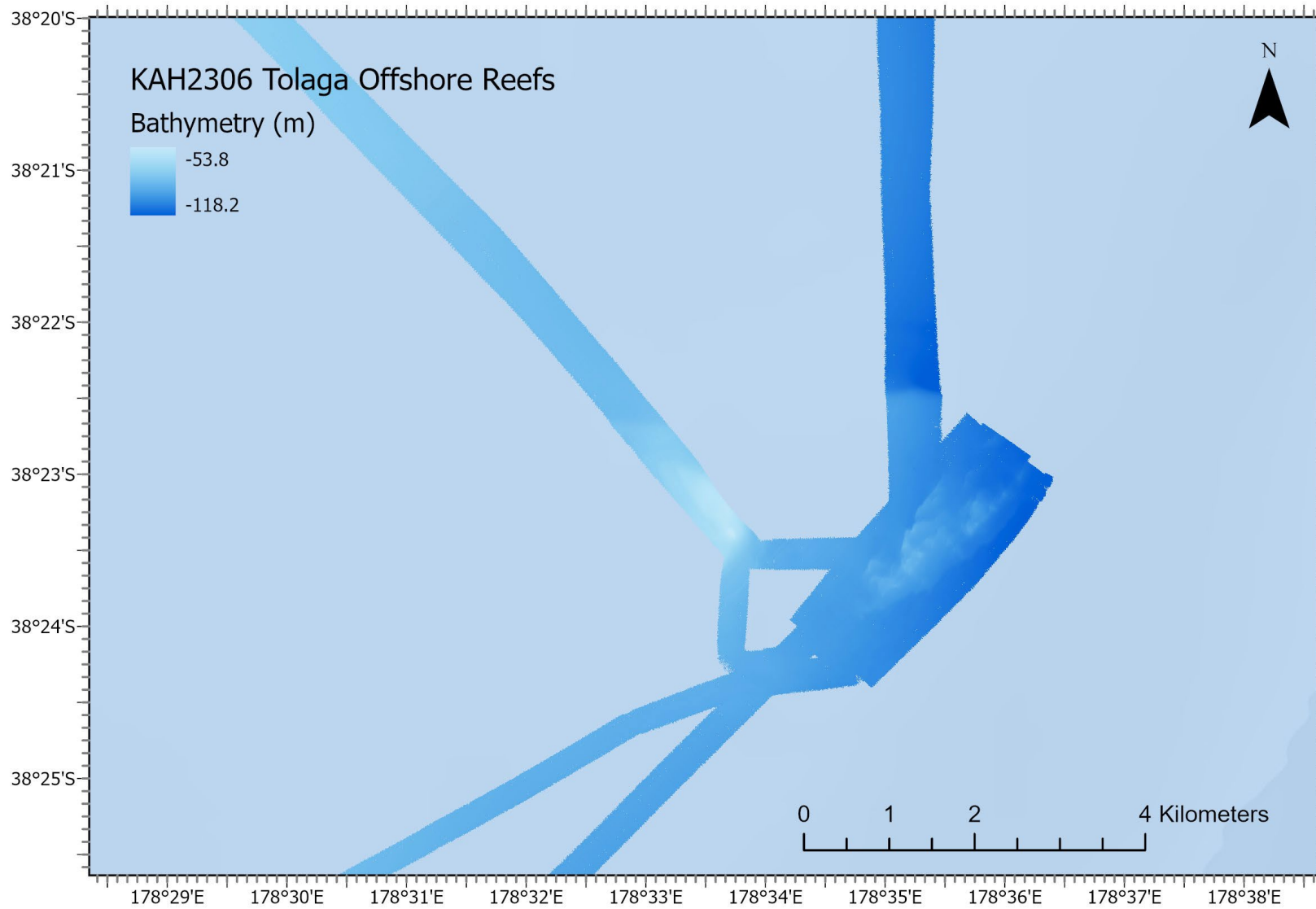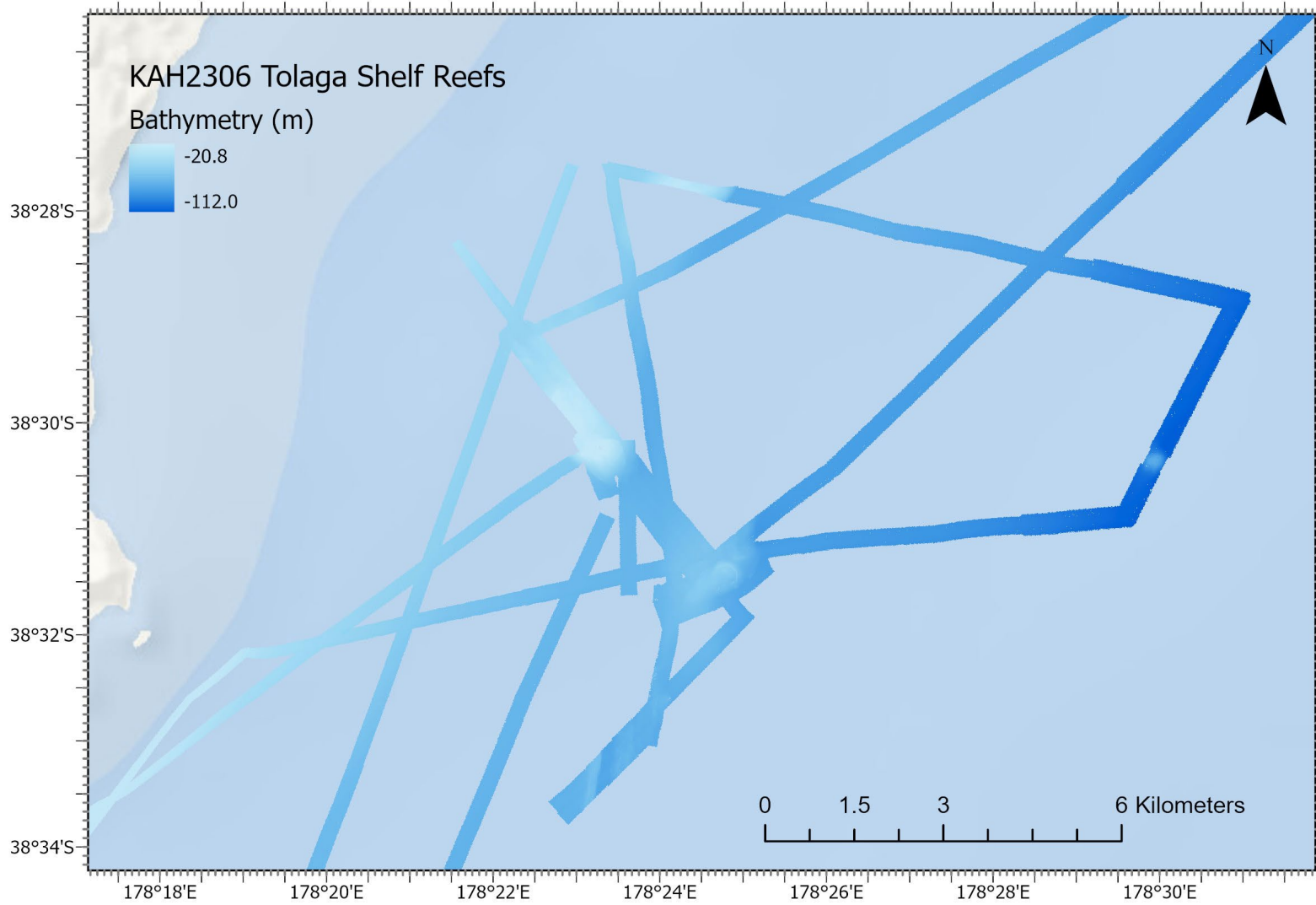
APPENDIX 5 – WOODY DEBRIS

Woody debris in macrofauna cores samples processed from 2010 (KAH1006 and KAH1010) and 2023 RV *Kaharoa* surveys (KAH202303 and KAH2306) in Hawke's Bay and Gisborne. Core samples were 9.5 cm in diameter and 5 cm deep. See Appendix 2 for details of sampling stations.

Survey	Station	Woody debris mg core^{-1}	g m^{-2}
KAH1006	203	16.37	2.31
KAH1006	204	86.16	12.16
KAH1006	206	884.45	124.78
KAH1006	208	45.22	6.38
KAH1006	209	67.36	9.50
KAH1006	210	55.43	7.82
KAH1006	217	145.45	20.52
KAH1006	232	348.00	49.10
KAH1006	235	136.32	19.23
KAH1006	237	778.19	109.79
KAH1010	317	36.39	5.13
KAH1010	318	66.87	9.43
KAH1010	323	55.85	7.88
KAH1010	329	54.66	7.71
KAH1010	332	10.56	1.49
KAH1010	333	27.29	3.85
KAH1010	334	28.13	3.97
KAH1010	339	27.07	3.82
KAH1010	352	86.19	12.16
KAH2303	9	193.55	27.31
KAH2303	10	9.52	1.34
KAH2303	11	345.32	48.72
KAH2303	12	244.58	34.51
KAH2303	13	34.53	4.87
KAH2303	15	20.47	2.89
KAH2303	16	31.42	4.43
KAH2303	17	43.04	6.07
KAH2303	20	2.52	0.36
KAH2303	21	28.75	4.06
KAH2303	24	3.75	0.53
KAH2303	29	2.47	0.35
KAH2303	31	1.82	0.26
KAH2303	36	44.19	6.23
KAH2303	43	205.72	29.02
KAH2303	45	181.7	25.63
KAH2303	46	33.30	4.70
KAH2303	52	41.61	5.87
KAH2303	53	41.61	5.87
KAH2303	53	122.48	17.28
KAH2303	58	11.77	1.66
KAH2303	61	37.62	5.31
KAH2303	66	103.52	14.60

KAH2303	67	28.29	3.99
KAH2306	1	31.43	4.43
KAH2306	2	174.11	24.56
KAH2306	3	37.17	5.24
KAH2306	13	831.79	117.35
KAH2306	14	93.37	13.17
KAH2306	15	113.91	16.07
KAH2306	21	228.11	32.18
KAH2306	25	48.85	6.89
KAH2306	28	2.04	0.29
KAH2306	35	271.71	38.33
KAH2306	38	67.82	9.57

APPENDIX 6 – MEIOFAUNA UNIVARIATE DATA

Meiofauna univariate parameters from June RV *Kaharoa* survey KAH2303. J´: Pielou's evenness; H´10: Shannon diversity index.

Station	Transect/Site	Depth (m)	Density core⁻¹	Density 10 cm⁻²	Taxon richness core⁻¹	Taxon evenness J´	Taxon diversity H´10
24	T1 #1	15	463	701.0	6	0.27	0.21
20	T1 #2	19	725	1 097.7	7	0.18	0.15
21	T1 #3	30	1 201	1 818.3	5	0.13	0.09
43	T1 #4	48	488	738.8	6	0.26	0.20
36	T2 #1	27	249	377.0	3	0.07	0.03
17	T2 #2	34	429	649.5	3	0.04	0.02
16	T2 #3	47	1 588	2 404.2	6	0.11	0.08
15	T2 #4	61	534	808.5	7	0.18	0.15
13	T3 #1	35	563	852.4	6	0.15	0.11
12	T3 #2	39	809	1 224.8	6	0.15	0.11
11	T3 #3	51	1 674	2 534.4	6	0.14	0.11
10	T3 #4	54	392	593.5	7	0.19	0.16
9	T3 #5	76	422	638.9	7	0.33	0.28
58	T4 #2	27	190	287.7	5	0.10	0.07
61	T4 #3	38	501	758.5	4	0.18	0.11
66	T4 #4	54	581	879.6	8	0.20	0.18
67	T4 #5	53	611	925.1	4	0.12	0.07
46	T5 #1	26	486	735.8	2	0.02	0.01
45	T5 #2	46	1 035	1 567.0	7	0.18	0.15
53	T6 #1	21	54	81.8	1	N/A	0.00
52	T6 #2	61	1 230	1 862.2	5	0.19	0.13
29	Pania Reef	16	513	776.7	5	0.09	0.06

APPENDIX 7 – MEIOFAUNA MULTIVARIATE DATA

Abundance of meiofauna taxa in core samples collected during the June RV *Kaharoa* survey KAH2303. Data are abundance per core (29 mm inner diameter, 5 cm deep).

KAH2303 station	Nematodes	Copepods	Nauplii	Tanaids	Amphipods	Isopods	Ostracods	Cumaceans	Mites	Kinorhynchs	Loriciferans	Annelids	Bivalves	Nemertean	Priapulid larvae	Flatworms
9	350	43	1	0	0	2	1	0	0	12	0	13	0	0	0	0
10	362	14	1	1	0	0	2	0	0	7	0	5	0	0	0	0
11	1 592	18	0	0	0	0	1	1	0	44	0	18	0	0	0	0
12	765	29	0	0	0	0	1	0	0	10	0	3	0	0	0	1
13	534	18	1	0	0	0	3	0	0	3	0	4	0	0	0	0
15	496	13	0	0	0	1	1	0	0	13	1	9	0	0	0	0
16	1 534	9	0	0	0	0	4	0	0	26	0	11	0	0	4	0
17	426	0	0	0	0	0	0	0	0	0	0	1	0	0	0	2
20	674	20	1	0	0	0	1	0	0	11	0	17	0	0	1	0
21	1 155	13	1	0	0	0	0	0	0	16	0	16	0	0	0	0
24	406	34	1	0	0	0	0	0	0	1	0	20	1	0	0	0
29	500	9	1	0	0	0	1	0	0	2	0	0	0	0	0	0
36	246	1	0	0	0	0	0	0	0	2	0	0	0	0	0	0
43	436	27	0	0	1	0	0	0	0	12	0	11	0	0	0	1
45	958	38	3	0	0	0	2	0	0	26	0	7	0	1	0	0
46	485	0	0	0	0	0	0	0	0	0	0	1	0	0	0	0
52	1 150	37	0	0	0	0	2	0	0	10	0	31	0	0	0	0
53	54	0	0	0	0	0	0	0	0	0	0	0	0	0	0	0
58	185	2	0	0	0	0	0	0	1	1	0	0	1	0	0	0
61	477	9	0	0	0	0	0	0	0	6	0	9	0	0	0	0
66	531	14	1	1	2	0	0	0	1	11	0	20	0	0	0	0
67	592	9	0	0	0	0	0	0	0	1	0	9	0	0	0	0

APPENDIX 8 – MACROFAUNA UNIVARIATE DATA

Macrofauna univariate parameters from 2010 and 2023 RV *Kaharoa* surveys. J´: Pielou's evenness; H´10: Shannon diversity index.

	Station	Transect/Site	Depth (m)	Abundance core^{-1}	Abundance 0.01m^{-2}	Taxon richness core^{-1}	Taxon evenness J´	Taxon diversity H´10
KAH2303*	24	T1 #1	15	7	9.9	2	0.59	0.18
	20	T1 #2	21	41	57.8	8	0.81	0.73
	21	T1 #3	30	54	76.2	12	0.78	0.84
	43	T1 #4	48	43	60.7	9	0.79	0.75
	36	T2 #1	29	10	14.1	4	0.95	0.57
	17	T2 #2	34	35	49.4	15	0.80	0.94
	16	T2 #3	47	30	42.3	9	0.82	0.78
	15	T2 #4	61	53	74.8	23	0.93	1.26
	13	T3 #1	35	15	21.2	10	0.96	0.96
	12	T3 #2	39	50	70.5	15	0.83	0.97
	11	T3 #3	40	5	7.1	3	0.87	0.41
	10	T3 #4	54	24	33.9	11	0.79	0.82
	9	T3 #5	76	68	95.9	15	0.57	0.67
	58	T4 #2	27	12	16.9	6	0.82	0.64
	61	T4 #3	42	12	16.9	7	0.92	0.78
	66	T4 #4	54	61	86.1	17	0.83	1.03
	67	T4 #5	53	59	83.2	16	0.85	1.02
	46	T5 #1	29	4	5.6	3	0.95	0.45
	45	T5 #2	42	33	46.6	14	0.89	1.02
	53	T6 #1	21	6	8.5	6	1.00	0.78
	52	T6 #2	61	30	42.3	11	0.87	0.91
	31	Tangoio	20	1	1.4	1	0.00	0.00
	29	Pania Reef	16	16	22.6	7	0.96	0.81
KAH2306**	3	T1 #1	15	33	46.5	8	0.72	0.65
	2	T1 #4	48	30	42.3	8	0.60	0.54
	1	T1 #5	61	88	124.1	23	0.76	1.03
	13	T2 #1	28	50	70.5	5	0.60	0.42
	21	T2 #2	34	52	73.3	8	0.63	0.57
	14	T2 #3	47	93	131.1	6	0.58	0.45
	15	T2 #4	61	155	218.6	24	0.58	0.81
	38	T4 #3	40	26	36.7	8	0.78	0.70
	25	T5 #3	64	65	91.7	14	0.75	0.86
	28	T6 #4	146	40	56.4	13	0.85	0.94
	35	Tolaga	49	37	52.2	11	0.86	0.90
KAH1006***	203	Poverty Bay	50	79	111.4	10	0.60	0.60
	204	Poverty Bay	47	84	118.4	12	0.58	0.63
	206	Poverty Bay	18	16	22.6	4	0.59	0.36
	208	Poverty Bay	30	39	55.0	8	0.67	0.60
	209	Poverty Bay	35	26	36.7	6	0.71	0.56
	210	Poverty Bay	35	32	45.1	9	0.79	0.76
	217	Poverty Bay	40	128	180.5	15	0.62	0.73
	232	Poverty Bay	25	30	42.3	9	0.88	0.84
	237	Poverty Bay	27	40	56.4	7	0.86	0.72
KAH1010***	317	Poverty Bay	24	84	118.4	13	0.61	0.68
	318	Poverty Bay	35	73	102.9	13	0.66	0.74
	323	Poverty Bay	58	17	24.0	6	0.84	0.65
	329	Poverty Bay	37	52	73.3	7	0.45	0.38
	332	Poverty Bay	50	77	108.6	12	0.75	0.81
	333	Poverty Bay	46	74	104.3	16	0.76	0.92
	334	Poverty Bay	42	41	57.8	14	0.84	0.96
	339	Poverty Bay	18	12	16.9	5	0.96	0.67
	352	Poverty Bay	36	57	80.4	9	0.66	0.63

* Molluscs (bivalves and gastropods), crustaceans (amphipods, cumaceans and isopods) and annelids identified to species/morphospecies.
** Molluscs (bivalves and gastropods), crustaceans (amphipods, cumaceans and isopods) identified to species/morphospecies.
*** Molluscs identified to species/morphospecies.

APPENDIX 9 – MACROFAUNA MULTIVARIATE DATA

Abundance of macrofauna taxa in core samples collected during the June 2023 RV *Kaharoa* survey KAH2303. Data are abundance per core (9.5 cm diameter, 5 cm deep).

					KAH2303 stations																						
Phylum	**Class**	**Order**	**Family**	**Taxon**	**9**	**10**	**11**	**12**	**13**	**15**	**16**	**17**	**20**	**21**	**24**	**29**	**31**	**36**	**43**	**45**	**46**	**52**	**53**	**58**	**61**	**66**	**67**
Cnidaria				Hydrozoans			1									1											
Cnidaria				*Edwardsia neozelanica*																		2				1	
Nemertea				Nemerteans																1						1	
Nematoda				Nematodes							1			1					14			5	1	1	1	1	10
Mollusca	Bivalvia	Cardiida	Tellinidae	*Moerella huttoni*																					1		
Mollusca	Bivalvia	Nuculanida	Malletiidae	*Neilo australis*										1													
Mollusca	Bivalvia	Nuculanida	Nuculanidae	*Saccella maxwelli*			1																			4	
Mollusca	Bivalvia	Nuculida	Nuculidae	*Ennucula sp.*	2																						
Mollusca	Bivalvia	Nuculida	Nuculidae	*Varinucula gallinacea*						1																	
Mollusca	Bivalvia	Nuculida	Nuculidae	*Linucula* sp. 1																1							
Mollusca	Bivalvia	Nuculida	Nuculidae	*Linucula* sp. 2																	2						
Mollusca	Bivalvia	Nuculida	Nuculidae	*Ennucula strangeiformis*						2																	
Mollusca	Bivalvia	Nuculida	Nuculidae	*Nucula* sp.					1					3		2											
Mollusca	Bivalvia	Solemyida	Nucinellidae	*Nucinella sp.*	2					2		1															
Mollusca	Bivalvia	Venerida	Mactridae	*Maorimactra ordinaria*					2				11		6			2									
Mollusca	Bivalvia		Lasaeidae	*Melliteryx* sp. 2			1																				
Mollusca	Bivalvia		Lasaeidae	*Myllita vivens*													1										
Mollusca	Bivalvia		Nuculidae	Nuculidae (juvenile)																				1			
Mollusca	Bivalvia		Semelidae	*Theora lubrica*				14	1	1	10	1		1				3	7								
Mollusca	Gastropoda	Neogastropoda	Muricidae	*Xymene plebeius*					1					2													
Mollusca	Gastropoda	Neogastropoda	Prosiphonidae	*Austrofusus glans*						1																	
Mollusca	Gastropoda		Acteonidae	*Punctacteon cratericulatus*																					1		
Mollusca	Gastropoda		Pyramidellidae	*Pyramidellidae* sp. (juveniles)					2	1			2								1						1
Mollusca	Scaphopoda			Scaphopoda	2																					1	1
Annelida		Spionida	Spionidae	*Paraprionospio* sp.1	4									1					1								

Phylum	Order	Family	Species																							
Annelida	Spionida	Spionidae	*Paraprionospio* sp. 2	1			1		4																
Annelida	Spionida	Spionidae	*Prionospio* sp. 1	1																					
Annelida	Spionida	Spionidae	*Boccardia* sp. 1	1													1								
Annelida		Capitellidae	*Capitella* sp. 1	42		9	2	2	8		19						12		3					9	
Annelida	Terebellida	Sternaspidae	*Sternaspis* sp. 1	1														2		1					
Annelida		Maldanidae	*Asychis trifilosus*	1				2																	
Annelida		Maldanidae	*Maldane* sp. 1	5				7										1		1					
Annelida		Maldanidae	*Axiothella serrata*																					8	
Annelida	Phyllodocida	Goniadidae	*Glycinde* sp. 1	1			2										1								1
Annelida		Terebellidae	Terebellidae sp. 1 (damaged)	1																					
Annelida		Magelonidae	*Magelona dakini*	10							1														
Annelida	Eunicida	Onuphidae	*Onuphis* cf *aucklandensis*	1			1		2		2										1				
Annelida	Eunicida	Onuphidae	*Kinbergonuphis* sp. 1		3																				
Annelida		Ampharetidae	*Amphicteis* sp. 1			4		2		2	12	4											2		
Annelida		Ampharetidae	*Ampharete* sp. 1				2								1								4		
Annelida	Eunicida	Lumbrineridae	*Lumbrineris* sp. 1			5			2			4									3				
Annelida		Nephytidae	*Aglaophamus* sp. 1				1			1															
Annelida		Pectinaridae	*Lagis australis*				1			1			1												
Annelida		Paraonidae	*Aricidea* sp. 1							1	15			4							6		16	11	
Annelida	Phyllodocida	Syllidae	*Exogone* sp. 1							9															
Annelida	Phyllodocida	Syllidae	*Syllis* sp. 1					6								3		4						5	9
Annelida	Phyllodocida	Polynoidae	*Lepidonotus* sp. 1				1	2								4		1					2		
Annelida	Phyllodocida	Polynoidae	*Disconatis* sp. 1								2													1	
Annelida	Phyllodocida	Nereididae	*Platynereis* sp. 1				1																		
Annelida		Oweniidae	*Owenia* sp. 1											3							1	1			
Annelida		Cossuridae	*Cossura consimils*							4	9							9	4					1	
Annelida	Terebellidae	Cirratulidae	*Chaetozone* sp. 1									5					2		9	4					
Annelida		Sabellidae	*Branchiomme* sp. 1									1													
Annelida	Eunicida	Dorvilleidae	*Schistomeringos* sp. 1													1									1
Annelida	Terebellida	Trichobranchidae	*Terebellides* cf *narribri*					2																	6

Phylum	Class	Order	Family	Taxon																		
Annelida				Plathelminthes					1													
Arthropoda	Ostracoda			Ostracods		1	1	3	6	1	1			2				2			1	1
Arthropoda	Copepoda			Copepods			1													1	2	1
Arthropoda		Amphipoda	Urothoidae	*Urothoe* sp. 1	2				1					2								
Arthropoda		Amphipoda	Phoxocephalidae	*Torridoharpinia hurleyi*	1		6				1				3		1		1			
Arthropoda		Amphipoda	Ampeliscidae	*Ampelisca chiltoni*	1				1												1	
Arthropoda		Amphipoda	Liljeborgiidae	*Liljeborgia* sp. (juv)																	1	1
Arthropoda		Amphipoda	Photidae	*Photis sp. 1*									1									
Arthropoda		Amphipoda	Tryphosidae	*Hippomedon* sp.1		1																
Arthropoda		Amphipoda	Melitidae	*Melita* n.sp. 1					1													
Arthropoda		Amphipoda	Photidae	*Gammaropsis* sp. (juv.)					1													
Arthropoda		Amphipoda	Amphilochidae	*Amphilochus* sp. 1																		1
Arthropoda		Tanaidacea		Tanaidacea	1									2								
Arthropoda		Cumacea	Diastylidae	*Diastylis* cf. *implanus*			2															
Arthropoda		Cumacea	Diastylidae	*Colurostylis* sp. 1	2				1													
Arthropoda		Cumacea	Diastylidae	*Diastylopsis elongata*							1	2				1						
Arthropoda		Cumacea	Leuconidae	*Eudorella hurleyi*	2		1		4						2						3	2
Arthropoda		Cumacea	Leuconidae	*Leucon* sp. 1											2							
Arthropoda		Cumacea	Leuconidae	*Hemileucon* sp. 1													1					2
Arthropoda		Cumacea	Bodotriidae	*Cyclaspis elegans*							1											
Arthropoda		Cumacea	Bodotriidae	*Cyclaspis argus*							1											
Arthropoda		Cumacea	Bodotriidae	*Bathycuma* sp. 1																	3	
Arthropoda		Cumacea	Gynodiastylidae	*Litogynodiastylis laevis*											1							
Arthropoda		Cumacea	Nannastacidae	*Campylaspis* sp. 1													1					6
Arthropoda		Isopoda		Isopods			1		2								1					
Arthropoda		Isopoda	Hemioniscidae	Hemioniscidae sp. 1			1															
Arthropoda		Isopoda	Paramunnidae	*Omonana* sp. 1					2								1					
Echinodermata	Ophiuroidea			Ophiuroidea		1				1			1		1				1			5
Echinodermata	Holothuroidea			Holothuroids	1																	1

Abundance of macrofauna taxa in core samples collected during the October 2023 RV *Kaharoa* survey KAH2306. Data are abundance per core (9.5 cm diameter, 5 cm deep).

Phylum	Class	Order	Family	Taxon	1	2	3	13	14	15	21	25	28	35	38
				KAH2306 stations											
Cnidaria	Hydrozoa			Hydrozoans				4		2			2		
Cnidaria	Anthozoa	*Edwardsia neozelanica*		*Edwardsia neozelanica*			1			1					
Nemertea				Nemerteans							2	1	1		
Nematoda				Nematodes	5	2		5	33	18			2		
Mollusca		Venerida	Mactridae	*Maorimactra ordinaria*			5	3							
Mollusca		Nuculida	Nuculidae	*Ennucula strangei*	2					4		1	1		
Mollusca		Solemyida	Nucinellidae	*Nucinella maoria*	1										
Mollusca		Nuculida	Nuculidae	*Linucula* sp. 1	3										
Mollusca		Cardiida	Cardiidae	*Pratulum pulchellum*	1										
Mollusca		Carditida	Carditidae	*Pleuromeris zelandica*						1					
Mollusca		Cardiida	Semelidae	*Theora lubrica*					4		2				
Mollusca		Cephalaspidea	Philinidae	*Philine auriformis*		1					1		1		
Mollusca		Pylopulminata	Pyramidellidae	*Odostomia* sp. 1										1	
Mollusca		Neogastropoda	Prosiphonidae	*Austrofusus glans*						1				1	
Mollusca		Opisthobranchia		Opisthobranchia		1					1				
Mollusca	Scaphopoda			Scaphopods									5		
Annelida	Polychaeta			Polychaetes	31	20	17	36	51	88	32	26	13	12	3
Sipunculida				Sipunculida	1	1									
Plathelminthes				Plathelminthes	2										
Crustacea	Ostracoda			Ostracods	15	1	1			3			5		
Crustacea	Copepoda			Copepods		3		2		2	2			2	
Crustacea	Malacostraca	Amphipoda	Melphidippidae	*Melphidippia* nsp. 1								2			
Crustacea	Malacostraca	Amphipoda	Ischyroceridae	*Ischyrocerus* sp. 1	2					6		3			
Crustacea	Malacostraca	Amphipoda	Phoxocephalidae	*Torridoharpinia hurleyi*			2		2		4	3	1	3	1
Crustacea	Malacostraca	Amphipoda	Liljeborgidae	*Liljeborgia* sp. 1	1				2	1		1			
Crustacea	Malacostraca	Amphipoda	Photidae	*Photis brevicaudata*			5			1	8			5	13

Crustacea	Malacostraca	Amphipoda	Aoridae	*Aora typica*			1						1
Crustacea	Malacostraca	Amphipoda	Oedicerotidae	*Monoculodes* sp. 1								1	3
Crustacea	Malacostraca	Amphipoda	Urothoidae	*Urothoe* sp. 1	2								
Crustacea	Malacostraca	Amphipoda	Lysianassidae	*Parawaldeckia kidderi*	5								
Crustacea	Malacostraca	Tanaidacea		Tanaidacea	1				2		2	2	
Crustacea	Malacostraca	Cumacea	Leuconidae	*Eudorella hurleyi*	3				2				
Crustacea	Malacostraca	Cumacea	Leuconidae	*Leucon latispina*	1				3		3	4	4
Crustacea	Malacostraca	Cumacea	Gynodiastylidae	*Litogynodiastylis laevis*	1								
Crustacea	Malacostraca	Cumacea	Nannastacidae	*Procampylaspis rhypakoceros*							1		
Crustacea	Malacostraca	Cumacea	Diastylidae	*Diastylopsis elongata*			1		1	2	2		
Crustacea	Malacostraca	Cumacea	Bodotriidae	*Cyclaspis thomsoni*					2			4	
Crustacea	Malacostraca	Cumacea	Diastylidae	*Diastylis* sp. 1								1	
Crustacea	Malacostraca	Isopoda	Leptanthuridae	*leptanthura* sp. 1	1						1		
Crustacea	Malacostraca	Isopoda	Paramunnidae	*Omonana* sp. 1					2				
Crustacea	Malacostraca	Isopoda	Paramunnidae	*Pentaceration* nsp. 1					1				
Crustacea	Malacostraca	Isopoda	Desmosomatidae	*Desmosoma* sp. 1							2		
Crustacea		Mysidacea		Mysids		1			2	1			2
Crustacea	Decapoda	Natantia		Natant decapods	1								
Crustacea		Reptantia		Crabs	1								2
Echinodermata	Ophiuroidea			Ophiuroids	2			1	3		6	3	1
Echinodermata	Holothuroidea			Holothuroids					1				
Chordata	Ascidiacea			Ascidians	1								
Forminifera				Foraminiferans	5				6		13		

Abundance of macrofauna taxa in core samples collected during the May 2010 RV *Kaharoa* survey KAH1006. Data are abundance per core (9.5 cm diameter, 5 cm deep).

Phylum	Class	Order	Genus	Taxon/species	203	204	206	208	209	210	217	219	232
Cnidaria	Hydrozoa			Hydrozoans				2		2		5	
Nemertea				Nemerteans		1							
Nematoda				Nematodes		1	1				3		
Mollusca		Nuculida	*Nucula*	*Nucula nitidula*				13					3
Mollusca		Venerida	*Maorimactra*	*Maorimactra ordinaria*									1
Mollusca		Galeommatida	*Arthritica*	*Arthritica bifurca*									5
Mollusca		Cardiida	*Bartschicoma*	*Bartschicoma edgari*				1					2
Mollusca		Nuculida	*Ennucula*	*Ennucula strangei*		2						1	
Mollusca		Nuculanida	*Saccella*	*Saccella maxwelli*		1				1	1		
Mollusca		Nuculida	*Linucula*	*Linucula sp. 1*		2					1		
Mollusca		Venerida	*Ruditapes*	*Ruditapes largillierti*									
Mollusca		Nuculanida	*Poroleda*	*Poroleda lanceolata*	1								
Mollusca		Anomalodesmata	*Thracia*	*Thracia vitrea*				1					
Mollusca		Cardiida	*Pratulum*	*Pratulum pulchellum*									
Mollusca		Neogastropoda	*Austrofusus*	*Austrofusus glans*									
Mollusca		Neogastropoda	*Amalda*	*Amalda novaezelandiae*									
Mollusca		Seguenziida	*Brookula*	*Brookula sp. 1*								1	
Mollusca		Opisthobranchia	*Philine*	*Philine powelli*	1								
Mollusca		Pylopulminata	*Odostomia*	*Odostomia sp. 1*							1		
Mollusca		Pylopulminata	*Turbonilla*	*Turbonilla sp. 1*									
Mollusca		Cephalaspidea	*Volvulella*	*Volvulella nesentus*									
Mollusca		Littorinimorpha	*Uberella*	*Uberella denticulifera*									
Mollusca		Pylopulminata	*Eulimella*	*Eulimella deplexa*									
Mollusca		Opisthobranchia		Opisthobranchia	1								
Mollusca	Scaphopoda			Scaphopods							2		
Mollusca				Solenogastres/Aplacophora		1							
Annelida	Polychaeta			Polychaetes	49	42	12	18	15	14	39	34	10

Phylum	Class	Order	Common name									
Sipunculida			Sipunculids									
Priapulida			Priapulids	1								
Arthropoda	Ostracoda		Ostracods	5	3		1		1	10		2
Arthropoda	Cirripedia		Cirripedia									1
Arthropoda	Copepoda		Copepods									
Arthropoda	Malacostraca	Amphipoda	Amphipods		2	1		2	3	1		3
Arthropoda		Tanaidacea	Tanaids								1	
Arthropoda		Cumacea	Cumaceans	7	2		1	2	4	4	1	
Arthropoda		Isopoda	Isopods						1	3	5	
Arthropoda		Mysidacea	Mysids									
Arthropoda	Decapoda	Natantia	Natant decapods					1				
Echinodermata	Ophiuroidea		Ophiuroids	3	1		3		1	2	1	3
Echinodermata	Holothuroidea		Holothuroids	2			1	1		1		
Chordata	Ascidiacea		Ascidians									
Foraminifera			Foraminiferans	9	26			5	5	5	9	

Abundance of macrofauna taxa in core samples collected during the October 2010 RV *Kaharoa* survey KAH1010. Data are abundance per core (9.5 cm diameter, 5 cm deep).

Phylum	Class	Order	Genus	Taxon	317	329	318	332	333	334	339	352	323
				KAH1010 stations									
Cnidaria	Hydrozoa			Hydrozoans	1					1			
Nemertea				Nemerteans		2				1			
Nematoda				Nematodes		1				1			2
Mollusca		Nuculida	*Nucula*	*Nucula nitidula*	3	3			3	12		2	
Mollusca		Venerida	*Maorimactra*	*Maorimactra ordinaria*						2			
Mollusca		Galeommatida	*Arthritica*	*Arthritica bifurca*	1					4			
Mollusca		Cardiida	*Bartschicoma*	*Bartschicoma edgari*						2			
Mollusca		Nuculida	*Ennucula*	*Ennucula strangei*				2	1				3
Mollusca		Nuculanida	*Saccella*	*Saccella maxwelli*			1	1				1	
Mollusca		Nuculida	*Linucula*	*Linucula sp. 1*					3				3
Mollusca		Venerida	*Ruditapes*	*Ruditapes largillierti*			1			1			
Mollusca		Nuculanida	*Poroleda*	*Poroleda lanceolata*									1
Mollusca		Anomalodesmata	*Thracia*	*Thracia vitrea*									
Mollusca		Cardiida	*Pratulum*	*Pratulum pulchellum*					1				
Mollusca		Neogastropoda	*Austrofusus*	*Austrofusus glans*						2		1	
Mollusca		Neogastropoda	*Amalda*	*Amalda novaezelandiae*			1						
Mollusca		Seguenziida	*Brookula*	*Brookula sp. 1*									2
Mollusca		Opisthobranchia	*Philine*	*Philine powelli*						1			3
Mollusca		Pylopulminata	*Odostomia*	*Odostomia sp. 1*									
Mollusca		Pylopulminata	*Turbonilla*	*Turbonilla sp. 1*									2
Mollusca		Cephalaspidea	*Volvulella*	*Volvulella nesentus*					1				
Mollusca		Littorinimorpha	*Uberella*	*Uberella denticulifera*						1			
Mollusca		Pylopulminata	*Eulimella*	*Eulimella deplexa*				2	1				
Mollusca		Opisthobranchia		Opisthobranchia						1			1
Mollusca	Scaphopoda			Scaphopods									
Mollusca				Solenogastres/Aplacophora						1			
Annelida	Polychaeta			Polychaetes	8	30	41	32	27	8	3	32	64

Phylum	Class	Order	Common name									
Sipunculida			Sipunculids		3	3					3	
Priapulida			Priapulids									
Arthropoda	Ostracoda		Ostracods	1	1	8	4	1	1			6
Arthropoda	Cirripedia		Cirripedia	2								
Arthropoda	Copepoda		Copepods	2	1			1	1			
Arthropoda	Malacostraca	Amphipoda	Amphipods	2		2	3		3	10	9	
Arthropoda		Tanaidacea	Tanaids				1					
Arthropoda		Cumacea	Cumaceans	2		8	6	1	3	4	2	
Arthropoda		Isopoda	Isopods									
Arthropoda		Mysidacea	Mysidacea						2			
Arthropoda	Decapoda	Natantia	Natant decapods				7	1				
Echinodermata	Ophiuroidea		Ophiuroids	2	2		3	3	4		1	1
Echinodermata	Holothuroidea		Holothuroids									
Chordata	Ascidiacea		Ascidians									1
Foraminifera			Foraminiferans		36	3	13	13			3	28
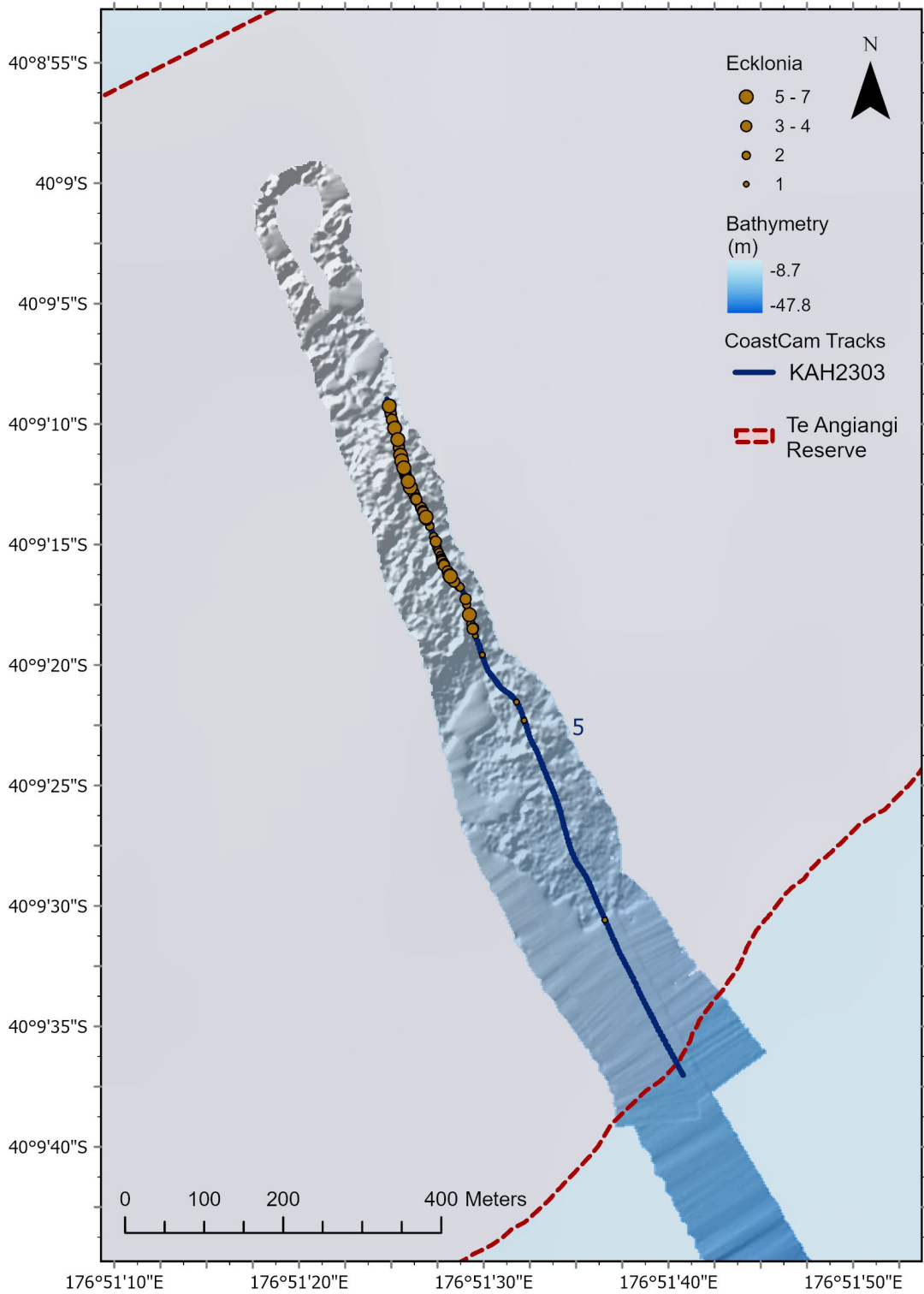
Paoanui Point – seafloor bathymetry, path of towed camera transect, and counts of kelp *Ecklonia radiata*. June survey KAH2303 station 5. Most of the transect was conducted within the Te Angiangi Reserve.
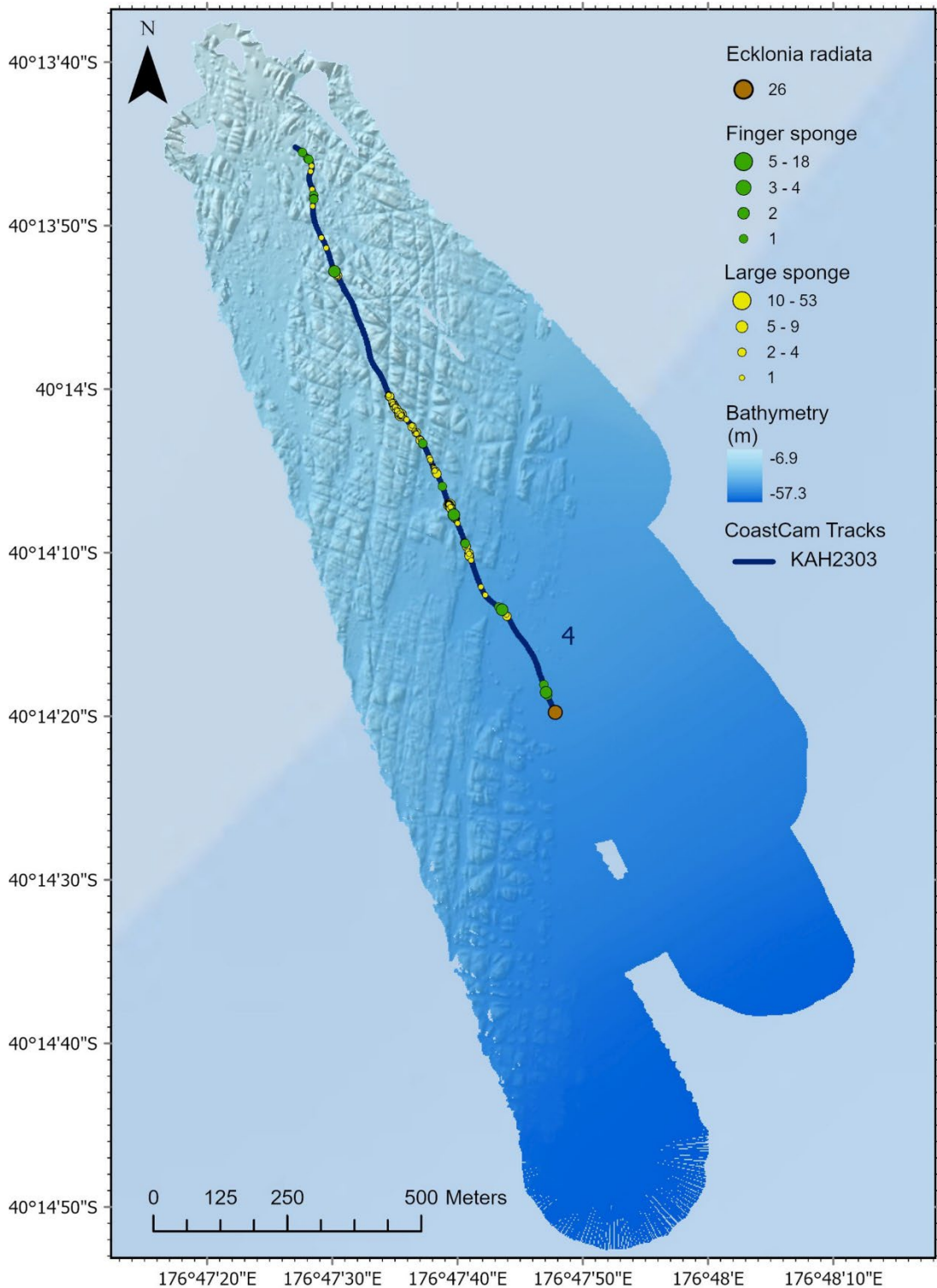
Blackhead Point – seafloor bathymetry, path of towed camera transect, and counts of kelp *Ecklonia radiata*, finger sponges, and large sponges (if present). June survey KAH2303 station 5.
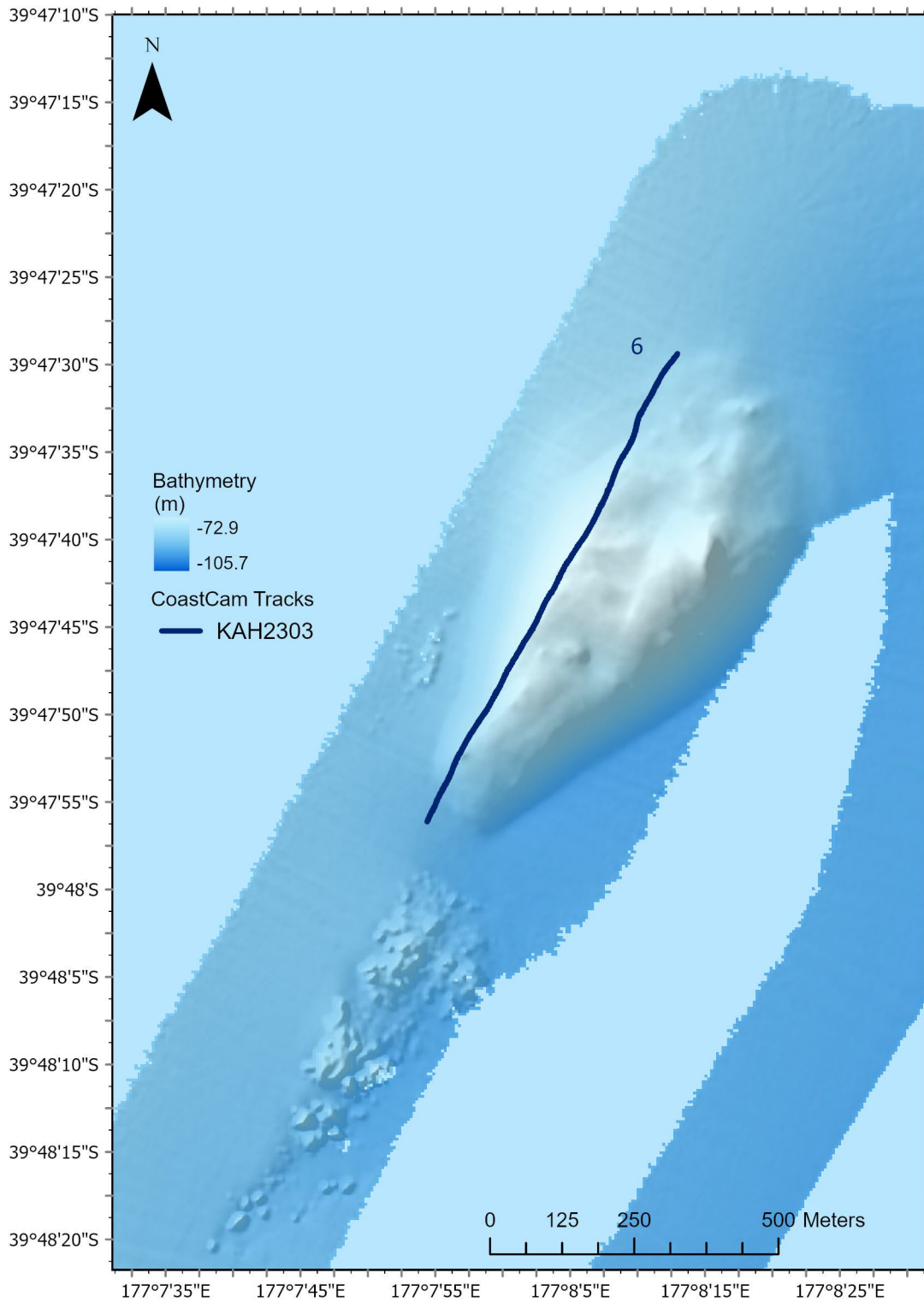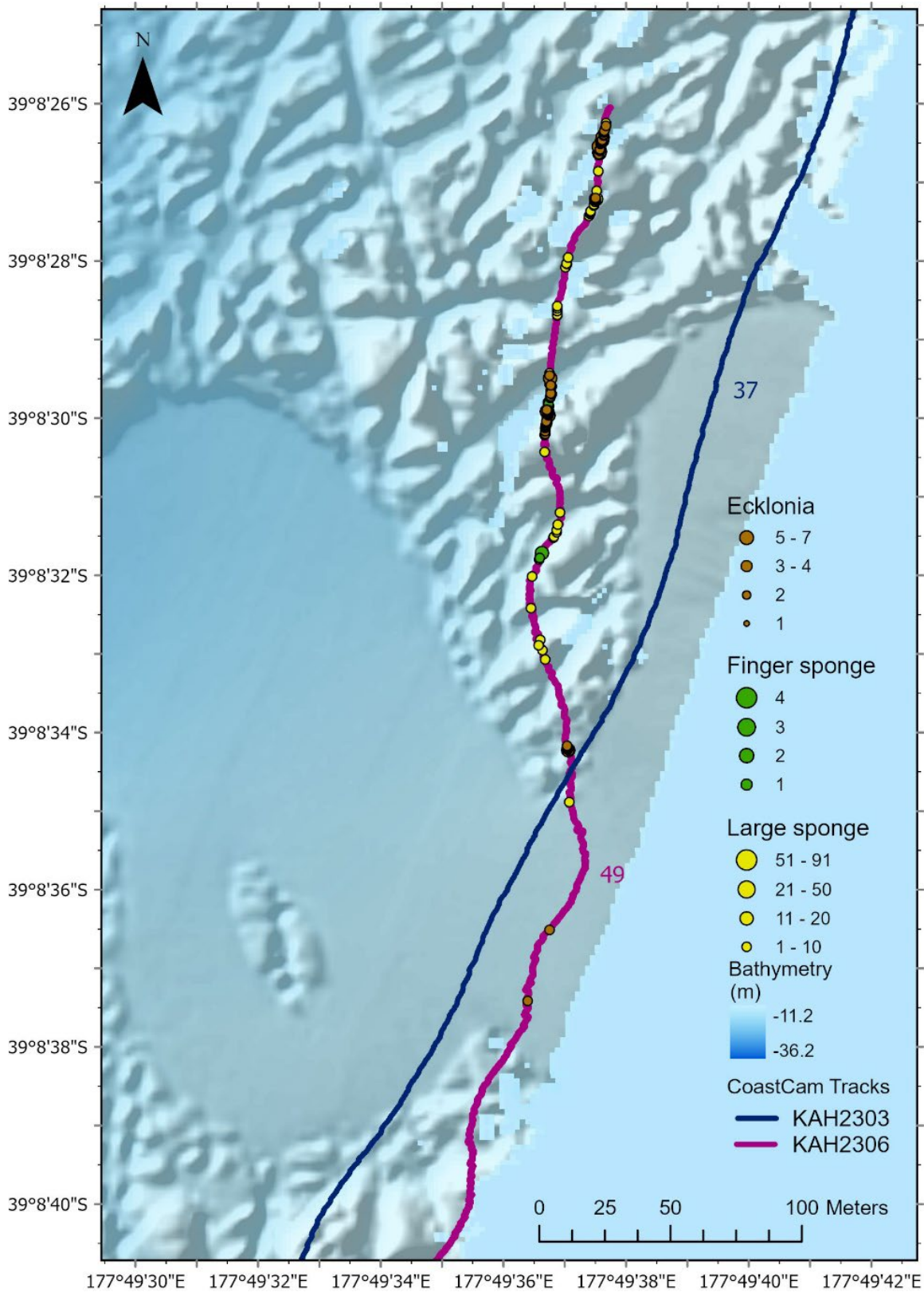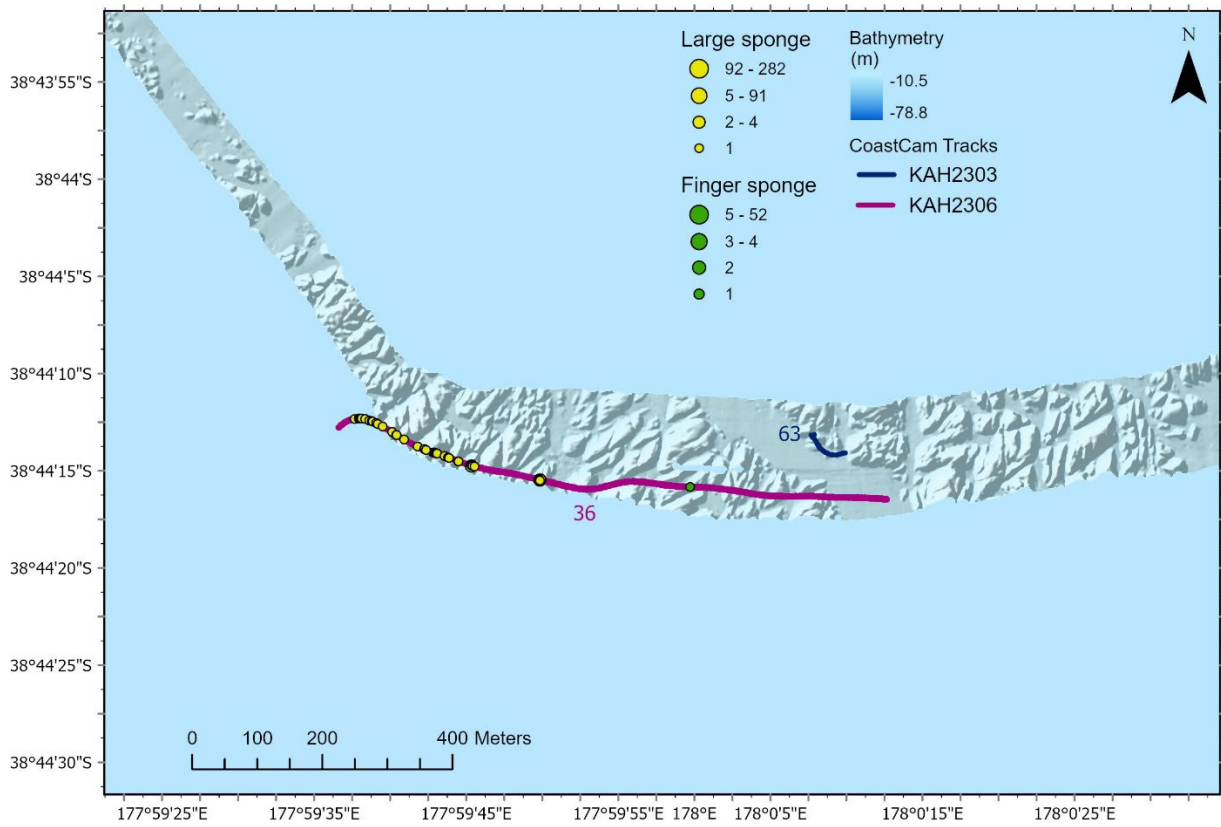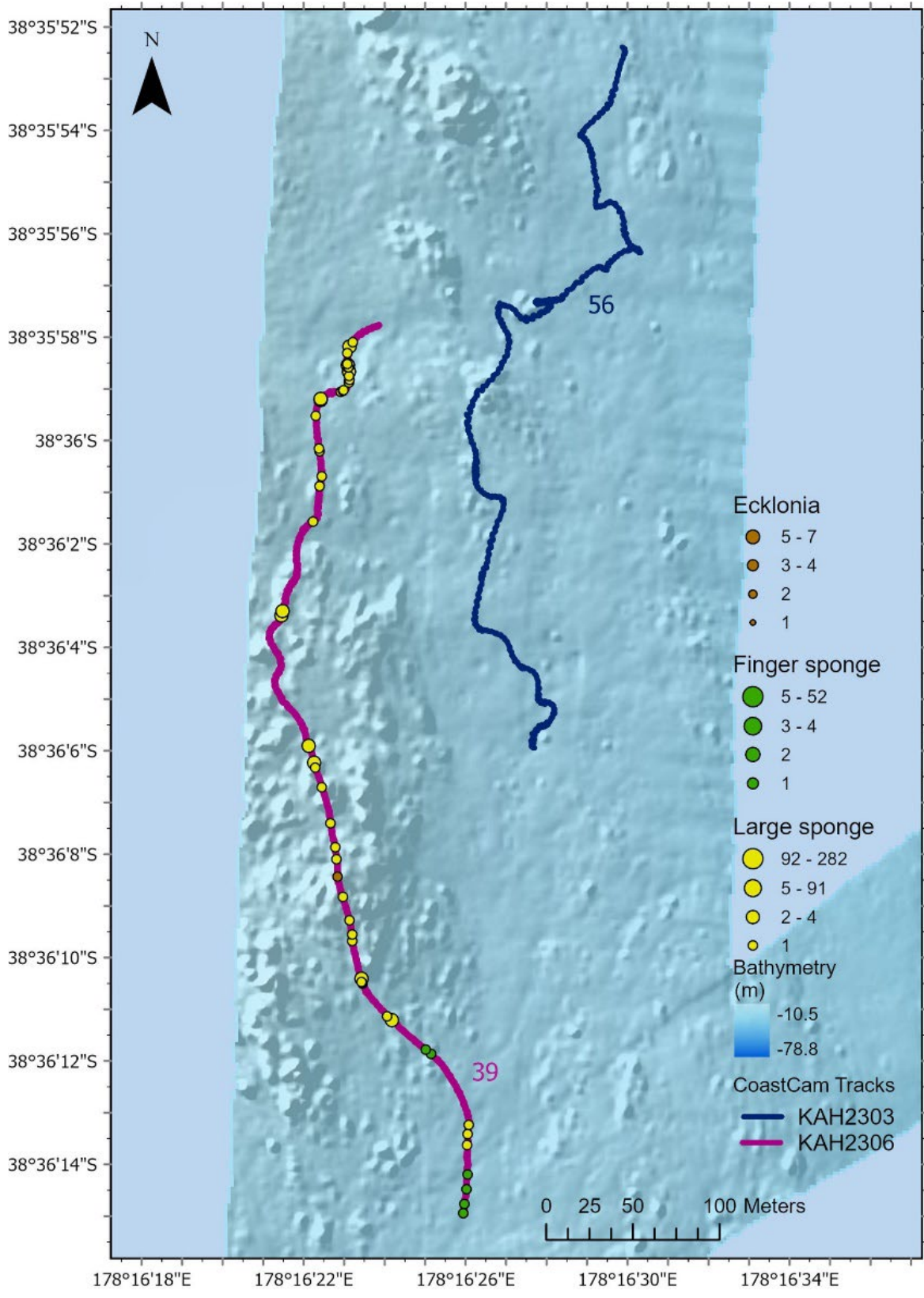
Motuokura Reef – seafloor bathymetry, path of towed camera transect. No kelp *Ecklonia radiata*, finger sponges, or large sponges were present. June survey KAH2303 station 5.
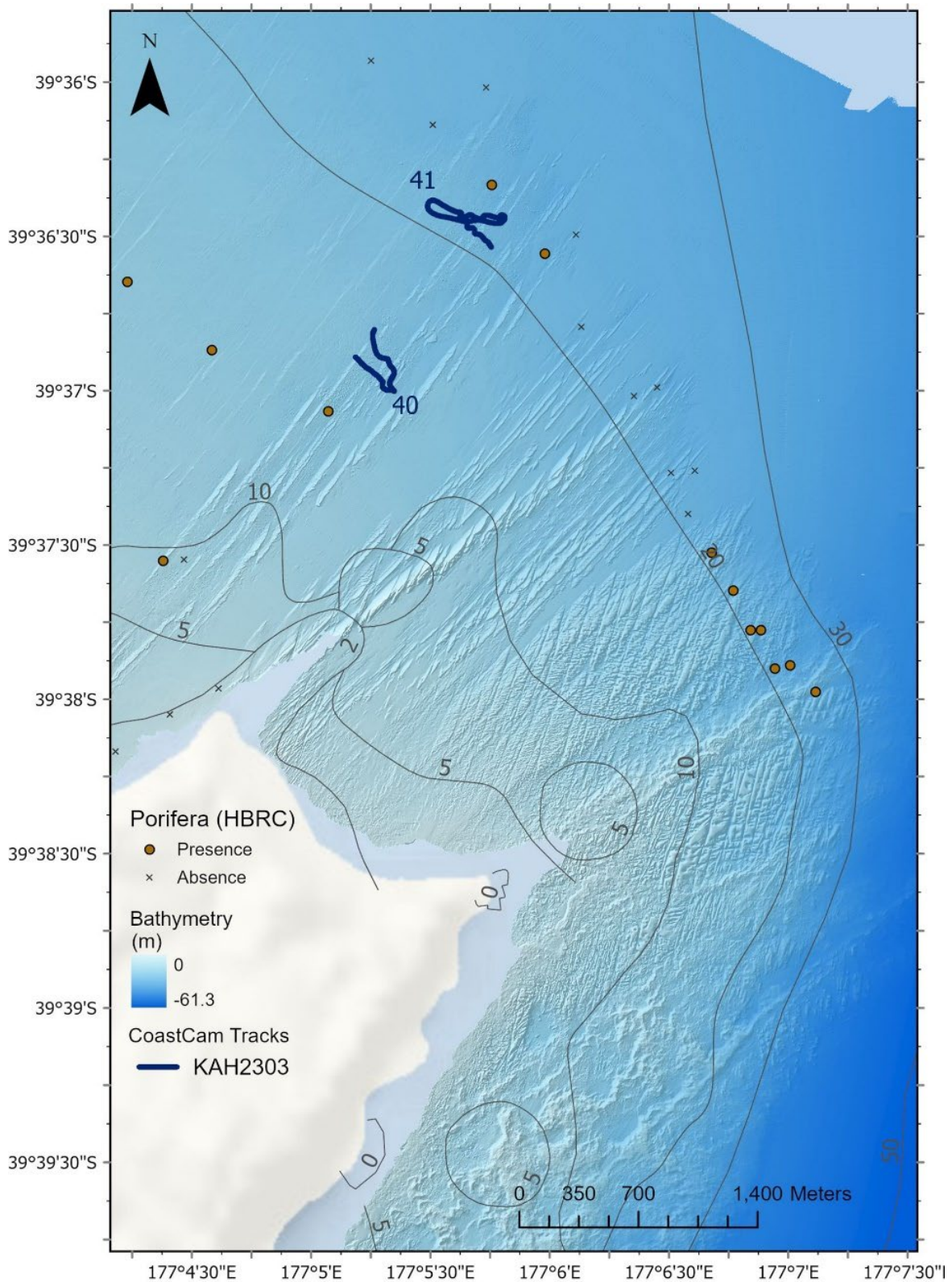
Cape Kidnappers – seafloor bathymetry and path of KAH2303 towed camera transects (which had very poor visibility). Pre-cyclone remotely operated vehicle (ROV) data from HBRC is shown for sponge/presence absence. No *Ecklonia radiata* kelp was observed in the HBRC data.
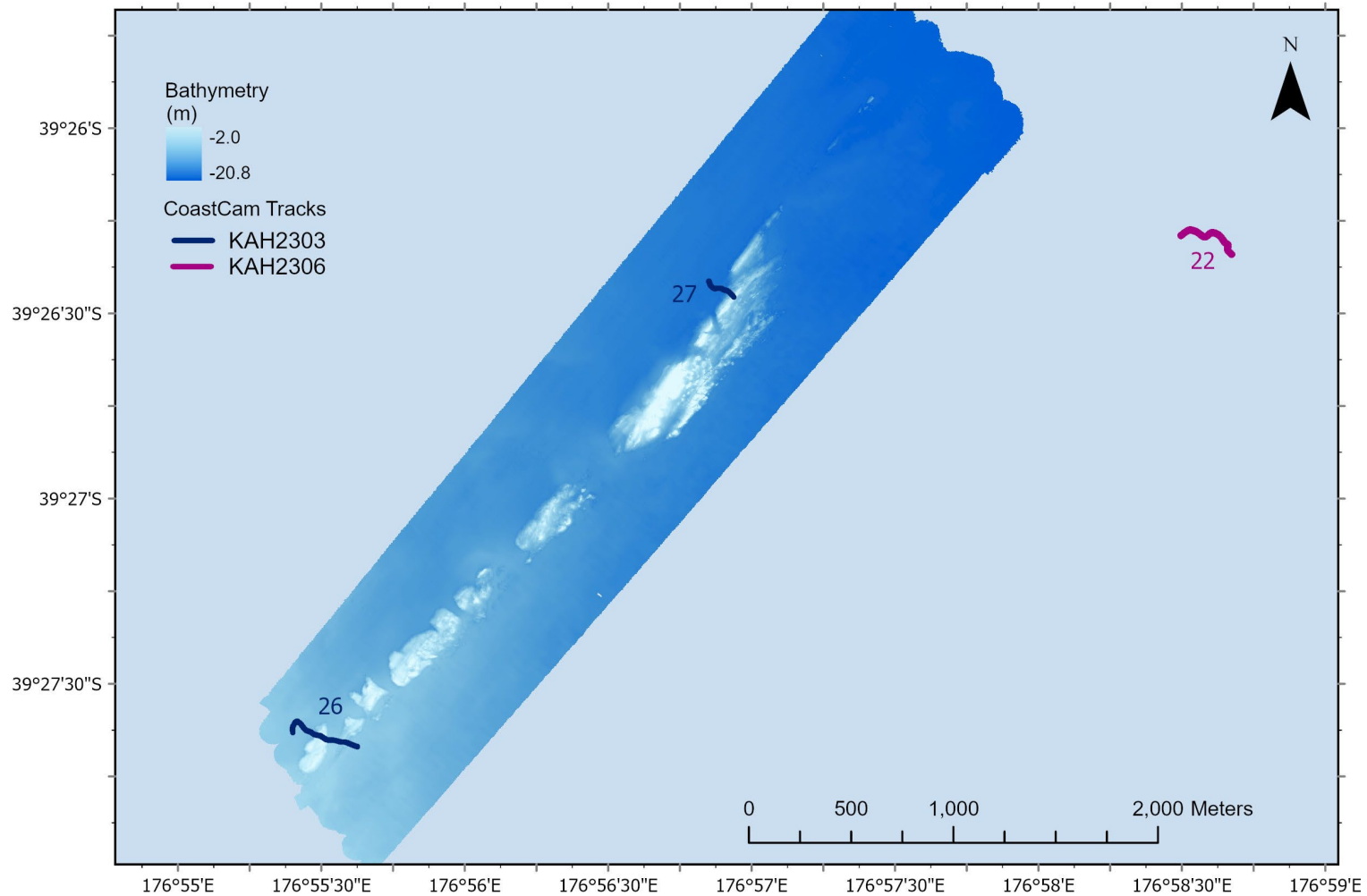
Pania Reef – seafloor bathymetry and path of towed camera transects (June RV *Kaharoa* survey KAH2303 stations 26 and 27). Path of the third June deployment (station KAH2303 station 28) could not be plotted due to corrupted GPS data. Station 22 (purple track) shows a camera deployment conducted as part of the Napier engagement day (October survey KAH2306 station 22) to demonstrate CoastCam operations.

Mahia west – seafloor bathymetry, path of towed camera transects, and counts of kelp *Ecklonia radiata*, finger sponges, and large sponges (if present). June survey KAH2303 station 37 and October survey KAH2306 station 49.

Poverty Bay south reef – seafloor bathymetry, path of towed camera transects, and counts of finger sponges and large sponges. June survey KAH2303 station 63 and October survey KAH2306 station 36.
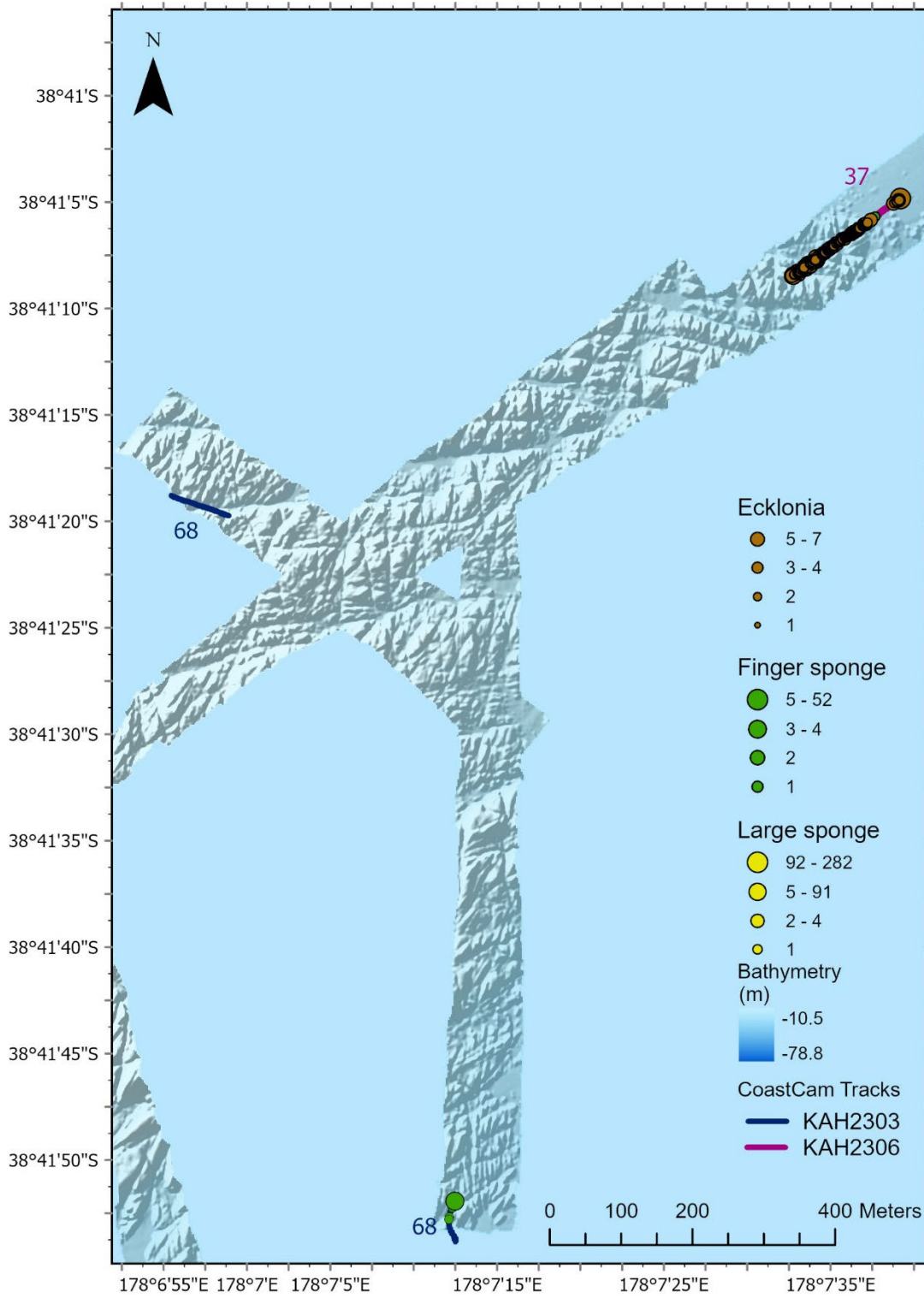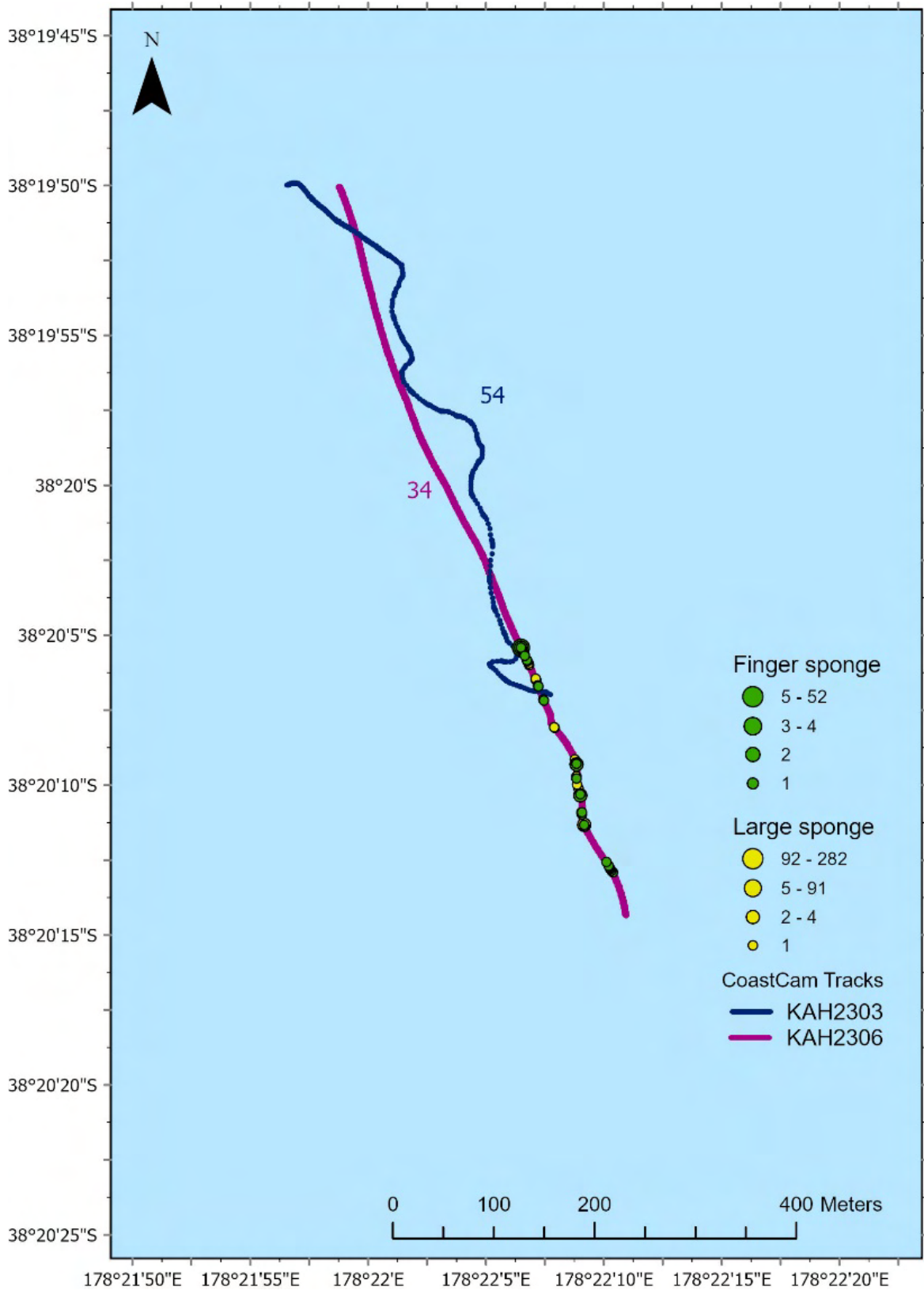
Poverty Bay north reef – seafloor bathymetry, path of towed camera transects, and counts of *Ecklonia radiata* kelp and finger sponges. June survey KAH2303 station 68 and October survey KAH2306 station 37.
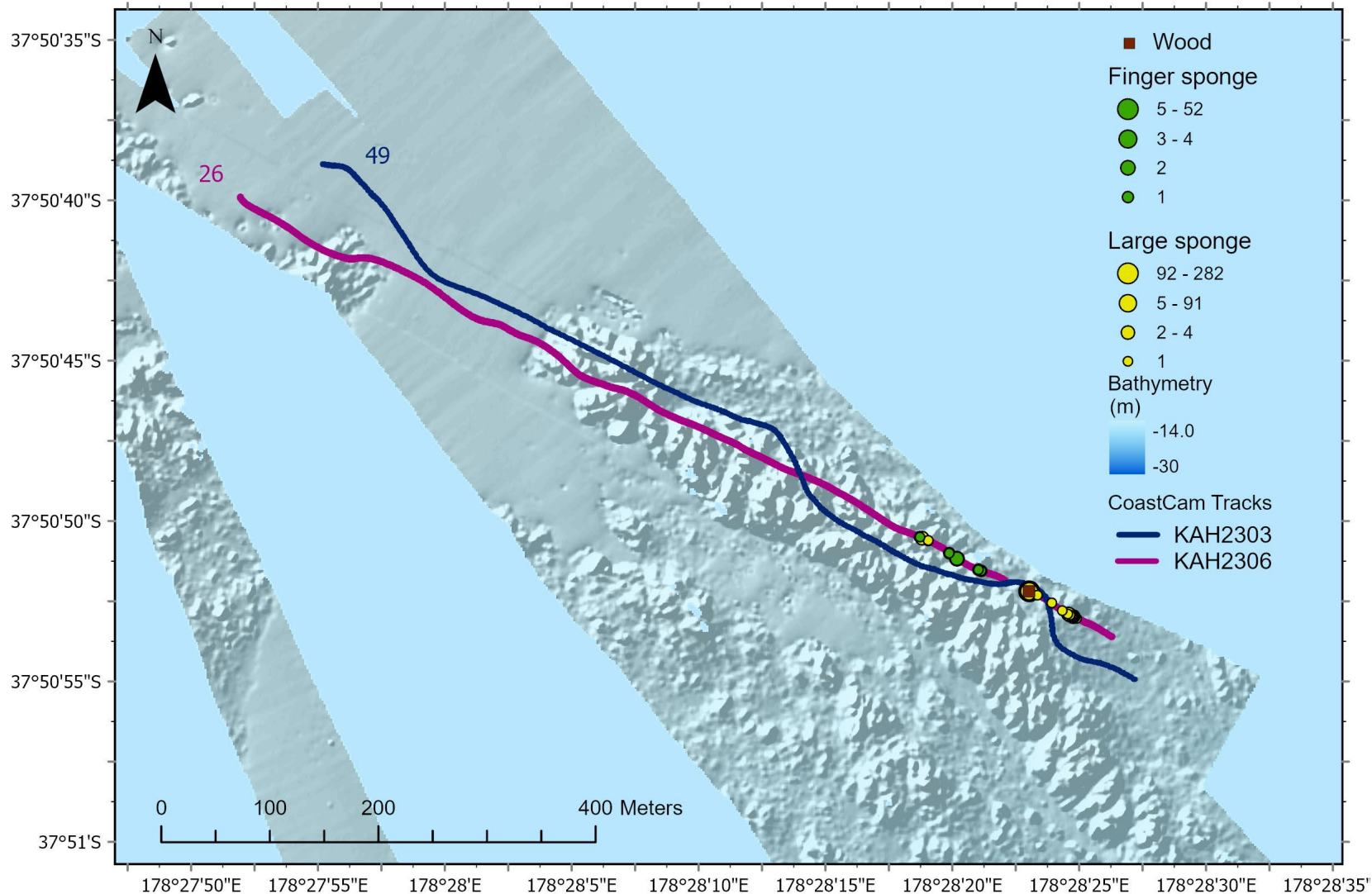
Whangara south reef – seafloor bathymetry, path of towed camera transects, and counts of finger sponges and large sponges. June survey KAH2303 station 56 and October survey KAH2306 station 39.
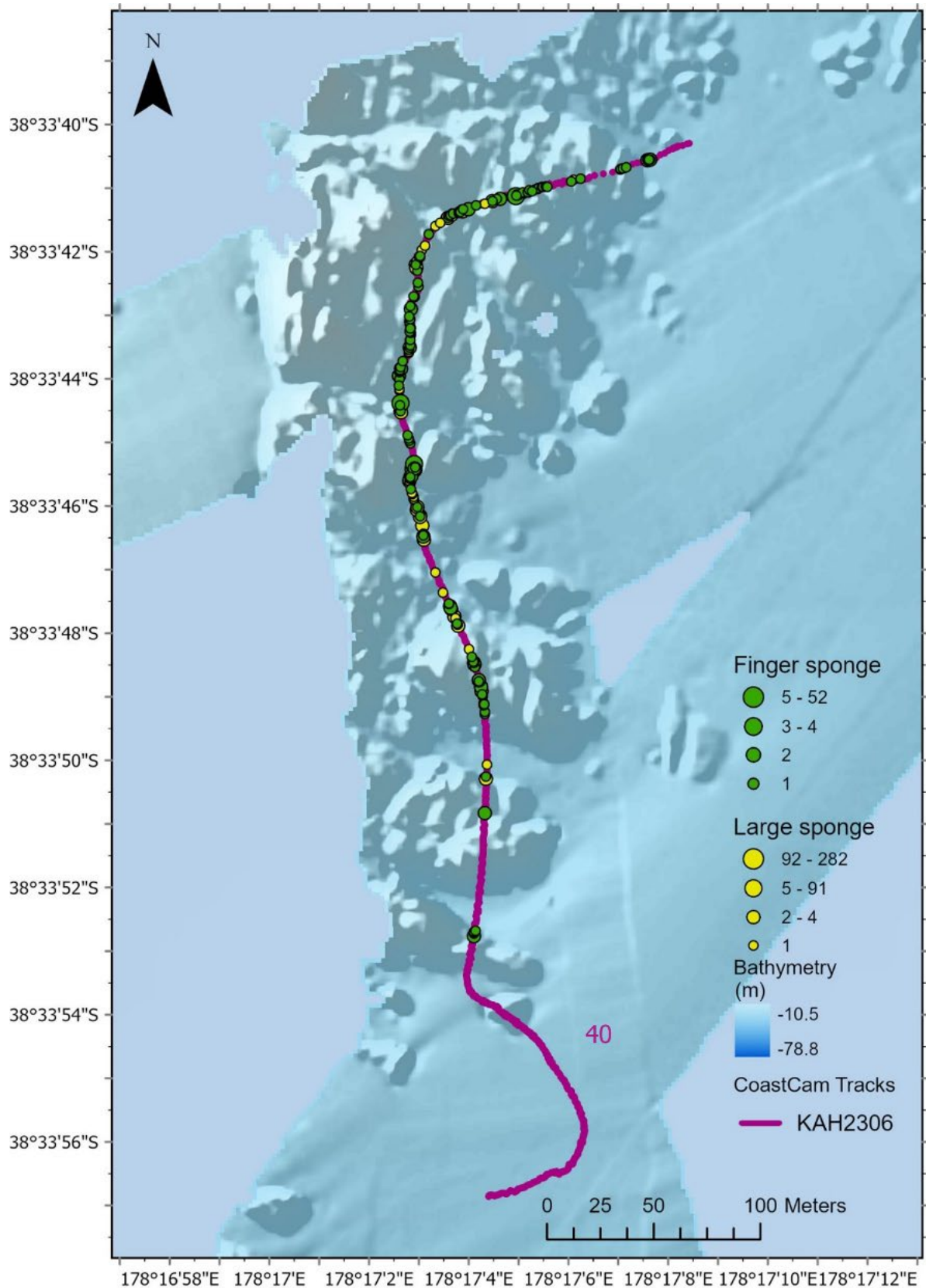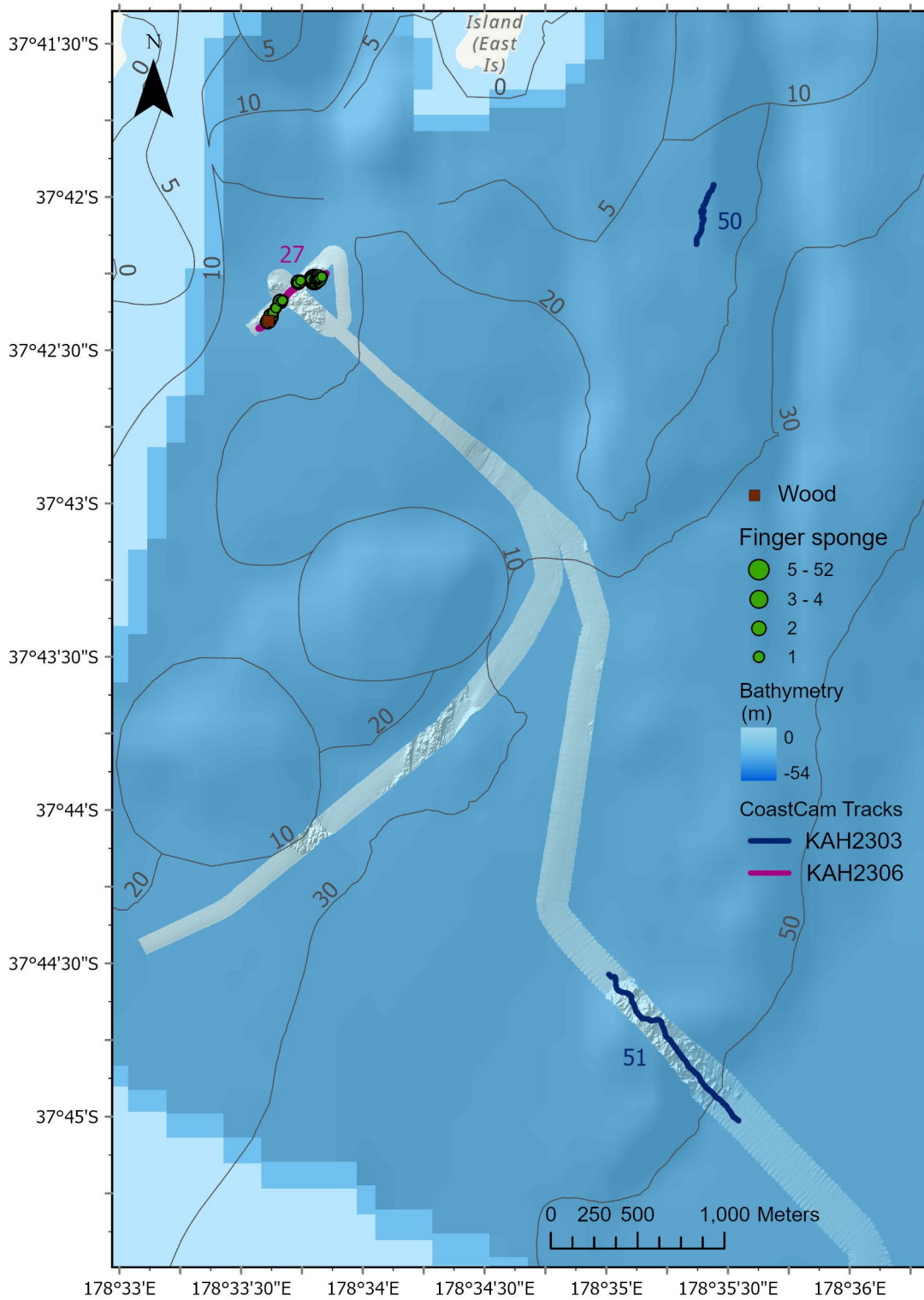
Whangara north reef – seafloor bathymetry, path of towed camera transects, and counts of finger sponges and large sponges. October survey KAH2306 station 40.

Tolaga north reef –path of towed camera transects, and counts of finger sponges and large sponges. June survey KAH2303 station 54 and October survey KAH2306 station 34. Seafloor bathymetry not shown.

Waiapu south reef – seafloor bathymetry, path of towed camera transects, and counts of finger sponges and large sponges. June survey KAH2303 station 49 and October survey KAH2306 station 26.

Waiapu north reef – seafloor bathymetry, path of towed camera transects, counts of finger sponges and location of wood on seafloor. June survey KAH2303 station 51 and October survey KAH2306 station 27.